ATOMIC LAYER DEPOSITION FOR FABRICATION OF ADVANCED POLYMER ELECTROLYTE MEMBRANE FUEL CELL CATALYSTS

by

WILLIAM WILSON MCNEARY IV

B.S., University of Missouri-Columbia, 2014

M.S., University of Colorado Boulder, 2016

A thesis submitted to the

Faculty of the Graduate School of the

University of Colorado in partial fulfillment

of the requirement for the degree of

Doctor of Philosophy

Department of Chemical and Biological Engineering

2018

This thesis entitled:

Atomic Layer Deposition for Fabrication of Advanced Polymer Electrolyte Membrane Fuel Cell Catalysts

written by William Wilson McNeary IV

has been approved for the Department of Chemical and Biological Engineering

_____

Alan W. Weimer, Committee Chair

_____

J. Will Medlin, Committee Member

Date_____

The final copy of this thesis has been examined by the signatories, and we find that both the content and the form meet acceptable presentation standards of scholarly work in the above mentioned discipline.

McNeary, William Wilson (PhD, Chemical Engineering)

Atomic Layer Deposition for Fabrication of Advanced Polymer Electrolyte Membrane Fuel Cell Catalysts

Thesis directed by Professor Alan W. Weimer

Polymer electrolyte membrane fuel cells (PEMFCs) are highly-efficient devices that convert the chemical energy stored in hydrogen and oxygen into electricity. The commercialization of this technology is hindered by the use of platinum metal to catalyze the oxygen reduction reaction (ORR) on the cathode. In this work, atomic layer deposition (ALD) was applied to the fabrication of PEMFC catalysts in order to improve the utilization of Pt in the ORR as well as the stability of the catalytic Pt nanoparticles over voltage cycling.

Nanostructures of TiO_2 were added via ALD to carbon-supported Pt catalysts (Pt/C) in order to investigate their stability effects. The durability of the catalysts was enhanced by the addition of TiO_2, with up to 70% retention in mass activity recorded over voltage cycling of the coated materials. A high-temperature treatment was found to produce Pt-Ti nanoparticles with high initial activity, but very poor durability. Atomic layer deposition was also used to add WN nanostructures to the catalysts. After a high-temperature treatment, highly stable W_2N blocking structures were formed around the Pt nanoparticles, which produced a catalyst with high activity and durability. Additional testing of these materials in a PEMFC showed that the addition of ALD nanostructures had significant effects on catalyst layer hydrophobicity, which has implications for water management during fuel cell operations.

In order to improve the utilization of Pt in the ORR, extended thin film electrocatalyst structures (ETFECS) were designed through the application of Pt ALD to a Ni nanowire (NiNW) substrate. Following a thermal annealing process to compress the lattice of the deposited Pt, the

ETFECS were found to be 4 times more active than nanoparticle Pt catalysts. Upon further testing in a PEMFC, the performance of these ALD materials surpassed that of previously-reported ETFECS as well as the DOE 2020 target for fuel cells. Additional research was conducted to develop a bimetallic Pt-Ni ALD process for ETFECS. It was observed that the quantity of deposited metal can be finely tuned by adjusting the ALD parameters, but further work will be required to improve the final performance of the materials produced through this method.

To my friends and family—thanks for always being there

ACKNOWLEDGMENTS

The mere existence of this thesis document would not have been possible without the assistance of a great number of people. I would first like to thank my external collaborators, who were an important part of the studies conducted over the course of my degree. As principal investigators in the Fuel Cell research group at the National Renewable Energy Laboratory (NREL), Drs. Bryan Pivovar, Shaun Alia, and K.C. Neyerlin provided excellent guidance and support for all work related to the extended thin film electrocatalyst structures (ETFECS) project. Chris Antunes was indispensable as manager of the ICP-MS equipment in the Fuel Cell group and was very helpful with sample preparation and data acquisition. Jason Zack performed all RDE analysis pertaining to the ETFECS project. Dr. Katherine Hurst performed hydrogen annealing on ETFECS samples and provided support with ALD experiments. Dr. Scott Mauger performed acid leaching on ETFECS samples and conducted studies on MEA incorporation of materials and fuel cell testing. At Colorado School of Mines, Prof. Svitlana Pylypenko and her group members Dr. Chilan Ngo and Sarah Zaccarine conducted extensive TEM and EDS mapping studies on ETFECS samples, as well as materials from my research on TiO_2 and WN ALD. Their contributions to this research were essential for developing a fundamental understanding of the systems I worked with, and I am very grateful for their time and expertise. Dr. Karen Buechler, Dr. Chris Gump, and Joe Spencer from ALDNanoSolutions, Inc. provided valuable feedback in ALD reactor design and operation that was crucial in the optimization of my experimental system.

Within the University of Colorado, I would like to thank Fred Luiszer in the Department of Geology for performing ICP measurements on many of my materials. In the Department of Chemical & Biological Engineering specifically, I am indebted to Dragan Mejic for his excellent

work in the machine shop. He was always willing to work with me to accommodate my experimental needs, and the custom reactor parts he fabricated were of unparalleled quality. Maria Toscano-Leary was extremely helpful in her capacity as the department electronics engineer, and I appreciate all her help in troubleshooting and building equipment. I am very grateful to Alex Roman in the Medlin/Holewinski groups for running CO-TPD experiments and his help with RDE reference electrode troubleshooting. Jeremiah Traeger was very generous in allowing me to use ultrapure water from the Schwartz lab on a regular basis for aqueous electrochemical experiments and provided assistance with the goniometer. Dr. Casey Lamarche from the Hrenya group also helped me to set up a custom contact angle measurement apparatus when the goniometer was out of commission. Finally, I would like to give an enormous thank you to Dominique De Vangel for his assistance with all academic matters large and small over the course of my graduate school experience. He is an invaluable asset to the ChBE department, and we graduate students would truly be lost without him.

I've been incredibly lucky to work with a number of excellent undergraduate and master's degree students who each made substantial contributions to my research. Megan Maguire, my first undergraduate research assistant, was a great help in the early days of my experimental work, in which we were establishing our RDE testing protocols essentially from scratch. She was a very dedicated presence in the lab who was driven to do high-quality research, and working alongside her made me a better scientist. Sarah van Rooij, a visiting master's student from EPFL in Switzerland, worked with me for a number of months synthesizing ALD catalysts, analyzing them electrochemically, and establishing protocols for TEM analysis of our materials. Sarah was also a devoted and reliable researcher, and her enthusiasm for our work was a great asset to me during some of the most difficult periods of my PhD. Annika Lai provided assistance with ALD synthesis,

as well as RDE, chemisorption, and BET analyses; she also worked independently to refine our method for calculating particle size distributions from TEM images. Audrey Linico worked with me for the final two years of my research and was an incredibly productive and dependable researcher. She worked tirelessly to gather results using RDE, chemisorption, and XRD, and also performed the majority of the preparation and execution of fuel cell testing with our catalysts. I'm immensely grateful to all of them for their contributions to this body of work.

I could not have hoped for a better group of colleagues than the members of Team Weimer. Firstly, I am grateful to Dr. Alia Lubers for introducing me to the world of fuel cells and ALD. She was an excellent mentor during the beginning of my research, and I appreciate her willingness to still answer my questions today, even after moving on to a career elsewhere. Dr. Brian Ehrhart was a very helpful source of scientific expertise and moral support during his tenure in the group, and I'm grateful to have known someone who was so astoundingly competent at everything. I'm thankful to BJ Ward for her friendship and her role in making our office a welcoming place to work. Caitlin Czernik was a valuable resource in running and repairing all of the analytical equipment in our lab. Thank you to Dr. Boris Chubukov for his willingness to help me with the lab furnaces. I'm very appreciative of the time sacrificed by Jacob Clary and Chris Bartel to explain fundamental aspects of catalysis to me. Becky O'Toole was a valuable contributor to many scientific discussions regarding ALD. Sarah Bull was very helpful in preparing membrane electrode assemblies during her independent study and also contributed greatly to the development of WN ALD in the fluidized bed. Samantha Millican provided many useful scientific insights from the dual perspective of a theorist/experimentalist, as well as good conversation in the office. I'd especially like to thank Amanda Hoskins for many years of assistance with troubleshooting,

interpretation of results, tales of her in-laws' corgi, and commiserating about experimental woes. I'm also eternally grateful for the baked goods she brought into the office on occasion.

None of this research would have been possible without funding. I would like to first acknowledge the National Science Foundation Graduate Research Fellowship Program (DGE 1144083), through which I was supported for the first three years of my degree. All work related to the ETFECS project was supported by the U.S. Department of Energy under Contract No. DE-AC36-08GO28308 with Alliance for Sustainable Energy, LLC, the Manager and Operator of the National Renewable Energy Laboratory, with funding provided by the U.S. Department of Energy Office of Energy Efficiency and Renewable Energy Fuel Cell Technologies Office. Finally, I received travel and research support from the U.S. Department of Education Graduate Assistance in Areas of National Need program (Award P200A120125).

I am very grateful to all the members of my thesis committee for their time and important feedback over the past many years. Prof. Michael Marshak from the Department of Chemistry provided many valuable insights into electrochemical phenomena suggestions for further analysis. Prof. Adam Holewinski was a reliable source of knowledge on electrocatalysis and provided honest analysis on my results and how to improve them. Prof. Will Medlin helped greatly with the development of a cohesive plan of study for the ETFECS materials and excelled at giving positive encouragement at the times it was most needed. Prof. Hans Funke was an invaluable asset to all of my experimental work, and I am truly appreciative of all the time he gave to help me troubleshoot and redesign equipment. My productivity and the quality of my research was immeasurably enhanced by his many contributions.

I'd like to especially thank my advisor and mentor, Prof. Alan Weimer. I distinctly remember my graduate school selection process getting a whole lot easier after meeting him during

my visit to CU Boulder, because of the certainty I felt that his research group would be the right place for me. Al places a great deal of trust in his students to pursue the details of their research as they see fit, and I am very grateful for his confidence in our abilities. Although this level of independence was somewhat daunting to me in the beginning, it resulted in me becoming much more confident in my ability to solve problems and answer difficult questions since I knew that Al trusted me to do so. Al helped me to expand my professional network exponentially, both through the many conferences he allowed me to attend, as well as introducing me to a number of his colleagues who were engaged in similar research to my own. I am incredibly grateful to Al for his steady presence and support throughout my entire graduate career. Even when it seemed like everything was going wrong and my world was (perhaps literally) on fire, he was always there to remind me of the bigger picture and help me push forward.

In addition to my professional colleagues, I owe a great debt to my family and friends for helping me through this process. I am so grateful to my parents, Charlotte and William McNeary, as well as my grandparents, Peggy and Bill McNeary, for their unwavering support and encouragement throughout my entire life, but especially over the last four and a half years. My sisters, Maggie and Mari McNeary, have also offered a great deal of reassurance and have been very tolerant of a brother who it seemed would never leave school and become a real adult. I've been incomprehensibly lucky to form many valuable friendships during my time in Boulder as well as to maintain special ones from previous years; each of you has added so much value to my life merely by being a part of it and I'm so thankful for you all. I'd like to particularly acknowledge the role played by my bandmates in Noctogon: Brooke Holman, Jeremiah Traeger, and Shawn Fortner. Making music with you all has been one of the greatest joys I've ever experienced, and the band was an essential creative outlet during some of the most harrowing periods of the past

few years. I truly couldn't have done this without you. Maybe someday we'll finish that Old West post-apocalyptic ragtime/space grunge concept album.

Thank you all so much.

CONTENTS

TABLES

Chapter 2:

Chapter 3:

Chapter 5:

FIGURES

Chapter 1:

Chapter 2:

Chapter 2, supplemental:

Chapter 3:

Chapter 3, supplemental:

Chapter 4:

Chapter 5:

Chapter 5, supplemental:

Chapter 6:

Chapter 6, supplemental:

CHAPTER 1

INTRODUCTION

The mitigation of anthropogenic climate change is one of the most significant challenges facing humanity in the 21st century. Beginning with the Arrhenius's initial quantification of carbon dioxide's (CO_2) contribution to the greenhouse effect [1], through Keeling's measurements of atmospheric CO_2 concentrations [2], and to the present-day reporting of the Intergovernmental Panel on Climate Change [3], a broad consensus has emerged that the emission of CO_2 from combustion of fossil fuels is the largest contributor to the global temperature increase observed since 1850 [4]. A rapid global reduction in CO_2 and other greenhouse gas (GHG) emissions is required in order to minimize future warming and mitigate the societal and environmental harm resulting from changes in the Earth's atmosphere, oceans, and cryosphere. A key component of effective GHG emissions reduction is the decarbonization of transportation through the development of advanced propulsion systems [3]. In most road vehicles, this may be accomplished by replacing the internal combustion engine with an electric motor powered by batteries or fuel cells, which do not produce CO_2 or other pollutants during operation. Both of these power sources have received significant research attention in recent years; however, the advancement of fuel cell technology will be imperative for the widespread implementation of long-range all-electric vehicles [5].

The work reported here is focused on the development of new methods for fabrication of fuel cell catalysts, with the goal of reducing cost and increasing performance—both necessary steps for advancement and eventual widespread adoption of the technology. This chapter will provide an overview of fuel cell technology and current barriers to commercialization; a primer on

atomic layer deposition, which was the catalyst fabrication method utilized in this work; and a description of the project objectives.

1.1. Overview of Fuel Cell Technology

A brief overview of the historical development of fuel cell technology and modern-day applications will be given, followed by a more extensive discussion on polymer electrolyte membrane fuel cells, as this classification is most relevant to the work reported here. The most prominent materials challenges in this field will be detailed, followed by subsequent reporting on the current outlook for innovations and solutions.

1.1.1. Applications

The fuel cell is an electrochemical energy conversion device that consumes fuel and oxidant and generates electricity. Unlike batteries, which are electrochemical energy storage devices, fuel cells require a constant supply of reactants to sustain their operation. The first operational fuel cell was demonstrated by W.R. Grove in 1839, and further development over the 19^{th} and 20^{th} centuries led to the use of fuel cells as auxiliary power sources onboard the NASA Apollo spaceflights [6]. The modern field of fuel cells encompasses devices that utilize a wide array of fuels, oxidants, electrolytes, and operating temperatures. A summary of the leading technologies is provided in Figure 1.1. The intermediate temperature phosphoric acid fuel cell (PAFC) is one of the most well-developed fuel cell technologies and was the first to be commercialized. High-temperature fuel cells, such as the molten carbonate fuel cell (MCFC) and solid oxide fuel cell (SOFC) are often used in large-scale utility power generation and military applications. Low-temperature direct methanol fuel cells (DMFC) may be used for power generation on a smaller scale. Of the devices listed, the low-temperature polymer electrolyte

membrane fuel cell (PEMFC) is the most relevant to the development of fuel cell electric vehicles and replacement of the internal combustion engine.

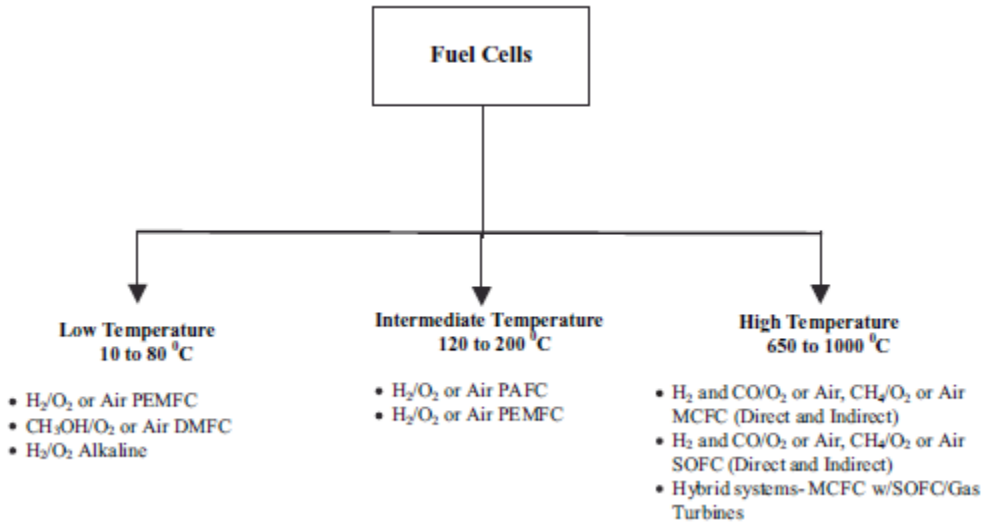

Figure 1.1: Leading fuel cell technologies classified by operating temperature.

1.1.2. Polymer Electrolyte Membrane Fuel Cells and the Oxygen Reduction Reaction

The PEMFC is a low-temperature fuel cell that utilizes hydrogen (H_2) as a fuel source, oxygen (O_2)/air as an oxidant, and a proton-conducting polymer membrane, also known as a proton exchange membrane (PEM), to separate the electrodes. On the anode, a catalyst—typically, some form of nanostructured platinum (Pt) supported on carbon—facilitates the oxidation of H_2 according to Equation 1.1 (E^0 = 0.00 V). The resulting protons move across the cell through the PEM, while the electrons are forced through an external circuit. At the cathode, the protons and electrons produced at the anode are utilized in the oxygen reduction reaction (ORR), which also requires a catalyst, according to Equation 1.2 (E^0 = 1.23 V). Movement of the electrons from the anode to cathode across an external circuit generates electricity that may be harnessed, while water (H_2O) is produced as a byproduct at the cathode. A schematic of this process is shown in Figure 1.2.

$$H_2 \rightarrow 4H^+ + 4e^- \quad (1.1)$$

$$O_2 + 4e^- + 4H^+ \rightarrow 2H_2O \quad (1.2)$$

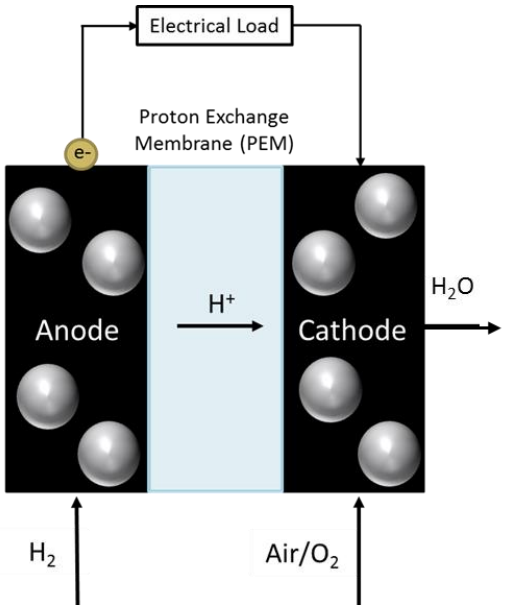

Figure 1.2: Schematic of the components of a PEMFC.

Based solely on thermodynamic properties at steady state, such a system has a maximum theoretical efficiency of 83% [6]. However, the real efficiency of a PEMFC will never match this value due to irreversible thermodynamic losses across the cell. These losses manifest as a recorded cell voltage that is lower than the ideal value of 1.23 V; this deviation is often referred to as overpotential. There are four primary contributing factors to overpotential [7]:

- activation losses, which are determined by the kinetics of the electrode reactions;
- fuel crossover, in which fuel diffuses through the PEM and is wasted;
- ohmic losses, which are caused by resistance to flow of electrons through the cell and ions through the PEM; and

- mass transport losses resulting from concentration changes of the reactant gases at the electrode surfaces.

Activation losses are directly influenced by the efficacy of catalyst materials on the electrodes, thus this source of overpotential is of primary interest to the electrocatalyst community.

The sluggish kinetics of the ORR on the cathode generate the majority of activation losses in the PEMFC. Typical activation overpotentials of 200-300 mV are often observed, thereby establishing the cathode reaction as the largest individual source of performance loss in the system [6]. The ORR is a complex, multi-step reaction whose exact mechanism remains a subject of vigorous debate. A general scheme of the reaction [6, 8] is shown in Figure 1.3. The inherently slow kinetics of the ORR may be overcome with the use of high surface area catalysts, which enhance the reaction rate such that the electrons moving from anode to cathode may be utilized for practical applications.

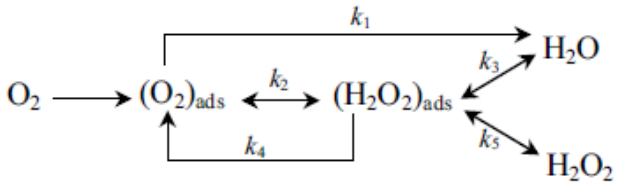

Figure 1.3: General scheme of the oxygen reduction reaction on the cathode of a PEMFC. Reprinted from [6].

As previously mentioned, nanostructured Pt on a carbon support has historically been used as a catalyst for both the anode and cathode reactions. In the case of the ORR, Pt exhibits optimal O and OH binding energies such that these adsorbed reaction intermediates are not bound too strongly to the catalyst surface and can freely proceed with the electron and proton transfer steps later in the reaction [9]. Unfortunately, although Pt is an effective ORR catalyst, its widespread use in PEMFCs presents a number of practical challenges and barriers to commercialization.

1.1.3. Materials Challenges

Platinum is one of the rarest elements in the Earth's crust. It is already used extensively as a catalyst in industrial processes such as refining and ammonia synthesis, as well as in modular applications, such as catalytic converters for internal combustion engines. Geological scarcity limits Pt production to around 180 tons per year, making it a highly valuable precious metal. Considering that any effective penetration of fuel cell vehicles into the market would involve the production of millions of cars, the availability and accessibility of Pt place limitations on its use in PEMFCs. These considerations have been taken into account by the U.S. Department of Energy (DOE) in their establishment of targets for fuel cell systems in both 2020 and 2025 [10]. Figure 1.4 shows the progress made towards these targets across the field as of November 2017. The feasibility of meeting the system cost and system durability metrics is strongly influenced by the catalyst material used in the PEMFC. These system parameters and their dependence on the choice catalyst will be discussed in greater detail below.

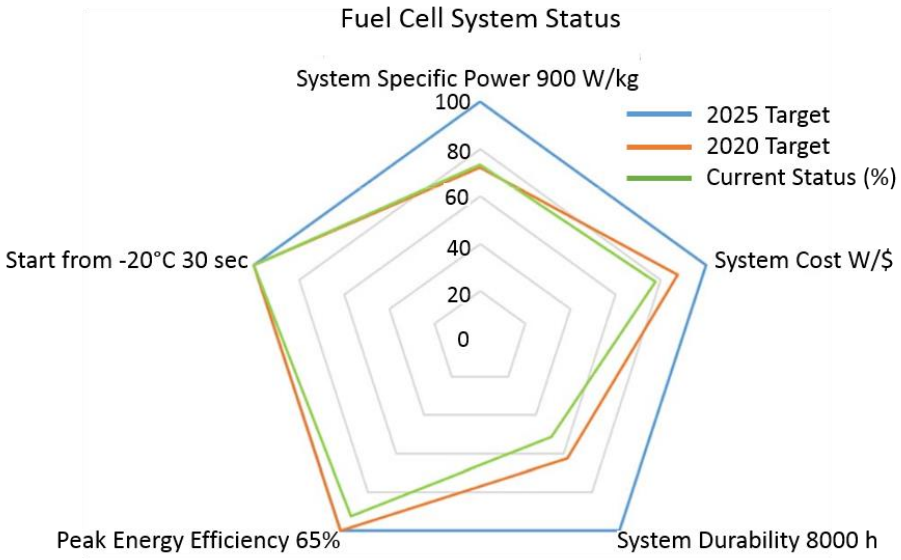

Figure 1.4: Status of current fuel cell system parameters as a percentage of the DOE 2020 and 2025 targets. Reprinted from [10].

1.1.3.1. Cost

In order for fuel cells to become a commercially viable alternative to the internal combustion engine as a source of transportation power, they must be cost-competitive. The cost target for automotive fuel cells systems put forth by the DOE is $35/kW by 2025. From Figure 1.4, it is observed that the system cost of current fuel cell systems stands at approximately 80% of this target. The attainment of this cost target is highly dependent on reducing the amount of platinum group metals (platinum, iridium, osmium, ruthenium, rhodium, and palladium) utilized in the cathode of the membrane electrode assembly (MEA). As such, it is anticipated that platinum group metal loading on the cathode must be reduced from its current minimum value of 0.125 mg cm^{-2} to a value below 0.10 mg cm^{-2} by 2020, while also maintaining similar or improved catalytic performance compared to state-of-the-art materials [10]. Thus, strategies must be devised to improve the utilization of Pt on the cathode such that precious metal loadings can be decreased without sacrificing device performance.

1.1.3.2. Durability

Similarly to cost, fuel cell systems must exhibit a lifetime durability akin to that of an internal combustion engine vehicle in order to be competitive in automotive applications. The DOE has identified a 2025 target of 8000 hours of operation (equivalent to 150,000 miles of driving) with less than 10% performance loss in order to meet this goal [10]. Given that the current status of fuel cell systems is less than 60% of the 2025 target, it is apparent that a great deal of work must be done to improve the durability of these systems.

The poor durability of existing systems is primarily due to the degradation of the Pt cathode catalyst under fuel cell operating conditions in vehicular applications. Startup of the motor,

acceleration/deceleration, and fuel starvation all result in highly variable voltage loads being placed on the fuel cell during operation. This potential cycling is known to degrade the catalyst material and reduce the performance of the fuel cell over time. Degradation of Pt catalysts on fuel cell cathodes occurs through four primary pathways: particle migration and coalescence, electrochemical Ostwald ripening, dissolution and precipitation into the electrolyte/membrane, and carbon corrosion [11]. A schematic of the first three degradation pathways can be found in Figure 1.5. Particle migration, which results in Pt sintering [12], occurs at potentials where Pt solubility is low (< 0.8 V) and is driven by minimization of surface energy. Electrochemical Ostwald ripening occurs when Pt becomes partially soluble in the acidic electrolyte, and involves the growth of larger particles at the expense of smaller ones. The smaller particles dissolve preferentially due to higher chemical potential; Pt ions then travel through the electrolyte and redeposit on larger Pt particles. The third mechanism, dissolution and precipitation, also occurs at higher potentials when Pt is soluble; however, in this case, dissolved Pt ions are reduced by residual H_2 gas from the anode and deposit in the membrane. A fourth mechanism involving the oxidation of the carbon support at potentials above 1.0 V may also cause detachment of Pt from the surface. The innate vulnerability of Pt catalysts to degradation under fuel cell operating conditions is a major barrier to the attainment of the DOE 2025 durability target, and there is an urgent need for new approaches to improve the stability of Pt in fuel cell catalysts.

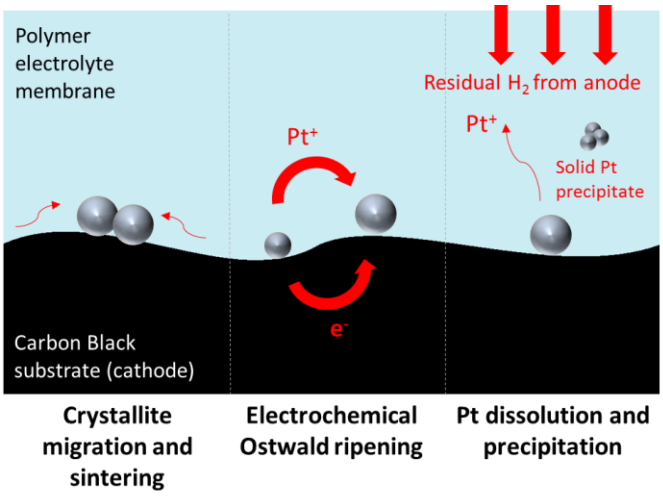

Figure 1.5: Schematic of Pt degradation pathways under potential cycling. Adapted from [11].

1.1.4. Current Outlook

1.1.4.1. Modification of Conventional Carbon-Supported Platinum (Pt/C) Catalyst

A number of researchers have sought to increase the performance of ORR catalysts by modifying conventional Pt/C materials. These strategies typically involve the addition of acid-stable chemical species to the carbon support or Pt nanoparticles to enhance the catalytic activity or the stability of Pt on the surface. One such approach is the direct coverage of both catalytic Pt and the carbon support by a protective nanometer-scale SiO_2 layer [13-16]. These inert silica layers were deposited across the catalyst surface via a hydrolysis process with the intent of stabilizing the Pt nanoparticles during potential cycling. Electrochemical characterization of the catalysts indicated only slight losses in initial catalytic activity due to the silica layers; additionally, electrochemical surface area (ECSA) and activity retention of coated catalysts over repeated potential cycling were far superior to uncoated. Further investigation with transmission electron microscopy and X-ray absorption indicated that Pt crystallite size in the coated catalysts did not change appreciably over voltage cycling, while Pt in the uncoated catalyst aggregated severely. Similar work has also established the efficacy of these silica layers in the stabilization of carbon-

supported Pd fuel cell catalysts [17-19]. Other direct layering strategies of inert materials have been tested, such as the addition of a rigid, intrinsically microporous polymer layer to a commercial Pt/C catalyst. This polymer layer was found to mechanically stabilize both the carbon support and the Pt nanoparticles, as well as enhance catalyst performance over time by selectively blocking larger impurity adsorbates from the Pt surface [20].

A related approach for modifying conventional Pt nanoparticle catalysts is the addition of nano-ceramics to the Pt/C matrix. Similar to the direct layering approaches, these materials may inhibit undesirable movement of the Pt nanoparticles and oxidation of the carbon support, but they do not typically cover the entire surface. Additionally, nano-ceramic additives such as TiO_2, ZrO_2, and others may promote synergistic metal-support interactions, such as increasing electron density around Pt [21], to enhance catalytic activity in ways that inert SiO_2 or polymer layers do not. An example of this is a composite catalyst that was prepared by physically mixing commercial Pt/C with WO_3 nanoplates [22]. It was seen that Pt nanoparticles gradually migrated onto the WO_3 nanoplates during potential cycling, which stabilized them without further agglomeration. The intrinsic catalytic activity of the Pt was also enhanced due to a hydrogen spillover effect between Pt and the WO_3. Another recent report detailed the incorporation of TiO_2 nanoflakes and a perfluorosulfonic acid (PFSA) polymer to create a three-dimensionally co-stabilized Pt catalyst supported on graphene nanosheets [23]. The modified catalyst was observed to retain considerably more of its initial ORR activity over potential cycling compared to Pt/C; Pt nanoparticle agglomeration was also mitigated. These durability improvements were attributed to the prevention of Pt migration in the x- and y-directions by the TiO_2 nanoflakes, as well as confinement in the z-direction by the PFSA molecules. The demonstrated durability and activity benefits of adding microporous layers, polymers, and nano-ceramics to conventional Pt/C

materials, in addition to the relative ease of modifying commercially-available materials, make this an area of research meriting further study.

1.1.4.2. Development of Extended Thin Film Electrocatalyst Structures

There is an extensive body of research concerning the development of Pt-M bimetallic nanoparticle ORR catalysts [24-27]. It has been well-established that the activity of Pt can be enhanced by alloying with another base metal, which often results in favorably-modified interactions with adsorbed O and OH species in the ORR [28]. Depending on the catalyst under scrutiny, these modified adsorbate interactions have been correlated with structural factors, such as smaller Pt-Pt bond distances in alloys that result in more favorable sites for dissociative adsorption of oxygen [29, 30], as well as electronic factors, such as increased Pt d-band vacancy in transition metal alloys that weakens binding with adsorbed OH intermediates [31-34]. These structure- and electronic-property correlations are often compared for various Pt-M alloys in volcano-type plots, such as the one shown in Figure 1.6. Though these bimetallic nanoparticle catalysts may represent an opportunity to fulfill the DOE goals of decreasing platinum group metal loading while also improving performance, they are still subject to many of the same nanoparticle degradation pathways as Pt/C. Additional activity benefits and advancements in durability may be possible by transferring knowledge gained from previous work in bimetallic nanoparticles into the investigation of alternative catalytic nanostructures [35, 36].

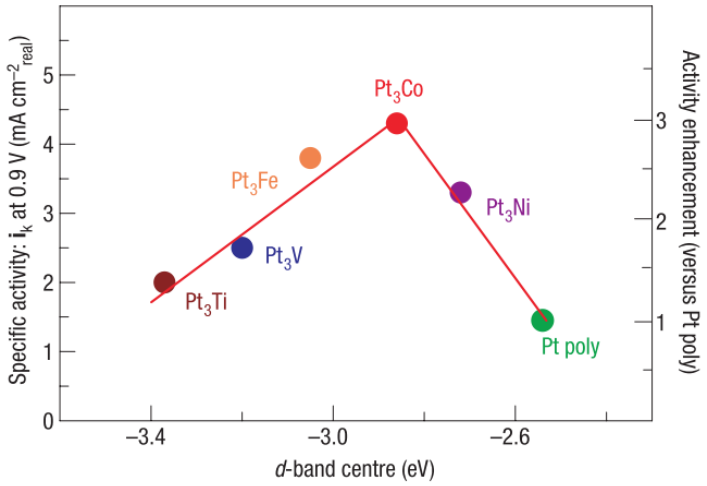

Figure 1.6: Relationships between catalyst performance and electronic properties. Reprinted from [32].

One of the most promising areas of research among these alternative nanostructures is the development of Pt-M alloy extended thin film electrocatalyst structures (ETFECS). These catalysts are typically based on high-aspect-ratio 1D materials such as nanotubes, nanorods, or nanowires and do not utilize a carbon support. Extended surface electrocatalysts have been shown to mitigate many of the persistent issues with nanoparticles; in particular, they exhibit site-specific activities that are typically an order of magnitude above those of nanoparticle catalysts, and their lack of carbon support and highly-coordinated metal surfaces impart higher electrochemical durability over potential cycling [37]. A crucial factor in the advancement of ETFECS technology is the optimization of a reproducible synthesis method that can be scaled to produce large quantities of material. One of the first demonstrations of these materials for ORR catalysis was 3M's nanostructured thin film (NSTF) catalyst, which was fabricated by vacuum sputtering various Pt-alloys onto PR149 whiskers [38]. Other examples include PtNi and PtCo nanowires synthesized via a wet chemistry surfactant-aided route [39, 40], as well as Pt-based nanowires made using a coordination effect-facilitated wet chemistry process [41].

Spontaneous galvanic displacement (SGD) has emerged as a promising route for the synthesis of extended surface electrocatalysts due to its tunable nature and ability to produce shape-controlled catalysts. This process utilizes a metal template in contact with a more noble metal cation in solution to thermodynamically corrode the template and replace the surface metal with the more noble species. The reaction typically forms a continuous layer of the noble metal on the surface of the template and can be halted at various stages of template corrosion or continued until the template is fully replaced [37]. A schematic of the process and images of a nanowire template before and after SGD can be seen in Figure 1.7. Galvanic displacement was initially used to synthesize Pt and Pt-Pd nanotubes on Ag templates [42]. These catalysts exhibited specific activities that were considerably higher than Pt/C, and the Pt nanotubes retained 70% more of their ECSA over potential cycling. Further work with Pt-coated Cu nanowires also showed promising initial mass activity and durability properties [43]. However, potential issues with residual template metals leaching from cathode during fuel cell operation necessitated the investigation of SGD on template metals with more negative redox potentials, such as Co and Ni.

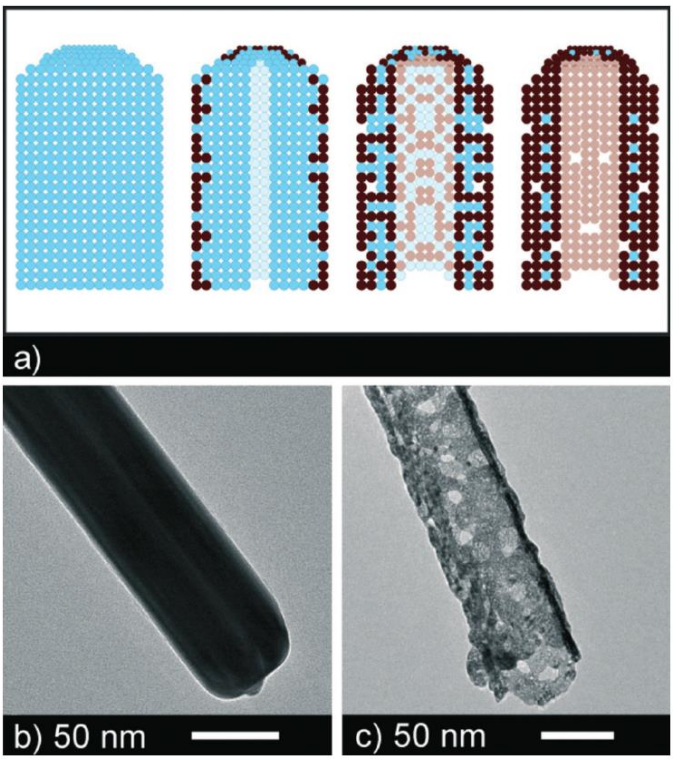

Figure 1.7: a) Schematic of spontaneous galvanic displacement (SGD). Transmission electron microscope images of (b) Ag nanowire template and (c) corresponding Pt nanowire after SGD. Reprinted from [37].

Cobalt nanowire (CoNW) templates were coated with Pt via galvanic displacement to produce PtCoNWs with a maximum specific activity of 2725 μA cm_{Pt}^{-2}, which was comparable to polycrystalline Pt [44]. It was observed that optimal performance for these catalysts occurred at low Pt displacements. The SGD of thin Pt layers onto Ni nanowire (NiNW) templates was also used to produce high-performing extended surface electrocatalysts [37, 44-47]. Various post-synthesis processing techniques, such as thermal annealing and selective acid leaching, were tested to optimize the performance of these materials for ORR [47]. An annealing step under hydrogen at 250°C was found to produce PtNiNWs with exceptionally high specific activity (> 6000 μA cm_{Pt}^{-2}) and ECSA (> 90 $m^2 g_{Pt}^{-1}$). The optimized materials also demonstrated an initial mass activity 11 times greater than traditional Pt nanoparticles supported on high surface area carbon (Pt/HSC) and lost less than 3% of their mass activity over electrochemical durability testing. However,

despite this highly promising performance in rotating disk electrode (RDE) half-cells, fuel cell testing will be needed to evaluate the performance of ETFECS under real-world conditions. In order to fabricate and optimize the fuel cell MEA, device testing of electrocatalysts requires larger quantities of materials than RDE analysis. The aforementioned SGD synthesis process has proven difficult to scale up while maintaining catalyst quality; it was observed that increasing the batch size from 40 mg to 400 mg resulted in significant losses in ECSA and specific activity [48]. The sample to sample variability in electrochemical measurements was also shown to be a concern with this fabrication method. Thus, in order advance the development of extended catalyst structures, it will be necessary to investigate synthesis routes that can overcome the documented shortcomings of SGD, while also producing analogous materials that match the exceptional performance previously reported for these catalysts.

1.2. Atomic Layer Deposition

Atomic layer deposition (ALD) is a thin film growth technique that is a subcategory of the chemical vapor deposition (CVD) family of nanofabrication methods. ALD, originally called atomic layer epitaxy (ALE), was initially developed by Finnish scientists in the 1970s for electroluminescent flat panel displays; a similar "molecular layering" technique was also explored by researchers in the USSR in the 1960s but received little attention outside the country at the time [49]. The ALD process utilizes vapor-phase, self-limiting surface reactions to deposit conformal films onto high aspect ratio substrates; these surface reactions are performed sequentially in ALD "cycles." Since this deposition technique is not line-of-sight dependent, it can be effectively used to coat a myriad of substrates, such as porous micron- or nano-sized powders, nanotubes, and nanowires [50]. A typical ALD cycle involves four steps: (1) dosing of an initial metalorganic precursor (A), which reacts with surface sites; (2) an inert purge to clear the reaction chamber of

excess A molecules and surface reaction byproducts; (3) dosing of a second precursor (B), which reacts with the ligands of the adsorbed A molecules; and (4) a second inert purge. This process is shown schematically in Figure 1.8. Atomic-scale control of the deposited materials can be achieved by varying the number of ALD cycles. The sections below review the uses of the ALD process in the stabilization and synthesis of various catalysts in order to demonstrate the potential utility of ALD in addressing the documented challenges in PEMFC ORR catalyst development.

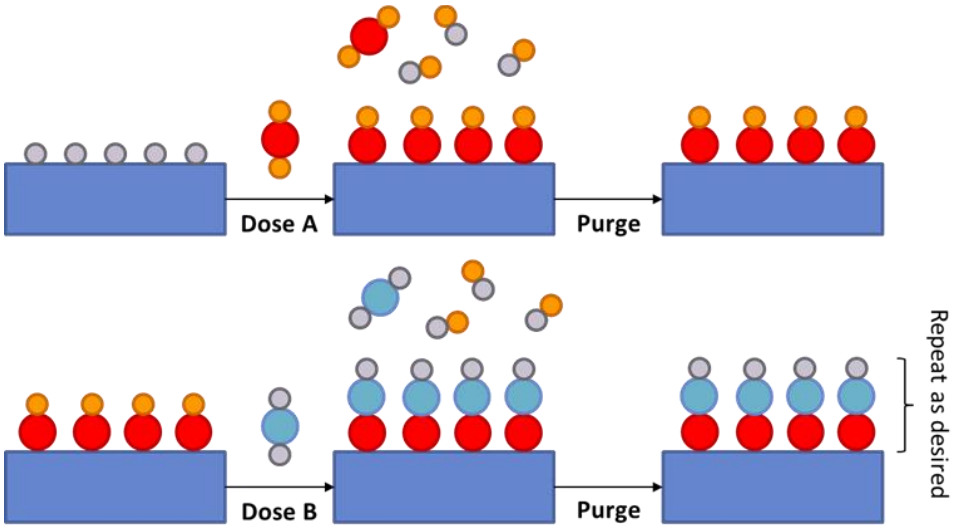

Figure 1.8: Schematic representation of a single ALD cycle.

1.2.1. ALD for Nanoparticle Catalyst Stabilization

The addition of metal oxide overcoats via ALD to supported noble metal catalysts has been demonstrated as an effective method for preventing the sintering of metal nanoparticles in high-temperature reactions. The first demonstration of ALD for nanoparticle catalyst stabilization involved the addition of a SiO_2 layer to a gold nanoparticle catalyst supported on TiO_2 [51]. It was seen through transmission electron microscopy (TEM) that the Au nanoparticles were stabilized by the SiO_2 coating at temperatures up to 700°C. Protective ALD alumina layers of 1-2 nm thickness were later found to prevent sintering and preserve the catalytic activity of Pd catalysts in

the methanol decomposition up to 500°C [52, 53]. Similarly, alumina overcoats of approximately 8 nm thickness have been found to prevent morphological changes in Pd nanoparticles after 28 hours of reaction at 675°C [54]. These ALD-coated catalysts also produced high yields in the dehydrogenation of ethane to ethylene that were on par with the best catalysts that had been reported for that reaction at the time. Ultrathin porous alumina layers were also deposited via a similar deposition process on silica-supported Pt catalysts for CO oxidation [55]. The protective films inhibited sintering of the catalytic nanoparticles at 800°C; however, the alumina-coated Pt nanoparticles were found to be less catalytically active due to the small size of the pores. Alumina layers were also used to protect Ni catalysts in the dry reforming of methane, a process in which high-temperature conditions result in catalyst sintering and deactivation [56]. When evaluated for activity at 700°C, the protected catalysts showed increasing reaction rates over time, followed by steady-state behavior, while the rate with an unprotected catalyst decreased continuously over the course of the experiment. Post-reaction particle size analysis showed a statistically significant difference in particle size between the coated and untreated Ni catalysts, indicating that the coatings did effectively reduce Ni sintering and agglomeration.

A number of researchers have investigated the effects of ALD coating strategies on electrocatalysts. Though not directly related to preventing the agglomeration of noble metal nanoparticles, early work in this field involved the application of CeO_2 [57], TiO_2 [58], and Co_3O_4 [59] ALD films onto porous nickel oxide MCFC cathodes to protect them from leaching and degradation. An area-selective ZrO_2 ALD process was recently evaluated for ORR catalyst stabilization; during ALD, the zirconia layers were coated around Pt catalyst particles suspended on a carbon nanotube support to create “nanocages,” [60]. In this case, the authors evaluated both thermal and electrochemical stability due to the zirconia ALD. A catalyst modified with 50 cycles

of ZrO_2 ALD retained its 2 nm Pt particle size after calcination at 600°C for 2 hours. When tested for electrochemical stability over 4000 potential cycles, it was found that the protected catalyst lost approximately 8% of its maximum ECSA, while the unprotected catalyst ECSA decreased by almost 74%. The ZrO_2 ALD catalyst also exhibited an initial mass activity 1.4 times greater than the corresponding unprotected catalyst and experienced very slight activity loss over potential cycling compared to the unprotected, which lost almost 73% of its activity. The authors attributed increased durability of their modified catalysts to the physical barrier to Pt sintering and dissolution created by encapsulation of Pt nanoparticles in the ZrO_2 nanocage. Researchers have also used ALD to deposit protective SnO_2 nanostructures onto a Pt-decorated carbon nanofiber ORR catalyst [61]. It was observed that the addition of the SnO_2 structures after 20 ALD cycles did not suppress ECSA, therefore indicating that reactants were not prevented from reaching the catalyst sites by the SnO_2. The deposited SnO_2 structures also appeared to promote enhanced catalytic effects due to their proximity to the Pt nanoparticles. After a 10,000 voltage cycle durability test, the coated catalyst was found to retain over 60% of its initial ECSA (compared to approximately 30% for uncoated catalyst). The agglomeration of Pt nanoparticles over the durability test was substantially mitigated by the presence of the SnO_2 ALD nanostructures. In a slightly modified approach, others have directly coated Pt/C electrodes with TiO_2 ALD before fabrication into MEAs with the goal of stabilizing Pt nanoparticles and inhibiting carbon support corrosion [62]. The electrodes modified with 10 cycles of TiO_2 ALD were found to have slightly lower fuel cell performance initially, due to coverage of the Pt sites, but the TiO_2 layer did improve catalyst durability over 2000 voltage cycles.

These examples of ALD for nanoparticle catalyst stabilization are analogous to the wet chemistry approaches for modifying conventional Pt/C discussed in Section 0. Indeed, the ALD

process integrates elements of direct layering—given the ability to tune layer thickness by modifying the number of ALD cycles—and the addition of nano-ceramics. The breadth of established ALD chemistries also allows for the addition of a wide range of stable metal oxides or nitrides to carbon support surfaces that may produce synergistic catalytic effects towards the ORR in the presence of Pt. The promising results that have been reported thus far in regards to ALD for stabilization of noble metal nanoparticles catalysts demonstrate the value of further investigations into novel strategies for ALD stabilization of Pt/C catalysts.

1.2.2. ALD for Catalyst Synthesis

In addition to the deposition of metal oxide or other ceramic films as described above, ALD can be used to deposit metal nanoparticles onto high aspect ratio substrates. The high surface energies of metals, as well as the high deposition temperatures often required in metal ALD processes, both contribute to the nucleation and growth of metal nanoparticles on the chosen substrate [63]. Though detrimental to the fabrication of thin film microelectronics, this phenomenon has been widely explored as a tunable, vapor-phase route to prepare supported nanoparticle catalysts in a "bottom-up" fashion. Of particular interest to the electrocatalyst community is the deposition of species active towards the ORR, particularly Pt and other transition metals such as those discussed in Section 0.

Atomic layer deposition of Pt is typically performed at temperatures between 200-300°C using methylcyclopentadienyl(trimethyl) platinum ($MeCpPtMe_3$) as the metal source and oxygen as the counter reagent. The established reaction mechanism for this ALD process [64] is detailed in Equations 1.3 and 1.4. Initially, the $MeCpPtMe_3$ precursor molecule reacts with O-containing substrate groups to form a $MeCpPtMe_2$(ads) surface species and gaseous byproducts CH_4, H_2O, and CO_2. It has been suggested that the Pt metal center may catalyze further hydrogenation and

incomplete combustion of the $MeCpPtMe_2$(ads) molecule after addition to the surface, resulting in a variety of carbonaceous species distributed across the surface [65]. During the subsequent O_2 dose, the remaining ligands on the adsorbed species (and any carbonaceous remnants of autocatalysis) are combusted, producing CO_2 and H_2O. The deposited Pt is also oxidized during this step, thereby producing new surface sites for further growth [66, 67]. Dispersed metal nanoparticles, rather than uniform films, are deposited in the early stages of Pt ALD nucleation and growth [68, 69]. At high numbers of ALD cycles, however, these Pt clusters may coalesce into uniform films [70].

$$2(MeCp)PtMe_3 + 3O(ads) \rightarrow 2(MeCp)PtMe_2(ads) + CH_4(g) + CO_2(g) + H_2O(g) \quad (1.3)$$

$$2(MeCp)PtMe_2(ads) + 24O_2(g) \rightarrow 2Pt(s) + 3O(ads) + 16CO_2(g) + 13H_2O(g) \quad (1.4)$$

The application of Pt ALD to carbon-based materials has been extensively studied, as these have historically been the standard ORR catalyst support. Early research found that dispersed Pt could be evenly deposited on the inner surfaces of carbon aerogels to produce high activity catalysts for CO oxidation [69]. Conformal Pt nanoparticles were later deposited on carbon nanotubes (CNT) for PEMFC catalysts; it was observed that acid pretreatment was necessary to functionalize the nanotube surface and provide active sites for ALD nucleation [71]. Researchers have also synthesized a Pt-SnO_2 ORR catalyst on nitrogen-doped CNT substrates via a combined ALD process [72] and deposited Pt onto 3D CNT/graphene oxide nanostructures [73]. Other recent work has consisted of studying the differences between Pt ALD on plain and acid-functionalized Vulcan XC72 carbon black substrate [74-76]. Although the functionalized carbon substrate allowed for the deposition of smaller, more dispersed Pt nanoparticles, it appeared that the residual oxygen-containing functional groups remaining after ALD decreased the hydrophobicity of the

catalyst surface. This created water management problems on the PEMFC cathode and decreased the fuel cell performance for the Pt ALD catalyst. In addition to carbon materials, ORR catalysts have been fabricated by applying Pt ALD to other supports such as polycrystalline Ni [77], ZrC [78], Mo_2C nanotubes [79], and $TiSi_2$ [80].

Platinum ALD may be combined with other chemistries, such as Ni or Co ALD, to produce bimetallic nanoparticle catalysts. Given that the performance of Pt-M catalysts is highly dependent on composition, the tunable nature of ALD offers great promise as an alternative to wet chemistry synthesis routes. Early work in the ALD synthesis of bimetallic nanoparticles was focused on developing constant temperature strategies for selective deposition of Pt, Pd, and Ru onto each other instead while avoiding deposition onto a metal oxide support material [81]. Bimetallic PtNi nanoparticles produced through a combined Ni and Pt ALD process were found to be more active towards dry reforming of methane than similar catalysts prepared through incipient wetness [82]. Various bimetallic PtCo nanoparticle catalysts for ORR were prepared by adjusting the deposition sequence and cycle ratio of Pt and Co ALD [83]. The authors found that the ALD method enabled them to fine-tune the nanoparticle properties and Pt:Co ratio and that the electrochemical performance of the catalysts varied greatly depending on the synthesis scheme used.

The demonstrated utility of ALD for catalyst synthesis, particularly in the field of ORR catalysis, positions it as a potentially useful tool in the development of extended thin film electrocatalysts. Like the SGD synthesis process described in Section 0, ALD can be used to deposit a catalytic metal, such as Pt, onto the surface of a nanowire [84, 85]. However, as ALD is a gas-phase process typically performed in a vacuum environment, it may allow for tighter control over process parameters and a greater degree of precision in materials produced. ALD is also widely regarded as a scalable process [86] and could likely produce quantities of material sufficient

for fuel cell MEA testing. Additionally, the promising results reported from the production of bimetallic nanoparticle catalysts using ALD suggest opportunities for the incorporation of multiple metals (in addition to the metallic nanowire substrate) into the extended surface, which is beyond the single-element replacement capabilities offered by SGD. Thus, there is a need for research into the use of ALD as an alternative synthesis method for the production of extended surface electrocatalysts.

1.3. Project Objectives

This dissertation will report on the use of ALD to address the two primary challenges associated with ORR catalyst materials for the PEMFC. First, ALD-based strategies for stabilizing Pt/C nanoparticle catalysts are discussed. Two separate ALD chemistries were examined for this purpose, and the synthesized catalysts were thoroughly characterized. The performance of select catalysts was also analyzed in a PEMFC device. Second, ALD was used as a means of improving utilization of Pt in ORR catalysts by engineering extended thin film electrocatalyst structures. A Pt ALD alternative to SGD synthesis process was developed, as well as a bimetallic Pt-Ni ALD process that enabled the creation of novel extended surface catalysts for ORR. Specific objectives for each of these research thrusts is detailed below, and the order of the dissertation will follow the sequence outlined here.

1.3.1. Titanium Dioxide ALD for Stabilization of Pt/C Catalysts

This work aimed to enhance the durability of Pt/C catalysts through the addition of TiO_2 ALD nanostructures to the catalyst surface. The ALD process was carried out in a fluidized bed on two different substrates—commercial Pt/C and a Pt nanoparticle catalyst on functionalized carbon. The catalysts were characterized using a variety of techniques in order to elucidate

differences in ALD growth between the substrates. Electrochemical performance of the catalysts was analyzed in aqueous RDE half-cell tests. The addition of TiO_2 ALD nanostructures alone was found have a slightly negative impact on catalytic activity, but yielded improvements in electrochemical durability. However, high-temperature treatment of the top-performing ALD catalyst resulted in a twofold increase in activity but was detrimental to durability. The possible reasons behind these observations and the trade-offs and benefits of this approach are also discussed.

1.3.2. Tungsten Nitride ALD for Stabilization of Pt/C Catalysts

The aforementioned strategy of using ALD nanostructures to stabilize Pt/C catalysts was extended to the use of a WN ALD chemistry. Tungsten nitride ALD was applied to the functionalized carbon-supported Pt catalyst, along with a high-temperature treatment after deposition, and the resulting materials were thoroughly characterized. Aqueous RDE testing was again used to gather information about the electrochemical properties of the active materials. Thermal treatment after the addition of 10 ALD cycles of WN was found to produce a highly-active catalyst with improved durability over other materials tested. Origins of this enhanced durability in the WN + Pt system are addressed, along with a comparison of the observed outcomes from the previous study with TiO_2 ALD.

1.3.3. Fuel Cell Testing of ALD-modified Pt/C Catalysts

Select catalysts were used to fabricate cathodes for membrane electrode assemblies for PEMFC testing in order to compare the performance of these materials in devices to that observed in RDE half-cell tests. Since previous studies with similar ALD-prepared Pt/C catalysts have shown the hydrophobicity of the catalyst layer to be strongly influenced by the presence and

identity of functional groups on the carbon support, this property was also examined on the prepared cathodes through contact angle measurement. It was observed that trends in fuel cell kinetic performance agreed well with previous data from RDE experiments, but catalyst performance at high current densities diverged significantly based on the relative hydrophobicity measured on each cathode. This behavior was attributed to water flooding, which was either mitigated or worsened depending on the surface species present on the catalyst support. A discussion of the implications of these results for development of ALD-modified Pt/C catalysts is included in the results.

1.3.4. Platinum ALD Synthesis of Extended Thin Film Electrocatalyst Structures

In order to explore the utility of ALD in the creation of novel catalyst motifs beyond nanoparticle Pt/C, Pt ALD was performed on Ni nanowires to fabricate extended thin film electrocatalyst structures. The ETFECS were synthesized at a range of Pt ALD cycles and the ALD growth was characterized. The physiochemical and electrochemical properties of the catalysts were examined before and after a hydrogen annealing step, which was found to substantially enhance the ORR activity of these materials in RDE testing. Following additional post-synthesis treatment steps and incorporation into a membrane electrode assembly for PEMFC testing, the ALD-fabricated ETFECS were observed to outperform analogous extended surface catalysts synthesized through spontaneous galvanic displacement. These catalysts made through ALD were contrasted with SGD ETFECS, as well as other advanced catalysts reported in the literature.

1.3.5. Development of Bimetallic Platinum-Nickel ALD for Extended Thin Film Electrocatalyst Structures

The previous strategy of Pt ALD growth on a nickel nanowire substrate for ETFECS was used as a basis for the development of a bimetallic Pt-Ni ALD process on a cobalt nanowire substrate to more precisely tailor the final Pt:Ni ratio in an extended surface electrocatalyst. The bimetallic ALD process was explored at a range of different conditions in order to assess the effects of process parameters on growth of the deposited metal species. The properties of the synthesized catalysts were examined in a similar manner to previous ETFECS, and recommendations for optimization and improvement of the bimetallic ALD process were proposed based on these preliminary results.

1.4. References

1. Arrhenius, S., *On the Influence of Carbonic Acid in the Air upon the Temperature of the Ground.* Philosophical Magazine and Journal of Science, 1896. **5**(41): p. 237-276.

2. Harris, D.C., *Charles David Keeling and the Story of Atmospheric CO2 Measurements.* Analytical Chemistry, 2010. **82**(19): p. 7865-7870.

3. IPCC, *Climate Change 2013: The Physical Science Basis. Contribution of Working Group I to the Fifth Assessment Report of the Intergovernmental Panel on Climate Change*, ed. T.F. Stocker, et al. 2013, Cambridge, United Kingdom and New York, NY, USA: Cambridge University Press. 1535 pp.

4. Cook, J., et al., *Quantifying the consensus on anthropogenic global warming in the scientific literature.* Environmental Research Letters, 2013. **8**(2): p. 024024.

5. Thomas, C.E., *Fuel cell and battery electric vehicles compared.* International Journal of Hydrogen Energy, 2009. **34**(15): p. 6005-6020.

6. Srinivasan, S., *Fuel Cell Principles*, in *Fuel Cells: From Fundamentals to Applications*. 2006, Springer: Boston, MA. p. 189-233.

7. Larminie, J. and A. Dicks, *Fuel Cell Systems Explained*, *Second Edition*. 2003, Hoboken, NJ: John Wiley & Sons Ltd.

8. Wroblowa, H.S., Yen-Chi-Pan, and G. Razumney, *Electroreduction of oxygen: A new mechanistic criterion.* Journal of Electroanalytical Chemistry and Interfacial Electrochemistry, 1976. **69**(2): p. 195-201.

9. Norskov, J.K., et al., *Origin of the Overpotential for Oxygen Reduction at a Fuel-Cell Cathode.* Journal of Physical Chemistry B, 2004. **108**: p. 17886-17892.

10. FCTT, *Fuel Cell Technical Team Roadmap*. 2017, U.S. Department of Energy Fuel Cell Technologies Office: https://www.energy.gov/sites/prod/files/2017/11/f46/FCTT_Roadmap_Nov_2017_FINAL.pdf.

11. Sasaki, K., M. Shao, and R. Adzic, *Dissolution and Stabilization of Platinum in Oxygen Cathodes*, in *Polymer Electrolyte Fuel Cell Durability*, F.N. Buchi, M. Inaba, and T.J. Schmidt, Editors. 2009, Springer New York: New York. p. 7-27.

12. Zhang, Y., et al., *Study of the degradation mechanisms of carbon-supported platinum fuel cells catalyst via different accelerated stress test.* Journal of Power Sources, 2015. **273**: p. 62-69.

13. Takenaka, S.M., H.; Nakagawa, K.; Matsune, H.; Tanabe, E.; Kishida, M., *Improvement in the Durability of Pt Electrocatalysts by Coverage with Silica Layers.* Journal of Physical Chemistry C Letters, 2007. **111**: p. 15133-15136.

14. Takenaka, S., et al., *High Durability of Carbon Nanotube-Supported Pt Electrocatalysts Covered with Silica Layers for the Cathode in a PEMFC.* Journal of The Electrochemical Society, 2008. **155**(9): p. B929-B936.

15. Takenaka, S., et al., *Highly active and durable silica-coated Pt cathode catalysts for polymer electrolyte fuel cells: control of micropore structures in silica layers.* Catalysis Science & Technology, 2015. **5**(2): p. 1133-1142.

16. Takenaka, S. and M. Kishida, *Functionalization of Carbon Nanotube-Supported Precious Metal Catalysts by Coverage with Metal Oxide Layers.* Catalysis Surveys from Asia, 2013. **17**(2): p. 71-84.

17. Takenaka, S., et al., *Highly durable Pd metal catalysts for the oxygen reduction reaction in fuel cells; coverage of Pd metal with silica.* Chemical Communications, 2010. **46**(47): p. 8950-8952.

18. Takenaka, S., et al., *Highly durable carbon nanotube-supported Pd catalysts covered with silica layers for the oxygen reduction reaction.* Journal of Catalysis, 2011. **279**(2): p. 381-388.

19. Fujii, K., et al., *Performance and durability of carbon black-supported Pd catalyst covered with silica layers in membrane-electrode assemblies of proton exchange membrane fuel cells.* Journal of Power Sources, 2015. **279**: p. 100-106.

20. He, D., et al., *Fuel cell anode catalyst performance can be stabilized with a molecularly rigid film of polymers of intrinsic microporosity (PIM).* RSC Advances, 2016. **6**(11): p. 9315-9319.

21. Wang, Y.J., D.P. Wilkinson, and J. Zhang, *Noncarbon support materials for polymer electrolyte membrane fuel cell electrocatalysts.* Chemical Reviews, 2011. **111**(12): p. 7625-7651.

22. Yang, C., et al., *Mitigating the Degradation of Carbon-Supported Pt Electrocatalysts by Tungsten Oxide Nanoplates.* Electrochimica Acta, 2016. **188**: p. 529-536.

23. Cheng, K., et al., *Three-Dimensionally Costabilized Metal Catalysts toward an Oxygen Reduction Reaction.* Langmuir, 2016. **32**(9): p. 2236-2244.

24. Markovic, N.M., et al., *Oxygen Reduction Reaction on Pt and Pt Bimetallic Surfaces: A Selective Review.* Fuel Cells, 2001. **1**(2): p. 105-116.

25. Mukerjee, S., et al., *Role of Structural and Electronic Properties of Pt and Pt Alloys on Electrocatalysis of Oxygen Reduction: An In Situ XANES and EXAFS Investigation.* Journal of The Electrochemical Society, 1995. **142**(5): p. 1409-1422.

26. Stassi, A., et al., *Electrocatalytic behaviour for oxygen reduction reaction of small nanostructured crystalline bimetallic Pt–M supported catalysts.* Journal of Applied Electrochemistry, 2006. **36**(10): p. 1143-1149.

27. Mukerjee, S., et al., *Effect of Preparation Conditions of Pt Alloys on Their Electronic, Structural, and Electrocatalytic Activities for Oxygen Reduction-XRD, XAS, and Electrochemical Studies.* Journal of Physical Chemistry, 1995. **99**(13): p. 4577-4589.

28. Greeley, J., et al., *Alloys of platinum and early transition metals as oxygen reduction electrocatalysts.* Nature Chemistry, 2009. **1**(7): p. 552-556.

29. Yang, H., et al., *Structure and Electrocatalytic Activity of Carbon-Supported Pt-Ni Alloy Nanoparticles Toward the Oxygen Reduction Reaction.* Journal of Physical Chemistry B, 2004. **108**: p. 11024-11034.

30. Min, M.-k., et al., *Particle Size and Alloying Effects of Pt-based Alloy Catalysts for Fuel Cell Applications.* Electrochimica Acta, 2000. **45**: p. 4211-4217.

31. Stamenkovic, V., et al., *Changing the Activity of Electrocatalysts for Oxygen Reduction by Tuning the Surface Electronic Structure.* Angewandte Chemie, 2006. **118**(18): p. 2963-2967.

32. Stamenkovic, V.R., et al., *Trends in electrocatalysis on extended and nanoscale Pt-bimetallic alloy surfaces.* Nature Materials, 2007. **6**(3): p. 241-247.

33. Gasteiger, H.A., et al., *Activity benchmarks and requirements for Pt, Pt-alloy, and non-Pt oxygen reduction catalysts for PEMFCs.* Applied Catalysis B: Environmental, 2005. **56**(1-2): p. 9-35.

34. Jia, Q., et al., *Structure–property–activity correlations of Pt-bimetallic nanoparticles: A theoretical study.* Electrochimica Acta, 2013. **88**: p. 604-613.

35. Stamenkovic, V., et al., *Improved Oxygen Reduction Activity on Pt3Ni(111) via Increased Surface Site Availability.* Science, 2007. **26**: p. 493-497.

36. Lai, J., R. Luque, and G. Xu, *Recent Advances in the Synthesis and Electrocatalytic Applications of Platinum-Based Bimetallic Alloy Nanostructures.* ChemCatChem, 2015. **7**(20): p. 3206-3228.

37. Alia, S.M., Y.S. Yan, and B.S. Pivovar, *Galvanic displacement as a route to highly active and durable extended surface electrocatalysts.* Catalysis Science & Technology, 2014. **4**(10): p. 3589-3600.

38. Debe, M.K., *Advanced Cathode Catalyst and Supports for PEM Fuel Cells*, in *2009 DOE Hydrogen Program Review*. 2009, DOE Hydrogen and Fuel Cells Program: https://www.hydrogen.energy.gov/pdfs/review09/fc_17_debe.pdf.

39. Bu, L., et al., *A General Method for Multimetallic Platinum Alloy Nanowires as Highly Active and Stable Oxygen Reduction Catalysts.* Advanced Materials, 2015. **27**(44): p. 7204-7212.

40. Bu, L., et al., *Surface engineering of hierarchical platinum-cobalt nanowires for efficient electrocatalysis.* Nature Communications, 2016. **7**: p. 11850.

41. Chen, T.-W., et al., *Ultralong PtNi alloy nanowires enabled by the coordination effect with superior ORR durability.* RSC Advances, 2016. **6**(75): p. 71501-71506.

42. Chen, Z., et al., *Supportless Pt and PtPd nanotubes as electrocatalysts for oxygen-reduction reactions.* Angewandte Chemie International Edition, 2007. **46**(22): p. 4060-4063.

43. Alia, S.M., et al., *Platinum Coated Copper Nanowires and Platinum Nanotubes as Oxygen Reduction Electrocatalysts.* ACS Catalysis, 2013. **3**(3): p. 358-362.

44. Alia, S.M., et al., *Platinum-Coated Cobalt Nanowires as Oxygen Reduction Reaction Electrocatalysts.* ACS Catalysis, 2014. **4**(8): p. 2680-2686.

45. Alia, S.M., et al., *Platinum Nickel Nanowires as Methanol Oxidation Electrocatalysts.* Journal of The Electrochemical Society, 2015. **162**(12): p. F1299-F1304.

46. Alia, S.M., et al., *Oxidation of Platinum Nickel Nanowires to Improve Durability of Oxygen-Reducing Electrocatalysts.* Journal of The Electrochemical Society, 2016. **163**(3): p. F296-F301.

47. Alia, S.M., et al., *Exceptional Oxygen Reduction Reaction Activity and Durability of Platinum–Nickel Nanowires through Synthesis and Post-Treatment Optimization.* ACS Omega, 2017. **2**(4): p. 1408-1418.

48. Pivovar, B.S., *Extended Surface Electrocatalyst Development*, in *2016 Annual Merit Review and Peer Evaluation Meeting*. 2016, DOE Hydrogen and Fuel Cells Program: https://www.hydrogen.energy.gov/pdfs/review16/fc142_pivovar_2016_o.pdf.

49. Puurunen, R.L., *A Short History of Atomic Layer Deposition: Tuomo Suntola's Atomic Layer Epitaxy.* Chemical Vapor Deposition, 2014. **20**(10-11-12): p. 332-344.

50. Van Bui, H., F. Grillo, and J.R. van Ommen, *Atomic and molecular layer deposition: off the beaten track.* Chemical Communications, 2016. **53**(1): p. 45-71.

51. Ma, Z., et al., *Surface Modification of Au/TiO2 Catalysts by SiO2 via Atomic Layer Deposition.* Journal of Physical Chemistry C, 2008. **112**: p. 9448-9457.

52. Feng, H., et al., *Palladium Catalysts Synthesized by Atomic Layer Deposition for Methanol Decomposition.* Chemistry of Materials, 2010. **22**(10): p. 3133-3142.

53. Feng, H., et al., *Alumina Over-coating on Pd Nanoparticle Catalysts by Atomic Layer Deposition: Enhanced Stability and Reactivity.* Catalysis Letters, 2011. **141**(4): p. 512-517.

54. Lu, J., et al., *Coking- and Sintering-Resistant Palladium Catalysts Achieved Through Atomic Layer Deposition.* Science, 2012. **335**(6073): p. 1205-1208.

55. Liang, X., et al., *Stabilization of Supported Metal Nanoparticles Using an Ultrathin Porous Shell.* ACS Catalysis, 2011. **1**(10): p. 1162-1165.

56. Gould, T.D., et al., *Stabilizing Ni Catalysts by Molecular Layer Deposition for Harsh, Dry Reforming Conditions.* ACS Catalysis, 2014. **4**(8): p. 2714-2717.

57. Meléndez-Ceballos, A., et al., *Electrochemical properties of Atomic layer deposition processed CeO2 as a protective layer for the molten carbonate fuel cell cathode.* Electrochimica Acta, 2014. **140**: p. 174-181.

58. Meléndez-Ceballos, A., et al., *TiO2 protective coating processed by Atomic Layer Deposition for the improvement of MCFC cathode.* International Journal of Hydrogen Energy, 2013. **38**(30): p. 13443-13452.

59. Meléndez-Ceballos, A., et al., *Electrochemical behavior of Mx−1Ox (M = Ti, Ce and Co) ultra-thin protective layers for MCFC cathode.* International Journal of Hydrogen Energy, 2014. **39**(23): p. 12233-12241.

60. Cheng, N., et al., *Extremely stable platinum nanoparticles encapsulated in a zirconia nanocage by area-selective atomic layer deposition for the oxygen reduction reaction.* Advanced Materials, 2015. **27**(2): p. 277-281.

61. Marichy, C., et al., *ALD SnO2 protective decoration enhances the durability of a Pt based electrocatalyst.* Journal of Materials Chemistry A, 2016. **4**(3): p. 969-975.

62. Chung, S., et al., *Atomic layer deposition of ultrathin layered TiO2 on Pt/C cathode catalyst for extended durability in polymer electrolyte fuel cells.* Journal of Energy Chemistry, 2016. **25**(2): p. 258-264.

63. Lu, J., J.W. Elam, and P.C. Stair, *Atomic layer deposition—Sequential self-limiting surface reactions for advanced catalyst "bottom-up" synthesis.* Surface Science Reports, 2016. **71**(2): p. 410-472.

64. Kessels, W.M.M., et al., *Surface reactions during atomic layer deposition of Pt derived from gas phase infrared spectroscopy.* Applied Physics Letters, 2009. **95**(1): p. 013114.

65. Mackus, A.J.M., et al., *Catalytic Combustion and Dehydrogenation Reactions during Atomic Layer Deposition of Platinum.* Chemistry of Materials, 2012. **24**(10): p. 1752-1761.

66. Setthapun, W., et al., *Genesis and Evolution of Surface Species during Pt Atomic Layer Deposition on Oxide Supports Characterized by in Situ XAFS Analysis and Water-Gas Shift Reaction.* Journal of Physical Chemistry C, 2010. **114**: p. 9758-9771.

67. Gould, T.D., et al., *Controlling Nanoscale Properties of Supported Platinum Catalysts through Atomic Layer Deposition.* ACS Catalysis, 2015. **5**(2): p. 1344-1352.

68. Christensen, S.T., et al., *Controlled growth of platinum nanoparticles on strontium titanate nanocubes by atomic layer deposition.* Small, 2009. **5**(6): p. 750-757.

69. King, J.S., et al., *Ultralow Loading Pt Nanocatalysts Prepared by Atomic Layer Deposition on Carbon Aerogels.* Nano Letters, 2008. **8**(8): p. 2405-2409.

70. Zhu, Y., K.A. Dunn, and A.E. Kaloyeros, *Properties of ultrathin platinum deposited by atomic layer deposition for nanoscale copper-metallization schemes.* Journal of Materials Research, 2007. **22**(05): p. 1292-1298.

71. Liu, C., et al., *Atomic layer deposition of platinum nanoparticles on carbon nanotubes for application in proton-exchange membrane fuel cells.* Small, 2009. **5**(13): p. 1535-1538.

72. Chen, Y., et al., *Atomic layer deposition assisted Pt-SnO2 hybrid catalysts on nitrogen-doped CNTs with enhanced electrocatalytic activities for low temperature fuel cells.* International Journal of Hydrogen Energy, 2011. **36**(17): p. 11085-11092.

73. Hsieh, C.-T., et al., *Atomic Layer Deposition of Platinum Nanocatalysts onto Three-Dimensional Carbon Nanotube/Graphene Hybrid*. The Journal of Physical Chemistry C, 2012. **116**(51): p. 26735-26743.

74. Lubers, A.M., et al., *Mechanistic studies for depositing highly dispersed Pt nanoparticles on carbon by use of trimethyl(methylcyclopentadienyl)platinum(IV) reactions with O2 and H2*. Journal of Nanoparticle Research, 2015. **17**(4): p. 179.

75. Lubers, A.M., et al., *Proton Exchange Membrane Fuel Cell Flooding Caused by Residual Functional Groups after Platinum Atomic Layer Deposition.* Electrochimica Acta, 2017. **237**: p. 192-198.

76. Lubers, A.M., et al., *Electrochemical hydrogen pumping using a platinum catalyst made in a fluidized bed via atomic layer deposition.* Powder Technology, 2016. **296**: p. 72-78.

77. Hoover, R.R. and Y.V. Tolmachev, *Electrochemical Properties of Pt Coatings on Ni Prepared by Atomic Layer Deposition.* Journal of The Electrochemical Society, 2009. **156**(1): p. A37-A43.

78. Cheng, N., Banis, M.N., Liu, J., Riese, A., Mu, S., Li, Ruying, Sham, T-S, Sun, X., *Atomic Scale Enhancement of Metal-Support Interactions Between Pt and ZrC for Highly Stable Electrocatalysts.* Energy & Environmental Science, 2015. **8**: p. 1450-1455.

79. Zhang, K., et al., *A highly active, stable and synergistic Pt nanoparticles/Mo2C nanotube catalyst for methanol electro-oxidation.* NPG Asia Materials, 2015. **7**(1): p. e153-e153.

80. Xie, J., et al., *Site-Selective Deposition of Twinned Platinum Nanoparticles on TiSi2 Nanonets by Atomic Layer Deposition and Their Oxygen Reduction Activities.* ACS Nano, 2013. **7**(7): p. 6337-6345.

81. Lu, J., et al., *Toward atomically-precise synthesis of supported bimetallic nanoparticles using atomic layer deposition.* Nature Communications, 2014. **5**: p. 4264.

82. Gould, T.D., et al., *Enhanced dry reforming of methane on Ni and Ni-Pt catalysts synthesized by atomic layer deposition.* Applied Catalysis A: General, 2015. **492**: p. 107-116.

83. Sairanen, E., et al., *Atomic layer deposition in the preparation of Bi-metallic, platinum-based catalysts for fuel cell applications.* Applied Catalysis B: Environmental, 2014. **148-149**: p. 11-21.

84. Lin, Y.-H., et al., *Enhancing the Photon-Sensing Properties of ZnO Nanowires by Atomic Layer Deposition of Platinum.* Electrochemical and Solid-State Letters, 2010. **13**(12): p. K93-K95.

85. Dai, P., et al., *Solar hydrogen generation by silicon nanowires modified with platinum nanoparticle catalysts by atomic layer deposition.* Angewandte Chemie International Edition, 2013. **52**(42): p. 11119-11123.

86. Goulas, A. and J.R. van Ommen, *Scalable Production of Nanostructured Particles using Atomic Layer Deposition.* KONA Powder and Particle Journal, 2014. **31**: p. 234-246.

CHAPTER 2

TITANIUM DIOXIDE ALD FOR STABILIZATION OF PT/C CATALYSTS

2.1. Abstract

Atomic layer deposition (ALD) was used to modify two different types of carbon black-based Pt oxygen reduction catalysts with protective TiO_2 nanostructures to increase catalyst durability. Rates of ALD growth and the structure of deposited TiO_2 were observed to be highly dependent on the oxygen content of the catalyst substrate. Electrochemical durability was enhanced with the addition of TiO_2 ALD nanostructures, with up to 70% retention in mass activity measured over accelerated durability testing. High-temperature treatment of the top-performing ALD catalyst, which was found to promote structural rearrangement of the TiO_2 and Pt phases into hybrid nanoparticles, yielded a twofold increase in activity but was detrimental to durability.

2.2. Introduction

As highly efficient, portable, non-greenhouse gas emitting sources of electrical power, proton exchange membrane fuel cells (PEMFCs) hold great potential as a performance- and cost-competitive alternative to internal combustion engines. One of the most significant developmental challenges in the commercialization of the PEM fuel cell is the long-term durability of the catalyst material [1, 2]. Cathode potential cycling—resulting from variable voltage loads imposed during vehicular operation—is known to promote agglomeration and growth of the Pt nanoparticle catalyst through combined mechanisms of particle migration and coalescence, electrochemical Ostwald ripening, and dissolution/precipitation of Pt into the electrolyte, all of which subsequently degrade the power output of fuel cells [3]. Poor catalyst stability necessitates the use of higher quantities of noble metals, which further increases the cost of these devices. The development of

novel catalysts with high activity and sufficient durability is essential for the advancement of PEMFC technology.

A promising approach to stabilizing ORR catalysts is the use of atomic layer deposition (ALD) to selectively deposit ultrathin films, which may protect Pt nanoparticles from dissolution and prevent crystallite migration and agglomeration on the carbon support while also ensuring unimpeded access to the catalytic sites. ALD is a sequential, self-limiting vapor-phase process that offers atomic-scale control in the growth of metal oxide films (or, in some cases, metal nanoparticles) by varying the number of surface reaction steps, or "cycles." [4]. Overcoats synthesized via ALD have been shown to preserve activity and prevent sintering and loss of active surface area in various high-temperature reactions [5-8]. Recent work focused specifically on the use of ALD films to stabilize ORR catalysts has demonstrated that both ZrO_2 ALD [9] and SnO_2 ALD [10] significantly improves the retention of electrochemical surface area (ECSA), catalytic activity, and Pt particle size. The number of ALD cycles can be chosen such that overcoats do not impede reactant access to the catalyst site. The proximity of metal oxides to the Pt nanoparticles has been suggested to promote beneficial metal-support interactions [9-11]; additionally, the ALD materials may induce changes in conductivity of the support material, thereby impacting the movement of electrons to the ORR reaction site on the catalyst particles.

Previously, TiO_2 has been applied as a support material and blocking agent against Pt nanoparticle coalescence for fuel cell catalysts due to excellent electrochemical stability and metal-support interactions [12, 13]. However, limited attempts have been made to utilize TiO_2 ALD for stabilization of Pt/C ORR catalysts [14]. Additionally, most previous ALD stabilization attempts have focused on catalysts supported by advanced carbon materials, such as carbon nanotubes and nanofibers, rather than more commercially available substrates such as carbon black. Even when

modifying carbon black-based catalysts [14], ALD was performed on the fully assembled fuel cell cathode, rather than the raw catalyst material. In this work, TiO_2 was grown on two varieties of carbon black-supported Pt nanoparticle catalysts (commercial Pt/C and ALD-synthesized Pt/acid-functionalized C) using titanium tetraisopropoxide (TTIP) and water as alternating ALD reagents in a fluidized bed reactor. This approach of coating primary particles offers a more scalable fabrication route and may also produce a more uniformly-coated catalyst material than performing ALD on pre-assembled electrodes. Rotating disk electrode (RDE) testing was used to assess the impact of the TiO_2 layers on the electrochemical durability of the catalysts.

2.3. Experimental

2.3.1. TiO_2 ALD on Pt/C Catalysts

Variable amounts of TiO_2 were grown on both a commercial 20 wt% Pt on Vulcan XC72R (Premetek P10A200; denoted as Pt/C) as well as a catalyst synthesized in-house using 25 cycles of Pt-H_2 ALD on HNO_3-functionalized Vulcan XC72R (denoted as ALD Pt/f-C; 19.8 wt% Pt). Details of the ALD Pt/f-C synthesis and its electrochemical properties can be found in [15] and [16]. The ALD Pt/f-C catalyst is known to have smaller Pt nanoparticles and higher dispersion than its Pt/C counterpart, as well as a greater concentration of oxygen-containing surface groups resulting from HNO_3 functionalization of the carbon black substrate. Commercial Pt/C catalysts modified with TiO_2 ALD are identified in the text by the number of ALD cycles (e.g., $50TiO_2$), while ALD Pt/f-C catalysts modified with TiO_2 are identified with the letter "f" and the number of ALD cycles (e.g., $f50TiO_2$). Titanium tetraisopropoxide (Sigma Aldrich) (heated to 38°C) and water were used as alternating ALD reagents to deposit TiO_2 in a fluidized bed reactor at 200°C, following the procedure developed by King et al [17, 18]. An in-line mass spectrometer (Stanford Research Systems QMS 200) was used to monitor relevant *m/z* peaks of 18, (H_2O), 28 (N_2), and

41, 43, and 45 (TTIP fragments). Vibrational motors at the base of the reactor were used to promote even mixing and gas exposure in the bed. The reactor was loaded with 3 g of catalyst, and N_2 carrier gas flow rates of 5 sccm were used for all TTIP dose and purge steps. Water doses were controlled via a needle valve to achieve a pressure drop across the reactor similar to that obtained with N_2 flow.

2.3.2. Thermal Treatment

Multiple TiO_2-modified ALD Pt/f-C catalysts were thermally treated after ALD synthesis to test the effects on catalytic performance. A low temperature oxidative thermal treatment was chosen in order to elucidate between catalytic effects of deposited TiO_2 and residual ligands from the Pt-H_2 ALD synthesis of ALD Pt/f-C, and a high-temperature partial reduction was used to promote mixing of the Pt and Ti phases. The catalysts ALD Pt/f-C, f10TiO_2, and f50TiO_2 were heated to 200°C in air for 2 hours to combust residual ligands from the Pt-H_2 ALD catalyst synthesis step. Following this treatment, the 200°C-f10TiO_2 and 200°C-f50TiO_2 were further treated at 700°C in 20% H_2 (balance Ar) for 3 hours in order to test the effect of high temperatures and a partial hydrogen atmosphere on ALD-deposited TiO_2 structures and their interactions with Pt on the surface. These catalysts are referred to as 700°C-f10TiO_2 and 700°C-f50TiO_2, respectively.

Temperature-programmed reduction (TPR) was used to verify the presence of residual ALD ligands on the surface of ALD Pt/f-C. Under a constant H_2 flow of 10 sccm, the catalyst was heated from room temperature to 700°C at a rate of 10°C/min, then held at 700°C for 30 minutes. Off-gases were measured using an in-line mass spectrometer (Stanford Research Systems QMS 200).

2.3.3. Physical Characterization

Metals weight loading of the catalysts was determined by inductively coupled plasma optical emission spectroscopy (ICP-OES) after digestion in an acid mixture. Bright field microscopy images were acquired by depositing catalyst powder on carbon film 200 mesh copper grids (Electron Microscopy Sciences) and examining under a transmission electron microscope (FEI Tecnai T12 Spirit). Particle size distributions were tabulated from these images using ImageJ, in which Feret diameters were calculated from a total of 200 Pt nanoparticles taken from 3 separate areas of the catalyst. Feret diameters initially and after durability testing were compared using a t-test assuming unequal variance. Dark field microscopy and energy dispersive X-ray spectroscopy (EDS) mapping were performed using a TEM operated at 300kV in scanning mode (FEI Talos F200X). Powder x-ray diffraction (XRD) measurements were collected using a Bruker D2 Phaser with a Cu source operating at 300 W and a Lynxeye 1D detector.

2.3.4. Electrochemical Characterization

Catalyst powders were made into ink dispersions using ultrapure water, isopropyl alcohol (Sigma Aldrich), and a 5% Nafion ionomer solution (Sigma Aldrich) [19, 20] and sonicated for 1 hour. A 10µL aliquot of ink was then drop-coated onto a 0.196 cm^2 polished glassy carbon working electrode (Pine Research Instrumentation) rotating in an inverted position at 100 rpm to give a Pt mass loading of (L_{Pt}) approximately 20 μg_{Pt} cm^{-2}. The ink was dried at 300 rpm with a heat gun positioned 6 inches above the electrode to aid in uniform airflow. After drying, the coated working electrode was used in an aqueous electrochemical cell with 0.1 M $HClO_4$ electrolyte (GFS Chemicals), a Pt coil as the counter electrode, and a regular hydrogen electrode (RHE) for the reference electrode.

Electrochemical evaluation of the catalysts was performed using rotating disk electrode (RDE) half-cell analysis [19]. Following a 100-cycle break-in procedure (0.025 to 1.2 V at 500 mV s^{-1}), cyclic voltammograms (CVs) were taken by scanning the voltage between 0.025 to 1.0 V and back at 20 mV s^{-1} in an N_2-purged cell with no rotation. Three cycles were recorded, and the third was used to estimate the hydrogen under potential desorption (H_{UPD}) charge by integrating the region of 0.06-0.4 V and removing capacitive and double layer charge contributions. The H_{UPD} value was converted into ECSA using L_{Pt}, the working electrode geometric surface area, and the conventional acidic hydrogen monolayer adsorption charge value of 210 μC cm_{Pt}^{-2}. Polarization curves were taken by scanning the voltage between 1.0 to -0.01 V and back at 20 mV s^{-1} in an O_2-purged cell with a rotation rate of 1600 rpm. One full cycle was recorded, and the anodic (positive-going) scan was used for analysis. Background curves were taken using the same scan conditions in an N_2-purged cell and subtracted from the raw polarization data. Kinetic current (I_k) was determined according to Equation 2.1, using the current at 0.9 V (I) and the mass-transfer limited current, taken at 0.4 V (I_{lim}). Mass activities were then calculated by normalizing I_k by L_{Pt}.

$$I_k = \frac{I_{lim} \times I}{I_{lim} - I} \tag{2.1}$$

Accelerated durability tests were conducted to evaluate the durability of the catalysts. An abbreviated version adapted from Marichy, et al. [10] was used in which the working electrode was subjected to cycling from 0.6 to 1.0 V at 100 mV s^{-1} under N_2 flow for 5000 cycles. Cyclic voltammograms and polarization curves were taken initially and after durability testing (ADT) to compare ECSA and activity loss.

2.4. Results and Discussion

2.4.1. TiO_2 ALD on Pt/C Catalysts

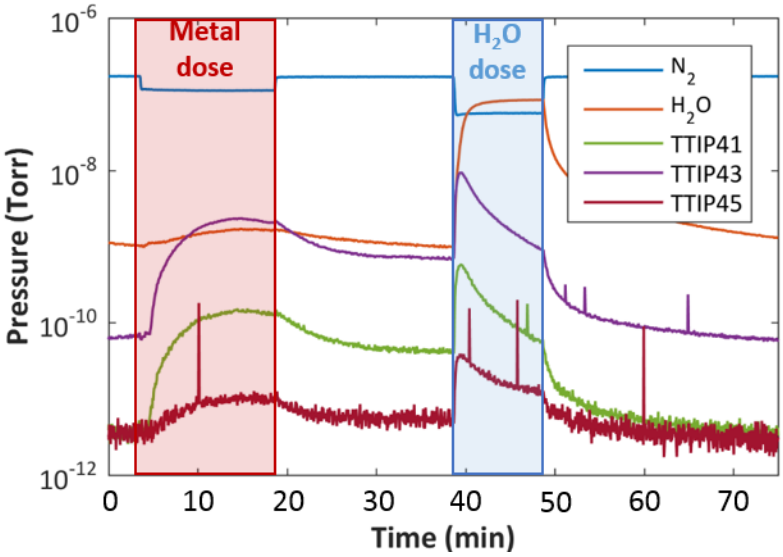

Figure 2.1: Mass spectrometry trace (m/z peak intensity expressed as pressure vs. time) for one cycle of TiO_2 ALD on ALD Pt/f-C; dose steps are denoted with colored boxes.

A representative mass spectrometry trace for TiO_2 ALD on ALD Pt/f-C catalyst is shown in Figure 2.1. Included in the figure are pressure (expression of peak intensity) vs. time traces for the *m/z* peaks of N_2, H_2O, and three primary TTIP fragments. During the metal dose (red box), TTIP fragments 41, 43, and 45 were produced as byproducts during TTIP adsorption on the surface; these fragments were also produced by unreacted TTIP reaching the MS filament and being ionized. Therefore, surface saturation was taken to be the point after the TTIP signals peaked and reached a lower steady state reading. Following this, the reactor was purged with N_2 until all signals returned to their baseline readings. The H_2O dose (blue box) showed an immediate spike in TTIP product signals, indicating removal of the TTIP ligands that remained bonded to adsorbed Ti metal centers after the metal dose. Once the H_2O signal increased to a steady state reading, the majority of TTIP ligands were assumed to have been oxidized, and the reactor was purged. This

ALD cycle process was repeated multiple times in order to investigate physical and electrochemical properties at different stages of TiO_2 nucleation and growth.

2.4.1.1. Physical Characterization

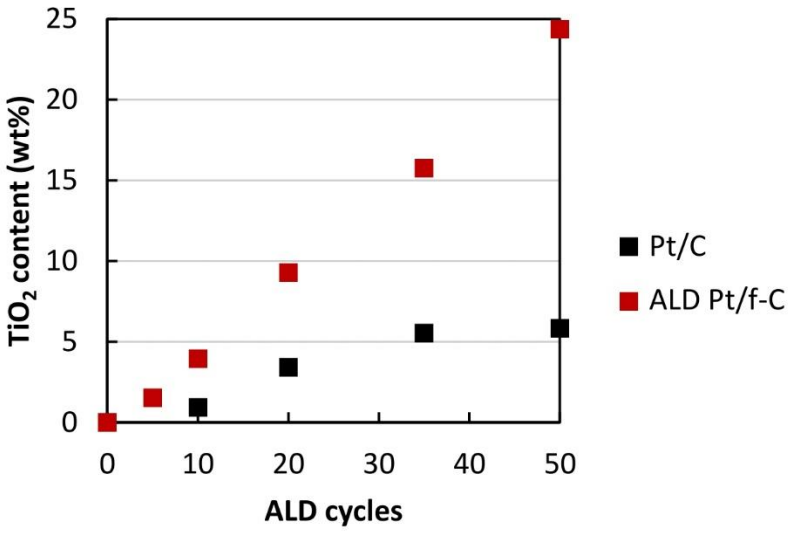

Figure 2.2: ICP-OES results for TiO_2 wt%.

Table 2.1: BET surface areas of Pt/C and ALD Pt/f-C catalysts before ALD.

Catalyst	BET surface area (m^2 g^{-1})
Pt/C	165
ALD Pt/f-C	79

Figure 2.2 displays ICP results that confirmed the presence of TiO_2 after ALD for both substrate materials. The growth rate on ALD Pt/f-C was considerably higher than on Pt/C, with 50 ALD cycles depositing almost five times more TiO_2 in the case of ALD Pt/f-C. Considering that ALD Pt/f-C had less than half as much available physical surface area for deposition as Pt/C before TiO_2 ALD (Table 2.1), the accelerated growth rate was likely due to the higher concentration of oxygen-containing functional groups on the carbon in this catalyst. The functional groups provided

more favorable nucleation sites for precursor adsorption, which led to higher amounts of TiO_2 deposited for a given number of ALD cycles.

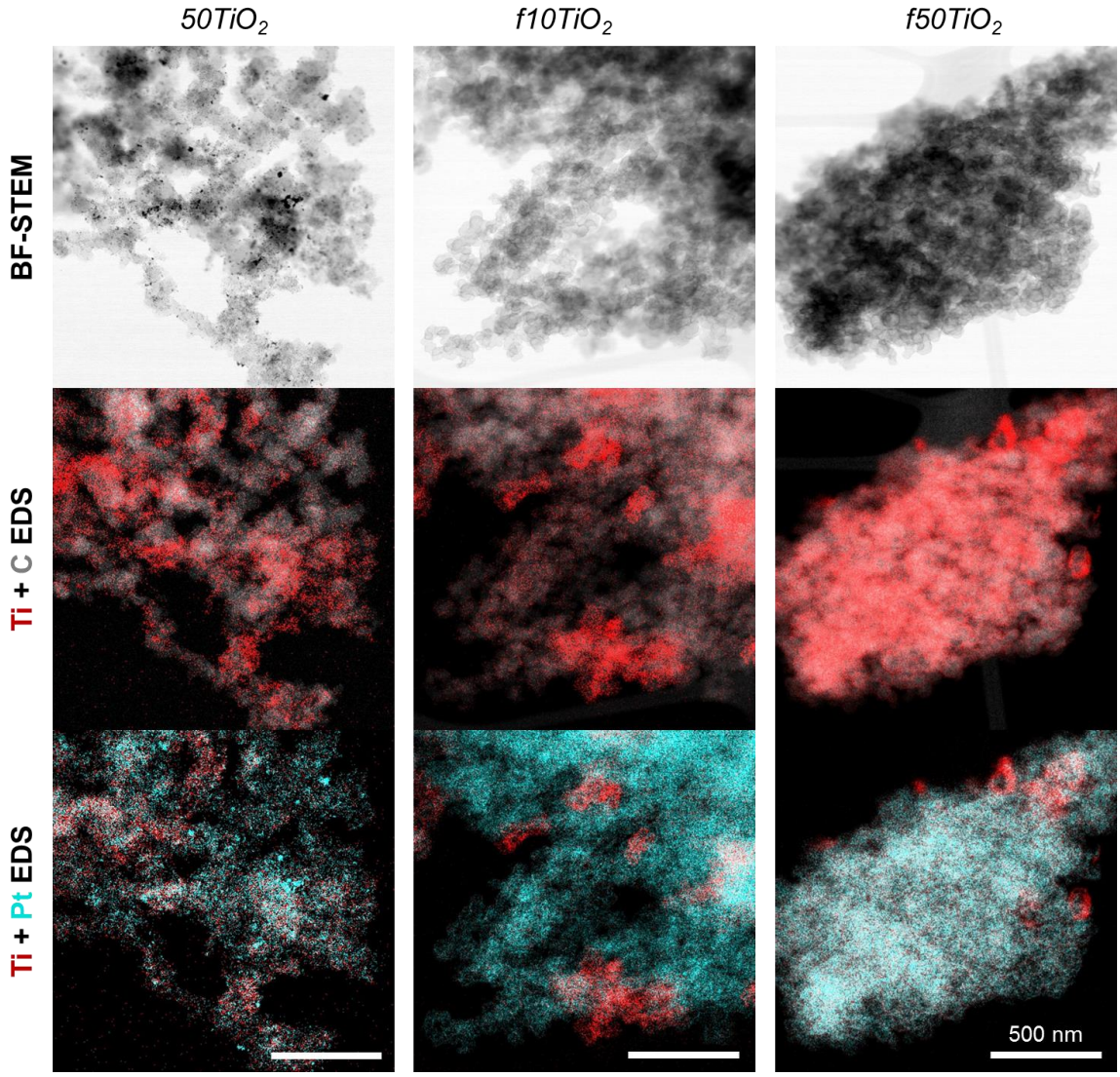

Figure 2.3: STEM images and corresponding EDS maps of as-synthesized 50 cycles TiO_2 ALD on Pt/C ($50TiO_2$); 10 cycles TiO_2 ALD on ALD Pt/f-C ($f10TiO_2$); and 50 cycles TiO_2 ALD on ALD Pt/f-C ($f50TiO_2$).

Further analysis and thermal treatments were conducted on a subset of the samples from Figure 2.2. Elemental mapping at various stages of growth (Figure 2.3) showed Ti dispersed across the surface for both Pt/C-based (50 TiO_2) and ALD Pt/f-C-based ($f10TiO_2$ and $f50TiO_2$) catalysts, though the catalysts based on ALD Pt/f-C also had large TiO_2 islands present across the surface.

Inhomogeneous distribution of nucleation sites will cause TiO_2 to grow at variable rates across the substrate; this appears to have been accentuated in the case of the HNO_3-functionalized substrate.

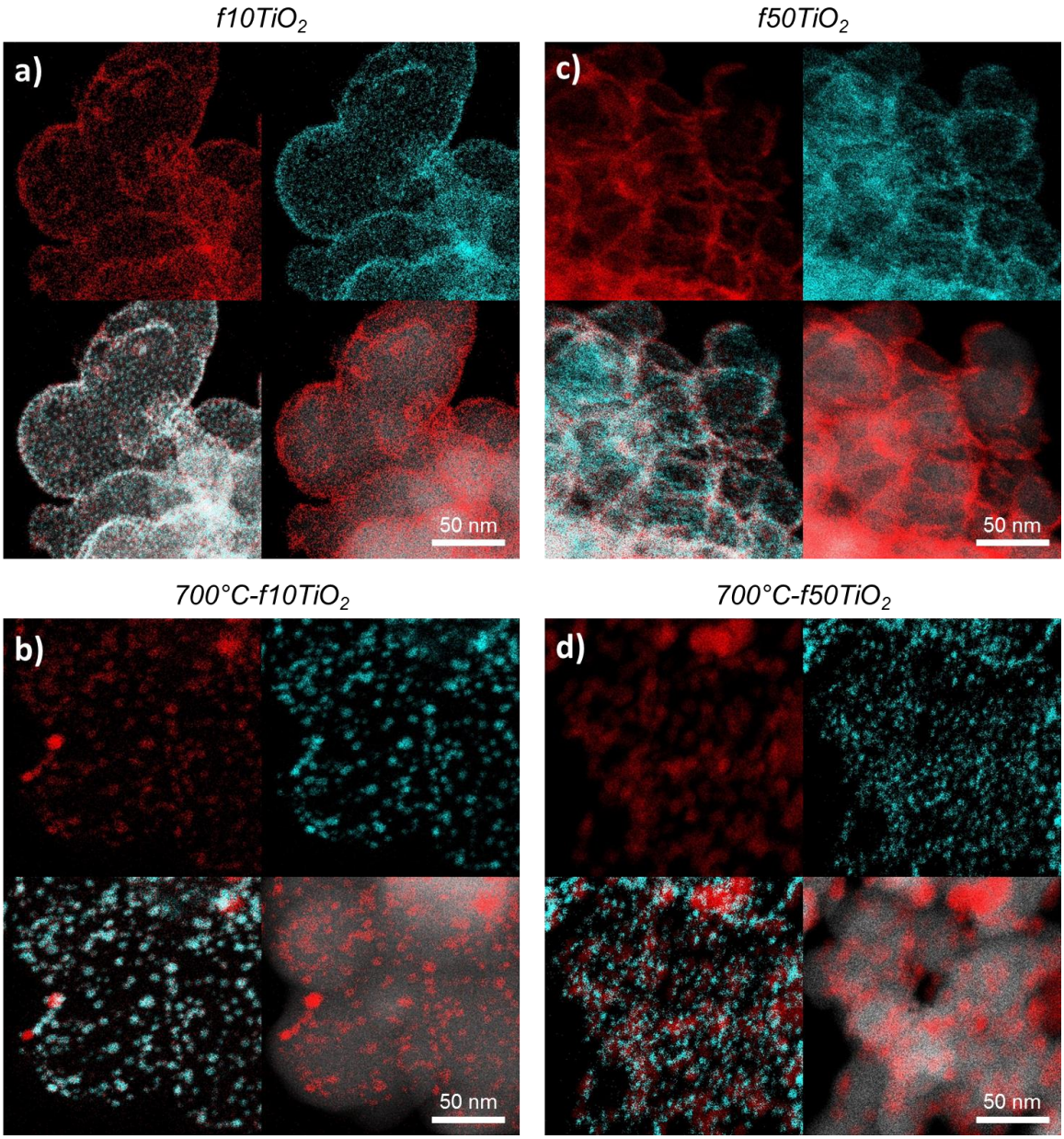

Figure 2.4: High-magnification EDS elemental maps and overlays of $f10TiO_2$ and $f50TiO_2$ as-made (a,c) and after treatment at 700°C in 20% H_2 (b,d), where light blue is Pt, red is Ti, and grey is carbon.

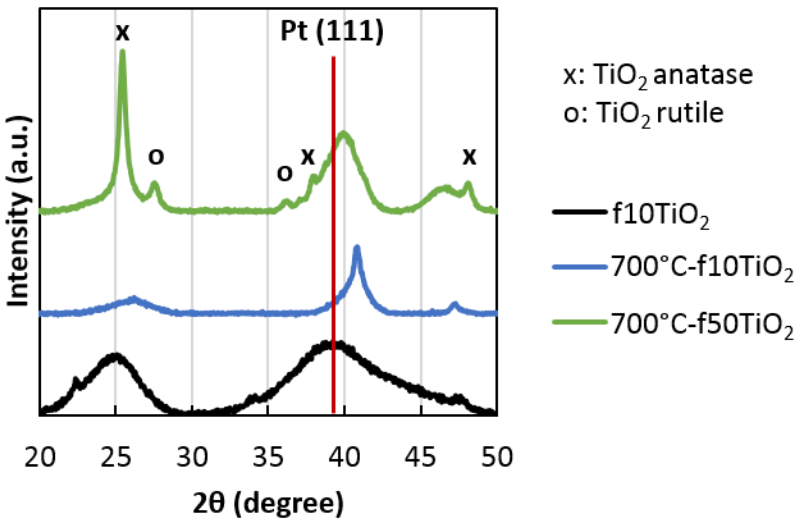

Figure 2.5: XRD patterns of $f10TiO_2$, 700°C-$f10TiO_2$, and 700°C-$f50TiO_2$; markers are used to denote relevant Pt and TiO_2 peaks.

Further examination by electron microscopy and EDS analysis of a small area of as-made $f10TiO_2$ showed localized TiO_2 homogeneity around Pt (Figure 2.4a). TiO_2 was dispersed much more evenly amongst the small, ALD-deposited Pt nanoparticles than for a Pt/C-based catalyst of similar TiO_2 content (Figure 2S.1). Following thermal treatment of $f10TiO_2$ at 700°C in 20% H_2, there was a distinct coarsening of the Pt nanoparticles (Figure 2.4b); additionally, the Ti on the surface migrated across the carbon support to concentrate at the Pt sites, suggesting the formation of new Pt-Ti intermetallic structures. Figure 2S.2 shows the crystalline lattice structure of these Pt-Ti nanoparticles. Comparison of XRD patterns across the catalysts (Figure 2.5) revealed a distinct positive shift in the Pt (111) peaks [21] by approximately 1.4 degrees for 700°C-$f10TiO_2$ and 0.5 degrees for 700°C-$f50TiO_2$, likely due to insertion of Ti into the Pt lattice. These shifted peaks are well-aligned with those various reference PtTi patterns, such as Pt_5Ti_3 (PDF 65-4265) and $TiPt_8$ (PDF 65-8378). The absence of distinct TiO_2 peaks in the diffraction pattern of 700°C-$f10TiO_2$ indicated that the 700°C partial reduction completely integrated the Ti and Pt phases (as implied by the overlapping Pt and Ti signals in Figure 2.4b), rather than forming separate

crystalline TiO_2. There are numerous examples in the literature of verified Pt-Ti catalysts prepared at similar temperatures [22-27], though this would represent the first synthesis using an ALD process in lieu of a wet chemistry procedure. Application of the same thermal treatment on f50TiO_2 (Figure 2.4d) showed decreased Pt agglomeration as well as the appearance of large Ti-based islands that remain separated from the Pt nanoparticles. Based on the XRD pattern of 700°C-50TiO_2, these islands were determined to be a mix of anatase and rutile TiO_2. The preservation of a distinct TiO_2 phase is in contrast to f10TiO_2, in which the elemental Ti signal correlated with that of Pt on the surface. This suggests that although greater amounts of ALD-deposited TiO_2 may have helped to prevent particle coarsening at high temperatures (as expected from other ALD layers [5, 6, 8]), there is also an upper limit to the amount of TiO_2 that can intermix with the Pt, and the remainder will exist as its own distinct phase after annealing.

2.4.2. Electrochemical Characterization

2.4.2.1. Effects of ALD on Catalytic Performance

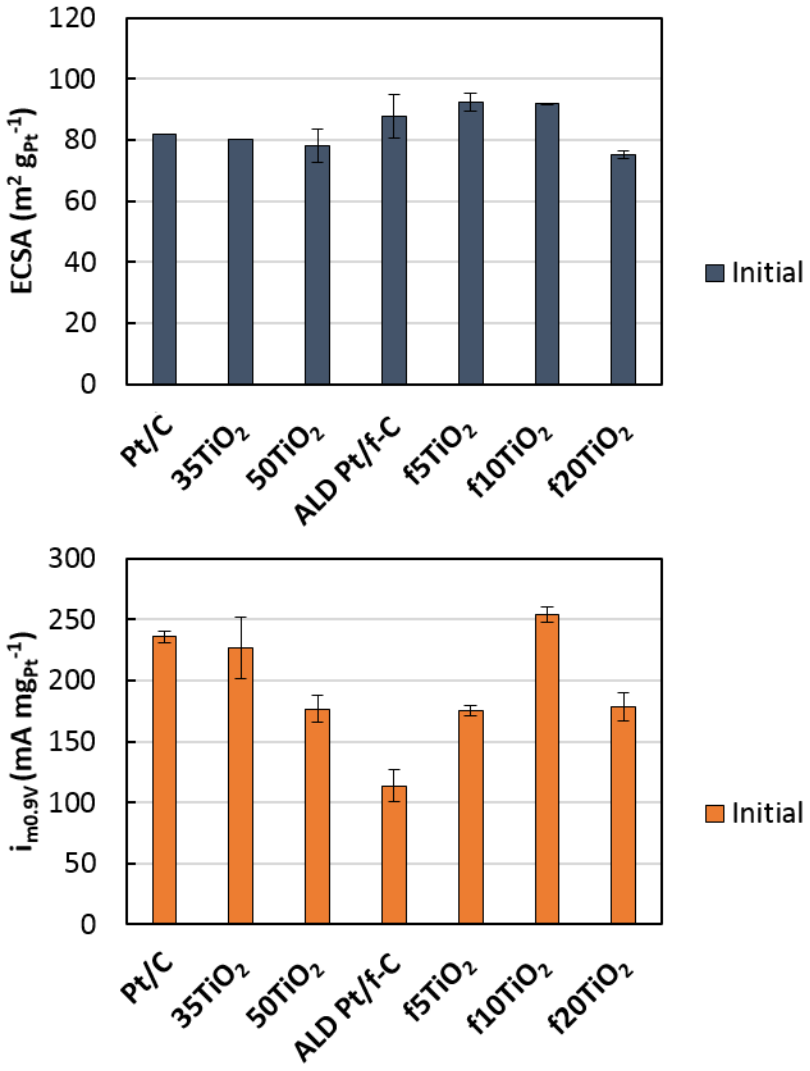

Figure 2.6: ECSA and mass activity values for ALD-coated catalysts.

Electrochemical performance of unmodified and TiO_2 ALD-coated catalysts is detailed in Figure 2.6. All catalysts based on ALD Pt/f-C had higher ECSA values than those based on Pt/C due to higher Pt dispersion. The mass activity of Pt/C-based catalysts was depressed with the addition of TiO_2, likely due to non-selective ALD growth over Pt active sites in addition to the carbon support, as was observed in Figure 2.3. Both ECSA and mass activity of ALD Pt/f-C were

enhanced with the addition of up to 10 ALD cycles; however, a significant drop in mass activity was observed at higher cycles. The increasingly poor performance of f35TiO_2 and f50TiO_2 catalysts (Figure 2S.3) indicated that unfavorable coverage of Pt sites also occurred past a certain threshold of ALD cycles in the case of the functionalized substrate. The f10TiO_2 catalyst appeared to be the best performer, with ECSA and activity slightly higher than Pt/C. The poor performance of ALD Pt/f-C and its activity enhancement with the addition of 10 TiO_2 ALD cycles was investigated through a series of subsequent thermal treatment processes detailed below.

2.4.2.2. Effects of Thermal Treatment on Catalytic Performance

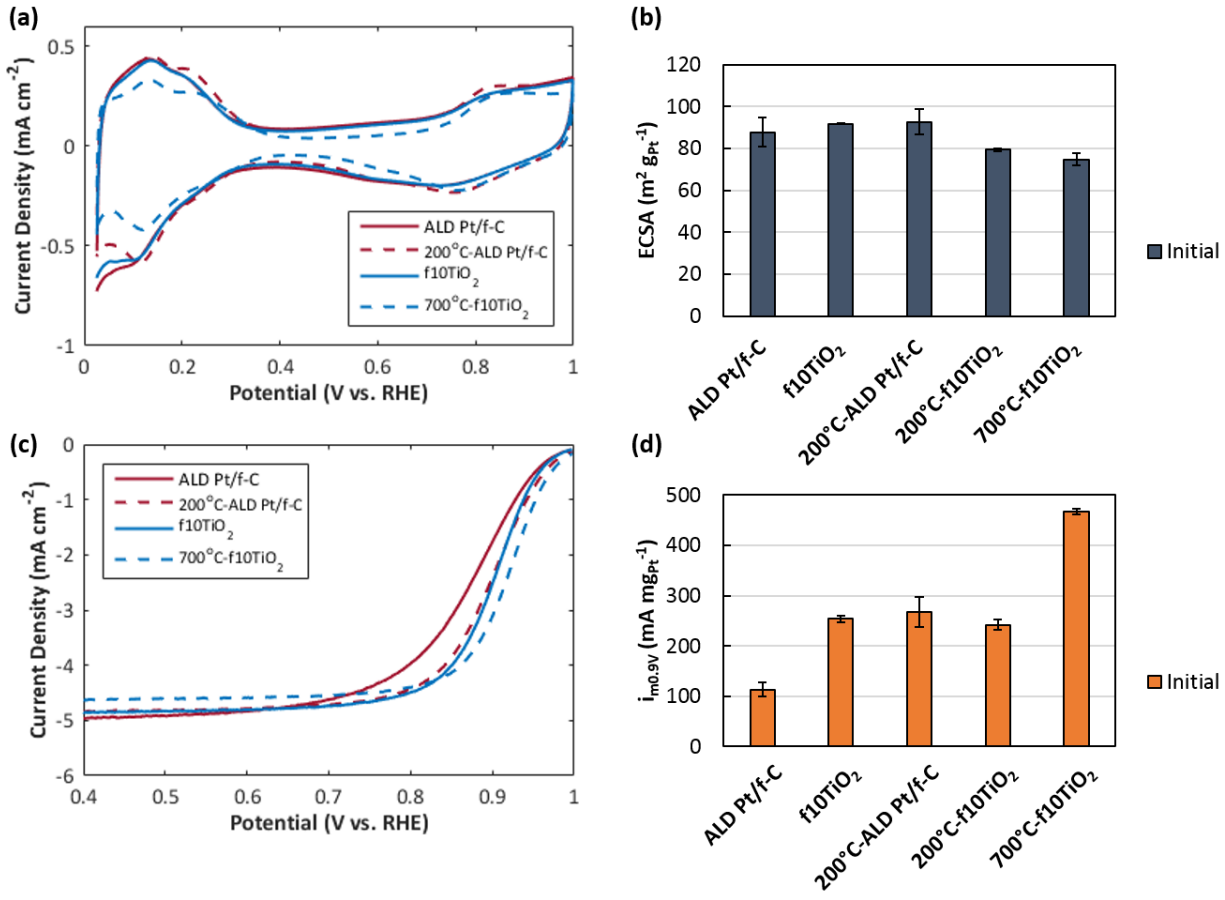

Figure 2.7: Electrochemical performance of thermally-treated catalysts: a) cyclic voltammograms; b) ECSA measurements; c) polarization curves; d) mass activities.

Treatment in air at 200°C enhanced the electrochemical performance of ALD Pt/f-C by combusting residual Pt ALD ligands and exposing Pt surface area, as evidenced by the emergence of the Pt_{HUPD} peak in Figure 2.7a. The mass activity of 200°C-ALD Pt/f-C was almost equivalent to f10TiO_2, which indicated that the activity increase from the addition of 10 ALD cycles was due not to the synergistic effects of deposited TiO_2 on Pt, but rather the removal of residual ligands that were not removed during the synthesis of ALD Pt/f-C. Typically, Pt ALD is performed using O_2 as a co-reactant to combust adsorbed ligands [28]; however, this catalyst was synthesized using H_2 in the ligand-removal step in order to promote the growth of dispersed Pt on the surface and protect the XC72 substrate from oxidation [15]. It was hypothesized that incomplete ligand elimination during hydrogenation may have led to site blocking and poor mass activity. The presence of residual Pt ALD ligands on this substrate was confirmed with H_2 TPR (Figure 2S.4). Given that the ligands were easily combusted in air at 200°C, the 200°C H_2O dose during TiO_2 ALD may have oxidized the ligands in a similar manner, thereby clearing off Pt sites and increasing the activity. The 200°C air treatment had a negligible effect on the activity of f10TiO_2, indicating that the residual Pt ALD ligands were fully removed after 10 cycles of TiO_2 ALD.

Treatment in 20% H_2 at 700°C significantly increased the mass activity of f10TiO_2, though ECSA was slightly decreased. A large positive shift in the half-wave potential was evident (Figure 2.7c), and the activity of this modified catalyst was almost twice that of the uncoated Pt/C catalyst. The ALD Pt/f-C catalyst also underwent the same 700°C treatment and displayed a mass activity that was roughly similar to 200°C-ALD Pt/f-C and f10TiO_2 (see initial data series in Figure 2S.5). This control experiment indicated that the high-temperature treatment alone was not enough to increase the activity to the degree observed in 700°C-f10TiO_2; the presence of TiO_2 on the surface during the 700°C treatment was essential to the observed catalytic benefit. The large activity

increase was likely the result of a structural rearrangement of the TiO_2 domain and infusion of reduced Ti into Pt (Figure 2.4b), which is typically associated with contraction of the Pt lattice and beneficial changes in electronic structure [23, 24, 26]. The 700°C-f10TiO_2 catalyst synthesized via ALD had similar performance to other high activity Pt-Ti catalysts synthesized through a wet chemistry process [26]. It is possible that other changes in the f10TiO_2 catalyst, such as removal of functional groups or exposure of more active Pt facets during thermally-induced coarsening, may have occurred during the 700°C treatment. Further research will be required to assess the contribution of these phenomena, relative to Pt-Ti structural rearrangement, in the observed mass activity improvement.

2.4.2.3. Effects of ALD Coatings on Catalyst Durability

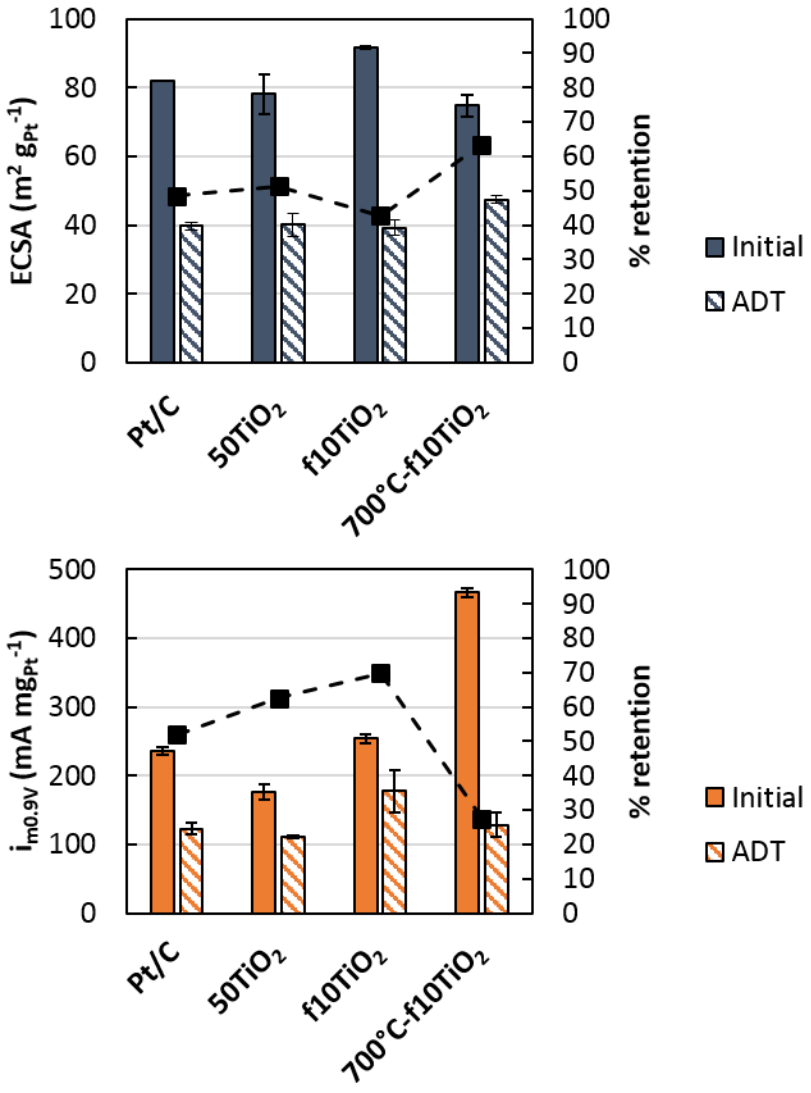

Figure 2.8: ECSA (blue) and mass activity (orange) of selected catalysts before and after durability testing; percent retention (black) of each property is also provided on the secondary y-axis.

Addition of TiO_2 ALD structures provided a modest improvement in ECSA retention (Figure 2.8), with most coated materials exhibiting greater retention of initial ECSA values over the durability test; however, f10TiO_2 lost slightly more ECSA due to its small initial nanoparticles, which had higher surface energy and were therefore prone to crystallite migration and electrochemical Ostwald ripening. Mass activity retention was also improved, with 10 cycles of

TiO_2 on ALD Pt/f-C producing a catalyst that retained 70% of its initial activity after the durability test. Though $50TiO_2$ had a similar TiO_2 content, the durability of $f10TiO_2$ was likely superior due to its enhanced proximity between Pt nanoparticles and ALD-deposited blocking structures, the deposition of which was facilitated by the functionalized XC72 substrate. The catalyst with the highest initial activity, 700°C-$f10TiO_2$, had the worst activity retention of all catalysts tested. The structural rearrangement and Pt-Ti intermixing that led to high initial activity for this catalyst appears to have also made the catalytic nanoparticles more prone to activity loss; when taken alongside the detrimental effects of excessive ALD coating (>10 ALD cycles), these findings demonstrate a trade-off between developing catalysts with high activity or high durability using the approach outlined in this work.

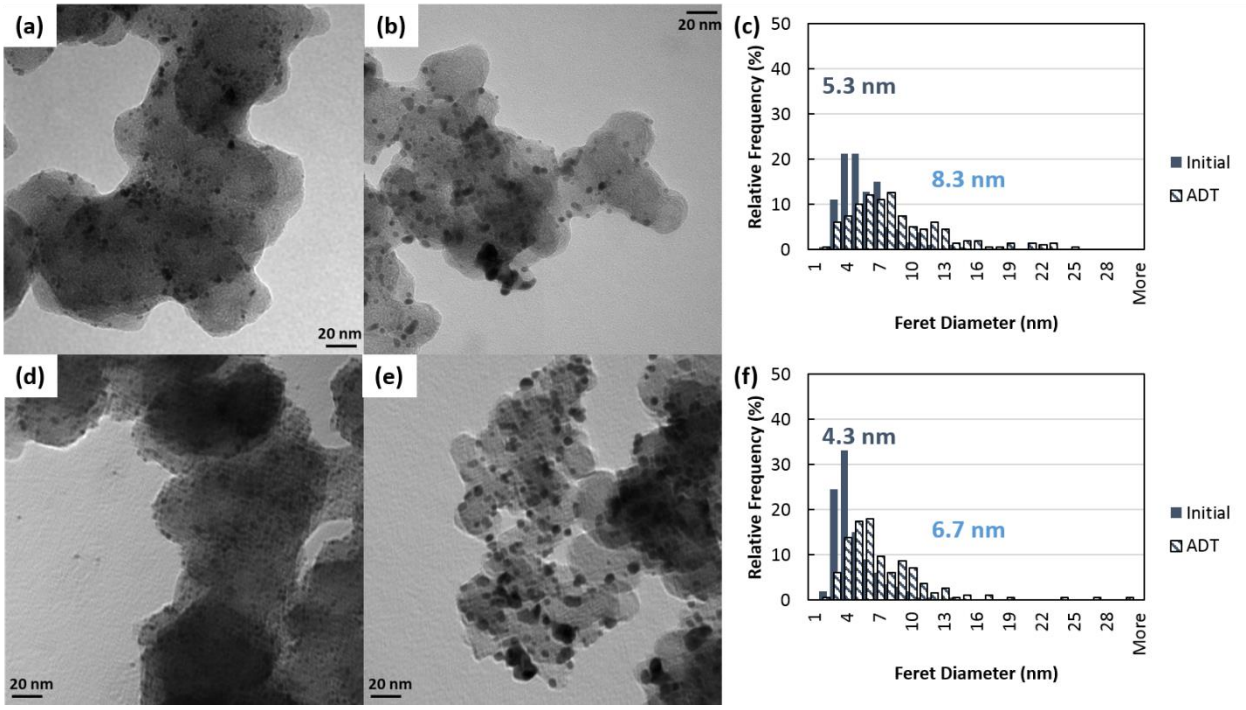

Figure 2.9: TEM images over durability testing: a) Pt/C initial; b) Pt/C ADT; c) Pt/C particle size distributions; d) $50TiO_2$ initial; e) $50TiO_2$ ADT; f) $50TiO_2$ particle size distributions. Mean diameters are provided next to particle size distributions.

Table 2.2: Statistical data for the comparison of Pt/C ADT and 50TiO_2 ADT particle size distributions.

	Pt/C ADT	**50TiO_2 ADT**
Mean (nm)	8.3	6.7
Variance (nm)	21.5	14.9
$\alpha < 0.05$ (t-test on means)	yes	

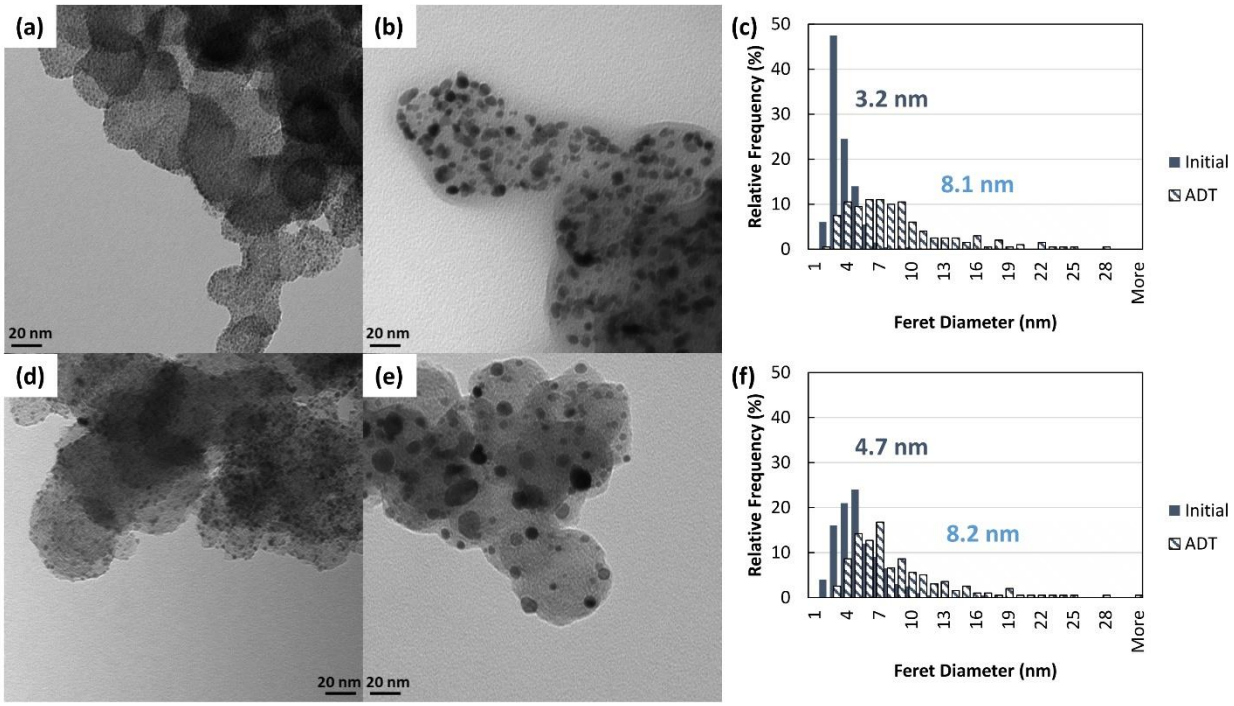

Figure 2.10: TEM images over durability testing a) f10TiO_2 initial; b) f10TiO_2 ADT; c) f10TiO_2 particle size distributions; d) 700°C-f10TiO_2 initial; e) 700°C-f10TiO_2 ADT; f) 700°C-f10TiO_2 particle size distributions. Mean diameters are provided next to particle size distributions.

Table 2.3: Statistical data for the comparison of f10TiO_2 ADT and 700°C-f10TiO_2 ADT particle size distributions.

	f10TiO_2 ADT	**700°C-f10TiO_2 ADT**
Mean (nm)	8.1	8.2
Variance (nm)	23.1	24.6
$\alpha < 0.05$ (t-test on means)	no	

Bright field TEM images were taken before and after electrochemical durability testing and used to calculate particle size distributions, which are shown in Figure 2.9 and Figure 2.10. Statistical data of the particle size distributions are provided in Table 2.2 and Table 2.3. These images showed obvious Pt nanoparticle coarsening over the durability test for all catalysts examined. However, analysis of variance (t-test assuming unequal variance) on the ADT particle size distributions for Pt/C and 50TiO_2 showed that the 50TiO_2 ADT mean diameter of 6.7 nm was significantly smaller than that of Pt/C, thereby indicating that the addition of 50 cycles of TiO_2 ALD did mitigate Pt agglomeration on this catalyst substrate. The f10TiO_2 catalyst in Figure 2.10 exhibited the greatest start-to-finish degree of coarsening, likely due to its small initial Pt nanoparticles, which would have been more prone to agglomeration. In the case of this catalyst, the efficacy of the TiO_2 ALD blocking structures in retention of mass activity over potential cycling observed in Figure 2.8 did not translate to improved Pt nanoparticle size retention. The hybrid Pt-Ti structures in 700°C-f10TiO_2 appeared to also agglomerate significantly, presenting an ADT mean diameter that was statistically indistinguishable from unprotected Pt/C. The poor particle size retention of these catalysts was consistent with their observed retention of only 27% of their initial mass activity.

It is not immediately apparent why the 700°C, 20% H_2 treatment decreased the durability to such a great extent, given that many similar Pt-Ti catalysts [25-27] have been shown to exhibit superior durability along with their enhanced ORR activity. The intermediate particle growth of the ALD Pt/f-C catalyst (distinctly smaller than 700°C-f10TiO_2; Figure 2S.6) suggests that the intermixing of Pt and Ti during annealing, in addition to improving the activity, also created a catalyst that is even more prone to particle coarsening than its unprotected starting material. Given that the individual weighted surface energies of Ti and Pt are 2.00 and 1.59 J/m^2, respectively [29],

one would expect that any combination of these species would result in an amalgam with higher surface energy, and, consequently, higher driving force for particle growth, than pure Pt. Indeed, early work with Pt-Ti alloys demonstrated that these materials, particularly at smaller particle sizes, may be more prone to dissolution under fuel cell operating conditions than conventional Pt/C catalysts [22]. Though more work is required to assess the activity and durability contributions of other surface changes, such as the elimination of carbon support functional groups and exposure of more active Pt facets during the 700°C treatment, it is clear that many of the properties that contributed to the high initial activity of 700°C-f10TiO_2 also had detrimental effects on the catalyst's electrochemical durability.

2.5. Conclusions

Atomic layer deposition of TiO_2 was used to modify commercial Pt/C catalysts and ALD-synthesized Pt catalysts on functionalized carbon black to improve ORR durability and protect catalytic Pt from agglomeration. Growth of TiO_2 was drastically enhanced on the functionalized substrate, leading to coverage of the Pt sites at high ALD cycles; however, 10 cycles of TiO_2 ALD on the functionalized substrate yielded a catalyst with dispersed, locally homogenous TiO_2 structures surrounding its small Pt nanoparticles that demonstrated catalytic activity on par with uncoated commercial Pt/C. Thermal treatment in air up to 200°C demonstrated that this activity increase was due to H_2O oxidation of residual ligands from the functionalized catalyst's Pt ALD fabrication. After thermal treatment up to 700°C in 20% H_2, ALD-deposited TiO_2 was observed to migrate onto Pt sites, likely forming Pt-Ti nanoparticles, which nearly doubled catalyst activity. Unfortunately, this surface rearrangement had detrimental effects on electrochemical durability, with the Pt-Ti catalyst retaining only 27% of its initial mass activity and displaying severe particle agglomeration in initial-ADT TEM comparisons. In contrast, the untreated 50TiO_2 and f10TiO_2

catalysts both had a mass activity retentions of over 60% and, in the case of 50TiO_2, did not agglomerate to as great an extent, thus demonstrating the benefits of TiO_2 ALD for Pt stabilization. Although ALD has many innate benefits over wet chemistry synthesis, further research is required to address challenges of using this method to increase both durability and activity of carbon black-based Pt catalysts.

2.6. Supplemental Information

This section contains figures with additional information.

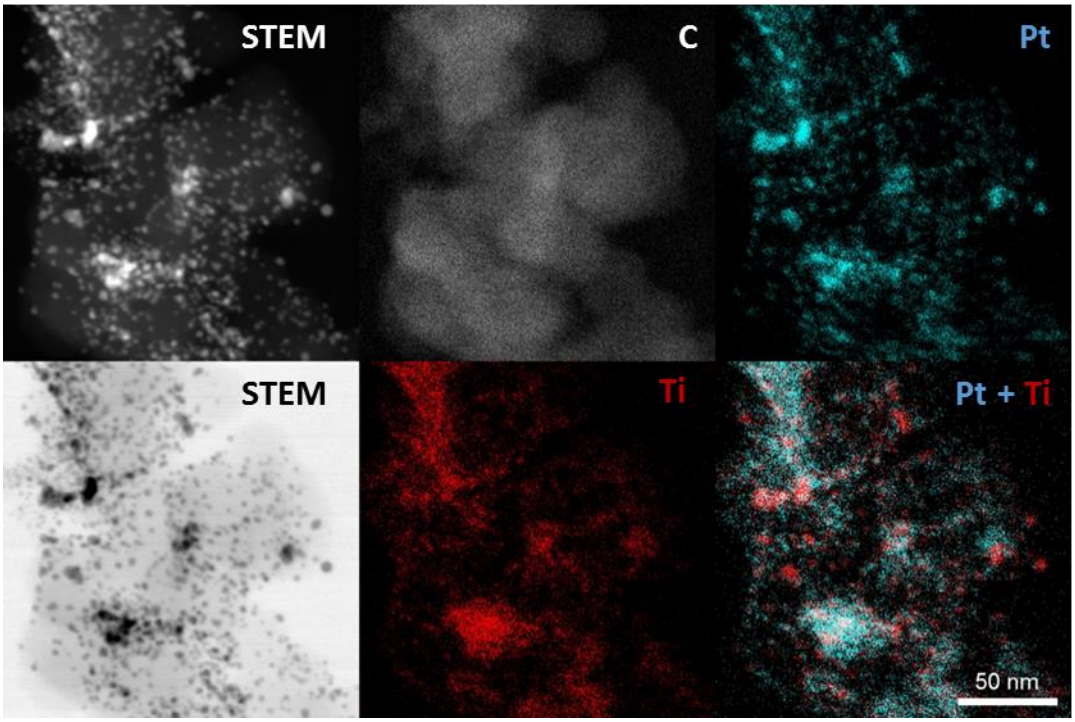

Figure 2S.1: High-magnification STEM + EDS images of 50 cycles TiO_2 ALD on Pt/C (50TiO_2) as-made.

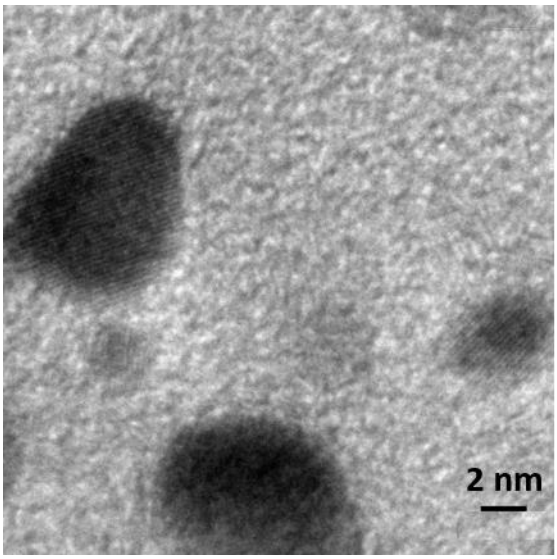

Figure 2S.2: High-resolution TEM of 700°C-f10TiO_2 nanoparticles showing crystalline lattice structure.

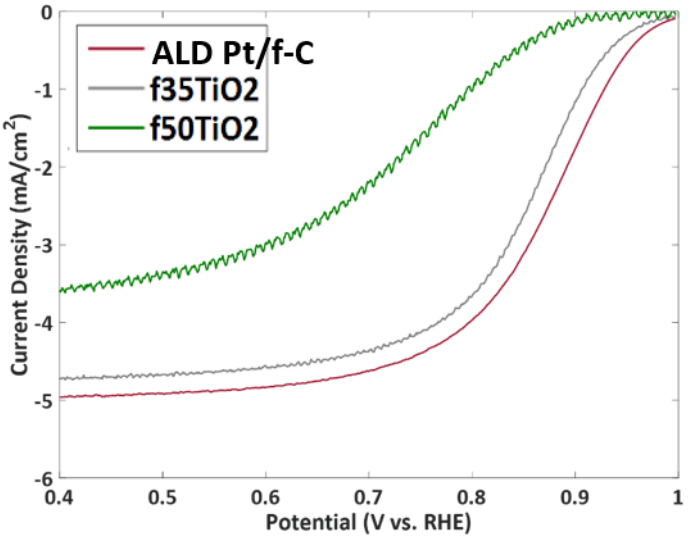

Figure 2S.3: Polarization curves of f35TiO_2 and f50TiO_2 against ALD Pt/f-C, illustrating significant mass transfer losses at high TiO_2 loadings.

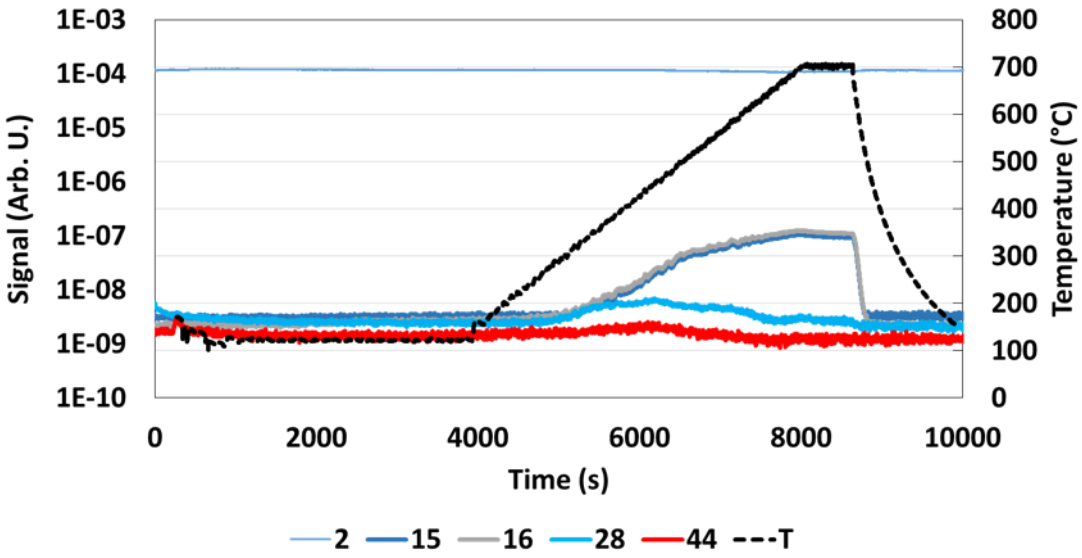

Figure 2S.4: Temperature-programmed reduction of ALD Pt/f-C catalyst showing CH_4 (m/z = 15,16) hydrogenation byproduct of ALD ligands being produced at temperatures >300°C. This indicates that the H_2 dose during Pt ALD synthesis of ALD Pt/f-C did not completely remove the ligands.

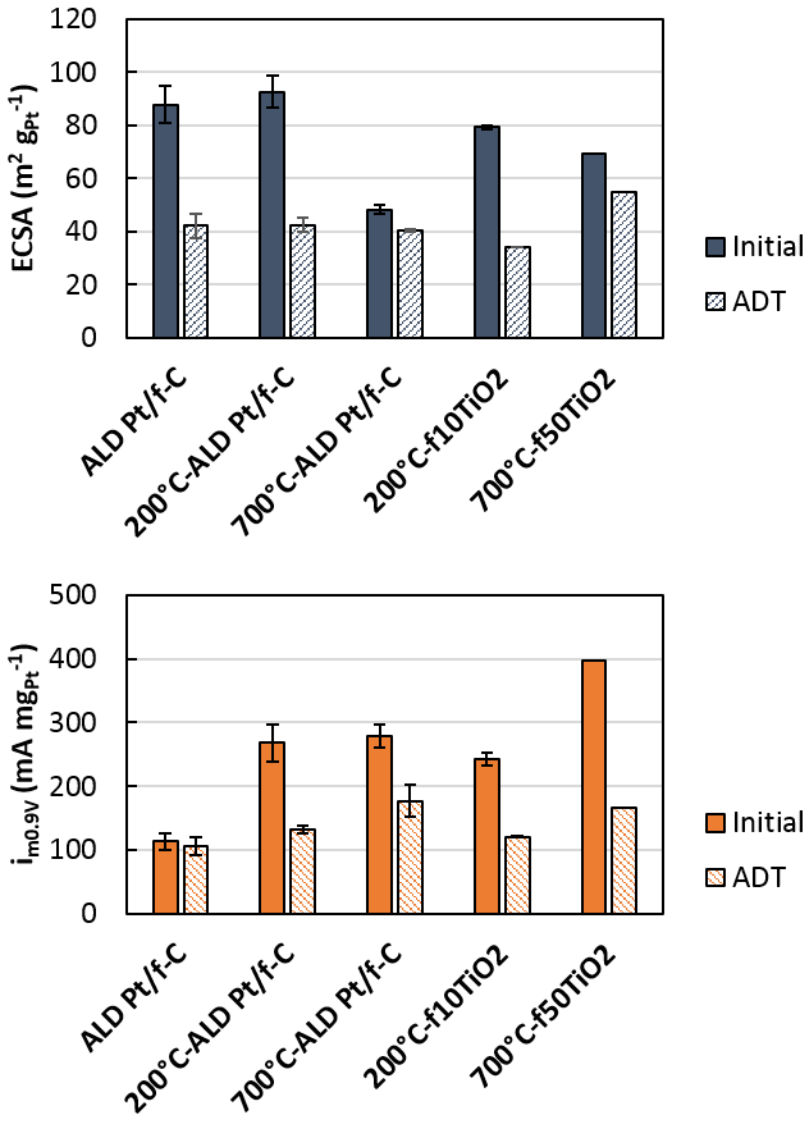

Figure 2S.5: ECSA and mass activity of various catalysts based on ALD Pt/f-C initially and after durability testing. The high mass activity retention of ALD Pt/f-C itself is an artifact of its carbonaceous residual ALD ligands—the site blocking effects reduce initial activity, and removal of those ligands by cycling > 1.0V creates the appearance of an ADT catalyst with high activity retention.

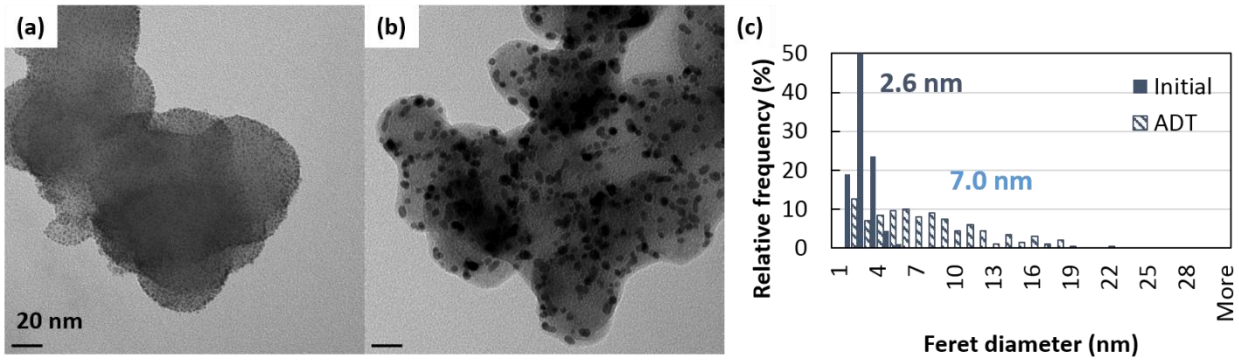

Figure 2S.6: Bright field TEM of ALD Pt/f-C catalyst a) before and b) after durability testing, with c) corresponding particle size distributions.

2.7. References

1. Takenaka, S.M., H.; Nakagawa, K.; Matsune, H.; Tanabe, E.; Kishida, M., *Improvement in the Durability of Pt Electrocatalysts by Coverage with Silica Layers.* Journal of Physical Chemistry C Letters, 2007. **111**: p. 15133-15136.

2. Takenaka, S., et al., *High Durability of Carbon Nanotube-Supported Pt Electrocatalysts Covered with Silica Layers for the Cathode in a PEMFC.* Journal of The Electrochemical Society, 2008. **155**(9): p. B929-B936.

3. Kocha, S.S., *Electrochemical Degradation: Electrocatalyst and Support Durability*, in *Polymer Electrolyte Fuel Cell Degradation*, M.M. Mench, E.C. Kumbur, and T.N. Veziroglu, Editors. 2012, Elsevier: Waltham, MA.

4. Lu, J., J.W. Elam, and P.C. Stair, *Atomic layer deposition—Sequential self-limiting surface reactions for advanced catalyst "bottom-up" synthesis.* Surface Science Reports, 2016. **71**(2): p. 410-472.

5. Feng, H., et al., *Alumina Over-coating on Pd Nanoparticle Catalysts by Atomic Layer Deposition: Enhanced Stability and Reactivity.* Catalysis Letters, 2011. **141**(4): p. 512-517.

6. Liang, X., et al., *Stabilization of Supported Metal Nanoparticles Using an Ultrathin Porous Shell.* ACS Catalysis, 2011. **1**(10): p. 1162-1165.

7. Gould, T.D., et al., *Stabilizing Ni Catalysts by Molecular Layer Deposition for Harsh, Dry Reforming Conditions.* ACS Catalysis, 2014. **4**(8): p. 2714-2717.

8. Lu, J., et al., *Coking- and Sintering-Resistant Palladium Catalysts Achieved Through Atomic Layer Deposition.* Science, 2012. **335**(6073): p. 1205-1208.

9. Cheng, N., et al., *Extremely stable platinum nanoparticles encapsulated in a zirconia nanocage by area-selective atomic layer deposition for the oxygen reduction reaction.* Advanced Materials, 2015. **27**(2): p. 277-281.

10. Marichy, C., et al., *ALD SnO2 protective decoration enhances the durability of a Pt based electrocatalyst.* Journal of Materials Chemistry A, 2016. **4**(3): p. 969-975.

11. Wang, Y.J., D.P. Wilkinson, and J. Zhang, *Noncarbon support materials for polymer electrolyte membrane fuel cell electrocatalysts.* Chemical Reviews, 2011. **111**(12): p. 7625-7651.

12. Cheng, K., et al., *Three-Dimensionally Costabilized Metal Catalysts toward an Oxygen Reduction Reaction.* Langmuir, 2016. **32**(9): p. 2236-2244.

13. Dhanasekaran, P., S. Vinod Selvaganesh, and S.D. Bhat, *Nitrogen and carbon doped titanium oxide as an alternative and durable electrocatalyst support in polymer electrolyte fuel cells.* Journal of Power Sources, 2016. **304**: p. 360-372.

14. Chung, S., et al., *Atomic layer deposition of ultrathin layered TiO2 on Pt/C cathode catalyst for extended durability in polymer electrolyte fuel cells.* Journal of Energy Chemistry, 2016. **25**(2): p. 258-264.

15. Lubers, A.M., et al., *Mechanistic studies for depositing highly dispersed Pt nanoparticles on carbon by use of trimethyl(methylcyclopentadienyl)platinum(IV) reactions with O2 and H2.* Journal of Nanoparticle Research, 2015. **17**(4): p. 179.

16. Lubers, A.M., et al., *Proton Exchange Membrane Fuel Cell Flooding Caused by Residual Functional Groups after Platinum Atomic Layer Deposition.* Electrochimica Acta, 2017. **237**: p. 192-198.

17. King, D.M., et al., *Atomic layer deposition of TiO2 films on particles in a fluidized bed reactor.* Powder Technology, 2008. **183**(3): p. 356-363.

18. King, D.M., et al., *Atomic layer deposition on particles using a fluidized bed reactor with in situ mass spectrometry.* Surface and Coatings Technology, 2007. **201**(22-23): p. 9163-9171.

19. Shinozaki, K., et al., *Oxygen Reduction Reaction Measurements on Platinum Electrocatalysts Utilizing Rotating Disk Electrode Technique.* Journal of The Electrochemical Society, 2015. **162**(10): p. F1144-F1158.

20. Garsany, Y., et al., *Experimental Methods for Quantifying the Activity of Platinum Electrocatalysts for the Oxygen Reduction Reaction.* Analytical Chemistry, 2010. **82**: p. 6321-6328.

21. Huong Nguyen, T.G., et al., *Nano-Pt/C electrocatalysts: synthesis and activity for alcohol oxidation.* Advances in Natural Sciences: Nanoscience and Nanotechnology, 2013. **4**(3): p. 035008.

22. Beard, B.C. and P.N. Ross, *Characterization of a Titanium-Promoted Supported Platinum Electrocatalyst.* Journal of The Electrochemical Society, 1986. **133**(9): p. 1839-1845.

23. Kawasoe, Y., et al., *Preparation and Electrochemical Activities of Pt–Ti Alloy PEFC Electrocatalysts.* Journal of The Electrochemical Society, 2007. **154**(9): p. B969-B975.

24. Ding, E., K.L. More, and T. He, *Preparation and characterization of carbon-supported PtTi alloy electrocatalysts.* Journal of Power Sources, 2008. **175**(2): p. 794-799.

25. Duan, H., Q. Hao, and C. Xu, *Hierarchical nanoporous PtTi alloy as highly active and durable electrocatalyst toward oxygen reduction reaction.* Journal of Power Sources, 2015. **280**: p. 483-490.

26. Kim, J., S. Yang, and H. Lee, *Platinum–titanium intermetallic nanoparticle catalysts for oxygen reduction reaction with enhanced activity and durability.* Electrochemistry Communications, 2016. **66**: p. 66-70.

27. Park, H.-Y., et al., *Carbon-Supported Ordered Pt-Ti Alloy Nanoparticles as Durable Oxygen Reduction Reaction Electrocatalyst for Polymer Electrolyte Membrane Fuel Cells.* Journal of Electrochemical Science and Technology, 2016. **7**(4): p. 269-276.

28. Li, J., et al., *Highly dispersed Pt nanoparticle catalyst prepared by atomic layer deposition.* Applied Catalysis B: Environmental, 2010. **97**(1-2): p. 220-226.

29. Tran, R., et al., *Surface energies of elemental crystals.* Scientific Data, 2016. **3**: p. 160080.

CHAPTER 3

TUNGSTEN NITRIDE ALD FOR STABILIZATION OF PT/C CATALYSTS

3.1. Abstract

Atomic layer deposition (ALD) of tungsten nitride was used to enhance the durability and activity of a carbon-supported Pt nanoparticle oxygen reduction reaction (ORR) catalyst by adding protective WN nanostructures to the surface. A post-synthesis thermal treatment sequence of low-temperature oxidation followed by high-temperature reduction was also performed on the ALD-modified catalyst. The effects the ALD process and thermal treatment on the structure and electrochemical properties of the catalyst were examined through a variety of techniques. Characterization through ICP-MS, STEM and EDS mapping, and X-ray diffraction showed that the ALD process deposited WN homogenously across the surface. Thermal treatment resulted in reduced amount of nitride on the surface and produced separate Pt and W domains. The electrochemical performance of the catalysts was measured through rotating disk electrode (RDE) voltammetry. The thermally-treated ALD catalyst was observed to have a high mass activity towards the ORR (465 mA mg_{Pt}^{-1}), surpassing benchmark Pt/C (277 mA mg_{Pt}^{-1}), and demonstrated superior retention of electrochemical properties after an accelerated durability test. Analysis of particle size distributions before and after durability testing also indicated that the mechanical stability of the Pt nanoparticles was enhanced in the thermally-treated ALD catalyst compared to the uncoated materials.

3.2. Introduction

The development of sufficiently active, durable, and cost-effective catalysts for the cathodic ORR is a major bottleneck in the commercialization of polymer electrolyte membrane

fuel cells (PEMFCs) [1]. Conventional carbon-supported Pt nanoparticle catalysts (Pt/C) can provide high surface areas and moderate activities; however, these materials are prone to performance degradation during fuel cell operation through Pt crystallite migration, electrochemical Ostwald ripening, and carbon support corrosion [2, 3]. As these degradation pathways are promoted by voltage perturbations induced during vehicle operation and the acidic environment of the PEMFC, it is essential to develop durable catalysts that can withstand these harsh operating conditions.

One promising approach to increasing the durability of Pt/C ORR catalysts is the stabilization of Pt nanoparticles through the addition of blocking structures, which are typically comprised of acid-stable metal oxides that mitigate Pt migration and agglomeration. These may be integrated during wet chemistry synthesis of catalyst [4-7] or added to the support material by ALD in a post-synthesis step. ALD is a self-limiting vapor-phase process that offers atom-level control over the growth of metal oxide films or metal nanoparticles by varying the number of surface reaction steps, or "cycles"[8]. Protective layers deposited onto metal nanoparticle catalysts for high-temperature reactions via ALD have been shown to preserve activity and prevent thermally-induced sintering and loss of active surface area [9-12]. Recently, the addition of ALD metal oxide nanostructures, such as ZrO_2 [13], SnO_2 [14], and TiO_2 [15], onto Pt/C ORR catalysts has shown great promise in improving retention of electrochemical surface area (ECSA), activity, and Pt nanoparticle size retention over electrochemical durability testing. In addition to increased durability, the proximity of these ALD blocking structures to the Pt may also enhance activity through beneficial metal support interactions [6, 13] or alloying effects after subsequent thermal treatment [16]. Tungsten nitride (WN) has been previously investigated as both an ORR co-catalyst and support material with promising results, [17, 18] but does not appear to have been

investigated as an ALD blocking agent for Pt/C. The corrosion resistance of WN under acidic and oxidizing conditions, along with its potential synergistic effects on Pt catalyst activity make it an attractive candidate for stabilization of Pt-based ORR catalysts.

This work reports the modification of a catalyst synthesized in-house through Pt-H_2 ALD on a functionalized carbon black substrate (ALD Pt/f-C) with WN nanostructures. To our knowledge, this is the first report of this particular ALD chemistry being applied to any type of Pt/C ORR catalyst. The ALD Pt/f-C catalyst was selected for this study because of the high amount of O-containing groups available on the functionalized carbon, which facilitate enhanced ALD growth rates over an unmodified carbon substrate. Ten cycles of WN ALD were applied to the Pt/f-C catalyst, and this material was subsequently treated with a 200°C oxidation to remove residual Pt-H_2 ALD ligands, followed by a 725°C anneal in 20% H_2 to reduce deposited WN to metallic W. This application of 10 WN ALD cycles was modeled after the TiO_2 ALD process discussed in Chapter 2, in which 10 cycles were found to be the optimum level to provide some protective benefits to the ALD Pt/f-C without allowing extreme coverage of Pt sites, as seen at higher cycle numbers. As-prepared catalysts were examined through elemental analysis, X-ray diffraction, and electron microscopy and the effects of WN ALD and thermal treatment on electrochemical activity and durability were characterized using RDE techniques.

3.3. Experimental

3.3.1. Catalyst Synthesis

WN ALD structures were added to the ALD Pt/f-C catalyst using bis(*tert*-butylimido)bis(dimethylamido)tungsten ((^{t}BuN)$_2$(Me$_2$N)$_2$W; Strem) and ammonia (Sigma-Aldrich) as alternating reagents in a fluidized bed reactor. In a single ALD cycle, the

(^{t}BuN)$_2$(Me$_2$N)$_2$W dose was held for 13 minutes, and the NH_3 was held for 20 minutes. Gases were purged between half-cycles with UHP N_2. The reactor and reactant bubbler were held at 300°C and 40°C, respectively. This WN ALD process was adapted from previous studies on flat substrates, [19, 20] as it has never been attempted in a fluidized bed setup. An in-line mass spectrometer (Stanford Research Systems) was used to monitor gases exiting the reactor. Ten ALD cycles were deposited to produce catalyst f10WN. The f10WN catalyst was subjected to a 200°C oxidation in air for 3 hours, followed by a 725°C anneal in 20% H_2 with balance Ar for 3 hours to produce material 725°C-f10WN for further analysis.

3.3.2. Analytical Characterization

The ALD Pt/f-C and f10WN catalysts were analyzed for Pt and W content using inductively coupled plasma mass spectroscopy (ICP-MS) after digestion in an aqua regia/HF mixture. Bright field microscopy images of catalysts before and after electrochemical durability testing were acquired by depositing catalyst powder on carbon film 200 mesh copper grids (Electron Microscopy Sciences) and examining under a TEM (FEI Tecnai T12 Spirit). Particle size distributions were tabulated from these images using ImageJ, in which Feret diameters were calculated from a total of 200 Pt nanoparticles taken from 3 separate areas of the catalyst. Feret diameters initially and after durability testing were compared using a t-test assuming unequal variance. Dark field and bright field microscopy and energy dispersive X-ray spectroscopy (EDS) mapping were performed on as-synthesized catalysts by depositing catalyst powder on carbon film 200 mesh copper grids (Ted Pella) using a transmission electron microscope (TEM) operated at 200kV in scanning mode (FEI Talos F200X). Powder x-ray diffraction (XRD) measurements were collected using a Bruker D2 Phaser with a Cu source operating at 300 W and a Lynxeye 1D detector.

3.3.3. Electrochemical Characterization

Catalyst powders were made into ink dispersions with ultrapure water, isopropyl alcohol (Sigma-Aldrich), and 5% Nafion ionomer (Sigma-Aldrich). After a 1 hour sonication, a 10 μL aliquot of ink was drop-coated onto a glassy carbon electrode and rotated at 700 rpm in an inverted position on a RDE test stand (Pine). After drying, the working electrode was submerged in an aqueous electrochemical cell with a Pt coil counter electrode and regular hydrogen electrode (RHE) reference. Data acquisition procedures followed those established by Shinozaki, et al [21]. Following a 100 cycle break-in (0.025 to 1.2 V at 500 mV s^{-1}), cyclic voltammograms (CVs) were taken from 0.025 to 1.0 V at 10 mV s^{-1} in an N_2-purged cell with no rotation. The calculated hydrogen under potential deposition (H_{UPD}) charge from 0.06 to 0.4 V was used to calculate the ECSA. Polarization curves were taken from 1.0 to -0.01 V at 20 mV s^{-1} in an O_2-purged cell at 1600 rpm and the anodic scan was used for analysis. Background curves were taken with the same parameters under N_2 and used to correct the polarization curves. Mass activities were calculated using the current at 0.9 V. ECSA and mass activity were calculated initially and after an accelerated durability test (ADT) of 5,000 voltage cycles from 0.6 to 1.2 V at 100 mV s^{-1} adapted from [14].

3.4. Results and Discussion

3.4.1. WN ALD on ALD Pt/f-C

A representative mass spectrometry trace during a single WN ALD cycle is shown in Figure 3.1. The emergence of signals corresponding to the $(^tBuN)_2(Me_2N)_2W$ fragments shown at ~25 minutes was indicative of saturation of the available surface sites; therefore, the metal precursor dose was ended with the appearance of these fragments. The NH_3 dose shown at ~65 minutes was marked by a rapid rise in the same fragments due to ligand composition (as detailed

in [20]), and the dose was held for 20 minutes. Elemental analysis with ICP-MS of the original and post-ALD catalysts (Table 3.1) showed the addition of 6.33 wt% W after 10 ALD cycles.

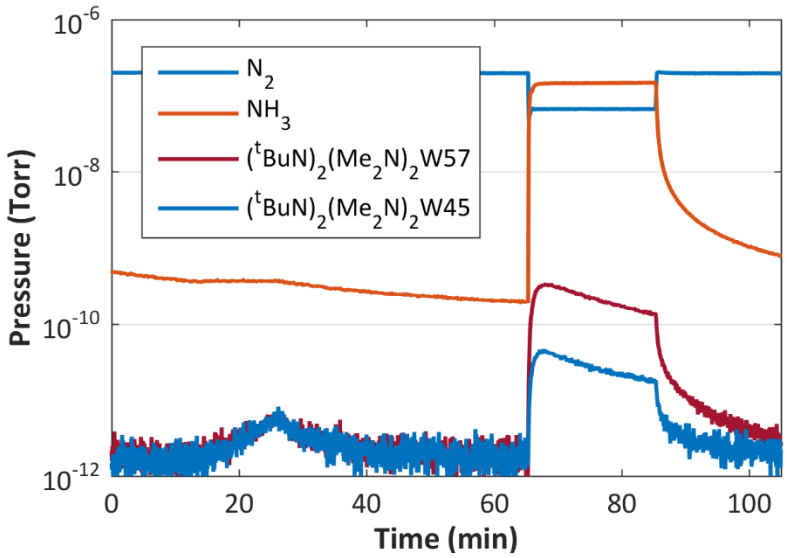

Figure 3.1: Time-resolved mass spectrometry traces of m/z = 28 (N_2), 17 (NH_3), 45, and 57 ($(^tBuN)_2(Me_2N)_2W$ fragments) during one WN ALD cycle.

Table 3.1: Elemental content of ALD Pt/f-C and f10WN catalysts as determined by ICP-MS.

	Pt wt%	**W wt%**
ALD Pt/f-C	19.8	--
f10WN	16.0	6.33

3.4.1.1. Physical Characterization

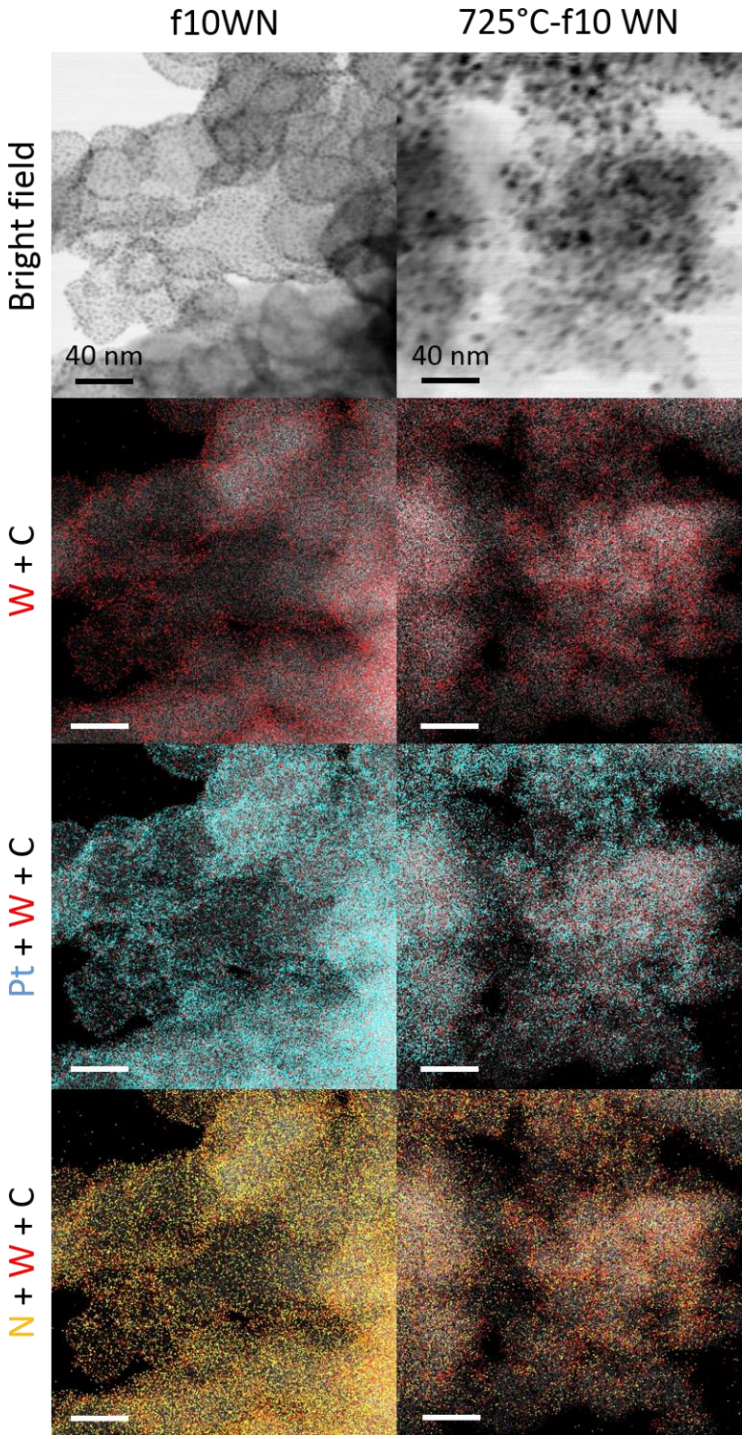

Figure 3.2: Bright field STEM images and corresponding EDS overlays of elemental maps showing the distribution of Pt, C, W, and N in 10WN and 725°C-10WN samples.

Table 3.2: EDS quantification of W, Pt, N, and C on a mass basis.

	W wt%	**Pt wt%**	**N wt%**	**C wt%**
f10WN	3.39	17.7	0.78	75.9
725°C-f10WN	8.02	17.8	0.35	70.8

Table 3.3: EDS quantification of W, Pt, N, and C on an atomic basis.

	W at%	**Pt at%**	**N at%**	**C at%**
f10WN	0.25	1.83	0.84	95.01
725°C-f10WN	0.73	1.68	0.39	95.83

Figure 3.2 shows STEM images and corresponding EDS maps for f10WN and 725°C-f10WN. EDS quantification values are listed in Table 3.2 and Table 3.3. Additional images and EDS maps for f10WN, 200°C-f10WN (the intermediate stage of thermal treatment), and 725°C-f10WN are provided in Figure 3S.1-Figure 3S.4. Analysis of the f10WN EDS maps showed the homogeneous presence of Pt, W, and N across the surface. The ALD Pt/f-C surface was initially covered in dispersed 2-3 nm Pt nanoparticles; the significant overlap between W and Pt in f10WN showed that during the ALD process WN was deposited evenly throughout the Pt nanoparticles. The further overlap between N and W confirmed the presence of a nitride. On an atomic basis, the stoichiometry of this species was approximately WN_3, which contains more nitrogen than is typical for the standard tungsten nitride configurations. It is possible that excess N was physisorbed to the carbon support during the NH_3 dose during ALD and was detected through EDS. The functionalized carbon substrate of ALD Pt/f-C has previously been demonstrated to facilitate TiO_2 ALD surface reactions (as seen in Chapter 2), as it provides O-terminated sites for nucleation and growth. It appears that the f-C carbon substrate was similarly active towards the WN ALD process performed here.

Thermal treatment at 725°C under 20% H_2/Ar induced a number of structural changes in the catalyst. Coarsening of the Pt nanoparticles following thermal treatment was apparent in the bright field images of 725°C-f10WN and corresponding Pt maps. Interestingly, it appeared that W was also slightly agglomerated during thermal treatment, but not to the same extent as Pt. The W map of 725°C-f10WN still showed dispersed W across the surface, though its presence was reduced at the edges of the carbon particles. The combined overlay of Pt and W showed distinct W-rich areas (shown in red) present between the Pt clusters (shown in blue) and less correlation between the positions of Pt and W after thermal treatment than before. These results indicate that the Pt and W species remained in mostly separate phases in the 725°C-f10WN catalyst and the thermal treatment likely did not produce alloy or intermetallic nanoparticles, as has often been observed with other Pt-W nanoparticle catalysts synthesized by colloidal or galvanic replacement methods [22, 23]. A significant decrease in the presence of N across the surface can be observed from 10 WN to 725°C-f10WN in the N+W maps in Figure 3.2; this is also reflected by the decrease in N wt% in Table 3.2 between the two catalysts. The W:N wt% ratio of f10WN was changed from 4 to almost 23 after thermal treatment, which indicated that the partial hydrogen atmosphere of the thermal treatment significantly changed the stoichiometry of the WN nanostructures to be more W-rich. On an atomic basis (Table 3.3), the stoichiometry of 725°C-f10WN appears to be closer to W_2N. This thermal treatment process created a catalyst surface with more metallic character but did not completely eliminate the presence of N.

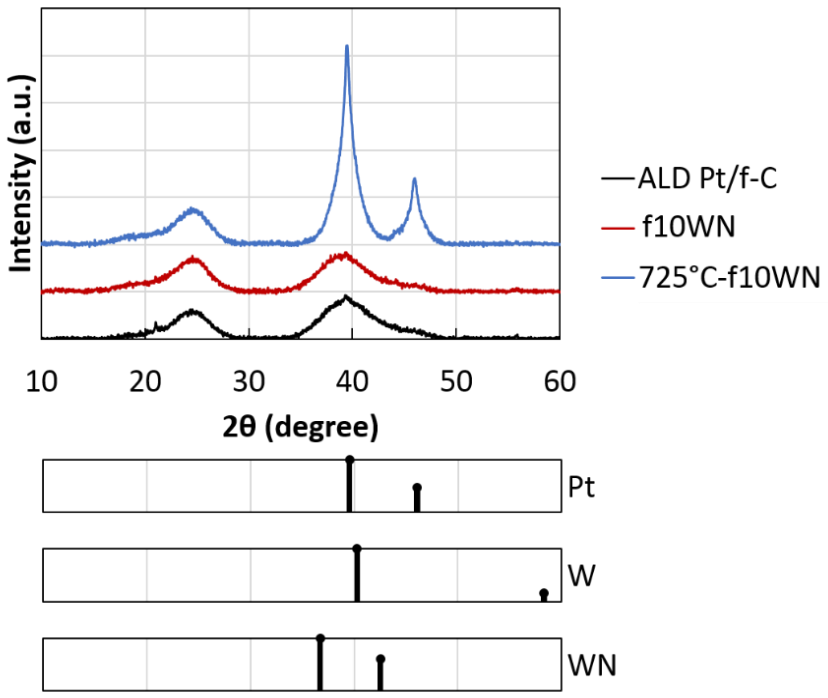

Figure 3.3: XRD patterns of all catalysts. Normalized XRD patterns for Pt, W, and WN are shown below the data.

All catalysts were probed with X-ray diffraction, and the results are shown in Figure 3.3, alongside normalized XRD patterns for Pt, W, and WN [24, 25]. The XRD pattern for ALD Pt/f-C catalyst showed broad Pt peaks around 39° and 46°, with a broad amorphous carbon peak near 25°. Addition of 10 WN ALD cycles did not result in any discernable changes in the f10WN pattern. Though the presence of WN in this catalyst was previously confirmed through ICP-MS and STEM-EDS, it is possible that the quantity of WN on the surface was not large enough to produce a distinct reflection during the XRD analysis. Additionally, thermal ALD processes, such as the one followed here, are known to deposit amorphous materials; thus, the WN present in the f10WN catalyst is likely not crystalline and would not be expected to produce clearly-defined XRD peaks. Application of thermal treatment greatly increased the sharpness and intensity of the Pt peaks in the 725°C-f10WN pattern. This can likely be attributed to the Pt coarsening observed in the bright field images in Figure 3.2. Also noteworthy is the relatively unchanged position of the

Pt peak at 39° after thermal treatment. This indicates that the Pt lattice was not detectably compressed by the surrounding W on the surface, which supports the assertion that Pt and W remain primarily in separate phases. The 725°C-f10WN pattern does not show any distinct reflections for W, despite an increased presence of metallic W (as seen in Figure 3.2) and a high likelihood that any W/WN species would exist in a crystalline phase by 725°C. This may be due to insufficient quantities of W for detection through this technique, or the presence of the primary W peak at 40° may be obscured by the larger Pt reflection at 39°.

3.4.2. Electrochemical Characterization

3.4.2.1. Effects of ALD and Thermal Treatment on Catalytic Performance

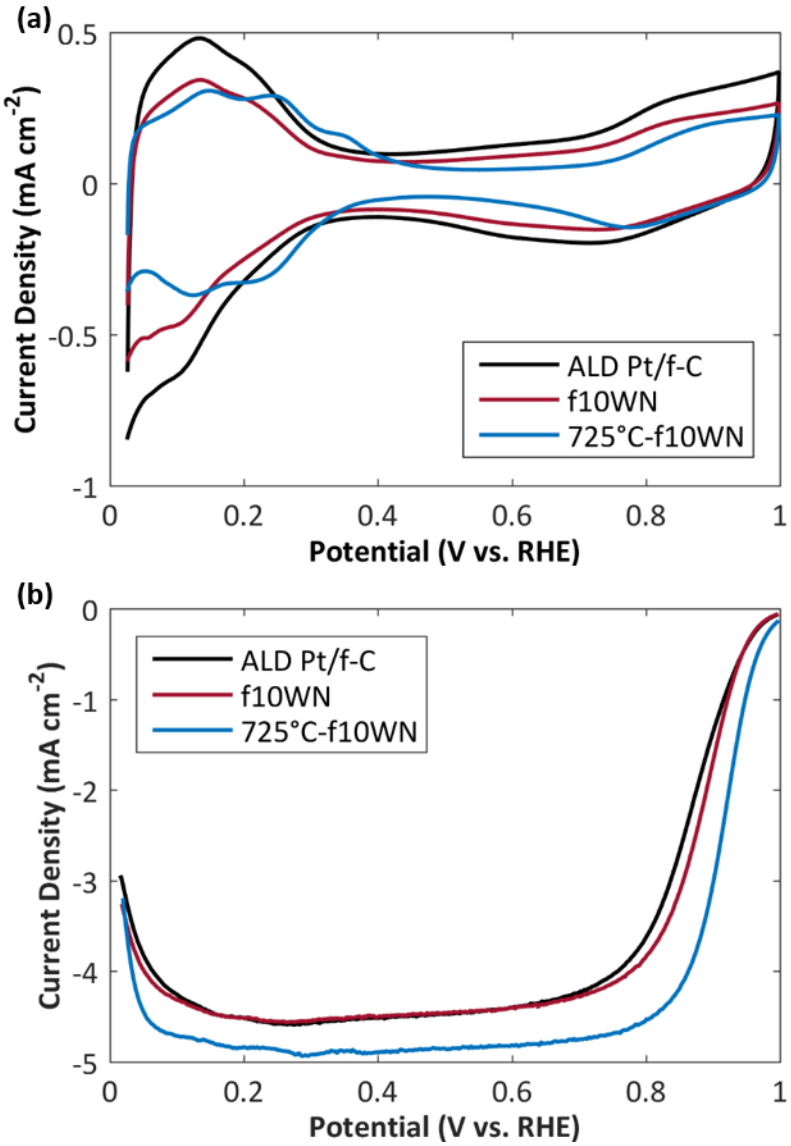

Figure 3.4: Initial cyclic voltammograms (a) and polarization curves (b) for all ALD catalysts.

Electrochemical performance of the catalysts was assessed through RDE voltammetry. Initial CVs and polarization curves for ALD Pt/f-C, f10WN, and 725°C-f10WN are shown in Figure 3.4. An apparent decrease in the magnitude of the Pt H_{UPD} peak was observed for f10WN and 725°C-f10WN in Figure 3.4a. This decrease was likely due to Pt nanoparticle coarsening

during ALD and thermal treatment; however, ECSA values for these catalysts were actually greater than ALD Pt/f-C after accounting for changes in Pt content with the addition of ALD (see Figure 3.5a). The CV for 725°C-f10WN exhibited a sharply-defined peak in the more positive potential region of the H_{UPD} (0.2 – 0.3 V) that was not prominent in the other catalysts. This peak is associated with strongly adsorbed hydrogen species on the Pt(100) surface [26, 27], and its emergence in the CV indicates that thermal treatment and the resultant Pt nanoparticle coarsening exposed more of this particular facet than was present in the initial catalysts. The CV for 725°C-f10WN also showed a positive shift in the oxygen adsorption/desorption peaks relative to the other catalysts, indicating that oxygenated species do not bind as tightly to the 725°C-f10WN catalyst sites. Finally, the 725°C-f10WN catalyst also exhibited the lowest double layer capacitance contribution in its CV, likely due to the elimination of any residual O-containing surface groups on the functionalized carbon substrate during thermal treatment.

The initial polarization curves in Figure 3.4b showed relatively similar ORR performance for ALD Pt/f-C and 10WN, though f10WN was slightly more active due to a more positive half-wave potential. Thermal treatment resulted in a significantly more positive half-wave potential as well as an increased limiting current for the 725°C-f10WN catalyst. A portion of this catalytic enhancement (primarily, the increase in limiting current) can be attributed to the removal of residual Pt-H_2 ALD ligands during the first phase of thermal treatment (200°C oxidation in air), as is shown in Figure 3S.5. This behavior has previously been observed for the ALD Pt/f-C catalyst, as was documented in Chapter 2. However, the majority of the increase in half-wave potential occurred after treatment of the catalyst at 725°C under 20% H_2. This indicates that the catalytic activity was distinctly enhanced by the creation of a W-rich surface surrounding the larger Pt nanoparticles of 725°C-f10WN, as was observed in Figure 3.2. The proximity of the W/WN

species may have induced changes in the catalytic behavior of Pt via a shifting of the metal d-band center that modified the adsorption strength of oxygen-based ORR intermediates. The previously-discussed CV results support the assertion that binding strength of oxygenated species is weakened in 725°C-f10WN. Even though XRD results do not indicate significant Pt lattice strain in 725°C-f10WN, it is possible that a d-band shift was induced through strong electronic ligand effects, which has been previously observed in Pt-W ORR catalysts [22]. There are numerous other reports in the literature detailing the catalytic influence of W-containing species in close proximity to Pt for ORR [18, 28, 29], as well for other reactions, such as toluene hydrogenation [30]. Though the current results clearly document the presence of an ALD-deposited W/WN species in close proximity to Pt and its influence on overall catalytic activity, further investigation into the Pt-W interactions in the thermally-treated catalyst, as well the effects of the residual nitrogen still present on the surface, may provide insight into the mechanism by which ORR performance is enhanced in this system.

3.4.2.2. Effects of ALD and Thermal Treatment on Catalyst Durability

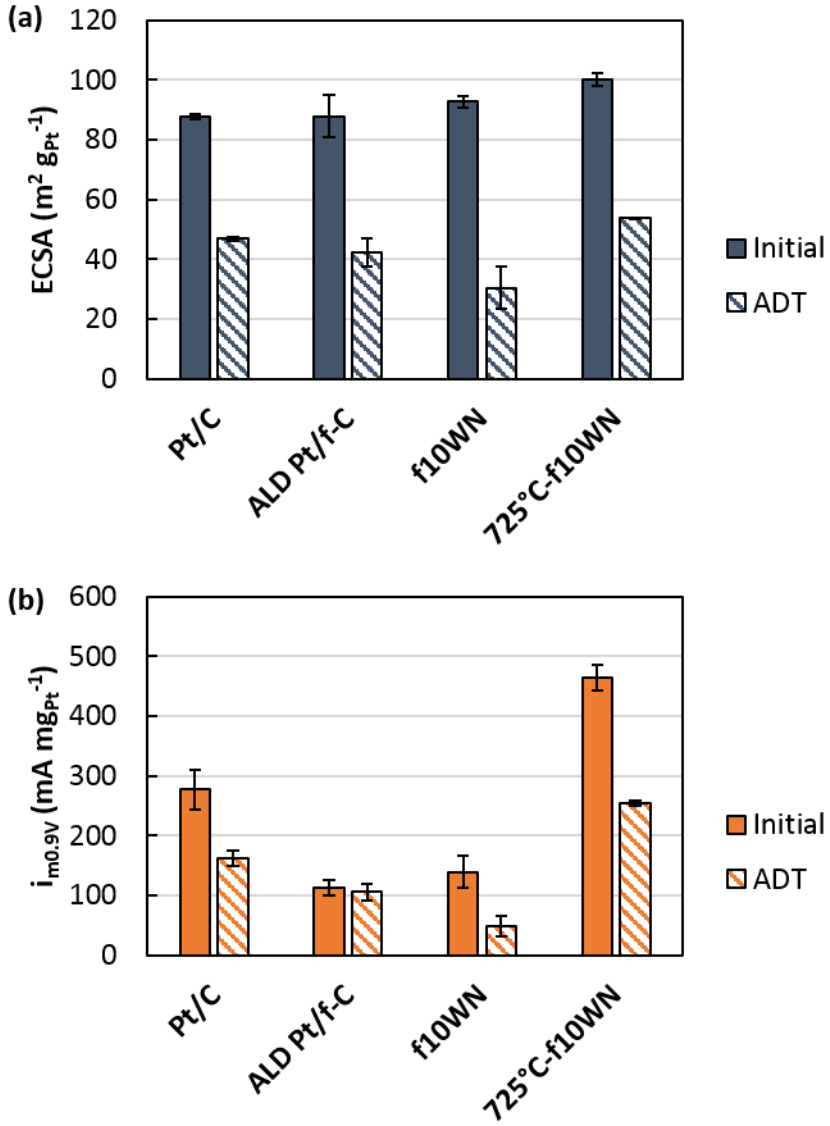

Figure 3.5: Electrochemical surface areas (a) and mass activities (b) of all catalysts initially and after a 5,000 voltage cycle durability test (ADT).

The electrochemical durability of the catalysts was assessed using an accelerated durability test; results of this analysis for ECSA and mass activity are presented in Figure 3.5. The performance of the ALD catalysts was benchmarked against a commercial Pt/C (Premetek P10A200). All catalysts were observed to lose ECSA over voltage cycling, with 725°C-f10WN

proving the most robust. Similarly, 725°C-f10WN had the best performance in mass activity over the durability test, starting with the highest value reported in the current study for any catalyst, 465 mA/mg, and retaining 55% of that over voltage cycling. The initial mass activity of 725°C-f10WN was considerably higher than that of commercial Pt/C, and its ADT value was on par with the initial activity of Pt/C. The enhanced durability of this catalyst is likely due to the stabilization of the Pt nanoparticles by nearby W/WN species on the carbon substrate. At first glance, the ALD Pt/f-C appeared to have superior retention of mass activity as a percentage of its initial value; however, this does not comport with the catalyst's observed ECSA loss. The apparent mass activity retention of ALD Pt/f-C was previously established in Chapter 2 to be an artifact of the residual Pt-H_2 ALD ligands on its surface and is the result of simultaneous oxidation of the ligands (activity increase) and Pt nanoparticle sintering (ECSA/activity decrease) during voltage cycling. Surprisingly, the f10WN catalyst appeared to have the worst retention of ECSA and mass activity, despite the addition of 10 cycles of WN ALD. This indicates that the as-deposited WN was not stable in the acidic environment under voltage cycling (perhaps due to its as-deposited amorphous state), and thermal treatment was necessary to realize any durability benefits from the deposited materials.

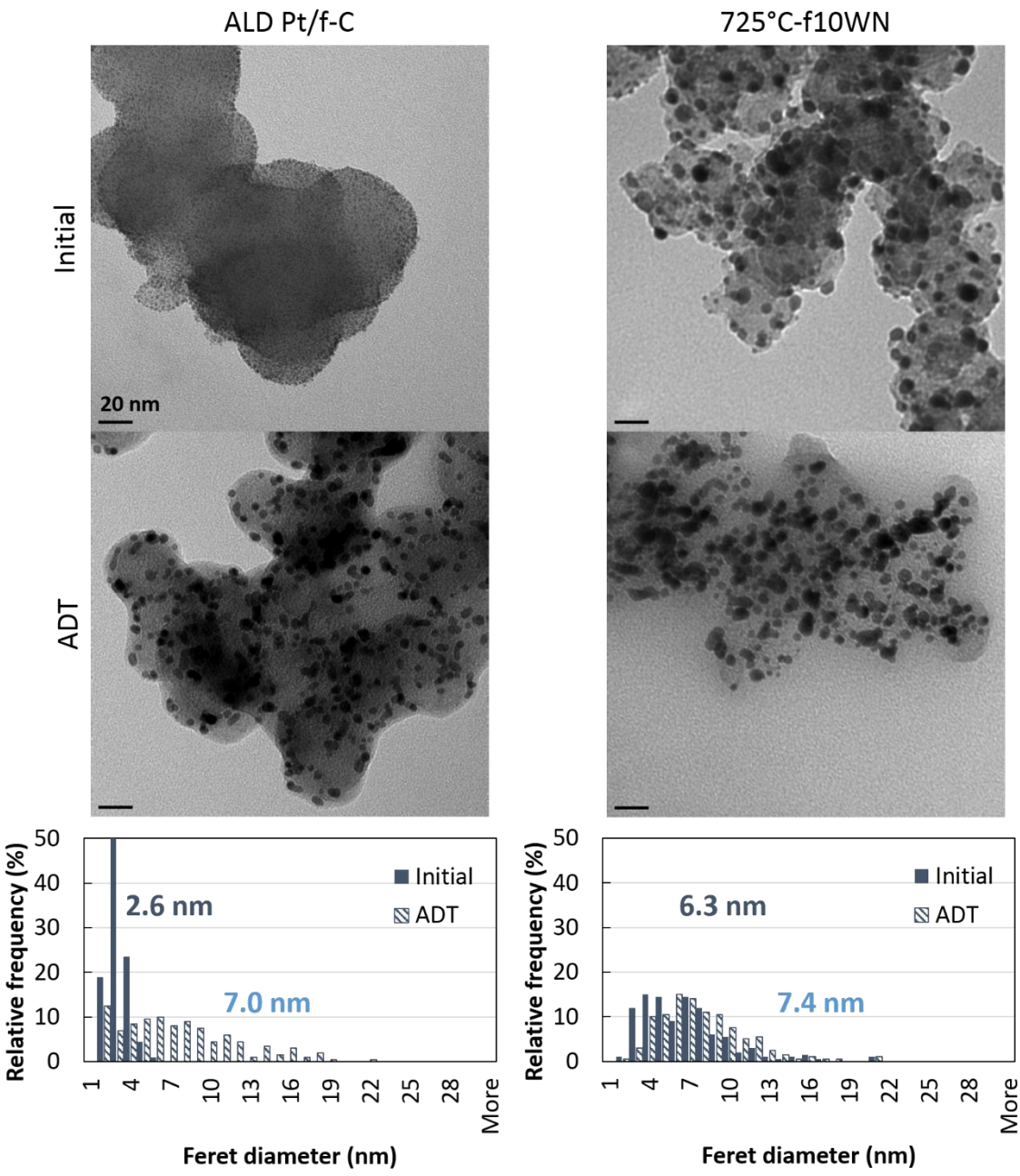

Figure 3.6: TEM images for ALD Pt/f-C and 725°C-f10WN catalysts initially and after durability testing (ADT). Particle size distributions tabulated from multiple images are shown below along with mean initial and ADT nanoparticle diameters.

Table 3.4: Statistical data for ALD Pt/f-C particle size distributions.

	Initial	**ADT**
Mean (nm)	2.6	7.0
Variance (nm)	0.6	19.3
$\alpha < 0.05$ (t-test on means)	yes	

Table 3.5: Statistical data for 725°C-f10WN particle size distributions.

	Initial	**ADT**
Mean (nm)	6.3	7.4
Variance (nm)	10.9	10.4
$\alpha < 0.05$ (t-test on means)	yes	

In order to further analyze the effects of voltage cycling on Pt nanoparticle stability, TEM images of the ALD Pt/f-C and 725°C-f10WN catalysts were analyzed to generate particle size distributions initially and after durability testing. Representative TEM images initially and after durability testing are shown in Figure 3.6, along with particle size distributions for each catalyst. Results of statistical analyses on the initial and ADT particle size distributions are provided in Table 3.4 and Table 3.5. Figure 3.6 shows a significant shift for ALD Pt/f-C from a narrow initial distribution with a mean diameter of 2.6 nm, to a much wider distribution with a mean diameter of 7.0 nm after the durability test. This is reflective of the catalyst's large ECSA loss and is the expected behavior for unprotected Pt nanoparticles over voltage cycling. The initial distribution for 725°C-f10WN in Figure 3.6 has a mean diameter of 6.3 nm, which shows that thermal treatment results in the considerable growth of the Pt nanoparticles from their original size. However, the durability test only resulted in a slight shift in the distribution, producing an ADT

mean diameter of 7.4 nm. This change in the particle size was also statistically significant, but considerably smaller in magnitude than that observed for the unmodified catalyst. Some of this improvement in particle size retention may be attributable to the larger initial mean diameter for 725°C-f10WN, as larger particles do not have as strong of a driving force to minimize surface energy and will be less prone to coalescence. However, comparison to the particle size distributions for commercial Pt/C (as documented in Chapter 2), which had an initial mean diameter of 5.3 nm—much closer to that of 725°C-f10WN, shows that the Pt nanoparticles in 725°C-f10WN were more stable and retained a smaller ADT mean diameter than Pt/C. Taken together, these results provide further evidence of the enhanced stability of the Pt nanoparticles in the 725°C-f10WN catalyst. The most likely source of this enhanced stability was the steric confinement provided by the stable W-rich nanostructures that were shown to reside in close proximity to the Pt nanoparticles on this catalyst. The presence of these structures likely inhibited migration and coalescence of the Pt nanoparticles across the carbon surface over potential cycling, though it did not appear to completely eliminate nanoparticle coarsening. It is possible that other catalyst degradation routes under voltage cycling, such as electrochemical Ostwald ripening and carbon corrosion, remain active in the ALD-modified catalysts due to the relatively low amount of W added after 10 ALD cycles. Taken alongside the electrochemical durability data reported above, these results show that WN ALD and subsequent thermal treatment can be used to greatly enhance the ORR activity and durability of a previously unremarkable Pt/f-C catalyst.

3.4.2.3. Comparison Between Thermally-Treated WN- and TiO_2-based ALD catalysts

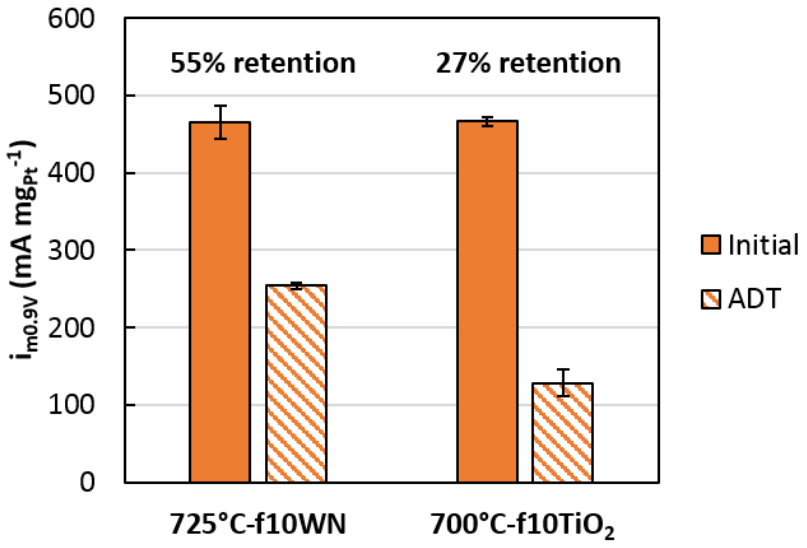

Figure 3.7: Comparison of initial and ADT mass activities for 725°C-f10WN and 700°C-f10TiO_2 catalysts, with % retention for each catalyst over durability testing denoted above the data.

Figure 3.7 compares the electrochemical performance of the 725°C-f10WN catalyst to that of the most active material from the TiO_2 ALD catalysts in Chapter 2, 700°C-f10TiO_2. Though both catalysts had very similar initial ORR mass activities, the WN-based catalyst exhibited considerably better durability over potential cycling than its TiO_2-based counterpart. In Chapter 2, it was observed that the thermal treatment used to make the 700°C-f10TiO_2 catalyst resulted in intermixing of the Pt and Ti phases. The creation of these Pt-Ti nanoparticles was determined to contribute to the observed mass activity increase after thermal treatment; however, these alloy nanoparticles were also postulated to be less stable than pure Pt nanoparticles surrounded by TiO_2, which led to the poor durability of this catalyst. In contrast to 700°C-f10TiO_2, the thermal treatment of 725°C-f10WN was shown to produce a catalyst surface with separate Pt and W phases. The observation that for similar treatment conditions, a mixed Pt-Ti phase was formed in the TiO_2-based catalyst, while separate Pt and W phases were maintained in the WN-based catalyst may be attributable to the higher mobility of Ti on the C support surface. Neglecting potential

differences in their crystal structures and simultaneous reduction of the oxide/nitride species during the H_2 treatment, titanium would be expected to have a higher rate of surface diffusion than tungsten due to its smaller atomic radius.

Based on the comparison in Figure 3.7, it appears that the atomic arrangement with W-rich nanostructures surrounding Pt is superior at preserving electrochemical activity over durability testing. The enhanced durability of 725°C-f10WN over 700°C-f10TiO_2 may be simply due to the presence of the W nanostructures blocking surface migration and agglomeration of the Pt nanoparticles, whereas the incorporation of the Ti nanostructures into the hybrid Pt-Ti nanoparticles seen in 700°C-f10TiO_2 left no residual blocking structures to mitigate agglomeration. It is also possible that the dissimilarity could result from different levels of chemical stability in the RDE environment between the W and Ti species; however, further research will be needed to assess leaching or similar degradation routes of these species during potential cycling.

3.5. Conclusions

Atomic layer deposition of WN and subsequent thermal treatment were used to enhance the activity and durability of an ALD Pt/f-C catalyst. It was observed that WN grew readily on the functionalized carbon substrate during the ALD process, depositing 6.33 wt% W after 10 ALD cycles. The WN nanostructures were homogeneously dispersed across the catalyst surface after ALD. Thermal treatment consisting of a 200°C oxidation in air followed by a 725°C treatment under 25% H_2 was seen to result in coarsening of the Pt nanoparticles, while the W on the surface remained dispersed and did not appear to form an alloyed phase with Pt. However, thermal treatment did change the character of the WN nanostructures by reducing the amount of N present, which resulted in a more W-rich surface. The thermally-treated catalyst was found to have vastly

superior activity towards the ORR than both the unmodified catalyst and the catalyst after 10 cycles of WN ALD; it also outperformed a benchmark Pt/C catalyst. This was attributed to synergistic metal-support effects induced by the W-rich nanostructures' proximity to the Pt nanoparticles. The thermally-treated catalyst also exhibited better electrochemical durability and retention of Pt nanoparticle size over accelerated durability testing due to the stabilizing effects of the W-rich structures. By examining the beneficial electrocatalytic effects of an ALD chemistry previously untested for this application, this work further demonstrates the utility of ALD in the modification of Pt/C ORR catalysts.

3.6. Supplemental Information

This section contains figures with additional information.

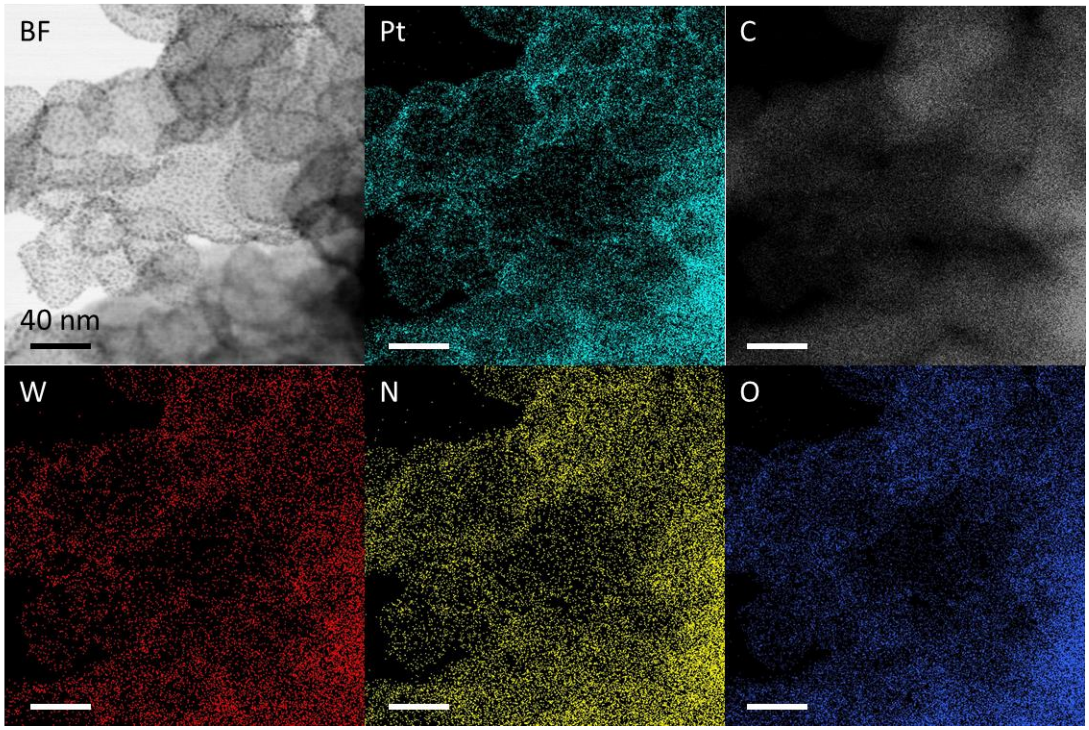

Figure 3S.1: Representative EDS elemental maps showing the distribution of Pt, C, W, N and O in f10WN sample.

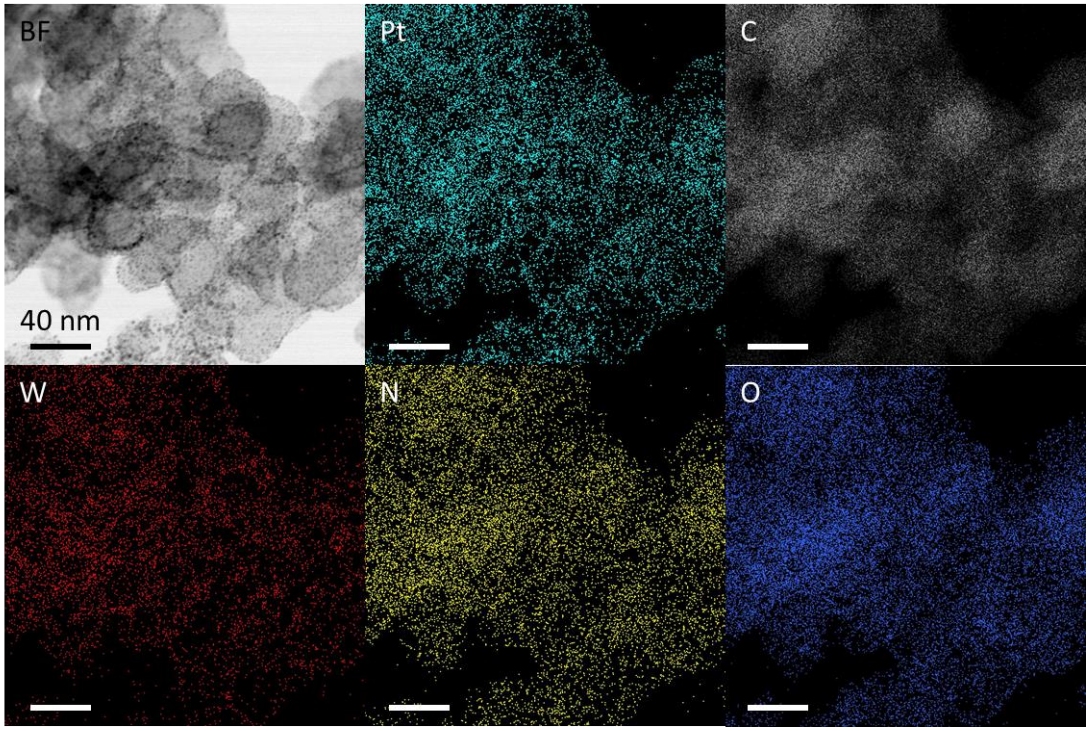

Figure 3S.2: Representative EDS elemental maps showing the distribution of Pt, C, W, N and O in 200°C-f10WN sample.

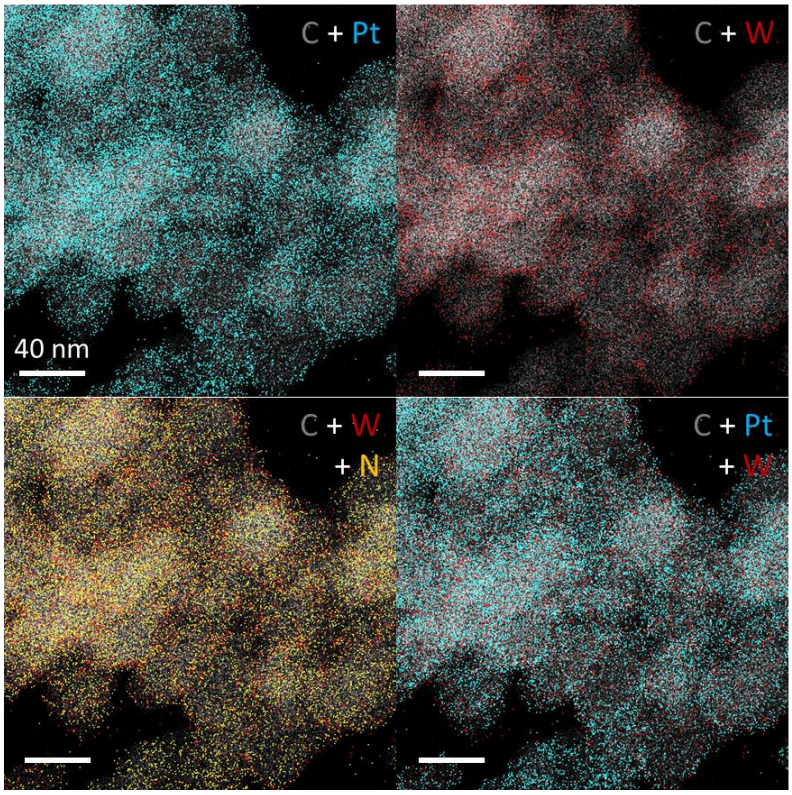

Figure 3S.3: EDS overlays for 200°C-10WN.

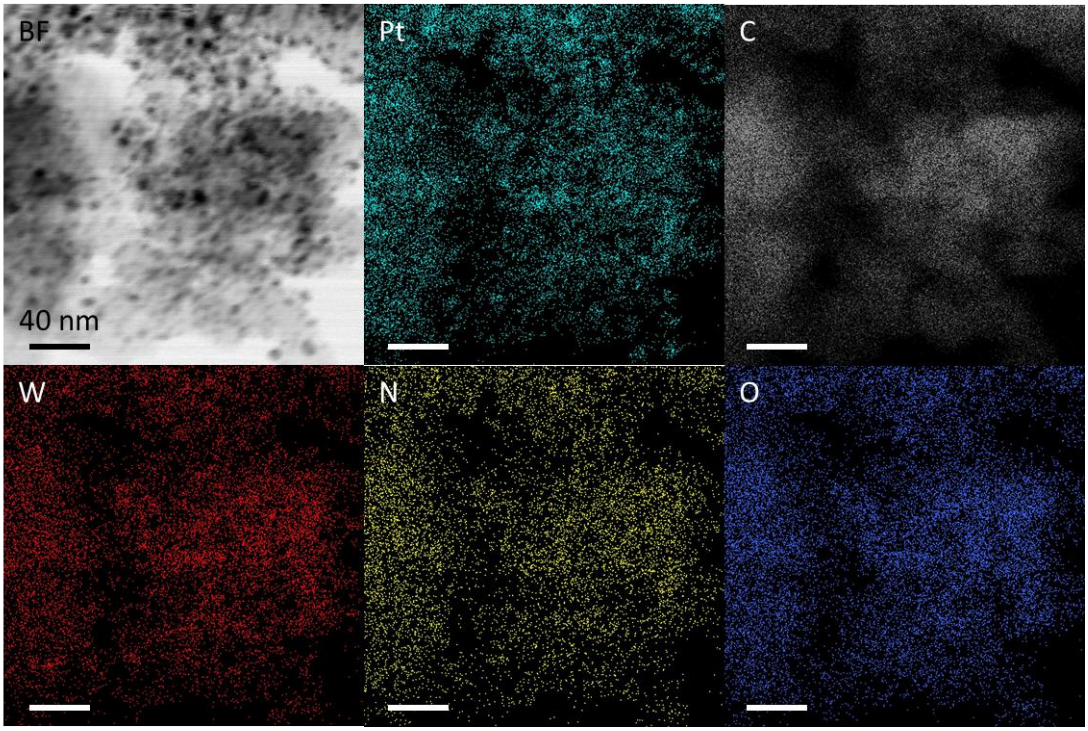

Figure 3S.4: Representative EDS elemental maps showing the distribution of Pt, C, W, N and O in 725°C-f10WN sample.

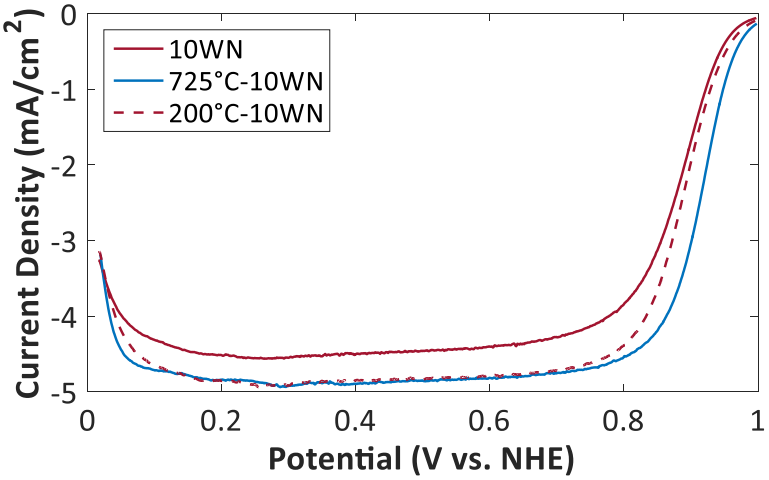

Figure 3S.5: Initial polarization curves for f10WN, 200°C-f10WN, and 725°C-f10WN, illustrating the separate effects of each phase of thermal treatment on ORR performance.

3.7. References

1. Cao, M., D. Wu, and R. Cao, *Recent Advances in the Stabilization of Platinum Electrocatalysts for Fuel-Cell Reactions.* ChemCatChem, 2014. **6**(1): p. 26-45.

2. Kocha, S.S., *Electrochemical Degradation: Electrocatalyst and Support Durability*, in *Polymer Electrolyte Fuel Cell Degradation*, M.M. Mench, E.C. Kumbur, and T.N. Veziroglu, Editors. 2012, Elsevier: Waltham, MA.

3. Virkar, A.V. and Y. Zhou, *Mechanism of Catalyst Degradation in Proton Exchange Membrane Fuel Cells.* Journal of The Electrochemical Society, 2007. **154**(6): p. B540-B547.

4. Takenaka, S.M., H.; Nakagawa, K.; Matsune, H.; Tanabe, E.; Kishida, M., *Improvement in the Durability of Pt Electrocatalysts by Coverage with Silica Layers.* Journal of Physical Chemistry C Letters, 2007. **111**: p. 15133-15136.

5. Takenaka, S., et al., *Highly active and durable silica-coated Pt cathode catalysts for polymer electrolyte fuel cells: control of micropore structures in silica layers.* Catalysis Science & Technology, 2015. **5**(2): p. 1133-1142.

6. Cheng, K., et al., *Three-Dimensionally Costabilized Metal Catalysts toward an Oxygen Reduction Reaction.* Langmuir, 2016. **32**(9): p. 2236-2244.

7. Yang, C., et al., *Mitigating the Degradation of Carbon-Supported Pt Electrocatalysts by Tungsten Oxide Nanoplates.* Electrochimica Acta, 2016. **188**: p. 529-536.

8. Lu, J., J.W. Elam, and P.C. Stair, *Atomic layer deposition—Sequential self-limiting surface reactions for advanced catalyst "bottom-up" synthesis.* Surface Science Reports, 2016. **71**(2): p. 410-472.

9. Feng, H., et al., *Alumina Over-coating on Pd Nanoparticle Catalysts by Atomic Layer Deposition: Enhanced Stability and Reactivity.* Catalysis Letters, 2011. **141**(4): p. 512-517.

10. Liang, X., et al., *Stabilization of Supported Metal Nanoparticles Using an Ultrathin Porous Shell.* ACS Catalysis, 2011. **1**(10): p. 1162-1165.

11. Gould, T.D., et al., *Stabilizing Ni Catalysts by Molecular Layer Deposition for Harsh, Dry Reforming Conditions.* ACS Catalysis, 2014. **4**(8): p. 2714-2717.

12. Lu, J., et al., *Coking- and Sintering-Resistant Palladium Catalysts Achieved Through Atomic Layer Deposition.* Science, 2012. **335**(6073): p. 1205-1208.

13. Cheng, N., et al., *Extremely stable platinum nanoparticles encapsulated in a zirconia nanocage by area-selective atomic layer deposition for the oxygen reduction reaction.* Advanced Materials, 2015. **27**(2): p. 277-281.

14. Marichy, C., et al., *ALD SnO2 protective decoration enhances the durability of a Pt based electrocatalyst.* Journal of Materials Chemistry A, 2016. **4**(3): p. 969-975.

15. Chung, S., et al., *Atomic layer deposition of ultrathin layered TiO2 on Pt/C cathode catalyst for extended durability in polymer electrolyte fuel cells.* Journal of Energy Chemistry, 2016. **25**(2): p. 258-264.

16. Kim, J., S. Yang, and H. Lee, *Platinum–titanium intermetallic nanoparticle catalysts for oxygen reduction reaction with enhanced activity and durability.* Electrochemistry Communications, 2016. **66**: p. 66-70.

17. Ham, D. and J. Lee, *Transition Metal Carbides and Nitrides as Electrode Materials for Low Temperature Fuel Cells.* Energies, 2009. **2**(4): p. 873-899.

18. Antolini, E. and E.R. Gonzalez, *Tungsten-based materials for fuel cell applications.* Applied Catalysis B: Environmental, 2010. **96**(3-4): p. 245-266.

19. Becker, J.S. and R.G. Gordon, *Diffusion barrier properties of tungsten nitride films grown by atomic layer deposition from bis(tert-butylimido)bis(dimethylamido)tungsten and ammonia.* Applied Physics Letters, 2003. **82**(14): p. 2239-2241.

20. Becker, J.S., S. Wang, and R.G. Gordon, *Highly Conformal Thin Films of Tungsten Nitride Prepared by Atomic Layer Deposition from a Novel Precursor.* Chemistry of Materials, 2003. **15**: p. 2969-2976.

21. Shinozaki, K., et al., *Oxygen Reduction Reaction Measurements on Platinum Electrocatalysts Utilizing Rotating Disk Electrode Technique.* Journal of The Electrochemical Society, 2015. **162**(10): p. F1144-F1158.

22. Dai, Y., et al., *Efficient and Superiorly Durable Pt-Lean Electrocatalysts of Pt−W Alloys for the Oxygen Reduction Reaction.* The Journal of Physical Chemistry C, 2011. **115**(5): p. 2162-2168.

23. Wang, Y., et al., *Carbon-Supported W@Pt Nanoparticles with a Pt-Enriched Surface as a Robust Electrocatalyst for Oxygen Reduction Reactions.* ChemistrySelect, 2018. **3**(4): p. 1056-1061.

24. Downs, R.T. and M. Hall-Wallace, *The American Mineralogist Crystal Structure Database.* American Mineralogist, 2003. **88**: p. 247-250.

25. Moharana, P.L., et al., *Structural and mechanical study of thermally annealed tungsten nitride thin films.* Perspectives in Science, 2016. **8**: p. 636-638.

26. Mukerjee, S., *Particle size and structural effects in platinum electrocatalysis.* Journal of Applied Electrochemistry, 1990. **20**: p. 537-548.

27. Karlberg, G.S., et al., *Cyclic voltammograms for H on Pt(111) and Pt(100) from first principles.* Physical Review Letters, 2007. **99**(12): p. 126101.

28. Shim, J.L., C-R; Lee, H-K; Lee, J-S; Cairns, EJ, *Electrochemical characteristics of Pt-WO3/C and Pt-TiO2/C electrocatalysts in a polymer electrolyte Fuel Cell.* Journal of Power Sources, 2001. **102**: p. 172-177.

29. Elezovic, N.R., et al., *Synthesis and characterization Pt nanocatalysts on tungsten based supports for oxygen reduction reaction.* Applied Catalysis B: Environmental, 2012. **125**: p. 390-397.

30. Alexeev, O., M. Shelef, and B.C. Gates, *MgO-Supported Platinum-Tungsten Catalysts Prepared from Organometallic Precursors: Platinum Clusters Isolated on Dispersed Tungsten.* Journal of Catalysis, 1996. **164**: p. 1-15.

CHAPTER 4

FUEL CELL TESTING OF ALD-MODIFIED PT/C CATALYSTS

4.1. Abstract

Device testing of polymer electrolyte membrane fuel cell (PEMFC) catalysts is essential for investigating the impact of catalyst properties on electrochemical performance. Platinum nanoparticle catalysts supported on functionalized XC72 carbon black that had been modified with both TiO_2 and WN atomic layer deposition (ALD) and subjected to various thermal treatments were incorporated into membrane electrode assemblies (MEAs) and tested for oxygen reduction reaction (ORR) activity in a fuel cell. The mass activities of the catalysts gathered at low current densities had comparable trends to those previously recorded in aqueous half-cell testing; however, significant deviations in catalyst performance became apparent at high current densities in the mass transport region of the polarization curves. The poor performance of the ALD-modified catalysts was attributed to water flooding induced by the low hydrophobicity of these catalysts layers, as determined by contact angle measurements on the cathode surfaces. It was seen that hydrophobicity was increased by thermal treatment and removal of surface groups known to be prone to hydrogen bonding, thereby improving the catalyst performance in the mass transport region. The field of research on fuel cell catalyst design via ALD is rapidly expanding, and this work demonstrates the importance of understanding the impact of ALD-deposited nanostructures on materials properties beyond the pure electrocatalytic activity.

4.2. Introduction

The commercialization of advanced propulsion systems powered PEMFCs depends on the development of catalysts with low precious metal content, high activity towards the ORR, and

sufficient durability under voltage cycling [1]. Atomic layer deposition offers highly tunable, nanoscale control over the growth of metal nanoparticles and protective nano-ceramics and the process may be utilized as a scalable method for ORR catalyst synthesis. Researchers have used ALD-deposited species, such as nanostructures of ZrO_2 and SnO_2, to stabilize Pt nanoparticles and mitigate their movement and agglomeration over voltage cycling [2, 3]. Chapters 2 and 3 of this thesis have detailed the application of TiO_2 and WN nanostructures to both commercial carbon-supported Pt nanoparticle catalysts (Pt/C) as well as an ALD-derived Pt nanoparticle catalyst on functionalized carbon (ALD Pt/f-C). These catalysts were analyzed through a variety of materials characterization techniques and their electrochemical performance was assessed through rotating disk electrode (RDE) half-cell testing. Though RDE measurements are useful for examining trends in catalyst activity and durability without the operational losses inherent to a fuel cell—e.g., membrane resistance, gas transport, and water management—a thorough evaluation of the efficacy of any new ORR catalyst must also involve performance testing in the PEMFC environment. Once incorporated into MEAs and placed in a PEMFC, catalysts may exhibit behaviors that were not apparent in the aqueous RDE testing environment; this allows for further probing of the materials properties beyond the catalytic activity. One such property is the hydrophobicity of the catalyst, which is strongly influenced by the composition of the support material.

Water management is a significant engineering issue in PEMFC design and operation [4-6]. Excessive liquid water accumulation in the cell, known as flooding, creates significant mass transport limitations for reactant gases by blocking pores in the gas diffusion layers and covering catalyst sites [7]. The propensity for liquid water accumulation is particularly acute at the cathode since water is the primary product of the ORR. Modern PEMFCs are designed to mitigate these issues, and the hydrophobic nature of conventional carbon-based catalyst supports impregnated on

carbon-based gas diffusion layers in the MEA assists with efficient water removal from the cell. However, the addition of a less-hydrophobic catalyst material to the gas diffusion layer may negatively impact the effectiveness of water removal and induce flooding on the cathode. This undesirable effect was previously documented for the ALD Pt/f-C catalyst in PEMFC testing [8]. In this case, HNO_3-functionalized carbon black was found to be a highly effective substrate for Pt ALD, producing catalysts with excellent Pt nanoparticle dispersion and uniformity. Despite its physical properties, the PEMFC performance of this catalyst was negatively impacted by the presence of residual oxygen-containing functional groups in the carbon substrate that were not consumed during the Pt ALD synthesis. These oxygenated carbon sites often behave like carboxylic acids [9], promoting hydrogen bonding with water and making the surface more hydrophilic [10]. When tested in the PEMFC, this property of the functionalized carbon led to severe water flooding even at low to moderate current densities, thereby rendering the ALD Pt/f-C virtually unusable as an ORR catalyst.

The work discussed in Chapters 2 and 3 utilized the residual oxygen-containing groups on the functionalized carbon to deposit TiO_2 and WN ALD nanostructures onto the ALD Pt/f-C catalyst. The consumption of these surface functional groups, the addition of ALD nano-ceramics, and subsequent thermal treatment were all expected to induce changes in catalyst hydrophobicity relative to the unmodified ALD Pt/f-C. In order to study the effects of these surface modifications on PEMFC performance and compare fuel cell activity trends to those observed in RDE testing, select catalysts from previous chapters were incorporated into MEAs and tested in a fuel cell device. The f10TiO_2 and f10WN catalysts were tested alongside ALD Pt/f-C to observe the impact of functional group consumption with different ALD processes; 725°C-f10WN and 700°C-ALD

Pt/f-C were tested to examine the effects of thermal treatment. A commercial Pt/C catalyst was also included as a control.

4.3. Experimental

4.3.1. Catalyst Synthesis and Membrane Electrode Assembly Fabrication

The catalysts were synthesized according to the TiO_2 ALD process detailed in Chapter 2 and the WN ALD process detailed in Chapter 3. The 700°C-ALD Pt/f-C catalyst was made according to the thermal treatment process used in Chapter 2, and 725°C-f10WN was made using the thermal treatment described in Chapter 3. Catalyst powders were made into ink dispersions by combining them with ultrapure water (0.416 mL/mg catalyst), isopropyl alcohol (0.32 mL/mg catalyst), and a 5 wt% Nafion ionomer solution (Sigma Aldrich; 0.874 g/g carbon) in a 20mL scintillation vial. This recipe was adapted from the Pt/C ink-making procedure in [11]. The catalyst inks were bath sonicated for 1 hour after mixing.

Electrodes were prepared by hand-spraying ink dispersions onto 10 cm^2 squares of Sigracet 25 BC gas diffusion layers with an airbrush (Harder & Steenbeck Evolution). Amounts of ink sprayed on each square were calculated based on the Pt content of each catalyst in the final ink dispersion, such that all electrodes had a weight loading of approximately 0.1 mg_{Pt} cm^{-2} after spraying. All MEAs were arranged with the catalyst of interest on the cathode, Pt/C on the anode, and a Nafion 212 membrane as a proton-conducting layer in between. The Nafion membranes were prepared by boiling in 0.5 M H_2SO_4 for 2 hours. MEAs were prepared following the procedure outlined in [8, 12], in which the anode and cathode were bonded to the proton conductor using a heated hydraulic press (Carver) under 500 psi at 130°C for 5 minutes.

4.3.2. Analytical Characterization

Contact angle measurements were taken on all cathode surfaces after catalyst ink spraying but before incorporation into MEAs. The cathode was placed on a backlit adjustable stage in a custom goniometer apparatus. A syringe used to deposit a 1μL drop of ultrapure water onto the cathode surface, and pictures were taken of the resulting drop by an attached camera. Three separate drops in different areas of the surface were analyzed for each cathode. The drop images were analyzed in ImageJ using the DropSnake plugin to calculate left and right contact angles.

4.3.3. Electrochemical Characterization

Electrochemical performance of the MEAs was evaluated in a single fuel cell (Fuel Cell Technologies) with 10 cm^2 active area. Gas flow, temperature, humidification, and current draw were controlled by a Ceres Technologies PEM 221 test stand, and the voltage across the cell was measured using a multimeter (Fluke). The cell temperature was held at 60°C for all experiments, with 92% relative humidity and UHP nitrogen/oxygen on the cathode and UHP hydrogen on the anode. All MEAs were initially broken in with a 1 hour warm-up with no current draw and N_2/H_2 on the cathode/anode at 50 sccm, followed by a 3-hour stabilization step at 0.1 mA/cm^2 and O_2/H_2 on the cathode/anode at 50 sccm. The polarization curves were recorded under the same conditions as the stabilization step, with a 6 minute stabilization time between data points. Electrochemical impedance spectroscopy from 100,000 Hz to 0.1 Hz at open circuit voltage was performed using a potentiostat (Gamry Reference 3000) and the real high-frequency intercept on the resulting Nyquist plot was used as ohmic resistance for the cell. All polarization curves were iR corrected accordingly. Mass-specific current density values used for mass activity and mass transport analysis were extracted from a smoothing spline fit of the discrete polarization curve data points in MATLAB using the default smoothing parameters.

4.4. Results and Discussion

4.4.1. Catalyst Hydrophobicity

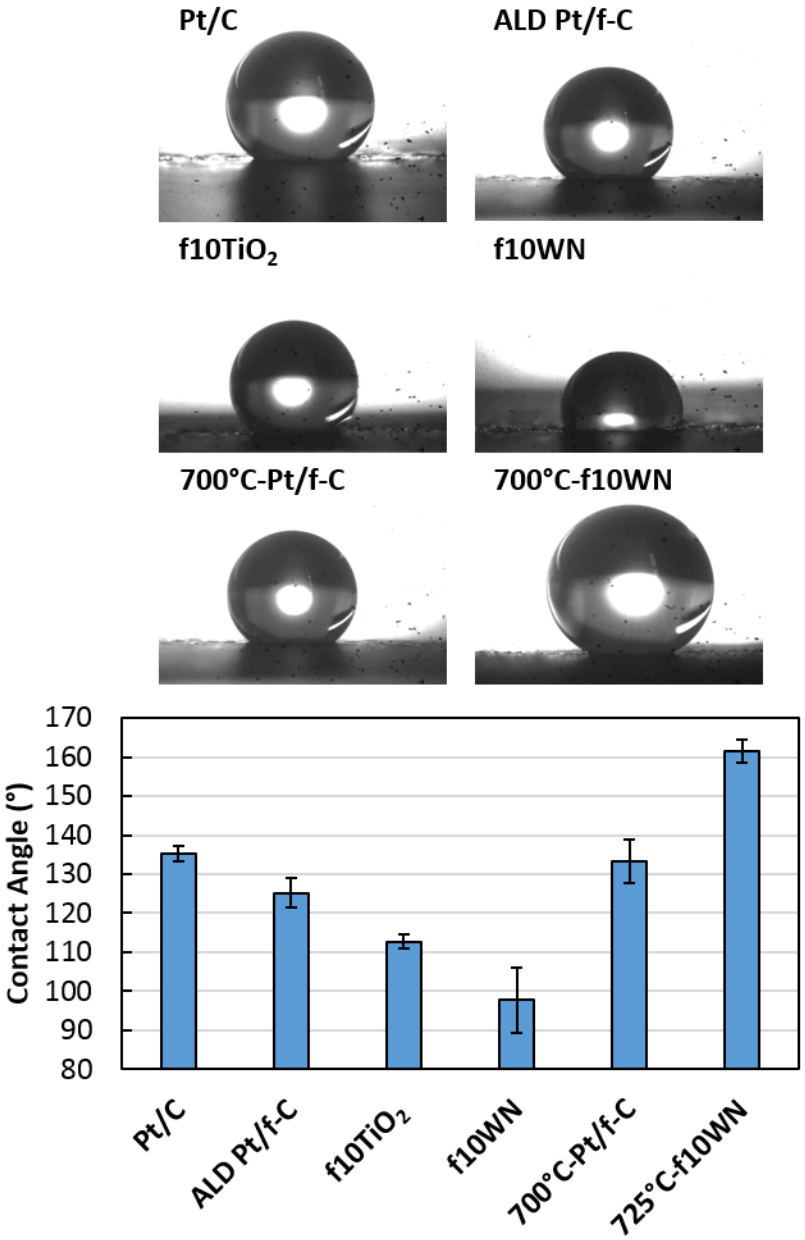

Figure 4.1: Contact angles of all cathode surfaces.

The contact angles for all cathode surfaces and images of their representative water droplets are shown in Figure 4.1. An obvious decrease in contact angle was observed in the ALD Pt/f-C

catalyst with the addition of both TiO_2 and WN ALD, though the magnitude of this decrease was greater for the application of 10 cycles of WN ALD. These observed changes in contact angle indicated that the hydrophobicity of the ALD Pt/f-C catalyst surface, which was initially lower than commercial Pt/C due to residual oxygen-containing groups in the functionalized carbon [8], was further lowered by the deposited ALD species. Though it was postulated that consumption of the functional groups during ALD might increase the hydrophobicity, the results imply that the deposited nano-ceramics also induced significant hydrophilic effects that may have counteracted any changes resulting from a less oxygenated carbon substrate. In the case of f10TiO_2, it is likely that the deposited TiO_2 promoted hydrogen-bonding interactions with the water droplet on the cathode, which increased the wettability of the surface. The hydrophilicity of many common ceramic oxides is well-documented in the literature [13, 14] and is particularly pronounced in metal oxides comprised of high-electronegativity metals due to the metal atoms' ability to act as Lewis acids and form coordinate bonds with water [15, 16]. The f10WN catalyst was observed to have the lowest contact angle of all the cathode surfaces. Though metal nitrides are generally expected to be more hydrophobic than metal oxides on account of fewer electron lone pairs on nitrogen available for hydrogen bonding [15], tungsten has a considerably higher Pauling electronegativity than titanium, which may have increased the wettability of the f10WN cathode. Additionally, the f10WN catalyst was observed in Chapter 3 to have a high nitrogen content through EDS mapping. The amount of N present was in excess of the stoichiometric amounts found in typical tungsten nitride configurations, indicating that some of the nitrogen detected may have been physisorbed to the carbon support during the NH_3 doses in the WN ALD process. The electron lone pairs on these excess nitrogen species may have further contributed to the hydrophilicity of this catalyst.

The application of thermal treatment to the ALD Pt/f-C and f10WN catalysts resulted in significant increases in contact angle for these catalysts. The 700°C-ALD Pt/f-C catalyst exhibited a contact angle approximately equal to that of Pt/C, which was attributed to the total removal of oxygen-containing groups by exposure to a high temperature and reducing atmosphere of 20% H_2, thereby leading to surface with similar hydrophobicity to Pt/C. The contact angle of 725°C-f10WN was the highest recorded of all the catalysts at 161°; this dramatic difference compared to the original f10WN catalyst may be due to the removal of excess nitrogen and change in the stoichiometry of the tungsten nitride species from WN_3 to W_2N over thermal treatment that was documented in Chapter 3. Removal of nitrogen species would be expected to decrease the amount of electron lone pairs present in the nitride available for hydrogen bonding, thereby increasing the hydrophobicity. The fact that the contact angle of this catalyst was higher than that of 700°C-ALD Pt/f-C indicates that the presence of the W-rich phase present in 725°C-f10WN induced additional hydrophobic effects. Though some nitrogen is still present on the surface, the W/WN species likely transitioned from amorphous to crystalline phase during the high-temperature treatment [17]. This transition would likely lower the surface energy [18] and decrease interactions between the water droplet and the cathode surface, leading to a higher contact angle.

4.4.2. Fuel Cell MEA Characterization

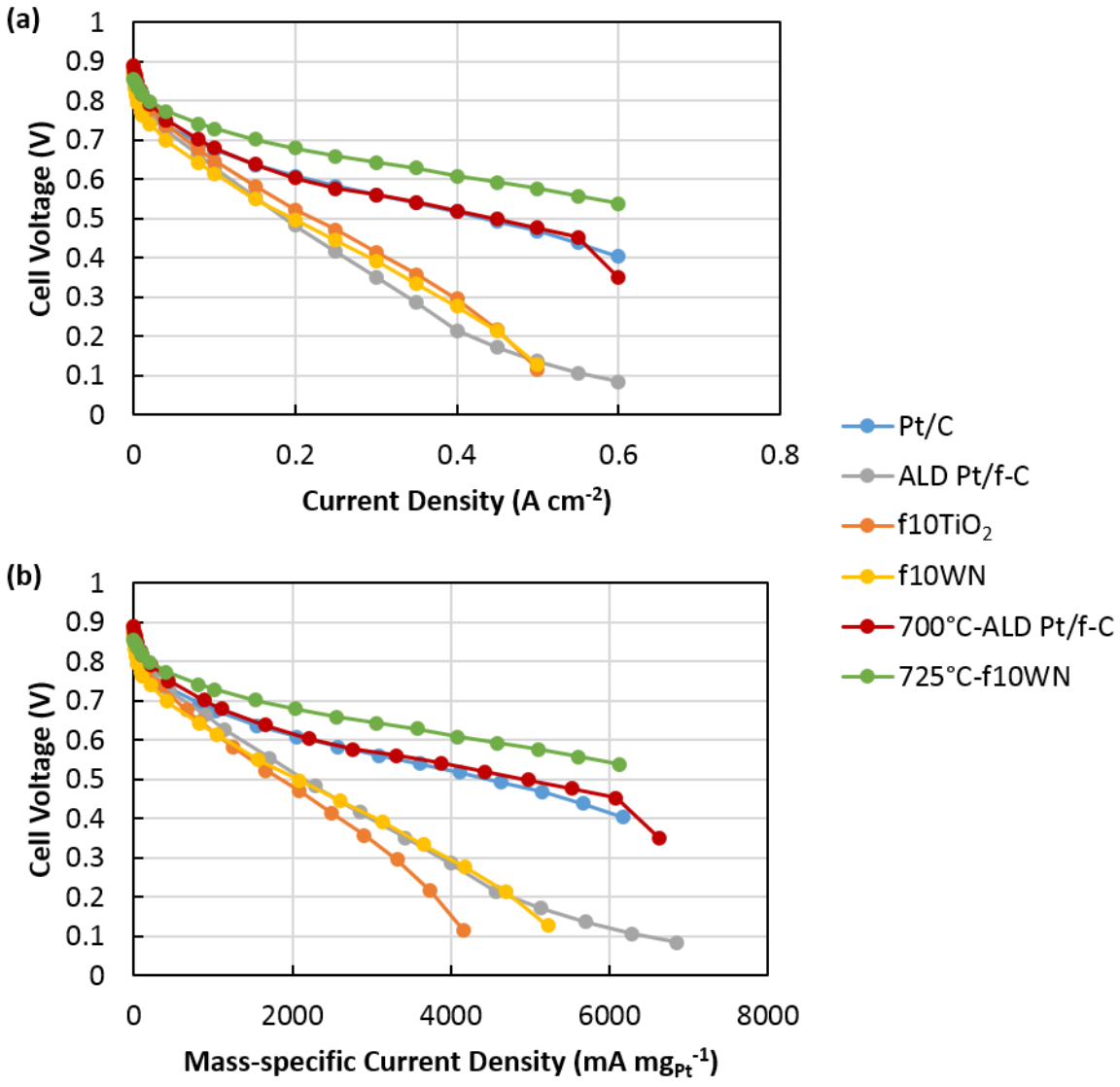

Figure 4.2: Polarization curves for all MEAs: (a) normalized by cathode active area and displayed as a function of current density; (b) normalized by cathode Pt weight loading and displayed as a function of mass-specific current density.

Polarization curves normalized by cathode active area and cathode Pt weight loading for all MEAs are shown in Figure 4.2. In both cases, there was an obvious qualitative difference in the performance of catalysts with contact angles <130° (ALD Pt/f-C, f10TiO_2, and f10WN) compared to those with higher contact angles (Pt/C, 700°C-ALD Pt/f-C, and 725°C-f10WN). The higher

contact angle catalysts exhibited higher cell voltages under moderate and large current draw, indicating that they are, in general, superior fuel cell catalysts than the low contact angle catalysts. In order to further quantify the differences between these catalysts, different regions of the polarization curves were isolated and examined in greater detail. The kinetic region at low current density values (0.9-0.7 V) represents voltage losses due to the intrinsic activity of the catalyst; conversely, the voltages losses in the mass transport region at high current density values are due to an inability of oxygen to reach catalyst sites that may be associated with low concentration of the reactant gases or other materials properties of the catalyst [4]. The observed catalyst performance in each of these regions was used to elucidate connections with previously-observed properties of these catalysts.

4.4.2.1. Kinetic Region

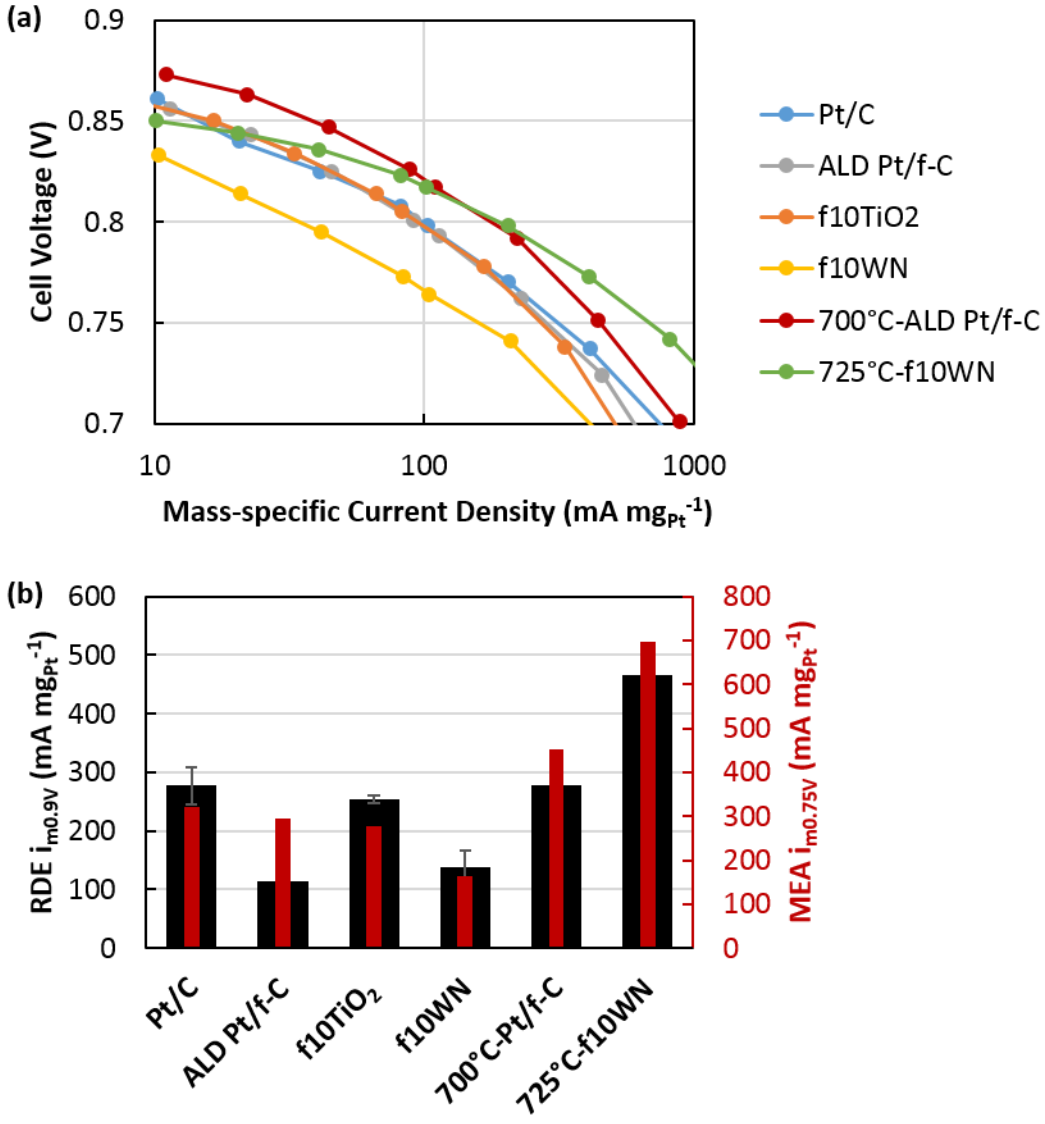

Figure 4.3: (a) Tafel plot of the kinetic region for all catalysts; (b) Mass activity trend comparison for RDE $i_{m0.9V}$ (shown in black) and MEA $i_{m0.75V}$ (shown in red).

An analysis of the kinetic region is shown in Figure 4.3. In Figure 4.3a, the kinetic region of the polarization curves is shown with logarithmic mass-specific current density on the x-axis to emphasize qualitative differences in the curves for each catalyst. A mass activity ($i_{m0.75V}$) was calculated using the mass-specific current density for each curve at 0.75 V. Conventionally, fuel cell mass activities are calculated at 0.9 V, but inefficiencies in the electrode spraying and MEA

preparation procedure used in this work prevented the use of that specific metric. As the kinetic region of the fuel polarization curve is the most accurate measure of intrinsic catalyst activity, the MEA $i_{m0.75V}$ was displayed alongside previous RDE mass activity data ($i_{m0.9V}$) from Chapters 2 and 3 in order to compare activity trends in the two systems (Figure 4.3b). Though the absolute activity values between RDE and MEA activities are different due to the use of different reference voltages, the trends across the catalysts tested appear to be consistent. As with RDE data, the MEA data shows that mass activities for the Pt/C and f10TiO_2 are very similar, while the f10WN catalyst is less active. Additionally, the thermally-treated catalysts are similarly high-performing, with 725°C-f10WN once again demonstrating the highest activity. The largest discrepancy between the RDE and MEA results is observed with the ALD Pt/f-C catalyst; its activity in proportion to the other catalysts in MEA testing is much higher than was seen in aqueous RDE testing. This may be due to the fact that the catalyst was exposed to an elevated temperature of 130°C in air during the MEA pressing step. It was previously observed in Chapter 2 that a 200°C treatment in air effectively oxidized residual ligands from the Pt-H_2 ALD used to prepare the ALD Pt/f-C catalyst. Though the thermal exposure in the MEA pressing step is certainly less intense than 200°C treatment in air, it is still possible that this extra preparation step that was not part of the RDE testing procedure may have resulted in a higher proportional activity for this catalyst in the fuel cell.

4.4.2.2. Mass Transport Region

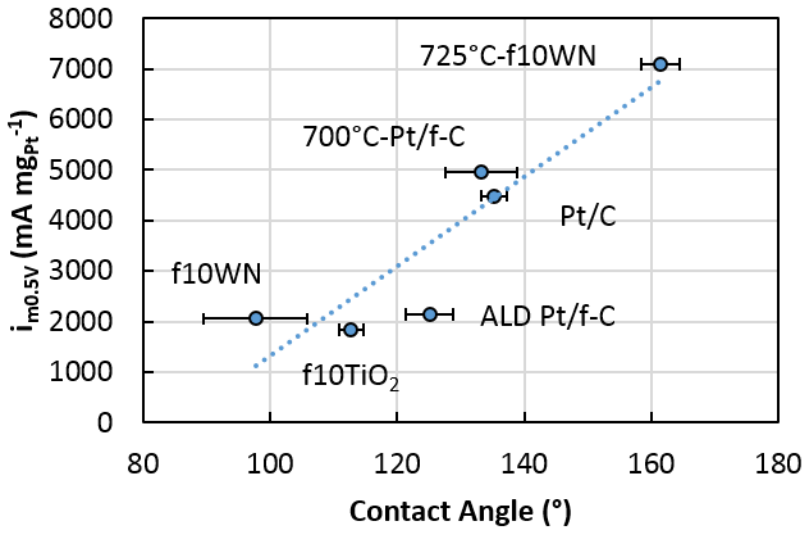

Figure 4.4: Mass-specific current density of each catalyst at 0.5 V plotted against the recorded contact angle of each catalyst.

The mass transport regions of the polarization curves in Figure 4.2 show obvious qualitative differences between the catalysts. As previously mentioned, the catalysts with contact angles below 130° had a significant drop-off in performance at higher current densities, which is consistent with observed water flooding behavior in PEMFCs [7]. In order to further elucidate the effects of cathode hydrophobicity on catalyst performance in the mass transport region, mass-specific current densities of each catalyst at 0.5 V ($i_{m0.5V}$) were plotted against corresponding contact angles and displayed in Figure 4.4. It should be noted that the $i_{m0.5V}$ value for 725°C-f10WN had to be extrapolated from existing data points. Though the relationship is not perfectly linear, this analysis shows a clear correlation between catalyst hydrophobicity and the ability of a catalyst to sustain high current densities without significant voltage losses. More hydrophilic catalysts, such as f10WN, f10TiO_2, and ALD Pt/f-C, were more prone to water flooding at high current densities due to their decreased ability to effectively wick moisture out of the catalyst layer. As the 725°C-f10WN was found to be considerably more hydrophobic than even commercial Pt/C,

water management was likely highly effective in that catalyst layer, which allowed the MEA to support high current densities with no evidence of water flooding.

4.5. Conclusions

In this work, ALD-modified Pt nanoparticle catalysts that had been previously examined through aqueous RDE testing were incorporated into MEAs and analyzed for ORR activity in a PEMFC. It was observed that general mass activity trends in the kinetic region of the polarization curve were consistent with the results acquired in the RDE setting, with some minor deviations attributed to the ink spraying and MEA fabrication procedures used before PEMFC testing. Significant voltage losses were seen in the mass transport region of the polarization curves for the ALD Pt/f-C, f10TiO_2, and f10WN catalysts, while the Pt/C, 700°C-ALD Pt/f-C, and 725°C-f10WN catalysts retained relatively high voltages at high current densities. The currents provided by the catalysts in the mass transport region were well-correlated with the contact angle of the cathode surfaces as measured after catalyst ink spraying; the hydrophilic catalysts (contact angle < 130°) had markedly lower mass-specific current density values at 0.5 V than the hydrophobic catalysts. This separation in catalyst performance was likely due to water flooding on the hydrophilic catalyst layers, a problem which was resolved after the thermal treatment procedures eliminated surface groups that were contributing to hydrogen bonding, such as O and N. These results show that the choice of ALD species applied to a Pt/C catalyst will impact materials properties other than catalytic activity. Given the increasing use of ALD-deposited metal oxide and nitride nanostructures in fuel cell catalyst development, it is essential to consider how these properties may affect various fuel cell system parameters beyond the catalytic activity, such as water management.

4.6. References

1. Cao, M., D. Wu, and R. Cao, *Recent Advances in the Stabilization of Platinum Electrocatalysts for Fuel-Cell Reactions.* ChemCatChem, 2014. **6**(1): p. 26-45.

2. Cheng, N., et al., *Extremely stable platinum nanoparticles encapsulated in a zirconia nanocage by area-selective atomic layer deposition for the oxygen reduction reaction.* Advanced Materials, 2015. **27**(2): p. 277-281.

3. Marichy, C., et al., *ALD SnO2 protective decoration enhances the durability of a Pt based electrocatalyst.* Journal of Materials Chemistry A, 2016. **4**(3): p. 969-975.

4. Srinivasan, S., *Fuel Cell Principles*, in *Fuel Cells: From Fundamentals to Applications*. 2006, Springer: Boston, MA. p. 189-233.

5. Avcioglu, G.S., B. Ficicilar, and I. Eroglu, *Improved PEM fuel cell performance with hydrophobic catalyst layers.* International Journal of Hydrogen Energy, 2018. **43**(40): p. 18632-18641.

6. Folgado, M.A., et al., *Single Cell Study of Water Transport in PEMFCs with Electrosprayed Catalyst Layers.* Fuel Cells, 2018. **18**(5): p. 602-612.

7. Li, H., et al., *A review of water flooding issues in the proton exchange membrane fuel cell.* Journal of Power Sources, 2008. **178**(1): p. 103-117.

8. Lubers, A.M., et al., *Proton Exchange Membrane Fuel Cell Flooding Caused by Residual Functional Groups after Platinum Atomic Layer Deposition.* Electrochimica Acta, 2017. **237**: p. 192-198.

9. Barton, S.S., et al., *Acidic and basic sites on the surface of porous carbon.* Carbon, 1997. **35**(9): p. 1361-1366.

10. Biniak, S., et al., *The characterization of activated carbons with oxygen and nitrogen surface groups.* Carbon, 1997. **35**(2): p. 1799-1810.

11. Mauger, S.A., et al., *Fuel Cell Performance Implications of Membrane Electrode Assembly Fabrication with Platinum-Nickel Nanowire Catalysts.* Journal of The Electrochemical Society, 2018. **165**(3): p. F238-F245.

12. Lubers, A.M., et al., *Electrochemical hydrogen pumping using a platinum catalyst made in a fluidized bed via atomic layer deposition.* Powder Technology, 2016. **296**: p. 72-78.

13. Azimi, G., et al., *Hydrophobicity of rare-earth oxide ceramics.* Nature Materials, 2013. **12**(4): p. 315-320.

14. Sankar, S., et al., *Hydrophobic and Metallophobic Surfaces: Highly Stable Non-wetting Inorganic Surfaces Based on Lanthanum Phosphate Nanorods.* Scientific Reports, 2016. **6**: p. 22732.

15. Zenkin, S., et al., *Hydrophobicity of Thin Films of Compounds of Low-Electronegativity Metals.* Journal of the American Ceramic Society, 2014. **97**(9): p. 2713-2717.

16. Musil, J., et al., *Flexible hydrophobic ZrN nitride films.* Vacuum, 2016. **131**: p. 34-38.

17. Becker, J.S. and R.G. Gordon, *Diffusion barrier properties of tungsten nitride films grown by atomic layer deposition from bis(tert-butylimido)bis(dimethylamido)tungsten and ammonia.* Applied Physics Letters, 2003. **82**(14): p. 2239-2241.

18. Graeser, K.A., et al., *The Role of Configurational Entropy in Amorphous Systems.* Pharmaceutics, 2010. **2**(2): p. 224-244.

CHAPTER 5

PLATINUM ALD SYNTHESIS OF EXTENDED THIN FILM ELECTROCATALYST STRUCTURES

5.1. Abstract

Extended thin film electrocatalyst structures based on PtNi nanowires, synthesized via spontaneous galvanic displacement, have shown great promise as efficient and durable catalysts for the oxygen reduction reaction in polymer electrolyte membrane fuel cells (PEMFCs). In this work, atomic layer deposition (ALD) of Pt onto Ni nanowire (NiNW) substrates is demonstrated for the first time with the goal to develop a more scalable synthesis route based on vapor phase deposition. ALD was used to deposit variable amounts of Pt onto NiNWs, producing PtNi nanowires with 3-16 wt% Pt. The Pt nanoparticle growth mechanism with increasing ALD cycles and physiochemical properties of as-received materials and ALD-modified catalysts were examined through a variety of techniques, including electron microscopy, X-ray diffraction, and rotating disk electrode analysis. Thirty cycles of Pt ALD followed by H_2 annealing was found to produce a catalyst with mass activity 4 times greater than Pt/HSC in rotating disk electrode analysis; subsequent acid leaching of the ALD-synthesized material and incorporation into membrane electrode assemblies produced a catalyst that outperformed previously-reported extended thin film electrocatalysts in fuel cell testing. The acid-leached ALD PtNiNWs also surpassed the DOE 2020 mass activity target for fuel cells, thereby demonstrating the potential of ALD as a method for producing gram-scale quantities of high-performing extended surface electrocatalysts.

5.2. Introduction

Polymer electrolyte membrane fuel cells (PEMFCs) have emerged as a potentially transformative technology in automotive power applications due to their portability, high theoretical maximum efficiency, and lack of CO_2 emissions. Commercial feasibility of this technology is currently limited by cost and durability of the catalyst layer, particularly on the cathode where the kinetically-sluggish oxygen reduction reaction (ORR) takes place. Conventional carbon-supported Pt nanoparticle catalysts (Pt/HSC) exhibit high surface area and moderate mass activities but are particularly vulnerable to Pt crystallite agglomeration, electrochemical Ostwald ripening, dissolution of Pt into the electrolyte, and carbon support degradation during fuel cell operation [1, 2]. There is a growing body of research concentrated on the development of alternative catalyst structures that address these shortcomings. One promising class of advanced catalysts is extended thin film electrocatalyst structures (ETFECS). These materials possess a number of inherent benefits over supported nanoparticle catalysts; in particular, their highly-coordinated metal surfaces and lack of carbon support improve their electrochemical durability over potential cycling. The extended surface structure also improves the utilization of Pt in the ORR, resulting in site-specific activities that are often an order of magnitude higher than those of nanoparticle catalysts [3, 4]. Additional research into Pt alloy nanoparticles, both as a means of cost reduction (by decreasing precious metal content) and ORR activity enhancement (by tuning adsorption energies of oxygen intermediates on the catalyst surface) [5-7], can be integrated into the development of extended surfaces to produce novel materials that significantly outperform conventional Pt nanoparticle catalysts.

A major unaddressed challenge in the advancement of ETFECS technology is the absence of a reproducible synthesis method that can be scaled to produce large quantities of material.

Spontaneous galvanic displacement (SGD) has been demonstrated as an effective solution-phase chemistry route to deposit thin Pt layers onto Ni nanowire (NiNW) templates for the production of high-performing extended surface electrocatalysts on the milligram scale [3, 8-11]. A number of post-synthesis processing techniques, such as thermal annealing and selective acid leaching, have also been utilized to optimize the activity of these materials towards the ORR [11]. However, despite exceptional performance in RDE half-cells (specific activity > 6000 μA cm_{Pt}^{-2}), challenges persist in the fabrication of high-quality materials of sufficient quantity for fuel cell membrane electrode assembly (MEA) testing and optimization [12]. Thus, there is a need for an investigation into ETFECS synthesis routes beyond SGD.

Atomic layer deposition (ALD) is a scalable, vapor-phase "bottom-up" synthesis method that provides atomic-scale control over the growth of metal oxide films or metal nanoparticles on a substrate [13]. This deposition technique is line-of-sight independent and is therefore well-suited for coating high-aspect-ratio substrates, such as porous micron- or nano-sized powders, nanotubes, and nanowires [14-17]. Catalytic Pt has been deposited with ALD on a variety of substrates for many diverse applications, including oxygen reduction [18-21]; however, there are currently no reports of Pt ALD for modification of NiNWs. This work represents the first demonstration of Pt ALD as a vapor-phase synthesis alternative to SGD for production of extended surface electrocatalysts. The ALD growth process and catalytic properties of synthesized materials were probed with mass spectrometry, electron microscopy, XRD, rotating disk electrode (RDE) voltammetry, and fuel cell testing. The effects of thermal annealing in a reducing atmosphere and acid leaching of the NiNW core were also investigated. PtNiNWs synthesized via ALD were found to have a mass activity almost 4 times greater than benchmark Pt/HSC after annealing in RDE

tests, and the acid-leached materials demonstrated activity in excess of the U.S. Department of Energy (DOE) 2020 target in fuel cell device testing.

5.3. Experimental

5.3.1. Atomic Layer Deposition of Pt

Atomic layer deposition of Pt was performed under a vacuum of approximately 1 Torr in a vertically-aligned viscous flow reactor at 295°C in which 0.5 g of as-received Ni nanowires (PlasmaChem) were immobilized by packed beds of quartz wool. The NiNWs had an average diameter of 171 ± 60 nm and were typically micron-scale in length [22]. The metal precursor, trimethyl(methylcyclopentadienyl)platinum (IV) ($MeCpPtMe_3$), was heated to 40°C in a stainless steel bubbler and transported to the reactor using N_2 as a carrier gas, while 5% O_2 in N_2 was used as a counter-reagent in order to minimize oxidation of the NiNW substrate. Ultra-high purity N_2 was used as a carrier and purge gas. Each ALD cycle consisted of: (1) a $MeCpPtMe_3$ dose with 10 sccm carrier gas flow rate (120 s), (2) a purge with 40 sccm N_2 flow rate (180 s), (3) a 5% O_2 dose with 45 sccm flow rate (140 s), and (4) a purge with 40 sccm N_2 flow rate (180 s). These ALD cycles were repeated 5, 10, 20, and 30 times, each on two separate batches of NiNWs, to assess reproducibility between runs and Pt growth at different numbers of ALD cycles. Gases exiting the reactor were monitored using an in-line mass spectrometer (Stanford Research Systems QMS 200); results are displayed for *m/z* peaks 16 (CH_4), 28 (N_2), 32 (O_2), 44 (CO_2), and 79 (MeCp precursor fragment).

5.3.2. Post-ALD Processing

The annealing procedure included first evacuating the material in a tube furnace over-night at room temperature and $1x10^{-7}$ Torr to eliminate any residual water or oxygen gas. A flow of

50% H_2/N_2 gas each at 200 sccm, was established and maintained at 400 Torr in the reactor. The sample was then heated at 250°C for 2 hours, using a 10°C min^{-1} heating and cooling rate.

Acid leaching was used to remove soluble Ni from the annealed PtNiNWs before incorporation into MEAs, similarly to SGD materials [23]. The PtNiNWs were added to 1 M H_2SO_4 in a 20 mL glass vial at a concentration of 40 mg PtNi/mL H_2SO_4 and soaked for 2 hours to achieve ~80 wt% Pt in the final material. In order to keep the PtNiNWs dispersed, the vial was placed on a roller during the duration of the soaking time. The mixture was subsequently diluted with deionized water and centrifuged at 2500 rpm for 15 min. The mixture was then decanted, and the process was repeated two more times. The rinsed wires were then dried in a vacuum oven at 110°C.

5.3.3. Physical Characterization

Elemental analysis was performed using inductively coupled mass spectrometry (ICP-MS). Solids were digested in concentrated aqua regia (3 parts HCl: 1 part HNO_3) overnight and then serially diluted to samples concentrations of 2, 20, and 200 ppb. These were then analyzed for Pt and Ni content on a Thermo Scientific iCAP Q that was calibrated to a blank, an internal standard, and three Pt-Ni standards. The Pt wt% was calculated assuming only Pt and Ni were present in each sample.

Scanning electron microscopy (SEM) and energy dispersive X-ray spectroscopy (EDS) were performed via JEOL JSM-700F field emission SEM, after mounting materials onto C tape. Samples for transmission electron microscopy (TEM) were prepared by gently dabbing holey C/Cu grids across the powders, after loosening the clumped material as necessary with a spatula. Scanning TEM (STEM) imaging and corresponding EDS maps were taken on an FEI FX200 Talos

operated at 200 kV. EDS data were acquired and processed with Bruker ESPRIT 1.9 software and presented as maps with signal average as a 3x3 pixel array (minimum binning possible with 9 pixels, e.g., 1 pixel with its surrounding neighbors).

Powder x-ray diffraction (XRD) measurements were collected using a Bruker D2 Phaser with a Cu source operating at 300 W and a Lynxeye 1D detector. Each sample was loaded onto a Si zero diffraction plate (MTI) and rotated at 60 rpm during a 65-minute scan over 2θ values from 35-80°.

Hydrogen chemisorption surface area was measured using a Quantachrome Autosorb-1. After weighing and being loaded into an analysis tube with quartz wool, samples were pretreated at 250°C under pure H_2 for 2 hours. A 10-point chemisorption isotherm (equilibration of 2 min per point; tolerance = 3) was then taken at 50°C. The monolayer uptake was determined using least-squares regression of the isotherm and converted to chemisorption surface area (per g of sample) using a Pt cross-sectional area of 8Å and an adsorption stoichiometry of 2. Values were further normalized by ICP Pt wt% to determine surface area per g of Pt.

Temperature programmed desorption (TPD) experiments were conducted in a vertically-aligned 0.5" quartz tube with ~75mg catalyst packed between two 100mg sections of quartz wool under continuous-flow at atmospheric pressure. The as-received NiNW samples were pretreated to remove residual carbon formed in the manufacturing process via calcination at 300ºC under 5% O_2/He at 80 sccm for 30 minutes. All samples were then annealed at 250ºC in 50% H_2/He at a flow of 50 sccm for 1.5 hours. The reactor tubes were then purged at 250ºC under 50 sccm He for 30 minutes before cooling to 50ºC. Pure CO was then dosed onto the catalyst while He continued to flow. After CO exposure was complete, the He flow rate was dropped to 15 sccm and the temperature was ramped from 50ºC to 550ºC at 5 K min^{-1}. The reactor effluent during the

temperature ramp was analyzed with a Pfeiffer mass spectrometer in order to track CO desorption from the surface.

5.3.4. Electrochemical Characterization

Electrochemical rotating disk electrode (RDE) testing was performed in accordance with previous analysis on SGD-synthesized PtNiNWs [11]. Tests were completed in RDE half-cells with 0.1 M perchloric acid electrolyte, glassy carbon (GC) working electrode, Pt mesh counter electrode, and RHE reference electrode. Pt-Ni nanowire inks were prepared by combining 7.6 mL of water, 2.4 mL of 2-propanol, 5 μL of Nafion (5 wt%, Sigma-Aldrich), and 0.6 mg of graphitized carbon nanofibers to the catalyst. The ink was horn sonicated for 60s, bath sonicated for 20 min, and horn sonicated for 60 s. Ink aliquots (10 μL each) were pipetted onto three separate GC electrodes on inverted rotator stands and dried at 700 rpm. During drying, the ink was again sonicated (20 min bath, 30 s horn). The ink aliquots were reapplied in this fashion until a total of 50 μL of ink had been deposited onto each electrode. Three electrodes were coated from each catalyst ink.

Following a 100-cycle break-in procedure (0.025 to 1.2 V at 500 mV s^{-1}) in the RDE, electrochemical surface area (ECSA) was determined by collecting cyclic voltammograms in the potential range of 0.025-1.0 at 20 mV s^{-1} in a nitrogen-saturated electrolyte with no rotation. The hydrogen under potential desorption (H_{UPD}) charge was converted into ECSA using the Pt loading of the working electrode and the conventional hydrogen monolayer adsorption charge value in acid (210 μC cm_{Pt}^{-2}). ORR polarization curves were taken anodically at 20 mV s^{-1} in the potential range of -0.01-1.05 V at 1600 rpm in an oxygen-saturated electrolyte. ORR mass and specific activities were reported at 0.9 V. Voltammetry measurements were repeated on three separate electrodes to generate averages and standard deviations for the reported values in this work.

MEA fabrication and fuel cell testing followed the optimized procedure for SGD PtNiNWs as outlined in [23]. Inks were prepared by weighing PtNiNWs into a glass vial and adding water (0.2 ml/mg PtNi) and 1-propanol (0.8 mL/mg PtNi). The vial was then placed in a beaker filled with ice water and tip sonicated for 2 min. Following this, a 20 wt% Nafion solution (D2020, Ion Power) was added, and then ink was tip sonicated for an additional 3 min. Membrane electrodes (5 cm^2) were ultrasonic spray coated (Sonotek Ultrasonic spray system with a 25 kHz Accumist spray heat) onto Nafion 212 membranes. Cathodes were coated with the PtNiNW ink to reach a loading of 0.1-0.2 mg_{Pt} cm^{-2}. All MEAs tested utilized Pt/HSC anodes with approximately 0.25 mg_{Pt} cm^{-2}. MEAs were placed into single test cells using Sigracet SGL 25BC gas diffusion layers (25% compression) and PTF gaskets. Hydrogen-oxygen polarization curves were measured at 80°C, 100% RH, 150 kPa_{abs}, and 0.4 slpm.

5.4. Results and Discussion

5.4.1. Atomic Layer Deposition of Pt

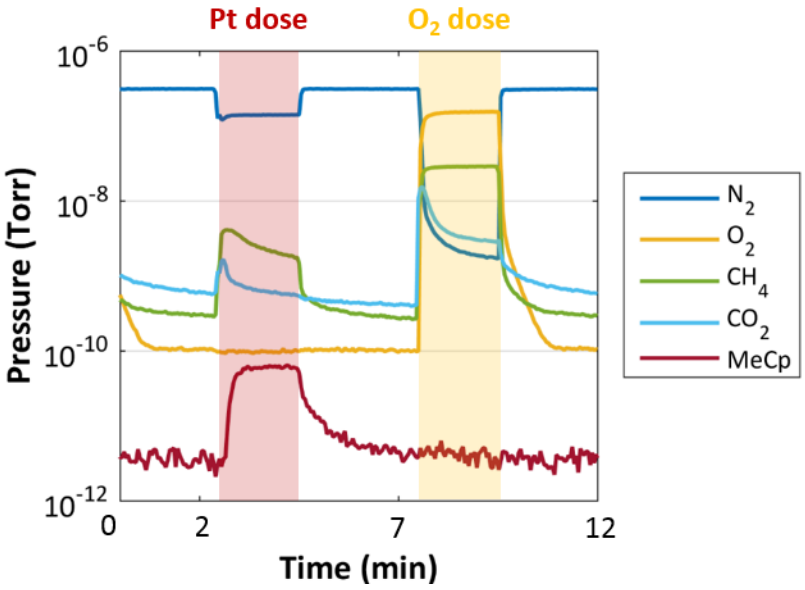

Figure 5.1: Time-resolved mass spectrometry traces of relevant *m/z* peaks during a representative Pt ALD cycle. Reactant doses are marked by colored boxes; purge steps are unmarked.

Pt ALD was performed on as-received NiNWs [22] and samples were produced at 5, 10, 20, and 30 ALD cycles in order to analyze Pt growth on this substrate. These catalysts are referred to throughout the manuscript as "as-made PtNiNWs." Representative mass spectrometry traces for relevant reaction byproducts over the course of a single Pt ALD cycle is shown in Figure 5.1. At the beginning of the $MeCpPtMe_3$ dose (denoted by the red box between 2.5 ~ 4.5 min), both CO_2 and CH_4 were detected as byproducts of the reactions on the surface of the Ni nanowires. The CO_2 contribution may result from combustion side reactions between the precursor and surface oxides [24]; the primary product, CH_4, results from adsorption of the $MeCpPtMe_3$ onto the substrate [25, 26]. This initial phase was followed by an increase and steady-state stabilization (known as "breakthrough") of the main $MeCpPtMe_3$ precursor fragment (MeCp), which indicated that the NiNW surface was saturated with adsorbed precursor molecules and the ALD half-cycle was complete. This dosing step was followed by a nitrogen purge to remove products and excess reactant gases. Dosing of O_2 (denoted by the yellow box between 7.5 ~ 9.5 min) resulted in the immediate response of CO_2 due to combustion of the adsorbed surface ligands, followed by the rapid breakthrough of O_2. The O_2 signal breakthrough implied that all reactive $MeCpPtMe_3$ ligands were removed and that only Pt, plus a thin oxide layer resulting from the O_2 exposure, remained deposited. The reactor was then purged again with N_2 to complete the ALD cycle.

5.4.2. Physical Characterization

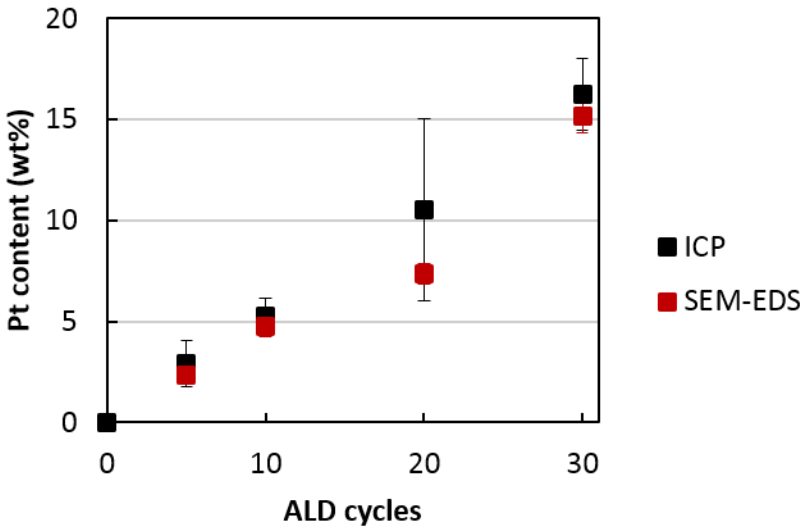

Figure 5.2: Pt content of as-made PtNiNWs as a function of ALD cycles.

The growth of Pt as a function of ALD cycles was examined using ICP-MS and SEM-EDS (Figure 5.2). Both methods showed that Pt content increased linearly with increasing ALD cycle number, as expected for oxidative Pt ALD [27]. Standard deviations for ICP data points make apparent some heterogeneity of as-made PtNiNWs within each 0.5 g sample; this was likely due to imperfect gas transport within the viscous flow reactor or variable extent of substrate oxidation in different areas of the reactor bed during the O_2 dose. Localized oxidation of the NiNW substrate may have promoted higher Pt ALD growth rates in some areas of the samples due to a higher concentration of O-based nucleation sites. Heterogeneity of the as-received NiNW substrates may have also been a contributing factor.

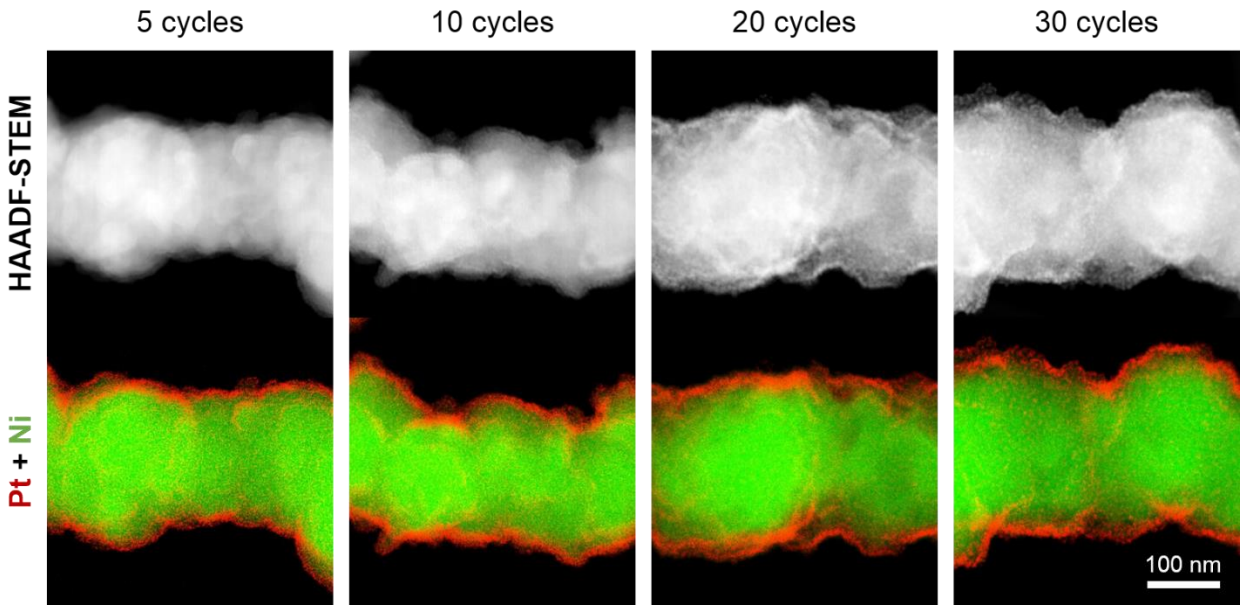

Figure 5.3: HAADF-STEM images and corresponding EDS maps of as-made PtNiNWs after 5, 10, 20, and 30 Pt ALD cycles.

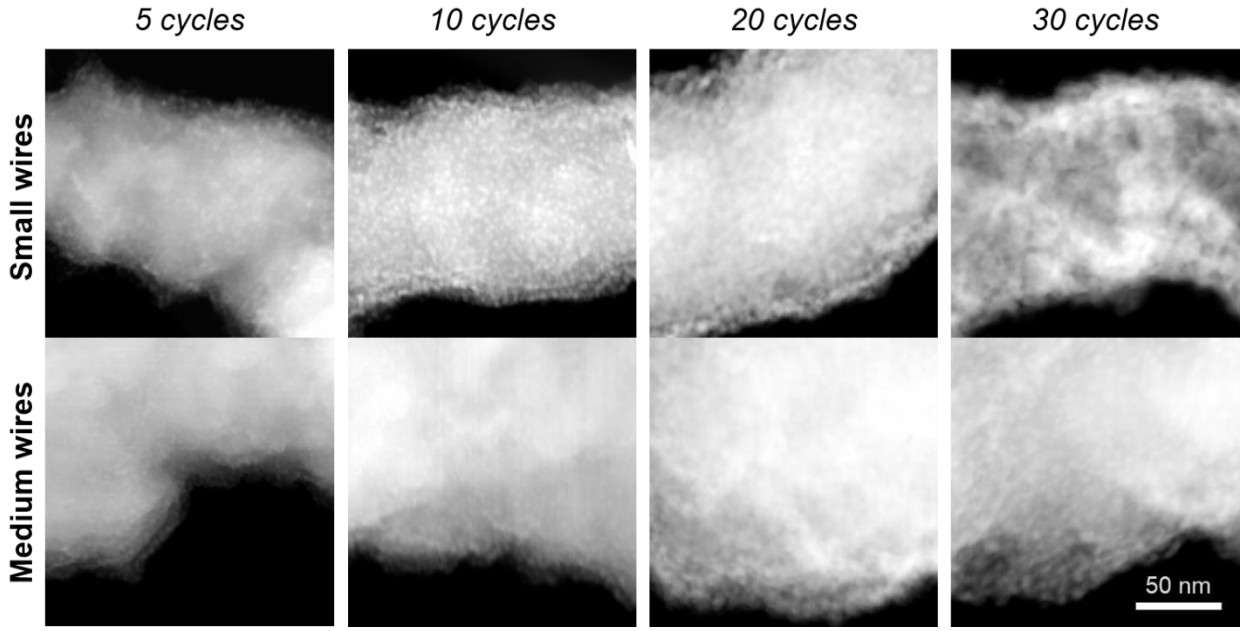

Figure 5.4: High-magnification HAADF-STEM images of as-made PtNiNWs after 5, 10, 20, and 30 Pt ALD cycles. Results are shown for small and medium diameter NiNWs, which were typical size variations in the as-received material.

HAADF-STEM images and corresponding EDS maps of as-made PtNiNWs (Figure 5.3 and Figure 5.4) were acquired after 5, 10, 20, and 30 cycles of Pt ALD. The uniform presence of

dispersed Pt nanoparticles was observed across the nanowire surface after 5 Pt ALD cycles. The propensity of Pt ALD to deposit dispersed nanoparticles in the initial stages of growth is well-established in the literature [27, 28]. There was a clear emergence of larger, more visible Pt nanoparticles seen in the progression of images taken after 10, 20, and 30 ALD cycles. This suggests that application of Pt ALD to a NiNW substrate follows the typical nucleation and self-growth behavior expected based on the observations of oxidative Pt ALD on other substrates [25, 29]. Previous studies of this chemistry showed that regeneration of the oxide surface during the O_2 dose of each ALD cycle produces favorable nucleation sites for the Pt dose in the following cycle; therefore, Pt is expected to form successively larger islands with increasing ALD cycles. Further evidence of the progressive growth of Pt nanoparticles on the NiNW surface can be observed in Figure 5S.2. It is also noteworthy that even after 30 ALD cycles on this substrate, a full uniform film of Pt has not been established. Observation of the 30 cycle PtNiNWs in Figure 5.3, Figure 5.4, and Figure 5S.2 clearly shows the continued presence of discrete, albeit large, Pt nanoparticles across the nanowire surfaces, thereby indicating that the ALD growth in this study remained in the nanoparticle regime and did not advance to the deposition of continuous films, which would be expected at higher numbers of ALD cycles [30].

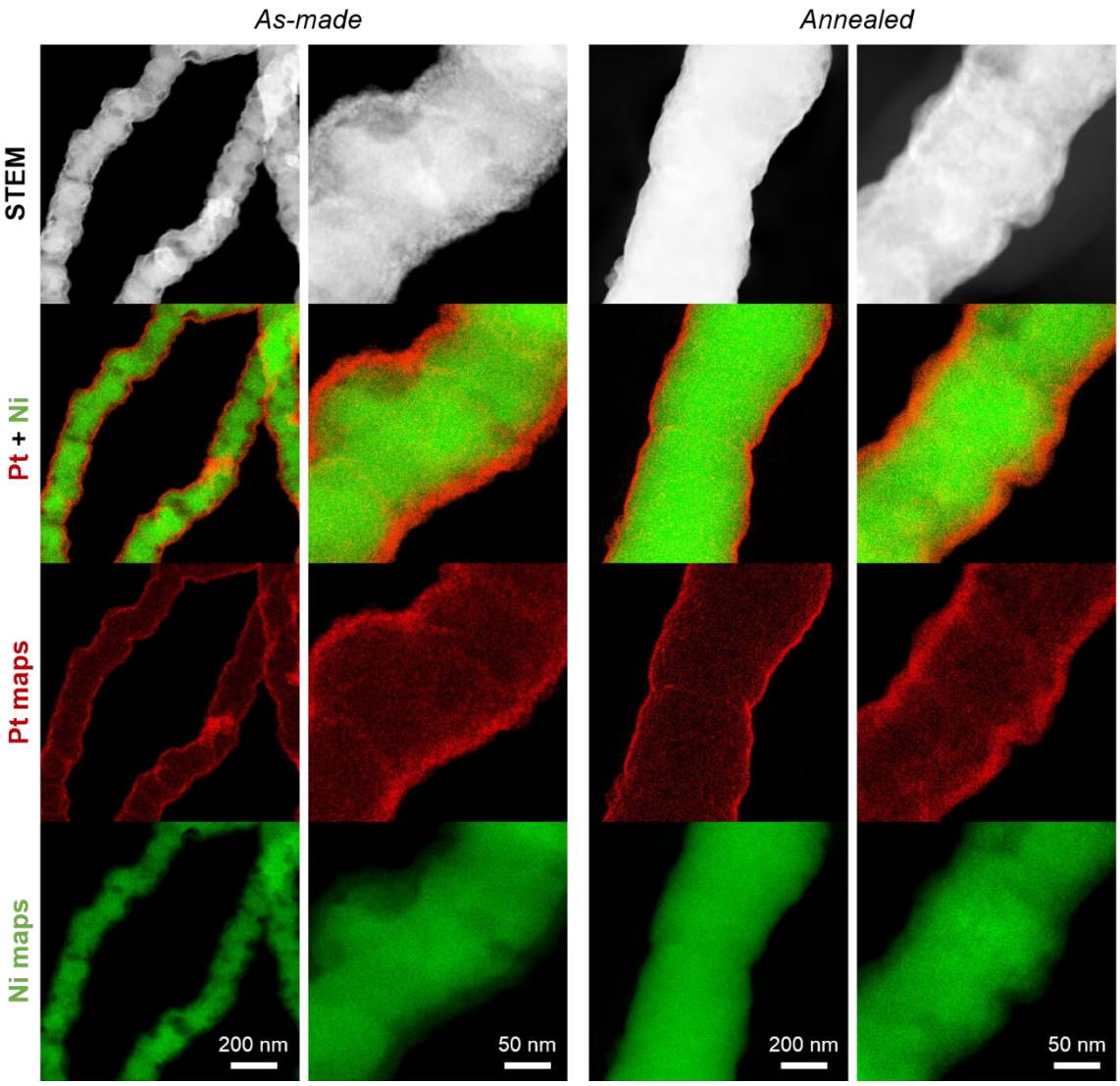

Figure 5.5: STEM images and corresponding EDS maps of 7.8 wt% Pt (20 ALD cycles) PtNiNWs as-made (left columns) and after annealing in H_2 at 250°C (right columns).

In previous work with SGD PtNiNWs, a thermal annealing treatment at 250°C under H_2 was used to promote mixing of the Pt and Ni phases and optimize electrochemical performance [11]. In order to compare the effects of this treatment on ALD PtNiNWs, all as-made catalysts in this study were annealed under H_2 at 250°C for 2 hours following ALD synthesis. Physical changes in the as-made PtNiNW structure after annealing were observed through STEM and EDS mapping (Figure 5.5). The top row of STEM figures shows that annealing treatment produced a structure with a distinctly smoother surface than the as-made material, which indicates that it was

thermodynamically favorable for the deposited Pt nanoparticles to coalesce into films under these treatment conditions. Additional STEM images in Figure 5S.3 further illustrate these physical changes on the PtNiNW surface. In addition to the thermodynamic driving force for reducing surface area, contributing factors to this physical change may include reduction of the surface Ni oxide layer and the increased surface mobility of the metallic Pt and Ni under these conditions. The corresponding elemental maps also showed a shift in the distribution of elements throughout the wires, particularly with greater Ni presence at the wire edges after annealing. Overall, the Pt and Ni phases at the wire surface were less segregated in the annealed sample, suggesting that heat treatment induced Pt diffusion into the Ni core of the wires.

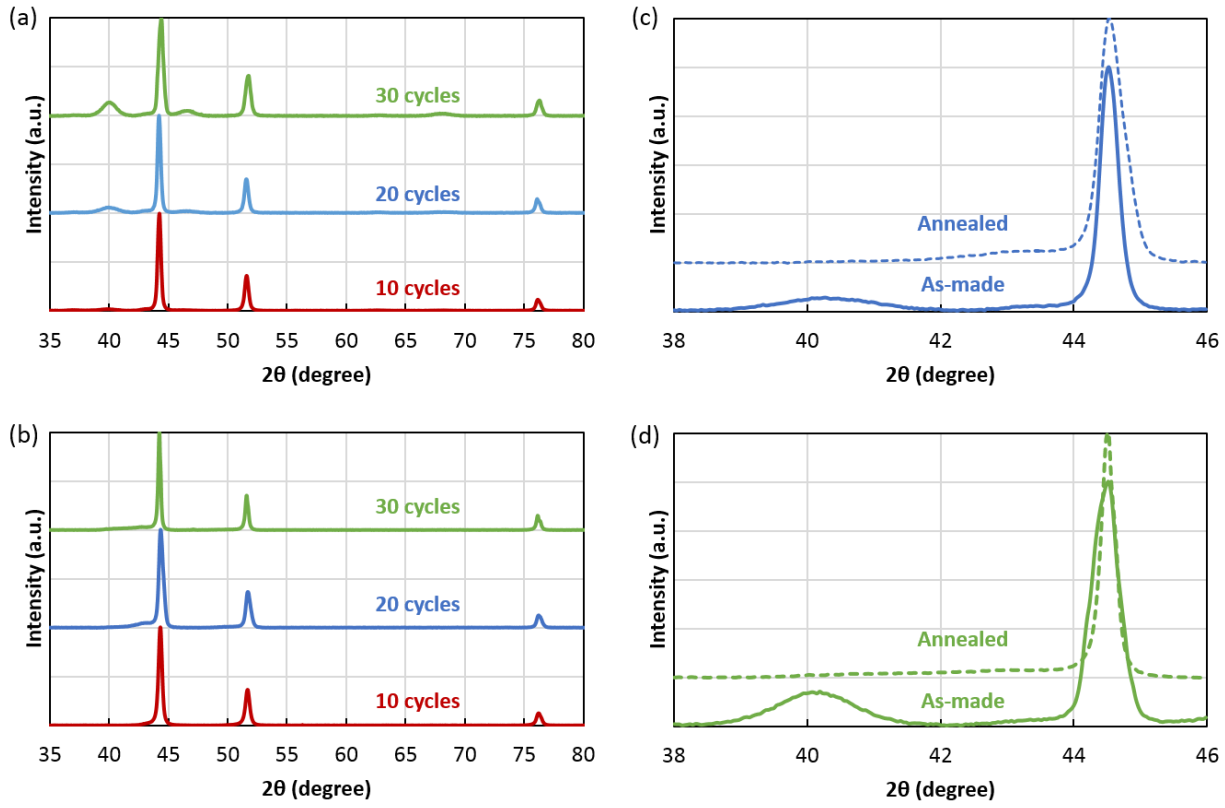

Figure 5.6: XRD patterns for PtNiNWs with >5wt% Pt: (a) full patterns for as-made catalysts; (b) full patterns for annealed catalysts; (c) selected patterns between 38-46° for 20 cycle catalyst as-made vs. annealed; (d) selected patterns between 38-45° for 30 cycle catalyst as-made vs.

annealed. Intensities of all patterns are normalized to the intensity value of the Ni(111) peak at 44.5°.

The effects of annealing on the Pt lattice were further probed through XRD analysis. It is noted that the Pt content of the 5 cycle catalysts resulted in insufficient signal for identification of Pt reflections and this catalyst was therefore omitted from these analyses. Initial diffraction patterns for the as-made catalysts provide baselines for these materials (Figure 5.6a). As Pt ALD cycles increased, the definition of the Pt(111) reflection around 40.2° also became sharper due to increased Pt content. After annealing, the corresponding patterns for each catalyst (Figure 5.6b) showed an obvious positive shift from the initial location for Pt(111) into the Ni(111) peak shoulder at 44.5°. These peak shifts are shown in greater detail in Figure 5.6c (20 cycles) and Figure 5.6b (30 cycles). Movement of the Pt(111) reflection after annealing has previously been tied to compression of the Pt lattice due to insertion of Ni during thermal treatment in SGD PtNiNWs [11] and is consistent with the qualitative changes seen in TEM (Figure 5.5 and Figure 5S.3).

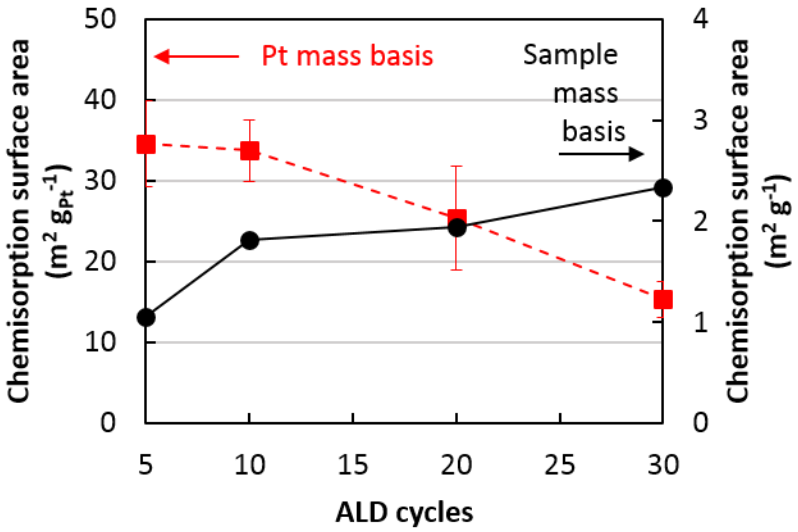

Figure 5.7: Hydrogen chemisorption surface area on a Pt mass basis and sample mass basis as a function of ALD cycles.

Chemisorption analysis with H_2 was used to quantify the Pt surface area of the ALD-modified samples after H_2 annealing at 250°C for 2 hours (Figure 5.7). Monolayer uptake data for as-made and annealed samples can be found in Figure 5S.4. As anticipated, the chemisorption surface area normalized by sample mass increased with ALD cycles; the highest amount of surface area was gained between 5 and 10 cycles. This is reflected in the qualitative differences in nanoparticle concentration and size seen between 5 and 10 cycles (Figure 5.4). However, when normalized by the corresponding Pt wt % from the ICP analysis, the chemisorption surface area showed a downward trend after 5 cycles, as additional ALD cycles resulted in greater loss of surface area. At higher numbers of ALD cycles, the additional deposited Pt mass did not increase the Pt surface area, therefore the overall utilization of Pt on the catalyst decreased. The observed trend in Pt-normalized chemisorption surface area is consistent with the increased particle size seen in at high ALD cycle numbers in Figure 5.3 and Figure 5.4, given that the evolution of larger nanoparticles would result in greater amounts of subsurface Pt.

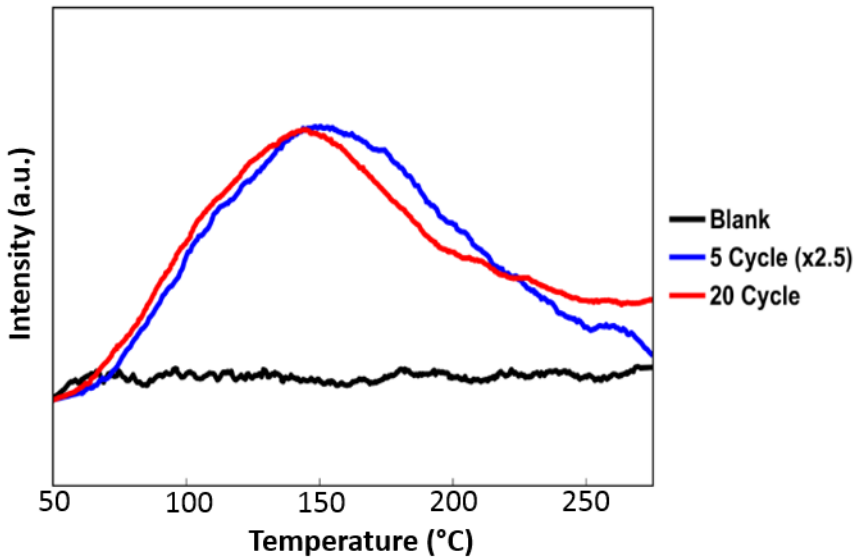

Figure 5.8: CO temperature programmed desorption traces measured from uncoated Ni nanowires and nanowires coated by 5 and 20 cycles of Pt ALD.

Temperature-programmed desorption (TPD) experiments were also conducted to provide information on the adsorbed amounts of CO on the as-received NiNWs and 5 and 20 PtNiNWs after H_2 annealing at 250°C for 2 hours. As expected, no CO desorption was detected from the uncoated wires. The integrated CO peak intensity from the 20 cycle sample was measured to be ~2.5 times greater than the 5 cycle sample, a consistent result with the surface areas reported from H_2 chemisorption data. We also analyzed the TPD peak shapes for the 5 and 20 cycle samples in an effort to identify any measurable shifts in CO desorption temperature. It is generally expected that the CO binding energy (and thus desorption temperature) will exhibit some sensitivity to the Ni content of the wires and the Pt nanoparticle size. However, as demonstrated in Figure 5.8, any shift in the desorption temperature with changing Pt loading was subtle; the small offset between peaks does not appear to be significant within the experimental reproducibility.

5.4.3. Electrochemical Characterization (As-made and Annealed)

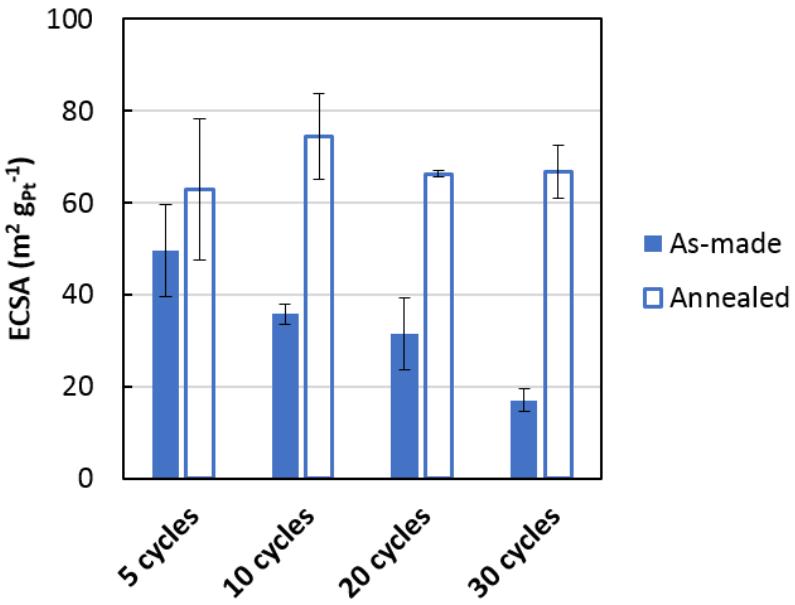

Figure 5.9: Electrochemical surface areas of as-made and annealed PtNiNWs at a range of ALD cycles.

Figure 5.9 displays the electrochemical surface area (ECSA) results for all catalysts as-made and annealed. Corresponding cyclic voltammograms can be found in Figure 5S.5 and Figure 5S.6. As anticipated based on increasing Pt nanoparticle size (Figure 5.3 and Figure 5.4), ECSA of as-made samples decreased in a relatively linear fashion with increasing ALD cycles. Annealing increased the ECSA of catalysts at all ALD cycles, which may seem unexpected given that smoother surfaces produced by annealing (Figure 5.5 and Figure 5S.3) should theoretically have a lower surface area. This expected decrease in surface area after annealing is also suggested by the chemisorption monolayer uptake data in Figure 5S.4. However, in this study, the RDE testing environment may have caused further changes in surface morphology that were not reflected in the STEM images and chemisorption data recorded with the annealed catalysts. The increased presence of Ni in the Pt phase indicated by XRD (Figure 5.6) likely created a surface that was more prone to etching in the aqueous electrolyte (0.1 M $HClO_4$) during RDE testing. Given that Ni is prone to dissolution upon exposure to acid and potential cycling [10], it is possible that some of this surface Ni was partially leached away during the electrochemical break-in step—thereby restructuring the extended surface to have additional roughness with higher ECSA than the as-made catalysts. Additionally, unlike the Pt chemisorption surface area (Figure 5.7), there did not appear to be a statistically significant trend for annealed Pt ECSA with increasing ALD cycles. These observations imply that the elimination of discrete nanoparticles and subsequent creation of an extended surface during annealing also eliminated the surface area-particle size relationship observed in the as-made samples.

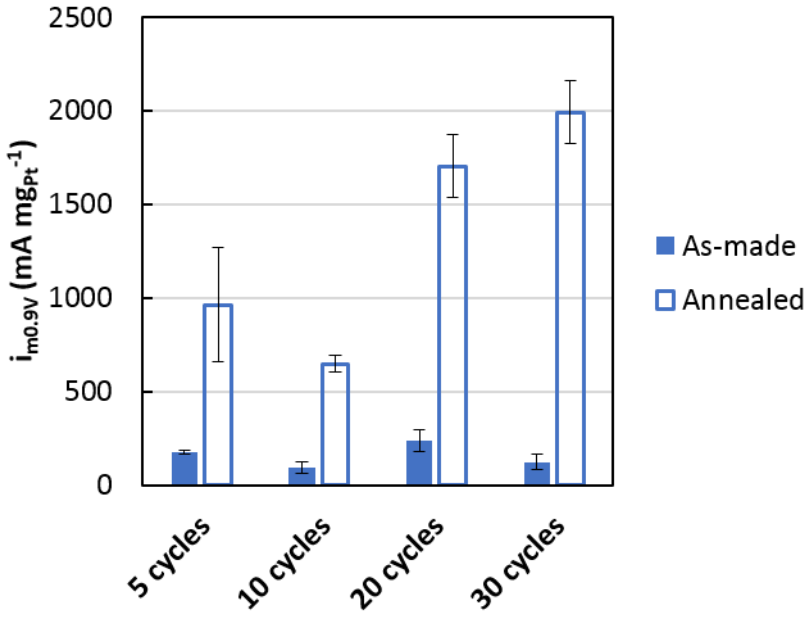

Figure 5.10: Mass activities of as-made and annealed PtNiNWs at a range of ALD cycles.

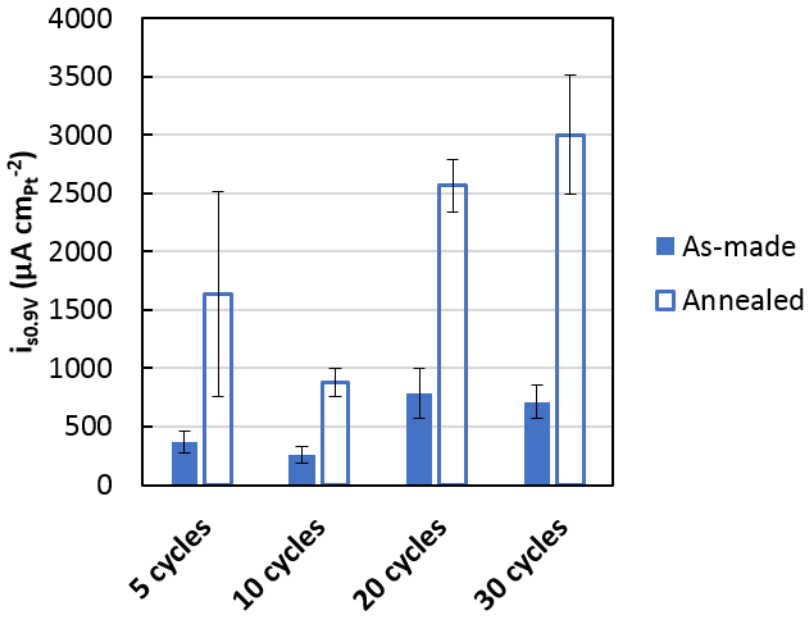

Figure 5.11: Specific activities of as-made and annealed PtNiNWs at a range of ALD cycles.

Oxygen reduction activities for all as-made and annealed catalysts are displayed in Figure 5.10 and Figure 5.11, with corresponding polarization curves in Figure 5S.5 and Figure 5S.6. Both mass (Figure 5.10) and specific activities (Figure 5.11) were significantly impacted by the H_2

annealing step, with the thermal process producing a 16-fold and 4-fold increase in mass activity ($i_{m0.9V}$) and surface activity ($i_{s0.9V}$), respectively, in the as-made 30 cycle catalyst. Analysis of the polarization curves of as-made (Figure 5S.5b) and annealed (Figure 5S.6b) PtNiNWs shows that annealing both dramatically increased the limiting currents of all as-made catalysts and shifted their half-wave potentials to more positive voltages. Electrochemical performance of all as-made PtNiNWs was unremarkable, which may be due in part to the presence of surface Ni surface oxides that accumulated during Pt ALD the O_2 half-cycles. The hydrogen atmosphere during annealing may have partially reduced these oxide species, thereby providing some activity benefit by creating a catalyst with more metallic character. However, compression of the Pt lattice, as was observed in XRD patterns for annealed materials (Figure 5.6), has previously been shown to weaken Pt-O binding interactions and enhance ORR activity [5, 31], and thus is likely the most significant contributor to the large activity increase of the annealed PtNiNWs.

Measured activity values appeared to trend upwards with increasing numbers of ALD cycles for annealed catalysts. It is possible that lattice compression in higher Pt wt% catalysts may produce a more optimal Pt-Pt interatomic distance at the nanowire surface. As the amount of Pt on the surface layer increases with more ALD cycles, the degree of penetration of Ni into the Pt lattice will be less for a fixed time and temperature of annealing. It has been previously shown for Pt-Ni nanoparticle catalysts that there is an optimal Pt:Ni ratio—i.e., Pt-Pt interatomic distance—at which catalytic activity is maximized [32]. A similar phenomenon may be present in the Pt-Ni extended surface catalysts studied in this work. As with the ECSA results in Figure 5.9, the fact that greater quantities of Pt in the extended surface catalysts was not detrimental to catalyst performance suggests that particle size was no longer a determining factor in activity after annealing.

In addition to an improvement over the as-made material, the annealed 30 cycle sample ($i_{m0.9V}$ = 1993 mA mg_{Pt}^{-1}) exhibited a mass activity almost four times higher than a benchmark Pt/HSC catalyst (500 mA mg_{Pt}^{-1}) [11]. In comparison to other advanced Pt-based catalysts in the literature, the mass activity of our annealed ALD PtNiNWs also surpasses PtPd nanodendrites (241 mA mg_{Pt}^{-1}) [33] and PtIrNi core-shell catalysts (1400 mA mg_{Pt}^{-1}) [34]. However, it is lower than recently reported advanced catalysts such as 1D PtNi nanostructures (4150 mA mg_{Pt}^{-1}) [4] and various polyhedron-designed Pt-based nanocrystal catalysts (>5000 mA mg_{Pt}^{-1}) [35]. The most direct comparison to these ALD PtNiNWs is the previously-discussed extended surface electrocatalysts produced through SGD. An optimized 7.3 wt% Pt PtNiNW catalyst that underwent the same H_2 annealing process was found to have considerably higher mass activity ($i_{m0.9V}$ = 5213 mA mg_{Pt}^{-1}) [11] than these ALD materials in RDE studies. This may be due to the presence of surface oxides in the ALD materials that were absent from the SGD catalysts. Though the ALD PtNiNWs were subjected to the same annealing procedure, the final degree of oxidation in the annealed SGD materials is likely lower, as no oxygen was purposefully introduced during this solution-phase synthesis method.

5.4.4. Electrochemical Characterization (Acid-leached)

Due to concerns over transition metal dissolution during fuel cell operation, it has been previously established that an acid preleaching step is essential in order to optimize the performance of SGD PtNiNWs in fuel cells and prevent the buildup of metal ions in the PEMFC membrane [23]. In order to directly compare the device performance of ALD PtNiNWs, a separate batch of PtNiNWs with 7-8 wt% Pt was synthesized using the ALD method described above and annealed under the same conditions. This batch was subjected to an additional acid leaching treatment to remove unalloyed Ni, such that the acid-leached PtNiNWs had 80 wt% Pt. The

electrochemical performance of these acid-leached ALD PtNiNWs was examined in RDE in the same manner as as-made and annealed catalysts. The acid-leached ALD PtNiNWs were also incorporated into MEAs and used in fuel cell tests.

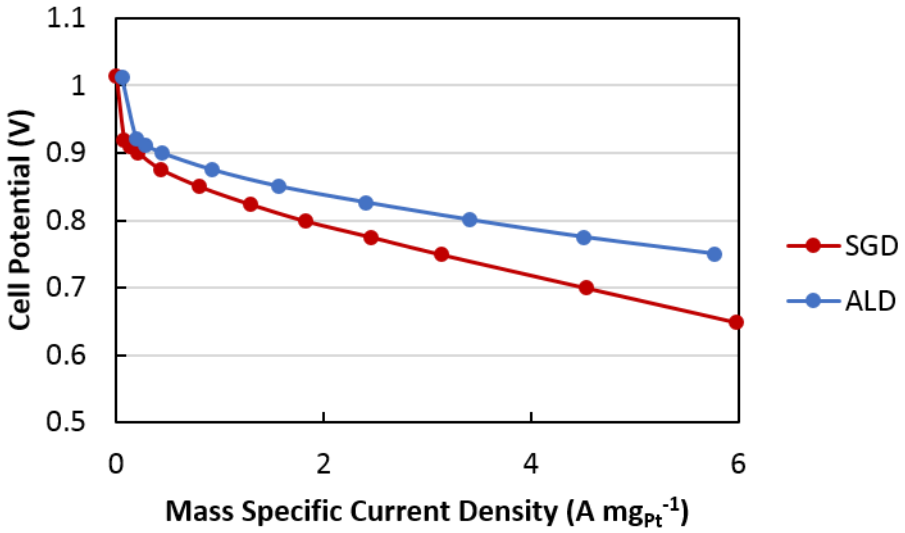

Figure 5.12: Fuel cell polarization curves for acid-leached SGD PtNiNWs (from [23]) and acid-leached ALD PtNiNWs.

Table 5.1: Mass activities for acid-leached SGD PtNiNWs (from [23]) and acid-leached ALD PtNiNWs in RDE analysis and MEA fuel cell analysis.

$i_{m0.9V}$ (mA mg_{Pt}^{-1})	SGD PtNiNWs	ALD PtNiNWs
RDE	518	700
MEA	238	577

Table 5.1 demonstrates that after acid leaching, both the SGD and ALD PtNiNWs showed considerable performance loss relative to their annealed counterparts in RDE analysis. This was expected due to the documented effects of acid leaching on the structure of these transition metal nanowire substrates [11, 23], though it is noteworthy that the acid leached-ALD PtNiNWs exhibited a higher mass activity than SGD PtNiNWs—a reversal from the RDE results with annealed materials. Figure 5.12 and Table 5.1 show that when incorporated into MEAs and tested

in a fuel cell, the acid-leached ALD PtNiNWs again outperformed acid-leached SGD materials. Additionally, acid-leached ALD PtNiNWs were found to surpass the DOE 2020 target for mass activity in fuel cells ($i_{m0.9V}$ = 440 mA mg_{Pt}^{-1}). The improved performance of ALD materials over SGD after acid leaching may be due to the introduction of an oxide during the ALD fabrication process. Though it likely contributed to the comparatively low maximum activity in the annealed ALD samples, the presence of a surface oxide may have imparted structural stability to the ALD PtNiNWs during acid leaching, resulting in a product with superior performance in the fuel cell environment. Further research will be required to examine the physiochemical properties of acid-leached ALD PtNiNWs and optimize their incorporation into MEAs, but the preliminary results discussed here clearly demonstrate that ALD can be used to produce high-performing extended surface catalysts. Additionally, given that this ALD procedure can reliably produce an order of magnitude more material than SGD per batch (500 mg vs. 40 mg), there is great value in the continued development of ALD as a high-throughput synthesis method for ETFECS.

5.5. Conclusions

ALD was successfully used to deposit Pt onto a Ni nanowire substrate in a vapor-phase analog to the synthesis process of spontaneous galvanic displacement, with the ability to produce gram-scale quantities of material. The ALD process was found to have a linear growth rate and followed a Pt self-growth mechanism, in which initial nucleation of Pt nanoparticles on the substrate was followed by addition of Pt mass to existing nanoparticles. The application of a thermal annealing step under H_2 caused qualitative changes in surface roughness of the PtNiNWs and was also seen to compress the Pt lattice through XRD patterns before and after annealing. In RDE analyses, electrochemical performance of the as-synthesized materials was unremarkable; however, annealing significantly increased the ECSA, mass activity, and surface activities of all

catalysts. These activity increases were primarily attributed to Ni-induced compression of the Pt lattice during the annealing step. The annealed 30 cycle PtNiNWs exhibited a mass activity almost 4 times greater than benchmark Pt/HSC, but lower than previously-reported annealed SGD PtNiNWs. Though it is a necessary step towards MEA incorporation, acid leaching was found to decrease the activity of ALD PtNiNWs in RDE. However, acid-leached ALD PtNiNWs showed superior performance over SGD materials in a single-cell fuel cell test. This catalyst's recorded mass activity of 577 mA mg_{Pt}^{-1} was also greater than the DOE 2020 activity target for fuel cells, thereby indicating the promise of extended surface electrocatalysts synthesized through a vapor-phase, high-throughput method such as ALD. Further study of MEA incorporation strategies to will be necessary to maximize Pt utilization and electrochemical durability of the ALD PtNiNWs will be examined by accelerated stress testing in the fuel cell environment.

5.6. Supplemental Information

This section contains figures with additional information.

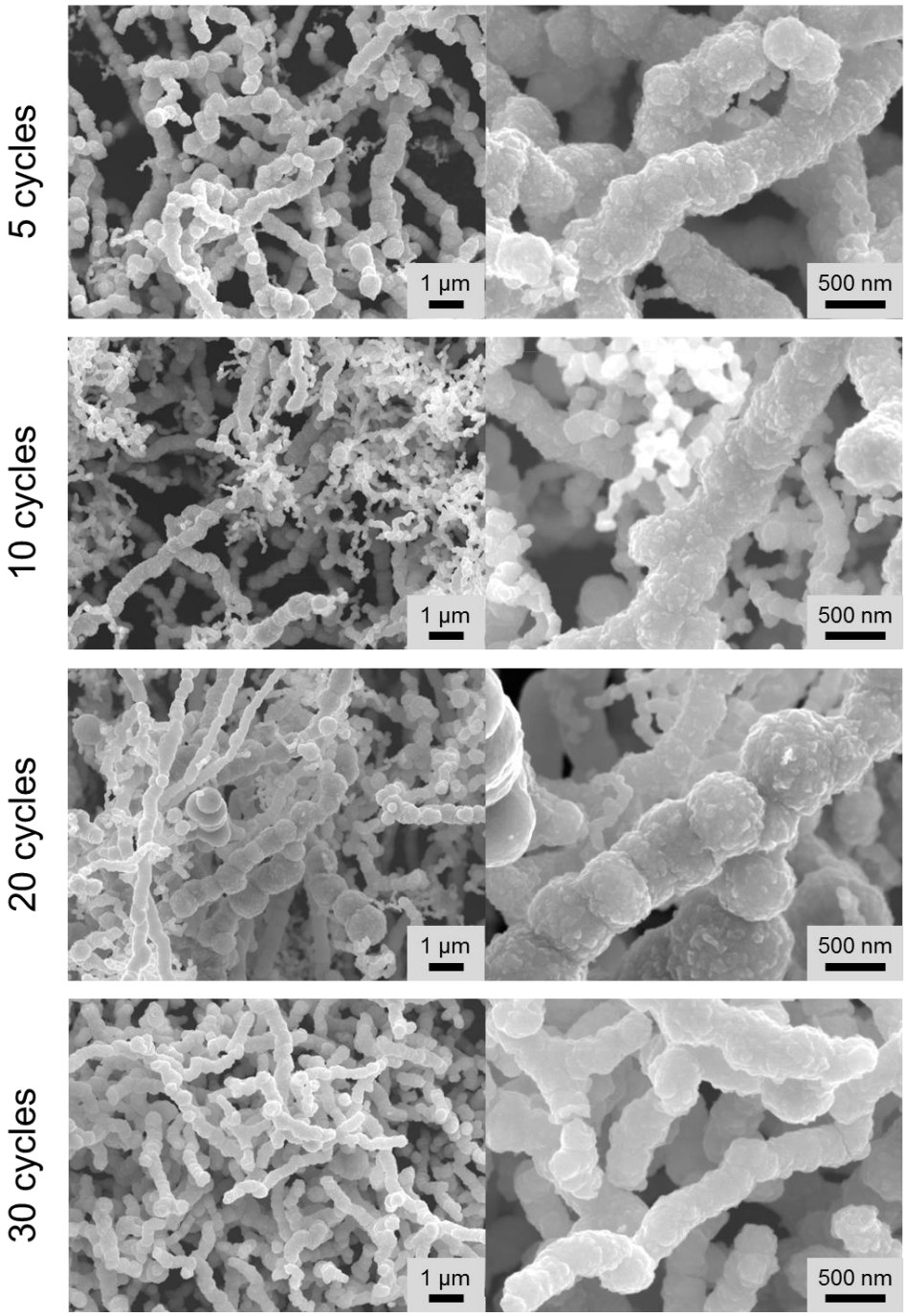

Figure 5S.1: SEM images of as-synthesized NiNWs after 5, 10, 20, and 30 cycles of Pt ALD.

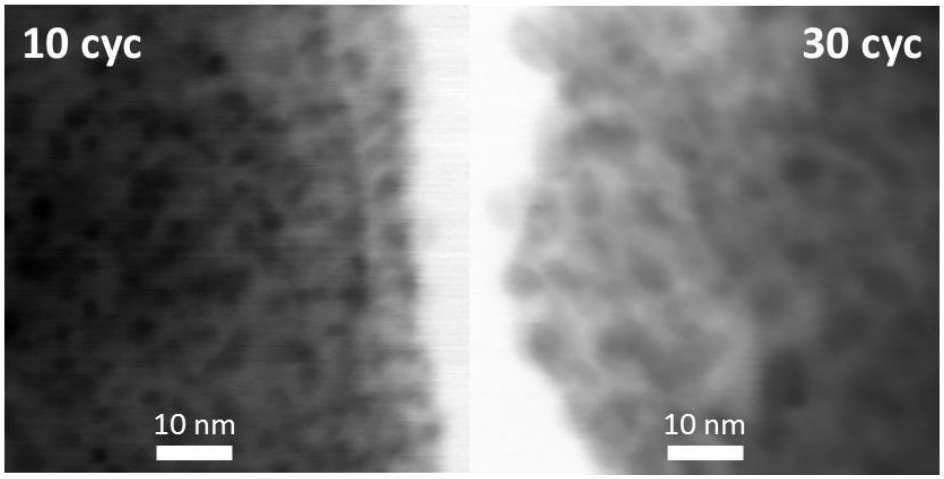

Figure 5S.2: Additional high magnification bright field STEM images illustrating the difference in Pt nanoparticle size between catalysts after 10 cycles of ALD and 30 cycles of ALD.

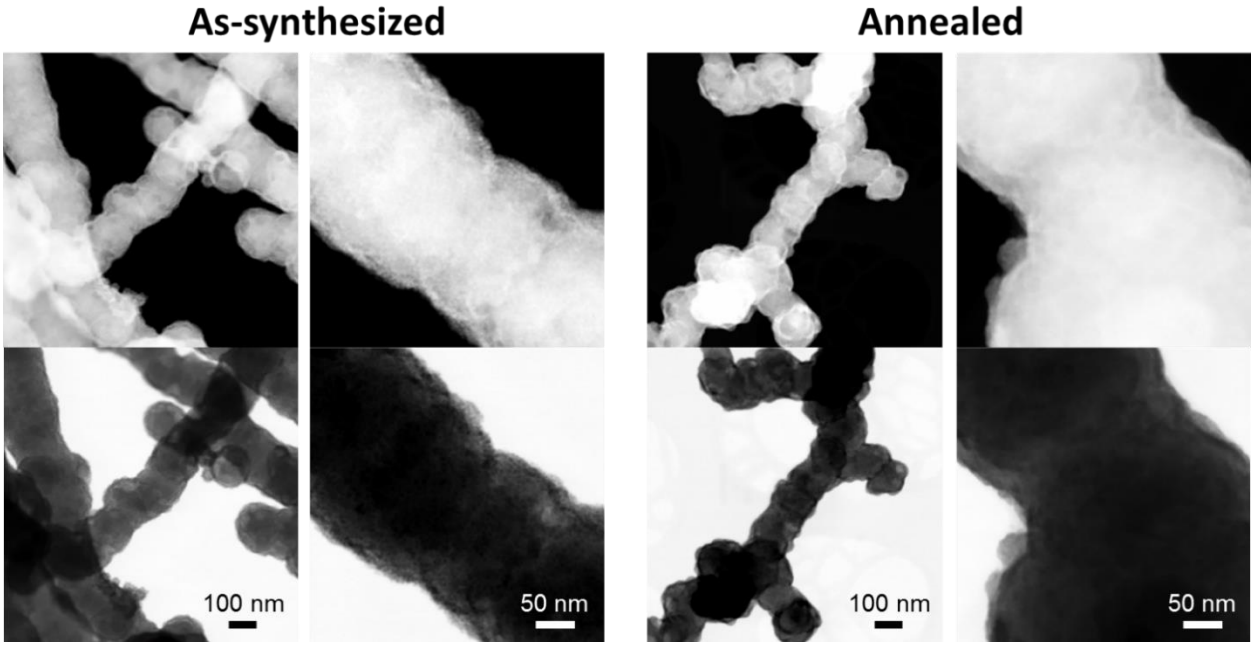

Figure 5S.3: Additional HAADF (top) and bright field (bottom) STEM images of 7.8 wt% Pt (20 cycles) before and after annealing. Differences in surface roughness before and after annealing can be observed in 50 nm scale bar images.

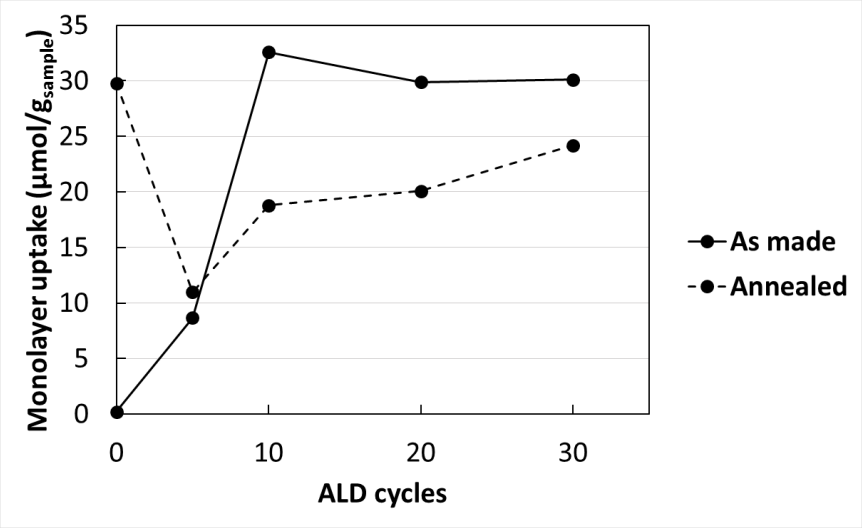

Figure 5S.4: Chemisorption H_2 monolayer uptake on a sample mass basis as-synthesized and after annealing. As-made data was extracted from an H_2 isotherm acquired at approximately 25°C, while annealed data was extracted from an H_2 isotherm at 50°C. Despite the difference in experiment temperature, the lower H_2 monolayer uptake after annealing may be corroborated with qualitatively smoother surfaces seen on annealed wires in Figures 5.5 and 5S.3.

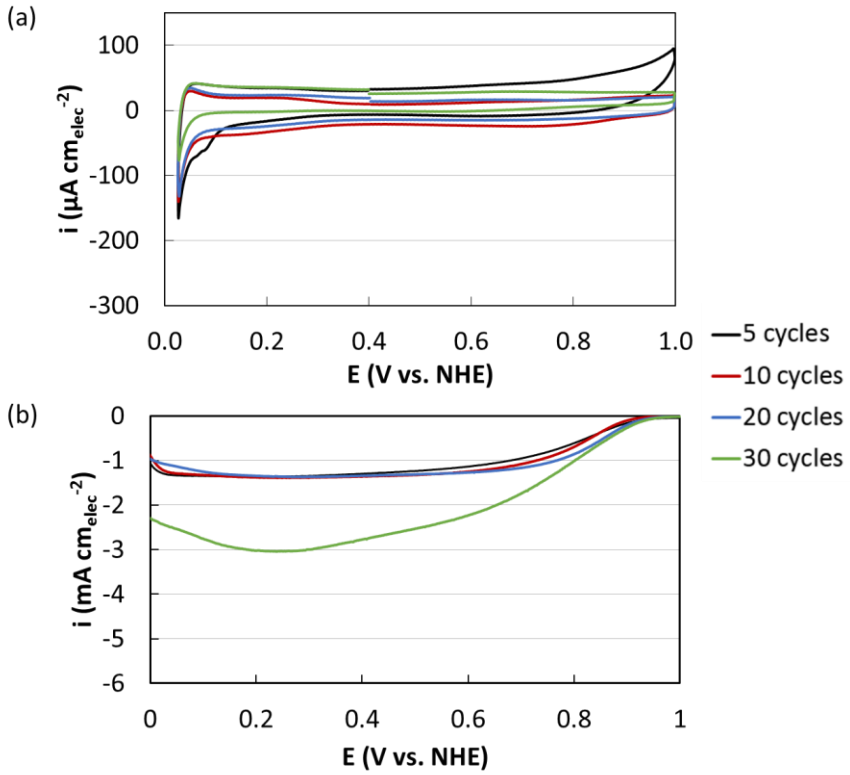

Figure 5S.5: RDE cyclic voltammograms (a) and polarization curves (b) for as-made PtNiNWs at 5, 10, 20, and 30 ALD cycles. Representative data are shown from one of the three electrodes tested for each catalyst in this study.

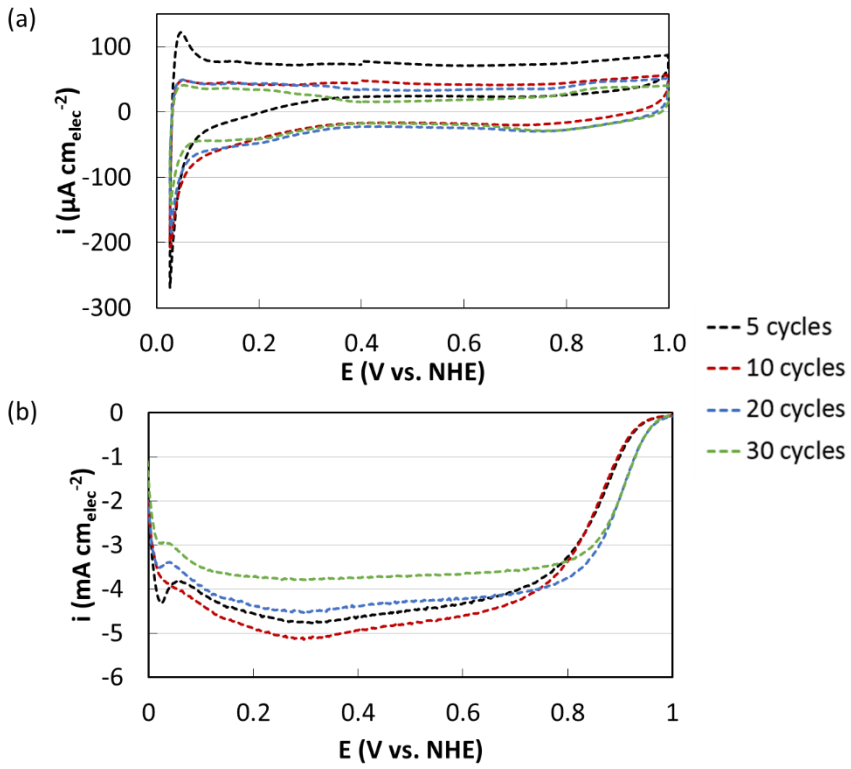

Figure 5S.6: RDE cyclic voltammograms (a) and polarization curves (b) for annealed PtNiNWs at 5, 10, 20, and 30 ALD cycles. Representative data are shown from one of the three electrodes tested for each catalyst in this study.

5.7. References

1. Kocha, S.S., *Electrochemical Degradation: Electrocatalyst and Support Durability*, in *Polymer Electrolyte Fuel Cell Degradation*, M.M. Mench, E.C. Kumbur, and T.N. Veziroglu, Editors. 2012, Elsevier: Waltham, MA.

2. Virkar, A.V. and Y. Zhou, *Mechanism of Catalyst Degradation in Proton Exchange Membrane Fuel Cells.* Journal of The Electrochemical Society, 2007. **154**(6): p. B540-B547.

3. Alia, S.M., Y.S. Yan, and B.S. Pivovar, *Galvanic displacement as a route to highly active and durable extended surface electrocatalysts.* Catalysis Science & Technology, 2014. **4**(10): p. 3589-3600.

4. Bu, L., et al., *A General Method for Multimetallic Platinum Alloy Nanowires as Highly Active and Stable Oxygen Reduction Catalysts.* Advanced Materials, 2015. **27**(44): p. 7204-7212.

5. Stamenkovic, V., et al., *Changing the Activity of Electrocatalysts for Oxygen Reduction by Tuning the Surface Electronic Structure.* Angewandte Chemie, 2006. **118**(18): p. 2963-2967.

6. Stamenkovic, V.R., et al., *Trends in electrocatalysis on extended and nanoscale Pt-bimetallic alloy surfaces.* Nature Materials, 2007. **6**(3): p. 241-247.

7. Greeley, J., et al., *Alloys of platinum and early transition metals as oxygen reduction electrocatalysts.* Nature Chemistry, 2009. **1**(7): p. 552-556.

8. Alia, S.M., et al., *Platinum-Coated Nickel Nanowires as Oxygen-Reducing Electrocatalysts.* ACS Catalysis, 2014. **4**(4): p. 1114-1119.

9. Alia, S.M., et al., *Platinum Nickel Nanowires as Methanol Oxidation Electrocatalysts.* Journal of The Electrochemical Society, 2015. **162**(12): p. F1299-F1304.

10. Alia, S.M., et al., *Oxidation of Platinum Nickel Nanowires to Improve Durability of Oxygen-Reducing Electrocatalysts.* Journal of The Electrochemical Society, 2016. **163**(3): p. F296-F301.

11. Alia, S.M., et al., *Exceptional Oxygen Reduction Reaction Activity and Durability of Platinum–Nickel Nanowires through Synthesis and Post-Treatment Optimization.* ACS Omega, 2017. **2**(4): p. 1408-1418.

12. Alia, S.M. and B.S. Pivovar, *Extended Surface Electrocatalyst Development*, in *2018 Annual Merit Review and Peer Evaluation Meeting*. 2018, DOE Hydrogen and Fuel Cells Program: https://www.hydrogen.energy.gov/pdfs/review18/fc142_pivovar_2018_o.pdf.

13. Lu, J., J.W. Elam, and P.C. Stair, *Atomic layer deposition—Sequential self-limiting surface reactions for advanced catalyst "bottom-up" synthesis.* Surface Science Reports, 2016. **71**(2): p. 410-472.

14. Van Bui, H., F. Grillo, and J.R. van Ommen, *Atomic and molecular layer deposition: off the beaten track.* Chemical Communications, 2016. **53**(1): p. 45-71.

15. Dai, P., et al., *Solar hydrogen generation by silicon nanowires modified with platinum nanoparticle catalysts by atomic layer deposition.* Angewandte Chemie International Edition, 2013. **52**(42): p. 11119-11123.

16. Meng, X., et al., *Atomic layer deposition for nanomaterial synthesis and functionalization in energy technology.* Materials Horizons, 2017. **4**(2): p. 133-154.

17. Li, J., et al., *Highly dispersed Pt nanoparticle catalyst prepared by atomic layer deposition.* Applied Catalysis B: Environmental, 2010. **97**(1-2): p. 220-226.

18. Liu, C., et al., *Atomic layer deposition of platinum nanoparticles on carbon nanotubes for application in proton-exchange membrane fuel cells.* Small, 2009. **5**(13): p. 1535-1538.

19. Lubers, A.M., et al., *Proton Exchange Membrane Fuel Cell Flooding Caused by Residual Functional Groups after Platinum Atomic Layer Deposition.* Electrochimica Acta, 2017. **237**: p. 192-198.

20. Cheng, N., Banis, M.N., Liu, J., Riese, A., Mu, S., Li, Ruying, Sham, T-S, Sun, X., *Atomic Scale Enhancement of Metal-Support Interactions Between Pt and ZrC for Highly Stable Electrocatalysts.* Energy & Environmental Science, 2015. **8**: p. 1450-1455.

21. Zhang, K., et al., *A highly active, stable and synergistic Pt nanoparticles/Mo2C nanotube catalyst for methanol electro-oxidation.* NPG Asia Materials, 2015. **7**(1): p. e153-e153.

22. Pivovar, B.S., *Extended Surface Electrocatalyst Development*, in *2017 Annual Merit Review and Peer Evaluation Meeting*. 2017, DOE Hydrogen and Fuel Cells Program: https://www.hydrogen.energy.gov/pdfs/review17/fc142_pivovar_2017_o.pdf.

23. Mauger, S.A., et al., *Fuel Cell Performance Implications of Membrane Electrode Assembly Fabrication with Platinum-Nickel Nanowire Catalysts.* Journal of The Electrochemical Society, 2018. **165**(3): p. F238-F245.

24. Aaltonen, T., et al., *Reaction Mechanism Studies on Atomic Layer Deposition of Ruthenium and Platinum.* Electrochemical and Solid-State Letters, 2003. **6**(9): p. C130-C133.

25. Setthapun, W., et al., *Genesis and Evolution of Surface Species during Pt Atomic Layer Deposition on Oxide Supports Characterized by in Situ XAFS Analysis and Water-Gas Shift Reaction.* Journal of Physical Chemistry C, 2010. **114**: p. 9758-9771.

26. Lubers, A.M., et al., *Mechanistic studies for depositing highly dispersed Pt nanoparticles on carbon by use of trimethyl(methylcyclopentadienyl)platinum(IV) reactions with O2 and H2.* Journal of Nanoparticle Research, 2015. **17**(4): p. 179.

27. Christensen, S.T., et al., *Controlled growth of platinum nanoparticles on strontium titanate nanocubes by atomic layer deposition.* Small, 2009. **5**(6): p. 750-757.

28. King, J.S., et al., *Ultralow Loading Pt Nanocatalysts Prepared by Atomic Layer Deposition on Carbon Aerogels.* Nano Letters, 2008. **8**(8): p. 2405-2409.

29. Gould, T.D., et al., *Controlling Nanoscale Properties of Supported Platinum Catalysts through Atomic Layer Deposition.* ACS Catalysis, 2015. **5**(2): p. 1344-1352.

30. Zhu, Y., K.A. Dunn, and A.E. Kaloyeros, *Properties of ultrathin platinum deposited by atomic layer deposition for nanoscale copper-metallization schemes.* Journal of Materials Research, 2007. **22**(05): p. 1292-1298.

31. Sha, Y., et al., *Mechanism for Oxygen Reduction Reaction on Pt3Ni Alloy Fuel Cell Cathode.* The Journal of Physical Chemistry C, 2012. **116**(40): p. 21334-21342.

32. Yang, H., et al., *Structure and Electrocatalytic Activity of Carbon-Supported Pt-Ni Alloy Nanoparticles Toward the Oxygen Reduction Reaction.* Journal of Physical Chemistry B, 2004. **108**: p. 11024-11034.

33. Lim, B., et al., *Pd-Pt Bimetallic Nanodendrites with High Activity for Oxygen Reduction.* Science, 2009. **234**: p. 1302-1305.

34. Kuttiyiel, K.A., et al., *Bimetallic IrNi core platinum monolayer shell electrocatalysts for the oxygen reduction reaction.* Energy & Environmental Science, 2012. **5**(1): p. 5297-5304.

35. Wang, Y.-J., et al., *Unlocking the door to highly active ORR catalysts for PEMFC applications: polyhedron-engineered Pt-based nanocrystals.* Energy & Environmental Science, 2018. **11**(2): p. 258-275.

CHAPTER 6

DEVELOPMENT OF BIMETALLIC PLATINUM-NICKEL ALD FOR EXTENDED THIN FILM ELECTROCATALYST STRUCTURES

6.1. Abstract

Atomic layer deposition, or ALD, has been demonstrated as an effective, reproducible method to synthesize extended thin film electrocatalyst structures (ETFECS) as high-performing catalysts for the cathodic oxygen reduction reaction (ORR) in polymer electrolyte membrane fuel cells (PEMFCs). This work details the development of a bimetallic Pt-Ni ALD process on a cobalt nanowire (CoNW) substrate to improve control over the final composition of the catalysts after an acid pre-leaching step, which is necessary for fuel cell stability. The tunability of the bimetallic ALD process was examined by synthesizing a range of catalysts at various ALD temperatures and Pt-Ni ALD "supercycle" configurations; the effect of in situ hydrogen annealing between ALD supercycles was also tested. The materials produced in these experiments were characterized through ICP-MS, electron microscopy, X-ray diffraction, hydrogen chemisorption, and rotating disk electrode (RDE) analysis. It was observed that acid leaching still removed undesirable amounts of the nickel that was deposited through ALD, indicating that in situ annealing is not sufficient for maintaining the deposited Pt:Ni ratio. Electrochemical performance of a subset of the synthesized materials was below that of previously-made ALD PtNiNWs, indicating the needs for further improvement of this bimetallic ALD process and subsequent treatment processes.

6.2. Introduction

In order to realize the potential of PEMFCs as power sources for advanced propulsion systems, the utilization of catalytic platinum in the cathodic ORR must be maximized [1, 2]. The

U.S. Department of Energy (DOE) has stated that platinum group metal loading on PEMFC cathodes must be reduced to below 0.10 mg cm^{-2} by 2020 from the current reported minimum of 0.125 mg cm^{-2}, while still maintaining high performance, to facilitate commercialization of these systems [3]. As the standard carbon-supported Pt nanoparticle catalyst is not sufficiently active to meet these DOE targets, the realization of these improvements will necessitate the exploration of new catalyst systems and structures.

One such intriguing area of research is the development of extended thin film electrocatalyst structures. These are systems in which the catalytic Pt is present as a thin layer spread across the surface of a high aspect ratio transition metal substrate, such as a nanowire, nanorod, or nanotube. This extended surface structure, along with Pt-M alloying effects from the transition metal substrate [4, 5], improves the utilization of Pt in the ORR, with many reported ETFECS demonstrating site-specific activities an order of magnitude higher than Pt-based nanoparticle catalysts [6, 7]. To date, most electrocatalysts of this nature are produced through a solution chemistry process, such as spontaneous galvanic displacement (SGD) [6]. The SGD process has been used to synthesize exceptionally high-performing ETFECS on the milligram scale by adding Pt to the surface of nickel or cobalt nanowires [8-11]; however, this technique was found to be difficult to scale up while retaining consistent properties of the synthesized materials [12], which may indicate the need for alternative approaches to ETFECS fabrication.

In the previous chapter, it was demonstrated that atomic layer deposition of Pt onto a Ni nanowire (NiNW) substrate could produce extended surface electrocatalysts with aqueous half-cell activities four times higher than Pt nanoparticle catalysts. Additionally, fuel cell activities of these materials were shown to surpass both the DOE 2020 target for mass activity as well as reported fuel cell activities of analogous materials synthesized via SGD. Before fuel cell testing,

both SGD and ALD materials were subjected to an acid pre-leaching step, which is essential for removing soluble transition metal from the nanowires [13]. Though the acid-leached ALD PtNiNWs still exhibited excellent device performance, the acid leaching preparation step, though necessary, represents an obstacle to the precise designation of the Pt:Ni ratio in the final catalyst material, as it is notoriously difficult to control the amount of Ni that is removed during this procedure.

With the viability of single-species ALD as a route to high-performing ETFECS established, this work aims to expand the scope of the deposition process to include both Pt and Ni, such that greater control over the metal species present in the acid-leached final catalyst may be achieved. A bimetallic Pt-Ni ALD process (shown schematically in Figure 6.1) was developed by sequentially depositing each metal at various ratios and process conditions onto a CoNW substrate. Given the demonstrated importance of thermal H_2 annealing in enhancing the ORR activity of these materials [11], various iterations of this treatment were also applied. A subset of the synthesized materials was subjected to an acid leaching to test the retention of the metallic species over this treatment. The ALD growth of Pt and Ni was examined through mass spectrometry and ICP, and the properties of the materials were probed with electron microscopy, XRD, hydrogen chemisorption, XRF, and RDE voltammetry. It was observed that ALD can be used to precisely tune the amount of Pt and Ni deposited on the CoNW substrate, but further improvements will be necessary to control the amount of transition metal removed during acid leaching and improve the electrochemical performance.

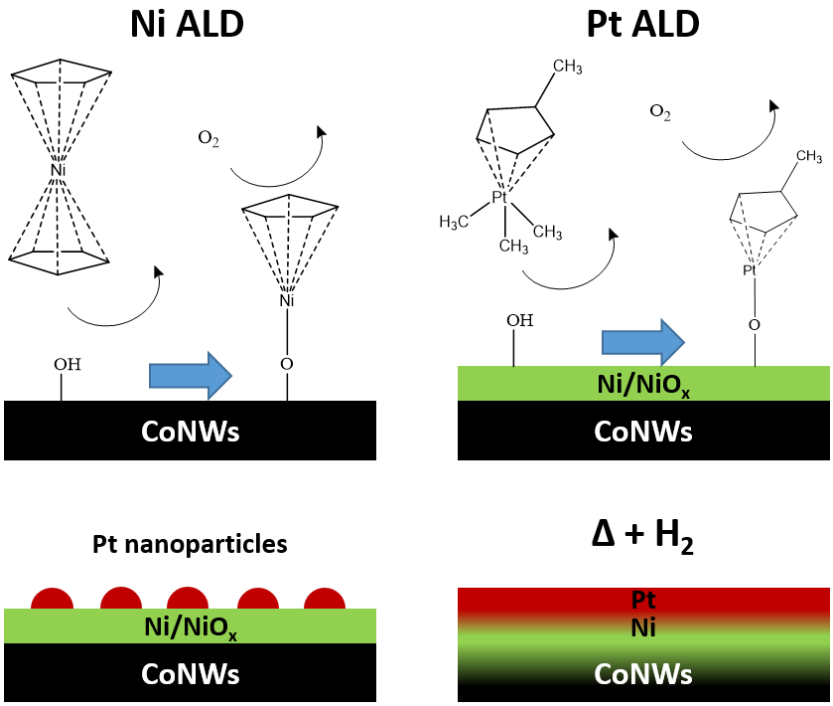

Figure 6.1: Schematic of the bimetallic Pt-Ni ALD process.

6.3. Experimental

6.3.1. Atomic Layer Deposition of Pt and Ni

Atomic layer deposition of Pt and Ni was performed under vacuum in a viscous flow reactor system as described in Chapter 5. The temperature for both ALD processes was held at 295°C, 250°C, or 210°C during the duration of synthesis, and 0.5 g of as-received cobalt nanowires (PlasmaChem) were loaded into the reactor for each batch. The Pt ALD was done using the precursor trimethyl(methylcyclopentadienyl)platinum (IV) ($MeCpPtMe_3$) as a metal source, and 5% O_2 in N_2 as a counter-reactant. The $MeCpPtMe_3$ was heated to 40°C in a stainless steel bubbler and transported to the reactor using ultrapure N_2 as a carrier gas. Each Pt ALD cycle consisted of: (1) a $MeCpPtMe_3$ dose with 10 sccm carrier gas flow rate (180 s), (2) a purge with 40 sccm N_2 flow rate (240 s), (3) a 5% O_2 dose with 45 sccm flow rate (240 s), and (4) a purge with 40 sccm N_2 flow rate (240 s). The Ni ALD utilized nickelocene ($NiCp_2$) as a metal source and 5% O_2 in N_2

as a counter-reactant. The $NiCp_2$ was heated to 95°C in a stainless steel bubbler and transported to the reactor using ultrapure N_2 as a carrier gas. Each Ni ALD cycle consisted of: (1) a $NiCp_2$ dose with 10 sccm carrier gas flow rate (360 s), (2) a purge with 40 sccm N_2 flow rate (240 s), (3) a 5% O_2 dose with 45 sccm flow rate (240 s), and (4) a purge with 40 sccm N_2 flow rate (240 s). For both processes, gases exiting the reactor were monitored using an in-line mass spectrometer (Stanford Research Systems QMS 200). Results for Pt ALD are displayed for *m/z* peaks 16 (CH_4), 28 (N_2), 32 (O_2), 44 (CO_2), and 79 (MeCp precursor fragment), while results for Ni ALD are displayed for *m/z* peaks 16 (CH_4), 28 (N_2), 32 (O_2), 44 (CO_2), 66 (Cp), and 187 ($NiCp_2$).

The Pt and Ni ALD were combined into ALD supercycles by depositing a fixed number of cycles of one metal, followed immediately by a fixed number of cycles of the other metal. The Pt:Ni supercycle ratio and the order in which the metals were deposited was varied in order to explore the range of materials that could be synthesized. A hydrogen annealing step was added between the ALD supercycles in some experiments. In these cases, ultrapure H_2 was flowed over the wires at 30 sccm for 30 minutes at the reaction temperature of 295°C.

6.3.2. Post-ALD Processing

In these experiments, annealing was either performed in situ during the ALD process (as described above) or as a pretreatment for hydrogen chemisorption. In the latter case, samples were loaded into the chemisorption analysis tube as described below and annealed under ultrapure H_2 for 2 hours at temperatures of 200°C, 250°C, 300°C, 400°C, of 500°C, depending on the specific experiment.

Acid leaching was used to remove soluble transition metals from the as-made PtNiCoNWs, as described in Chapter 5 and [13]. The PtNiCoNWs were added to 1 M H_2SO_4 in a 20 mL glass

vial at a concentration of 40 mg PtNi/mL H_2SO_4 and soaked for 20 mins in order to minimize loss of Ni. The mixture was subsequently diluted with deionized water and centrifuged at 2500 rpm for 15 min. The mixture was then decanted, and the process was repeated two more times. The rinsed wires were then dried in a vacuum oven at 110°C.

6.3.3. Physical Characterization

Elemental analysis was performed on as-made PtNiCoNWs using inductively coupled mass spectrometry (ICP-MS). Solids were digested in concentrated aqua regia (3 parts HCl: 1 part HNO_3) overnight and then serially diluted to samples concentrations of 2, 20, and 200 ppb. These were then analyzed for Pt, Ni, and Co content on a Thermo Scientific iCAP Q that was calibrated to a blank, an internal standard, and three Pt-Ni-Co standards. The metal weight loadings were calculated assuming only Pt, Ni, and Co were present in each sample. Elemental composition of leached PtNiCoNWs was analyzed using a Fisherscope XDV-SDD X-ray fluorescence (XRF) spectrometer with a 50 kV, 50 W X-ray source.

Samples for transmission electron microscopy (TEM) were prepared by gently dabbing holey C/Cu grids across the powders, after loosening the clumped material as necessary with a spatula. Scanning TEM (STEM) imaging and corresponding EDS maps were taken on an FEI FX200 Talos operated at 200 kV. EDS data were acquired and processed with Bruker ESPRIT 1.9 software and presented as maps with signal average as a 3x3 pixel array (minimum binning possible with 9 pixels, i.e., 1 pixel with its surrounding neighbors).

Powder x-ray diffraction (XRD) measurements were collected using a Bruker D2 Phaser with a Cu source operating at 300 W and a Lynxeye 1D detector. Each sample was loaded onto a

Si zero diffraction plate (MTI) and rotated at 60 rpm during a 65-minute scan over 2θ values from 35-80°.

Hydrogen chemisorption surface area was measured using a Quantachrome Autosorb-1. After weighing and loading into an analysis tube with quartz wool, samples were pretreated at variable temperatures under pure H_2 for 2 hours. A 10-point chemisorption isotherm (equilibration of 2 min per point; tolerance = 3) for H_2 was then taken at 50°C. The monolayer uptake was determined using least-squares regression of the isotherm. Surface areas for individual metal species were not calculated due to the potential for all three metals to adsorb hydrogen.

6.3.4. Electrochemical Characterization

Electrochemical RDE testing was performed in accordance with a previous analysis on SGD-synthesized PtNiNWs [11] and the procedure laid out in Chapter 5. Tests were completed in RDE half-cells with 0.1 M perchloric acid electrolyte, glassy carbon (GC) working electrode, Pt mesh counter electrode, and RHE reference electrode. Pt-Ni nanowire inks were prepared by combining 7.6 mL of water, 2.4 mL of 2-propanol, 5 μL of Nafion (5 wt%, Sigma-Aldrich), and 0.6 mg of graphitized carbon nanofibers to the catalyst. The ink was sonicated, and ink aliquots (10 μL each) were pipetted onto three separate GC electrodes on inverted rotator stands and dried at 700 rpm. The ink aliquots were reapplied in this fashion until a total of 50 μL of ink had been deposited onto each electrode. Three electrodes were coated from each catalyst ink.

Following a 100-cycle break-in procedure (0.025 to 1.2 V at 500 mV s^{-1}) in the RDE, electrochemical surface area (ECSA) was determined by collecting cyclic voltammograms in the potential range of 0.025-1.0 at 20 mV s^{-1} in a nitrogen-saturated electrolyte with no rotation. The hydrogen under potential desorption (H_{UPD}) charge was converted into ECSA using the Pt loading

of the working electrode and the conventional hydrogen monolayer adsorption charge value in acid (210 μC cm_{Pt}^{-2}). ORR polarization curves were taken anodically at 20 mV s^{-1} in the potential range of -0.01-1.05 V at 1600 rpm in an oxygen-saturated electrolyte. ORR mass and specific activities were reported at 0.9 V. Voltammetry measurements were repeated on three separate electrodes to generate averages and standard deviations for the reported values in this work.

6.4. Results and Discussion

6.4.1. Atomic Layer Deposition of Pt and Ni

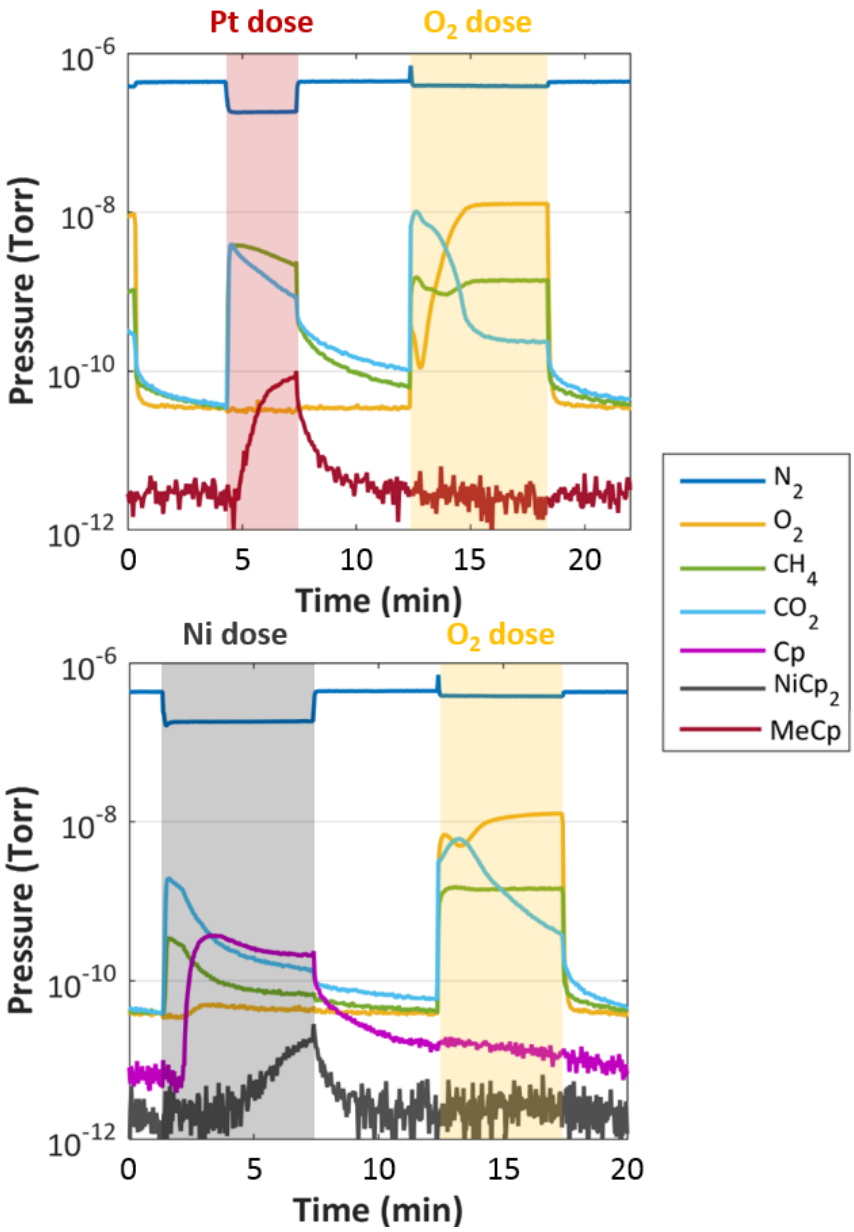

Figure 6.2: Time-resolved mass spectrometry traces of relevant *m/z* peaks during representative Pt ALD (top) and Ni ALD (bottom) cycles. Reactant doses are marked by colored boxes; purge steps are unmarked.

Representative mass spectrometry traces for a single cycle of Pt ALD and Ni ALD on the as-received CoNW substrate are shown in Figure 6.2. The Pt ALD mechanism on CoNWs

appeared to function very similarly to the deposition process observed on a NiNW substrate in Chapter 5, although more CO_2 was producing during the O_2 dose, indicating there were higher amounts of adsorbed $MeCpPtMe_3$ ligands on the surface to be combusted in this case. The Ni ALD process shown in the bottom panel began with the $NiCp_2$ dose (denoted by the grey box between 1~7 min). Initially, CO_2 was detected as the primary reaction product, which may have resulted from oxidation of the incoming nickelocene ligands by adsorbed O_2 on the surface of the CoNWs. This was followed by a rise in the signal corresponding to the Cp ring, which has been previously associated with cleavage of the ring during deposition of the precursor on the substrate [14]. Once the Cp byproduct signal fell from its maximum to a lower steady-state value, breakthrough of $NiCp_2$ peaks was observed, indicating saturation of the CoNW surface in the reactor and completion of the nickelocene dose. The O_2 dose (denoted by the yellow box between 13~17 min) proceeded much as expected, with high initial levels of CO_2 as the primary ligand combustion product, followed by the breakthrough of oxygen. These individual Pt and Ni ALD cycles were repeated at various ratios and combined into ALD supercycles in order to promote intermixing of the deposited metal species.

6.4.2. Physical Characterization

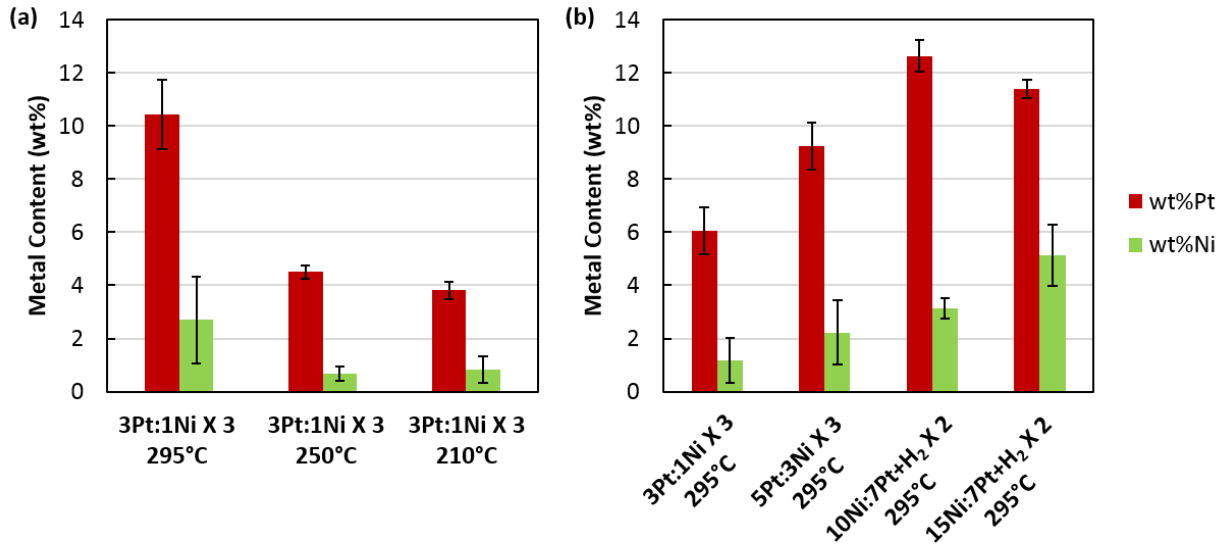

Figure 6.3: Metal content of various ALD PtNiCoNWs as measured by ICP-MS: (a) varying ALD temperature; (b) varying Pt-Ni ALD supercycle ratio and incorporating H_2 annealing step.

The growth of Pt and Ni at various ALD temperatures and supercycle configurations was analyzed using ICP-MS (Figure 6.3). The supercycle sequence is described by the number of ALD cycles of the first metal, followed by the number of cycles of the second metal as well as the number of times this sequence was repeated—e.g., 3Pt:1Ni X 3 denotes a supercycle comprised of 3 Pt ALD cycles followed by 1 Ni ALD cycle repeated three times. Figure 6.3a shows that for a given supercycle configuration, decreasing the ALD temperature decreased the amount of metal deposited; this temperature effect appeared to be stronger for Pt ALD than for Ni. This is to be expected, given that temperature is known to greatly impact mechanisms and rates for most ALD processes [15]. Figure 6.3b displays the results of a separate series of experiments in which the supercycle sequence was changed at a constant ALD temperature of 295°C. Increasing the supercycle ratio from 3Pt:1Ni to 5Pt:3Ni was observed to increase the amount of metals deposited, though, again, the amount of Pt deposited appeared to be more sensitive than Ni. In the case of the

10Ni:7Pt+H_2 X 2 and 15Ni:7Pt+H_2 X 2 samples, the order of the ALD processes was reversed, and a 30 minute H_2 annealing step at the reaction temperature was added after every supercycle. Changing the order in which the metals were added did not appear to significantly affect the final elemental content any more so than changing the number of ALD cycles in previous samples. However, comparison between these two samples showed that the amount of Ni could be increased to its highest level observed in this study by holding the amount of Pt cycles constant and increasing the amount of Ni cycles. The fact that the 15Ni:7Pt+H_2 X 2 sample required over double the amount of Ni ALD cycles than Pt ALD to produce a material in which the Ni wt% is almost half the Pt wt% illustrates that the Ni ALD rate is considerably slower than that of Pt at 295°C.

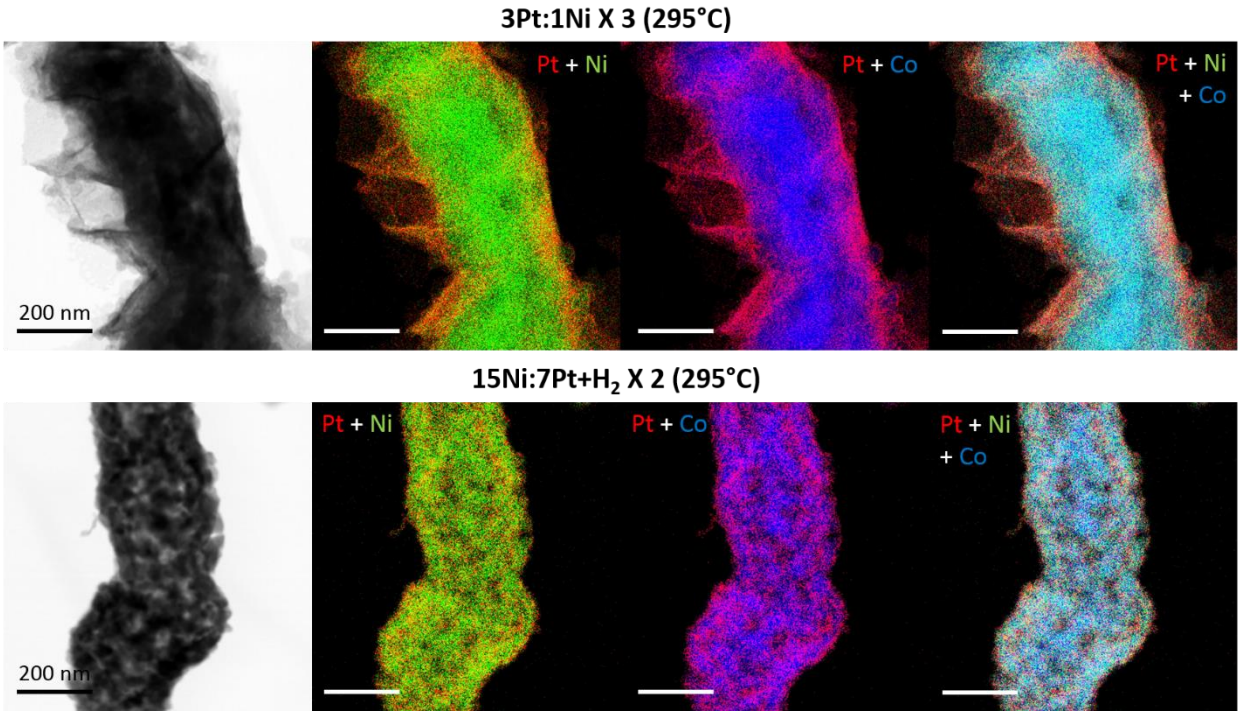

Figure 6.4: Bright field STEM images and corresponding EDS overlays of as-made 3Pt:1Ni X 3 and 15Ni:7Pt+H_2 X 2, both synthesized at 295°C.

Two of the aforementioned samples made at 295°C, 3Pt:1Ni X 3 and 15Ni:7Pt+H_2 X 2, were analyzed using STEM and EDS mapping in order to examine the differences between PtNiCoNWs synthesized with and without in situ annealing between ALD supercycles. The STEM

images of these samples and EDS overlays for Pt, Ni, and Co are shown in Figure 6.4, while individual elemental maps are provided in Figure 6S.1 and Figure 6S.2. In the initial case of 3Pt:1Ni X 3, a high degree of segregation between the Pt and Ni was observed. Though the metals were laid down in an alternating sequence, the Pt appeared to have been deposited mostly on the sheet-like structures at the edges of the wire, while Ni was more concentrated in the inner core of the wire. Based on the individual EDS maps for O, Co, and Ni (Figure 6S.1), it is likely that the sheet-like structures were comprised of both Co oxides, which may have been present in the as-received CoNWs, and Ni oxides, which were deposited during the Ni-O_2 ALD process. The Ni ALD process used in this work with $NiCp_2$ as a metal source and an oxidizing agent as a counter reactant has been previously established to deposit nickel oxide species, rather than metallic nanoparticles as is typical with Pt ALD [16-18]. Significant qualitative changes in the PtNiCoNW structure were evident in the case of the 15Ni:7Pt+H_2 X 2. All three metals present appeared to be much more thoroughly mixed with the inclusion of the H_2 annealing step, though examination of the Pt elemental map in Figure 6S.2 suggests that Pt still predominated at the wire edges. Additionally, the sheet-like structures present in the 3Pt:1Ni X 3 sample were no longer present, indicating that the metal oxide species were reduced during annealing.

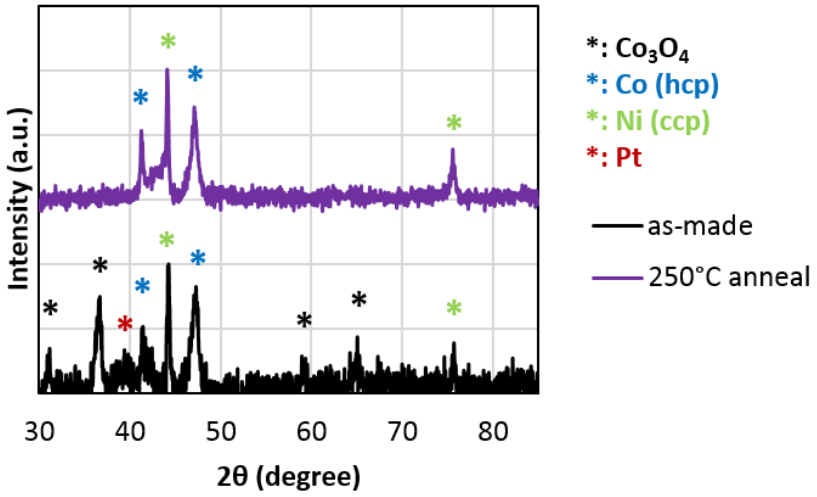

Figure 6.5: XRD patterns of PtNiCoNWs as-made and after a 250°C H_2 annealing treatment. The data shown was collected on a 6Pt:5Ni X 3 batch synthesized at 250°C (~15wt% Pt, ~4 wt% Ni).

X-ray diffraction patterns were collected on an as-made sample of 6Pt:5Ni X 3 synthesized at 250°C (~15wt% Pt, ~4 wt% Ni), as well as the same sample subjected to an ex-situ H_2 annealing step at 250°C for 2 hours. These patterns are shown in Figure 6.5, along with indicators of peak identity as determined by comparison with standard crystal structures from [19]. Analysis of the XRD pattern for the as-made PtNiCoNWs showed the presence of metallic Pt, Ni, and Co, as well as peaks corresponding to Co_3O_4, thereby further confirming the identity of the sheet-like structures observed in Figure 6.4 with a similar catalyst. After the 250°C annealing treatment, the Co_3O_4 peaks were no longer present in the XRD pattern, which suggests that these species were reduced and the annealed bulk material is primarily metallic in nature. Additionally, the individual Pt peak at ~39° was seen to disappear after annealing, with a shoulder appearing between Co and Ni peaks from ~41-44°. This is indicative of compression of the Pt lattice as seen previously with annealed ETFECS in Chapter 5 and [11], though in this case, both Co and Ni may contribute to the compression.

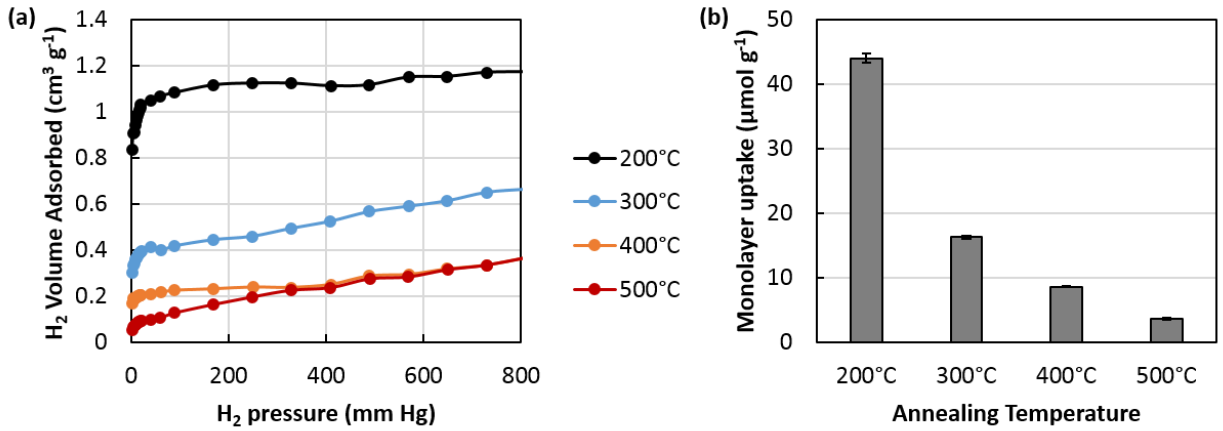

Figure 6.6: (a) H_2 chemisorption isotherms and (b) H_2 monolayer uptake on PtNiCoNWs after H_2 annealing treatments of various temperatures. The data shown was collected on the 5Pt:3Ni X 3 batch synthesized at 295°C.

Chemisorption analysis was used to examine the effects of annealing at various temperatures on the surface uptake of hydrogen in the gas phase. The H_2 chemisorption isotherms recorded on the 5Pt:3Ni X 3 PtNiCoNWs after these annealing treatments are shown in Figure 6.6, along with calculated H_2 monolayer uptake values. The highest uptake of hydrogen, which was indicative of the greatest amount of active surface area, was recorded after a 200°C annealing step. The H_2 uptake dropped precipitously when the annealing temperature was increased to 300°C and continued decreasing monotonically up to 500°C. These results indicate that higher annealing temperatures produce extended surfaces that are less favorable to the binding of gas-phase hydrogen. As observed in Figure 6.4 and Figure 6S.2, the in situ 295°C annealing step between the ALD supercycles eliminated the Pt-decorated metal oxide sheets at the wire edges and resulted in an extended surface that had greater mixing between the metallic species, but retained a Pt-rich outer layer. Bimetallic overlayer catalysts comprised of platinum monolayers on nickel and/or cobalt nanoparticles have previously shown decreased hydrogen adsorption compared to non-structured bimetallic catalysts due to lowering of the Pt d-band [20]; it is possible that similar phenomena were at play in these annealed PtNiCoNWs. The drop in hydrogen adsorption may

also have been due to loss of Pt surface area after reduction of the surface oxide sheets that the Pt nanoparticles were initially dispersed on. Given that the higher annealing temperatures likely made the physical changes observed at 295°C even more pronounced, this may have in turn increased the influence of Co and Ni on Pt, thereby lowering the adsorption of H_2. Given the clear impact of annealing temperature on hydrogen uptake, these results may be useful in tuning the in situ H_2 annealing process in future iterations of the bimetallic ALD process.

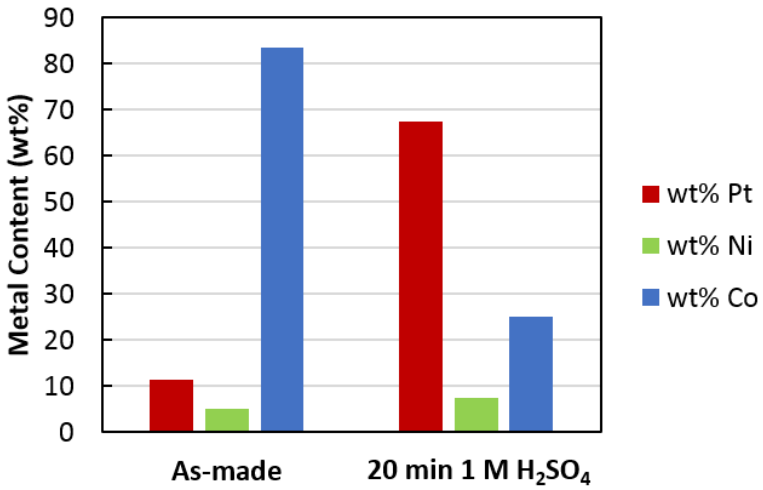

Figure 6.7: Metal content of 15Ni:7Pt+H_2 X 2 as-made and after acid pre-leaching. Acid-leached wt% data was collected with XRF.

An acid pre-leaching treatment was conducted on the 15Ni:7Pt+H_2 X 2 sample in order to test the effects of this procedure on a batch of PtNiNWs with relatively high nickel content as well as to prepare the catalyst for electrochemical testing. A 20-minute acid leach was observed to significantly reduce the amount of cobalt present, while also increasing the weight loading of Pt to almost 70 wt%. The weight loading of Ni was marginally increased from 5.1 to 7.5 wt%; however, given the disproportionately large rise in Pt content, it appeared that some of the original Ni was removed along with the soluble Co. For instance, had the initial Pt:Ni weight ratio remained intact over acid leaching, the final composition would have been closer to ~50 wt% Pt and ~25

wt% Ni. Thus, it is apparent that the bimetallic ALD process with an in situ H_2 annealing in this iteration was not capable of creating an ETFECS system in which the template transition metal could be selectively leached out without affecting the Pt:Ni ratio set during the ALD.

6.4.3. Electrochemical Characterization

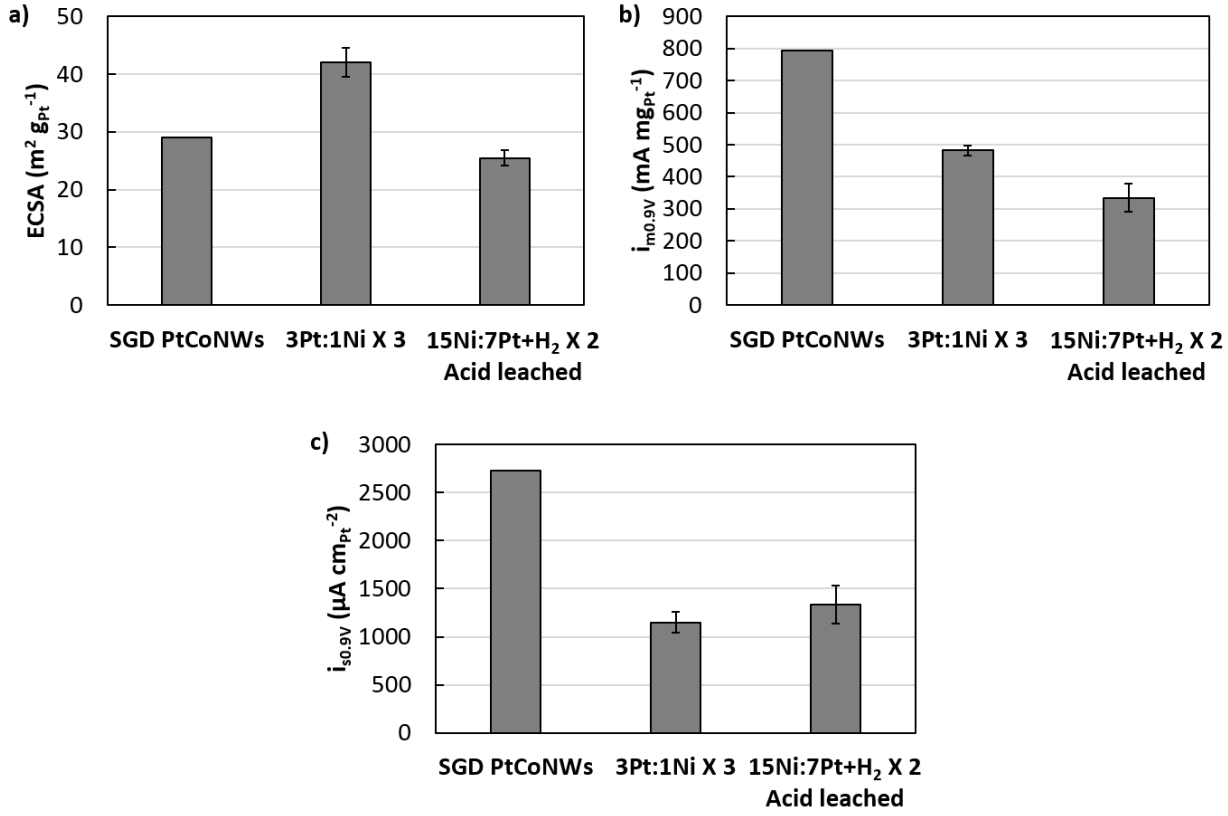

Figure 6.8: Electrochemical results for SGD PtCoNWs [9], as-made 3Pt:1Ni X 3 (295°C), and acid-leached 15Ni:7Pt+H_2 X 2.

The electrochemical performance of select PtNiCoNWs was tested in RDE voltammetry. Figure 6.8 shows electrochemical parameters for the as-made 3Pt:1Ni X 3 (295°C) and the acid-leached 15Ni:7Pt+H_2 X 2 samples, along with reported parameters for PtCoNWs synthesized via SGD [9]. The ECSA of 3Pt:1Ni X 3 was found to be higher than the other catalysts, likely due to the presence of dispersed Pt nanoparticles on the ridges and edges of the nanowire substrate. In terms of mass activity, the SGD PtCoNWs outperformed materials made with ALD, with the acid

leached 15Ni:7Pt+H_2 X 2 sample exhibiting the lowest activity. It was anticipated that acid leaching would degrade the performance of the materials; however, the performance of this catalyst after acid leaching is considerably lower than the acid leached PtNiNWs from Chapter 5 ($i_{m0.9V}$ = 700 mA mg_{Pt}^{-1} in RDE), indicating that the cobalt nanowire substrate may not be as robust over this treatment. Future changes in the ALD or acid leaching processes may help to improve the activity of acid leached materials, particularly if Ni content can be retained. When assessing specific activity, both sets of ALD PtNiCoNWs were found to outperform commercial Pt/HSC ($i_{s0.9V}$ = 500 mA mg_{Pt}^{-1}) but were still significantly less active than SGD PtNiNWs. Though the presence of a cobalt oxide layer was evident in the SGD PtNiNWs [9], it is likely that the oxide content of the ALD materials was greater due to oxygen exposure during both the Pt and Ni ALD cycles. A high presence of oxygen was evident in the individual elemental maps of both 3Pt:1Ni X 3 and 15Ni:7Pt+H_2 X 2 (Figure 6S.1and Figure 6S.2), indicating that the in situ H_2 anneal did not completely remove oxygen. The discrepancy in performance observed between the SGD and ALD materials, in this case, may be attributable to higher oxide content in the ALD PtNiCoNWs; the presence of Ni/Ni oxide in the ALD samples is another complicating factor that may affect the ORR activity of these materials. Further research will be required to analyze the surface chemistry of the PtNiCoNWs synthesized with bimetallic ALD, as well as the physical and chemical changes introduced by the acid leaching treatment and their role in the observed electrochemical performance.

6.5. Conclusions

In order to expand the flexibility of the ALD synthesis process for extended surface electrocatalysts, a bimetallic ALD process was developed for deposition of Pt and Ni onto a Co nanowire substrate. The Pt and Ni ALD processes were analyzed using mass spectrometry and

were combined in various iterations of ALD supercycles. It was observed that the deposited amount of each metal could be effectively controlled by tuning process parameters, such as the ALD temperature and the Pt:Ni ratio of the supercycles. Physical characterization via STEM and XRD showed that a simple bimetallic ALD synthesis produced PtNiCoNWs with highly segregated surfaces and high oxide content, while the addition of an in situ H_2 annealing step improved metal mixing and reduced bulk cobalt oxides. The effects of annealing temperature on gas-phase hydrogen uptake were also probed with hydrogen chemisorption. Application of an acid pre-leaching step was found to remove a considerable amount of ALD-deposited Ni from the annealed PtNiCoNWs in addition to soluble Co, indicating the need for further changes in the bimetallic ALD process to improve Ni retention. As-made and annealed/acid leached catalysts showed higher specific activity than Pt/HSC in preliminary RDE testing, but were outperformed by previous ALD-synthesized PtNiNWS as well as PtCoNWs synthesized by galvanic displacement. Though modifications to the bimetallic ALD process will be necessary to improve control over the Pt:Ni ratio during acid leaching and final performance of the catalysts, this work is an important proof of concept for the advancement of ALD-derived extended surface electrocatalysts.

6.6. Supplemental Information

This section contains tables and figures with additional information.

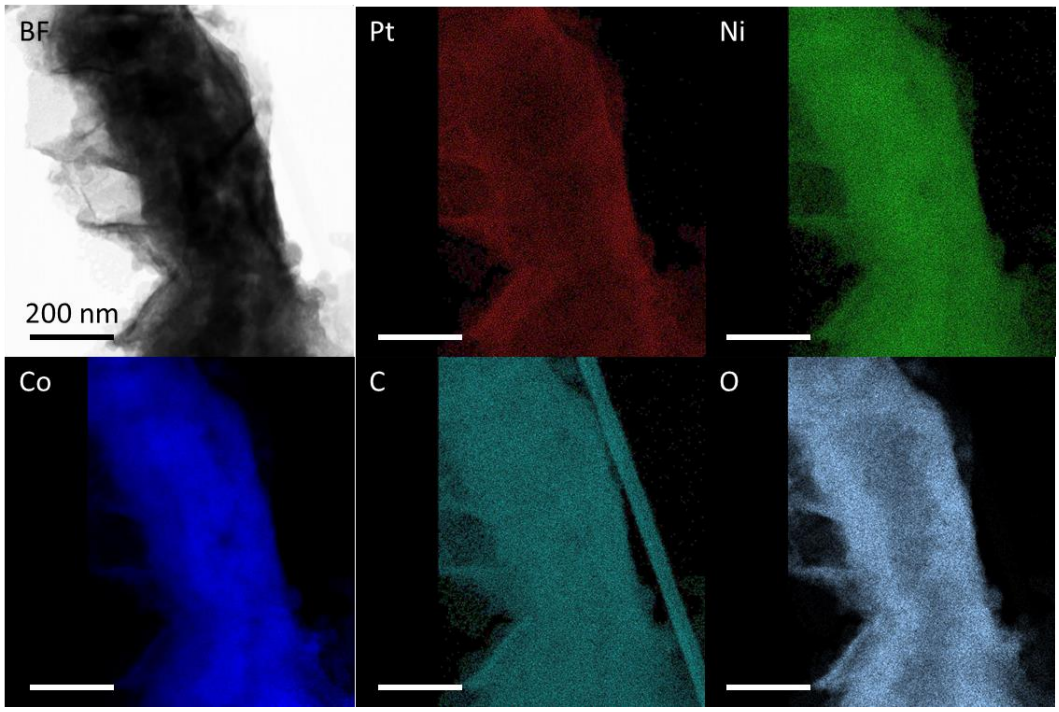

Figure 6S.1: Individual elemental maps for 3Pt:1Ni X 3.

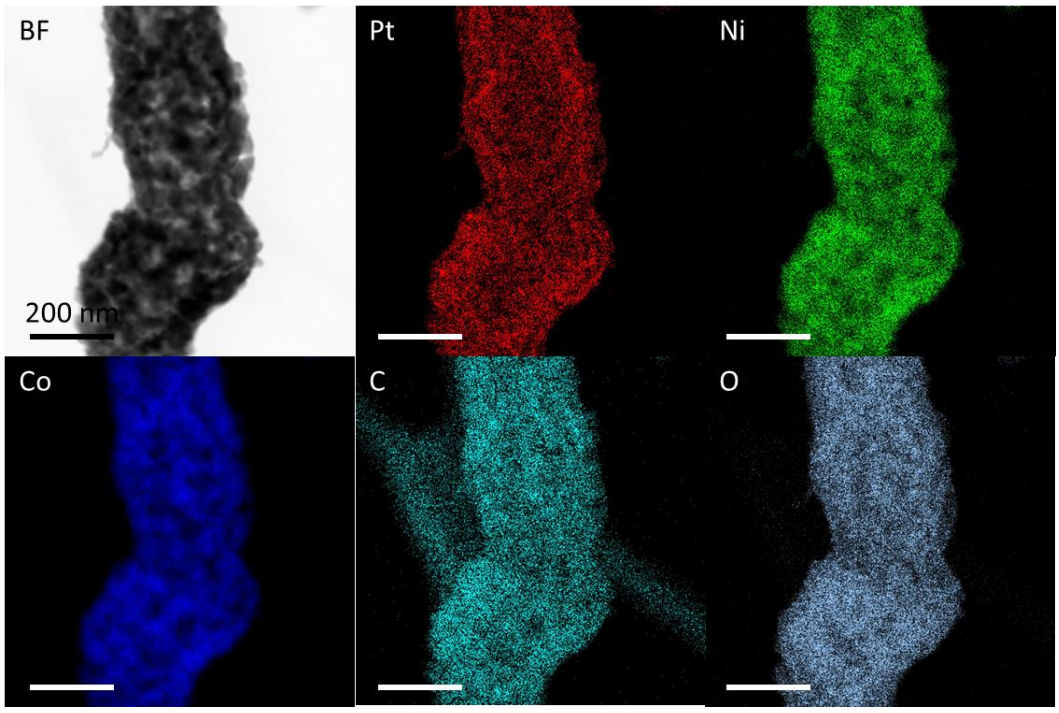

Figure 6S.2: Individual elemental maps for 15Ni:7Pt+H_2 X 2.

6.7. References

1. Stamenkovic, V., et al., *Improved Oxygen Reduction Activity on Pt3Ni(111) via Increased Surface Site Availability.* Science, 2007. **26**: p. 493-497.

2. Wang, Y.-J., et al., *Unlocking the door to highly active ORR catalysts for PEMFC applications: polyhedron-engineered Pt-based nanocrystals.* Energy & Environmental Science, 2018. **11**(2): p. 258-275.

3. FCTT, *Fuel Cell Technical Team Roadmap*. 2017, U.S. Department of Energy Fuel Cell Technologies Office: https://www.energy.gov/sites/prod/files/2017/11/f46/FCTT_Roadmap_Nov_2017_FINAL.pdf.

4. Stamenkovic, V., et al., *Changing the Activity of Electrocatalysts for Oxygen Reduction by Tuning the Surface Electronic Structure.* Angewandte Chemie, 2006. **118**(18): p. 2963-2967.

5. Greeley, J., et al., *Alloys of platinum and early transition metals as oxygen reduction electrocatalysts.* Nature Chemistry, 2009. **1**(7): p. 552-556.

6. Alia, S.M., Y.S. Yan, and B.S. Pivovar, *Galvanic displacement as a route to highly active and durable extended surface electrocatalysts.* Catalysis Science & Technology, 2014. **4**(10): p. 3589-3600.

7. Bu, L., et al., *A General Method for Multimetallic Platinum Alloy Nanowires as Highly Active and Stable Oxygen Reduction Catalysts.* Advanced Materials, 2015. **27**(44): p. 7204-7212.

8. Alia, S.M., et al., *Platinum-Coated Nickel Nanowires as Oxygen-Reducing Electrocatalysts.* ACS Catalysis, 2014. **4**(4): p. 1114-1119.

9. Alia, S.M., et al., *Platinum-Coated Cobalt Nanowires as Oxygen Reduction Reaction Electrocatalysts.* ACS Catalysis, 2014. **4**(8): p. 2680-2686.

10. Alia, S.M., et al., *Oxidation of Platinum Nickel Nanowires to Improve Durability of Oxygen-Reducing Electrocatalysts.* Journal of The Electrochemical Society, 2016. **163**(3): p. F296-F301.

11. Alia, S.M., et al., *Exceptional Oxygen Reduction Reaction Activity and Durability of Platinum–Nickel Nanowires through Synthesis and Post-Treatment Optimization.* ACS Omega, 2017. **2**(4): p. 1408-1418.

12. Pivovar, B.S., *Extended Surface Electrocatalyst Development*, in *2016 Annual Merit Review and Peer Evaluation Meeting*. 2016, DOE Hydrogen and Fuel Cells Program: https://www.hydrogen.energy.gov/pdfs/review16/fc142_pivovar_2016_o.pdf.

13. Mauger, S.A., et al., *Fuel Cell Performance Implications of Membrane Electrode Assembly Fabrication with Platinum-Nickel Nanowire Catalysts.* Journal of The Electrochemical Society, 2018. **165**(3): p. F238-F245.

14. Gould, T.D., et al., *Synthesis of supported Ni catalysts by atomic layer deposition.* Journal of Catalysis, 2013. **303**: p. 9-15.

15. Lu, J., J.W. Elam, and P.C. Stair, *Atomic layer deposition—Sequential self-limiting surface reactions for advanced catalyst "bottom-up" synthesis.* Surface Science Reports, 2016. **71**(2): p. 410-472.

16. Tong, X., et al., *Enhanced catalytic activity for methanol electro-oxidation of uniformly dispersed nickel oxide nanoparticles-carbon nanotube hybrid materials.* Small, 2012. **8**(22): p. 3390-3395.

17. Bachmann, J., et al., *Stoichiometry of Nickel Oxide Films Prepared by ALD.* Chemical Vapor Deposition, 2011. **17**(7-9): p. 177-180.

18. Lu, H.L., et al., *Atomic Layer Deposition of NiO Films on Si(100) Using Cyclopentadienyl-Type Compounds and Ozone as Precursors.* Journal of The Electrochemical Society, 2008. **155**(10): p. H807-H811.

19. Downs, R.T. and M. Hall-Wallace, *The American Mineralogist Crystal Structure Database.* American Mineralogist, 2003. **88**: p. 247-250.

20. Skoglund, M.D., et al., *Characterization of Ni@Pt and Co@Pt overlayer catalysts using adsorption, reactivity descriptors, and X-ray absorption spectroscopy.* Applied Catalysis A: General, 2013. **467**: p. 355-362.

CHAPTER 7

CONCLUSIONS AND RECOMMENDATIONS FOR FUTURE WORK

7.1. Conclusions

Polymer electrolyte fuel cells (PEMFCs) are highly appealing as sources of clean transportation power, but the widespread adoption of these devices in advanced propulsion systems will require overcoming significant materials chemistry and engineering challenges. This work contributes to the understanding of the use of atomic layer deposition (ALD) as a tool for PEMFC catalyst synthesis and stabilization. Overall conclusions for each research thrust will be summarized below, followed by recommendations for future areas of study.

7.1.1. Oxygen Reduction Reaction Electrocatalysts and the Applications of ALD

The oxygen reduction reaction (ORR), which takes place on the cathode of a PEMFC, is the largest source of overpotential in the fuel cell. Nanoparticle Pt/C catalysts are the current commercial standard for ORR catalysts, but, at present, the utilization and stability of Pt in these systems is insufficient to meet the Department of Energy targets for PEMFC system cost and durability. One promising approach to ORR catalyst advancement is the modification of conventional Pt/C, which typically involves the addition of nano-ceramics or direct layering via solution phase chemistry to prevent the agglomeration of the Pt nanoparticles. A second strategy that has yielded impressive results involves the translation of Pt-M bimetallic nanoparticle catalysts into a new class of extended thin film electrocatalyst structures (ETFECS); however, though these materials have demonstrated excellent electrochemical performance in RDE half-cell testing, their development has been stymied by the lack of a reproducible synthesis method that can be scaled to produce materials sufficient for fuel cell testing.

Atomic layer deposition (ALD) has been utilized previously to stabilize metal nanoparticle catalysts in high-temperature reactions as well as in the acidic ORR environment under potential cycling. A wide research space in this area remains unexplored due to the tunability inherent to the ALD process and the variety of chemistries yet to be examined for ORR catalyst stabilization. The ability of ALD to uniformly coat high aspect ratio substrate materials also presents opportunities for the development of a vapor-phase synthesis process for ETFECS with higher reproducibility and scalability than previously reported solution-phase methods.

7.1.2. Titanium Dioxide ALD for Stabilization of Pt/C Catalysts

Two varieties of carbon black-supported Pt nanoparticle catalysts, commercial Pt/C and an ALD-produced Pt catalyst supported on functionalized carbon (ALD Pt/f-C), were modified with TiO_2 ALD in a fluidized bed reactor system. The rate of TiO_2 deposition on the catalyst with the functionalized carbon substrate was found to be substantially higher due to a large number of oxygen groups available on its surface. Examination of the catalysts after ALD showed that TiO_2 was dispersed across each surface, but was more heterogeneous in the case of the functionalized carbon substrate. A 700°C thermal treatment was applied to the ALD Pt/f-C catalyst with 10 cycles of TiO_2 ALD (f10TiO_2); this was observed to create Pt-Ti nanoparticles due to simultaneous reduction and migration of the deposited TiO_2.

Electrochemical analysis of the catalysts after ALD showed that high amounts of TiO_2 deposition on both catalyst varieties had the undesirable effect of blocking Pt sites and reducing the catalytic performance. An interesting phenomenon was documented in the case of the ALD Pt/f-C catalyst in which the catalytic activity increased from the unmodified case up to 10 cycles of TiO_2 ALD. Subsequent analyses indicated that residual ligands from the Pt-H_2 ALD used to synthesize this catalyst were responsible for the low initial activity of the unmodified catalyst;

these ligands were inadvertently oxidized during the H_2O dose step of the TiO_2 ALD process, thereby improving the catalytic activity to the same degree as a designated thermal oxidation step on the unmodified material. The application of the 700°C treatment to the f10TiO_2 catalyst was found to significantly increase the catalyst's ORR activity to almost double that of its initial value, which was attributed to the creation of Pt-Ti nanoparticles and the resultant compression of the Pt lattice.

The electrochemical durability of the catalysts was probed through accelerated durability testing in the RDE. After 5000 voltage cycles, the TiO_2 ALD-modified catalysts were found to retain higher percentages of their initial catalytic activity than commercial Pt/C, though all catalysts experienced nanoparticle growth and loss of electrochemical surface area (ECSA). Surprisingly, the highly-active 700°C-f10TiO_2 was observed to have the worst durability of all catalysts tested, retaining only 27% of its initial activity and forming large nanoparticles after voltage cycling with a mean diameter of 8.2 nm. It was postulated that the Pt-Ti nanoparticles formed through thermal treatment may have had higher surface energy than pure Pt, thereby making them more prone to agglomeration. This study illustrates the utility of TiO_2 in mitigating Pt nanoparticle growth over voltage cycling as well as some of the shortcomings and trade-offs associated with this approach.

7.1.3. Tungsten Nitride ALD for Stabilization of Pt/C Catalysts

The ALD Pt/f-C catalyst was chosen as a substrate for WN ALD in a fluidized bed reactor system due to its documented propensity for high rates of ALD growth. Ten cycles of WN ALD were performed in order to avoid blocking Pt sites with excess deposited species, as seen previously at a high number of ALD cycles. Following ALD, the catalyst was also subject to a series of thermal treatments (low-temperature oxidation followed by high-temperature reduction).

Electron microscopy showed that WN was deposited evenly across the catalyst surface and was well-dispersed throughout the small Pt nanoparticles. The amount of nitrogen present after ALD was in excess of the standard tungsten nitride stoichiometries, indicating that some nitrogen may have been physisorbed to the carbon support during the NH_3 dose in the ALD process. Thermal treatment was found to change the distribution of elements on the catalyst surface; the Pt nanoparticles coarsened, as expected, but the WN species remained dispersed between the Pt agglomerates, indicating that the W and Pt were in separate phases and did not form mixed metal nanoparticles. Additionally, the 725°C reduction treatment removed considerable amounts of nitrogen from the deposited species, changing the stoichiometry to W_2N.

Upon evaluation in electrochemical RDE half-cell tests, the 725°C-f10WN catalyst was found to be significantly more active than both the ALD Pt/f-C catalyst and commercial Pt/C. Though no evidence for Pt lattice compression by W species was observed in XRD, the proximity of the W to the Pt nanoparticles may have impacted the ORR performance through electronic ligand effects. This thermally treated catalyst was found to have excellent performance over accelerated durability testing, retaining 55% of its mass activity over voltage cycling. The agglomeration of Pt nanoparticles in this catalyst was also mitigated, with the mean diameter growing from 6.3 nm initially to 7.4 nm after durability testing; for comparison, uncoated ALD Pt/f-C grew from 2.6 nm to 7.0 nm. The enhanced stability of this 725°C-f10WN catalyst was attributed to the observed structure of the catalyst surface after heat treatment—Pt nanoparticles surrounded by W-rich nanostructures that impeded the movement and agglomeration of Pt during voltage cycling. This stood in contrast to the highly unstable Pt-Ti nanoparticles obtained after thermal treatment in the case of TiO_2 ALD, which demonstrates the impact of the ALD chemistry used on how effective the resultant catalyst is as an ORR catalyst.

7.1.4. Fuel Cell Testing of ALD-modified Pt/C Catalysts

Select catalysts from the TiO_2 and WN research thrusts were incorporated into membrane electrode assemblies (MEAs) and tested in a PEMFC in order to characterize the behavior of these materials in an operational fuel cell device, particularly in regards to water management. Before bonding the proton exchange membrane, each catalyst-coated cathode had its hydrophobicity probed by contact angle measurement. It was observed that the application of TiO_2 and WN ALD to the ALD Pt/f-C catalyst resulted in lower contact angles, which was attributed to the interactions of the metal oxides/nitrides with water. Since thermal treatment removed oxygen and nitrogen from the surface of these catalysts, heat-treated materials such as 725°C-f10WN were found to be very hydrophobic in nature.

Electrochemical behavior of each catalyst in the fuel cell was analyzed in both the kinetic and mass transport regions of the polarization curve. In the kinetic region, it was found that the trends in catalyst mass activity at 0.75 V mostly followed those observed in previous RDE experiments, with minor exceptions likely due to the preparation methods required to fabricate the MEAs. In the mass transport region, the behavior of each catalyst at high current densities was found to correlate largely with the contact angle of the cathode measured before PEMFC testing. Relatively hydrophilic catalysts with contact angles below 130° had significantly larger voltage losses at moderate-to-high current densities than hydrophobic catalysts with higher contact angles. This behavior was likely due to water flooding in the catalysts with larger voltage losses, as their decreased hydrophobicity would be expected to lower the moisture wicking ability of the catalyst layer, thereby causing water buildup in the pores of the electrode and impeding access to Pt sites. This work shows the importance of understanding the macro-scale effects of changing the surface

chemistry of a Pt/C catalyst with ALD, especially when depositing species that may affect water management in a fuel cell environment.

7.1.5. Platinum ALD Synthesis of Extended Thin Film Electrocatalyst Structures

In order to develop a vapor-phase analog to spontaneous galvanic displacement (SGD), the current method for fabricating high-performing ETFECS, Pt ALD was applied to a Ni nanowire (NiNW) substrate in a viscous flow reactor system. Based on gaseous effluent from the reactor, the Pt ALD process on these substrates was determined to follow the standard Pt ALD mechanism outlined in the literature. The synthesis of samples at 5, 10, 20, and 30 ALD cycles showed that the growth rate of Pt was linear under these conditions, and that the Pt followed a self-growth mechanism, in which small nanoparticles were initially deposited on nickel oxide or nickel hydroxide surface sites and continued growth occurred on the deposited Pt at higher numbers of ALD cycles. The deposited Pt was present on the surface as nanoparticles in all samples and did not form a continuous film, even after 30 cycles of ALD. All of the ALD PtNiNWs were exposed to a 250°C hydrogen annealing step, which was found to create a smoother surface and increase mixing of the Pt and Ni phases and the wire edge. Evidence of Pt lattice contraction was found after comparison between XRD patterns of the as-made and annealed PtNiNWs. Hydrogen chemisorption and CO temperature programmed desorption illustrated changes in the adsorption of gas-phase species to the annealed PtNiNWs at different numbers of ALD cycles.

In RDE half-cell tests, the ECSA of the as-made catalysts was found to decrease as the number of ALD cycles was increased, which was attributed to the increasing size of the Pt nanoparticles with more ALD cycles. The H_2 annealing step increased the ECSA of all catalysts and eliminated the observed particle size effect, which further affirmed the creation of an extended surface after annealing. The mass and specific activities of the catalysts were significantly

impacted by the annealing treatment as well, with the 30 cycle PtNiNWs exhibiting a 16-fold increase in mass activity after thermal treatment. This activity increase over annealing was ascribed to the contraction of the Pt lattice observed in the XRD results, as well as partial reduction of surface Ni oxides to create a catalyst with more metallic character. The mass activity of the annealed 30 cycle PtNiNWs was almost four times higher than benchmark Pt/HSC. However, the ALD materials were found to be less active when compared to PtNiNWs of similar composition synthesized through SGD that had also been subjected to a 250°C hydrogen anneal.

The annealed ALD PtNiNWs were also subjected to an acid pre-leaching treatment to remove soluble transition metals and prepare them for use in a PEMFC. Following incorporation into MEAs and fuel cell testing, the mass activity of ALD PtNiNWs ($i_{m0.9V}$ = 577 mA mg_{Pt}^{-1}) was found to surpass the highest reported value for SGD PtNiNWs in a device. Additionally, the ORR performance of the ALD PtNiNWs exceeded the DOE 2020 target for mass activity ($i_{m0.9V}$ = 400 mA mg_{Pt}^{-1}). The superior performance of the ALD materials compared to SGD after acid leaching may have been due to nickel oxides created during the ALD process that were not completely reduced by the annealing step, which imparted greater structural stability upon exposure to acid. This study shows that ALD can be used to synthesize extended surface catalysts at the gram scale with performance exceeding that of SGD-fabricated materials.

7.1.6. Development of Bimetallic Platinum-Nickel ALD for Extended Thin Film Electrocatalyst Structures

In a continuation of the research thrust to advance the use of ALD as a synthesis method for ETFECS, a bimetallic ALD process was developed to deposit both Ni and Pt onto a Co nanowire (CoNW) substrate. The standard processes for Pt and Ni ALD were combined in various ratios and configurations into ALD supercycles and the mechanisms were again studied using mass

spectrometry. Elemental analysis of synthesized materials showed that the content of each deposited metal could be tuned by adjusting the ALD reaction temperature or Pt:Ni ratio in each supercycle. Significant differences in the morphology of the PtNiCoNWs depending on the supercycle configuration were elucidated through electron microscopy and XRD. It was observed that simple bimetallic ALD produced materials with high cobalt oxide content and separate domains of Ni and Pt, while the addition of an in situ hydrogen annealing step between ALD supercycles considerably reduced the bulk oxide species present and resulted in materials with a high degree of mixing between all three metals. Effects of annealing temperature on gas-phase H_2 uptake were probed using hydrogen chemisorption; annealing temperatures above 200°C were found to greatly decrease H_2 adsorption on the surface. One sample of PtNiCoNWs with high deposited Ni content was subjected to an acid leaching step to test the retention of Pt and Ni. Considerable amounts of nickel were removed along with the cobalt in this treatment, indicating that further improvements in the bimetallic ALD process are necessary to ensure the preservation of the deposited Pt:Ni ratio over acid leaching.

Preliminary electrochemical characterization of these catalysts was carried out RDE half-cell tests. Both the simple bimetallic ALD process, as well as bimetallic ALD with in situ H_2 annealing followed by acid leaching, produced catalysts with specific activity above Pt/HSC but considerably lower than previously-reported PtCoNWs synthesized through SGD. The acid leached PtNiCoNWs also exhibited mass activity less than half that of previously-reported ALD PtNiNWs after acid leaching, indicating that these materials may not be as robust as those based on NiNW substrates. The work detailed here is an important proof of concept showing that controlled deposition of Pt and Ni for extended surfaces can be achieved through bimetallic ALD,

but further research is needed to understand the surface chemistry of the synthesized materials as well as to improve the ALD process.

7.2. Recommendations for Future Work

7.2.1. ALD for Stabilization of Pt/C Catalysts

The application of ALD for stabilization of Pt/C catalysts reported here was often negatively impacted by the addition of too many ALD cycles such that coverage of Pt sites decreased the reactivity of the catalyst. However, the stability benefits of adding metal oxide or nitride nanostructures to the surface may be more fully realized at higher concentrations of deposited material, which will help to keep the Pt nanoparticles confined and prevent agglomeration. As such, the ideal strategy for ALD stabilization would involve area-selective deposition solely on the carbon support so that protective nanostructures can be built around the Pt nanoparticles but not impede access of reactants to the catalyst surface.

Area-selective atomic layer deposition is often accomplished by blocking the ALD precursors from accessing certain sites on the surface so that deposition happens only in the desired area. Organic blocking agents such as oleylamine are often used to cover active metal sites during ALD and can be easily combusted after deposition to regain access to the metal surface. Preliminary experiments (not reported in this thesis) were conducted to test the efficacy of oleylamine as a blocking agent for the ALD Pt/f-C catalyst during the WN ALD process detailed in Chapter 3. Following solution-phase addition of the oleylamine to Pt sites, 35 cycles of WN ALD were added to the catalyst. A post-ALD thermal treatment of 200°C in air was used to combust the oleylamine and prepare the catalyst for analysis. The electrochemical performance of the catalyst was unremarkable, with low initial activity indicating that the Pt sites were thoroughly

covered, despite attempts to avoid this outcome. It is likely that the high temperature of the WN ALD process (300°C) caused oleylamine to desorb from the surface (assuming it was there initially) and resulted in WN growth over the unprotected Pt sites.

Future work in this research thrust should involve a more systematic study of oleylamine adsorption to the Pt and its presence before and after ALD as well as after subsequent thermal treatment. An analysis technique such as diffuse reflectance infrared Fourier transform spectroscopy (DRIFTS) may be used to confirm the presence of oleylamine molecules on the surface. This area selective ALD approach may also be attempted with lower-temperature ALD processes, such as TiO_2, to ensure adherence of the blocking agent to the ALD sites. It may also be beneficial to explore the availability of blocking agents other than oleylamine that bind more tightly to Pt and can tolerate higher ALD temperatures, assuming that those molecules can still be efficiently removed after ALD.

7.2.2. ALD Synthesis of Extended Thin Film Electrocatalyst Structures

The application of Pt ALD to NiNWs was found to be an effective method for producing high-performing extended surface catalysts at a scale of 0.5 g per batch. However, this quantity must be further scaled up if this process is to become useful for widespread commercialization of PEMFCs. Preliminary work in the viscous flow reactor system reported here has shown that this reactor configuration is not effective for coating large quantities of NiNWs > 0.5 g due to diffusion limitations of the Pt ALD precursor through the packed bed of NiNWs. Additionally, the oxidation of the NiNWs in the viscous flow reactor contributes to some variability from batch to batch. For larger-scale batches, it may be more effective to coat the NiNWs in a stop-flow system in which the wire agglomerates could “soak” in a chamber for enough time to ensure even exposure of the $MeCpPtMe_3$ to all surface sites. Given that these materials do not fluidize in a manner similar to

powders, it may also be worthwhile to examine the effects of agitation, such as rotary motion or vibration, to ensure even gas contact.

Though the bimetallic ALD process was shown to be an effective means of tuning the deposition of Pt and Ni onto the CoNWs, the retention of Ni over acid leaching and electrochemical performance of the PtNiCoNWs left much to be desired in the final use of materials prepared through this method. One potential route to increasing the amount of Ni retained during acid leaching may be a pre-oxidation of the cobalt wires before application of ALD. This may prevent Ni migration into the CoNW core during the ALD process, and leave more Ni available for alloying with the Pt during the annealing step. The results obtained through H_2 chemisorption on PtNiCoNWs annealed at different temperatures showed that gas-phase adsorption of hydrogen was extremely sensitive to the annealing temperature. Lowering the temperature of the in situ annealing step from the ALD temperature of 295°C may yield PtNiCoNWs with improved hydrogen uptake, which would likely presage higher ECSAs and ORR activities as well.

BIBLIOGRAPHY

Aaltonen, T., et al., *Reaction Mechanism Studies on Atomic Layer Deposition of Ruthenium and Platinum.* Electrochemical and Solid-State Letters, 2003. **6**(9): p. C130-C133.

Alexeev, O., M. Shelef, and B.C. Gates, *MgO-Supported Platinum-Tungsten Catalysts Prepared from Organometallic Precursors: Platinum Clusters Isolated on Dispersed Tungsten.* Journal of Catalysis, 1996. 164: p. 1-15.

Alia, S.M., et al., *Platinum Coated Copper Nanowires and Platinum Nanotubes as Oxygen Reduction Electrocatalysts.* ACS Catalysis, 2013. **3**(3): p. 358-362.

Alia, S.M., et al., *Platinum-Coated Nickel Nanowires as Oxygen-Reducing Electrocatalysts.* ACS Catalysis, 2014. **4**(4): p. 1114-1119.

Alia, S.M., et al., *Exceptional Oxygen Reduction Reaction Activity and Durability of Platinum–Nickel Nanowires through Synthesis and Post-Treatment Optimization.* ACS Omega, 2017. **2**(4): p. 1408-1418.

Alia, S.M. and B.S. Pivovar, *Extended Surface Electrocatalyst Development*, in *2018 Annual Merit Review and Peer Evaluation Meeting*. 2018, DOE Hydrogen and Fuel Cells Program: https://www.hydrogen.energy.gov/pdfs/review18/fc142_pivovar_2018_o.pdf.

Alia, S.M., et al., *Oxidation of Platinum Nickel Nanowires to Improve Durability of Oxygen-Reducing Electrocatalysts.* Journal of The Electrochemical Society, 2016. **163**(3): p. F296-F301.

Alia, S.M., et al., *Platinum-Coated Cobalt Nanowires as Oxygen Reduction Reaction Electrocatalysts.* ACS Catalysis, 2014. **4**(8): p. 2680-2686.

Alia, S.M., et al., *Platinum Nickel Nanowires as Methanol Oxidation Electrocatalysts.* Journal of The Electrochemical Society, 2015. **162**(12): p. F1299-F1304.

Alia, S.M., Y.S. Yan, and B.S. Pivovar, *Galvanic displacement as a route to highly active and durable extended surface electrocatalysts.* Catalysis Science & Technology, 2014. **4**(10): p. 3589-3600.

Antolini, E. and E.R. Gonzalez, *Tungsten-based materials for fuel cell applications.* Applied Catalysis B: Environmental, 2010. **96**(3-4): p. 245-266.

Arrhenius, S., *On the Influence of Carbonic Acid in the Air upon the Temperature of the Ground.* Philosophical Magazine and Journal of Science, 1896. **5**(41): p. 237-276.

Avcioglu, G.S., B. Ficicilar, and I. Eroglu, *Improved PEM fuel cell performance with hydrophobic catalyst layers.* International Journal of Hydrogen Energy, 2018. **43**(40): p. 18632-18641.

Azimi, G., et al., *Hydrophobicity of rare-earth oxide ceramics.* Nature Materials, 2013. **12**(4): p. 315-320.

Bachmann, J., et al., *Stoichiometry of Nickel Oxide Films Prepared by ALD.* Chemical Vapor Deposition, 2011. **17**(7-9): p. 177-180.

Barton, S.S., et al., *Acidic and basic sites on the surface of porous carbon.* Carbon, 1997. **35**(9): p. 1361-1366.

Beard, B.C. and P.N. Ross, *Characterization of a Titanium-Promoted Supported Platinum Electrocatalyst.* Journal of The Electrochemical Society, 1986. **133**(9): p. 1839-1845.

Becker, J.S. and R.G. Gordon, *Diffusion barrier properties of tungsten nitride films grown by atomic layer deposition from bis(tert-butylimido)bis(dimethylamido)tungsten and ammonia.* Applied Physics Letters, 2003. **82**(14): p. 2239-2241.

Becker, J.S., S. Wang, and R.G. Gordon, *Highly Conformal Thin Films of Tungsten Nitride Prepared by Atomic Layer Deposition from a Novel Precursor.* Chemistry of Materials, 2003. 15: p. 2969-2976.

Biniak, S., et al., *The characterization of activated carbons with oxygen and nitrogen surface groups.* Carbon, 1997. **35**(2): p. 1799-1810.

Bu, L., et al., *A General Method for Multimetallic Platinum Alloy Nanowires as Highly Active and Stable Oxygen Reduction Catalysts.* Advanced Materials, 2015. **27**(44): p. 7204-7212.

Bu, L., et al., *Surface engineering of hierarchical platinum-cobalt nanowires for efficient electrocatalysis.* Nature Communications, 2016. 7: p. 11850.

Cao, M., D. Wu, and R. Cao, *Recent Advances in the Stabilization of Platinum Electrocatalysts for Fuel-Cell Reactions.* ChemCatChem, 2014. **6**(1): p. 26-45.

Chen, T.-W., et al., *Ultralong PtNi alloy nanowires enabled by the coordination effect with superior ORR durability.* RSC Advances, 2016. **6**(75): p. 71501-71506.

Chen, Y., et al., *Atomic layer deposition assisted Pt-SnO2 hybrid catalysts on nitrogen-doped CNTs with enhanced electrocatalytic activities for low temperature fuel cells.* International Journal of Hydrogen Energy, 2011. **36**(17): p. 11085-11092.

Chen, Z., et al., *Supportless Pt and PtPd nanotubes as electrocatalysts for oxygen-reduction reactions.* Angewandte Chemie International Edition, 2007. **46**(22): p. 4060-4063.

Cheng, K., et al., *Three-Dimensionally Costabilized Metal Catalysts toward an Oxygen Reduction Reaction.* Langmuir, 2016. **32**(9): p. 2236-2244.

Cheng, N., Banis, M.N., Liu, J., Riese, A., Mu, S., Li, Ruying, Sham, T-S, Sun, X., *Atomic Scale Enhancement of Metal-Support Interactions Between Pt and ZrC for Highly Stable Electrocatalysts.* Energy & Environmental Science, 2015. 8: p. 1450-1455.

Cheng, N., et al., *Extremely stable platinum nanoparticles encapsulated in a zirconia nanocage by area-selective atomic layer deposition for the oxygen reduction reaction.* Advanced Materials, 2015. **27**(2): p. 277-281.

Christensen, S.T., et al., *Controlled growth of platinum nanoparticles on strontium titanate nanocubes by atomic layer deposition.* Small, 2009. **5**(6): p. 750-757.

Chung, S., et al., *Atomic layer deposition of ultrathin layered TiO2 on Pt/C cathode catalyst for extended durability in polymer electrolyte fuel cells.* Journal of Energy Chemistry, 2016. **25**(2): p. 258-264.

Cook, J., et al., *Quantifying the consensus on anthropogenic global warming in the scientific literature.* Environmental Research Letters, 2013. **8**(2): p. 024024.

Dai, P., et al., *Solar hydrogen generation by silicon nanowires modified with platinum nanoparticle catalysts by atomic layer deposition.* Angewandte Chemie International Edition, 2013. **52**(42): p. 11119-11123.

Dai, Y., et al., *Efficient and Superiorly Durable Pt-Lean Electrocatalysts of Pt−W Alloys for the Oxygen Reduction Reaction.* The Journal of Physical Chemistry C, 2011. **115**(5): p. 2162-2168.

Debe, M.K., *Advanced Cathode Catalyst and Supports for PEM Fuel Cells*, in *2009 DOE Hydrogen Program Review*. 2009, DOE Hydrogen and Fuel Cells Program: https://www.hydrogen.energy.gov/pdfs/review09/fc_17_debe.pdf.

Dhanasekaran, P., S. Vinod Selvaganesh, and S.D. Bhat, *Nitrogen and carbon doped titanium oxide as an alternative and durable electrocatalyst support in polymer electrolyte fuel cells.* Journal of Power Sources, 2016. 304: p. 360-372.

Ding, E., K.L. More, and T. He, *Preparation and characterization of carbon-supported PtTi alloy electrocatalysts.* Journal of Power Sources, 2008. **175**(2): p. 794-799.

Downs, R.T. and M. Hall-Wallace, *The American Mineralogist Crystal Structure Database.* American Mineralogist, 2003. 88: p. 247-250.

Duan, H., Q. Hao, and C. Xu, *Hierarchical nanoporous PtTi alloy as highly active and durable electrocatalyst toward oxygen reduction reaction.* Journal of Power Sources, 2015. 280: p. 483-490.

Elezovic, N.R., et al., *Synthesis and characterization Pt nanocatalysts on tungsten based supports for oxygen reduction reaction.* Applied Catalysis B: Environmental, 2012. 125: p. 390-397.

FCTT, *Fuel Cell Technical Team Roadmap.* 2017, U.S. Department of Energy Fuel Cell Technologies Office: https://www.energy.gov/sites/prod/files/2017/11/f46/FCTT_Roadmap_Nov_2017_FINAL.pdf.

Feng, H., et al., *Palladium Catalysts Synthesized by Atomic Layer Deposition for Methanol Decomposition.* Chemistry of Materials, 2010. **22**(10): p. 3133-3142.

Feng, H., et al., *Alumina Over-coating on Pd Nanoparticle Catalysts by Atomic Layer Deposition: Enhanced Stability and Reactivity.* Catalysis Letters, 2011. **141**(4): p. 512-517.

Folgado, M.A., et al., *Single Cell Study of Water Transport in PEMFCs with Electrosprayed Catalyst Layers.* Fuel Cells, 2018. **18**(5): p. 602-612.

Fujii, K., et al., *Performance and durability of carbon black-supported Pd catalyst covered with silica layers in membrane-electrode assemblies of proton exchange membrane fuel cells.* Journal of Power Sources, 2015. 279: p. 100-106.

Garsany, Y., et al., *Experimental Methods for Quantifying the Activity of Platinum Electrocatalysts for the Oxygen Reduction Reaction.* Analytical Chemistry, 2010. 82: p. 6321-6328.

Gasteiger, H.A., et al., *Activity benchmarks and requirements for Pt, Pt-alloy, and non-Pt oxygen reduction catalysts for PEMFCs.* Applied Catalysis B: Environmental, 2005. **56**(1-2): p. 9-35.

Goulas, A. and J.R. van Ommen, *Scalable Production of Nanostructured Particles using Atomic Layer Deposition.* KONA Powder and Particle Journal, 2014. 31: p. 234-246.

Gould, T.D., et al., *Stabilizing Ni Catalysts by Molecular Layer Deposition for Harsh, Dry Reforming Conditions.* ACS Catalysis, 2014. **4**(8): p. 2714-2717.

Gould, T.D., et al., *Controlling Nanoscale Properties of Supported Platinum Catalysts through Atomic Layer Deposition.* ACS Catalysis, 2015. **5**(2): p. 1344-1352.

Gould, T.D., et al., *Synthesis of supported Ni catalysts by atomic layer deposition.* Journal of Catalysis, 2013. 303: p. 9-15.

Gould, T.D., et al., *Enhanced dry reforming of methane on Ni and Ni-Pt catalysts synthesized by atomic layer deposition.* Applied Catalysis A: General, 2015. 492: p. 107-116.

Graeser, K.A., et al., *The Role of Configurational Entropy in Amorphous Systems.* Pharmaceutics, 2010. **2**(2): p. 224-244.

Greeley, J., et al., *Alloys of platinum and early transition metals as oxygen reduction electrocatalysts.* Nature Chemistry, 2009. **1**(7): p. 552-556.

Ham, D. and J. Lee, *Transition Metal Carbides and Nitrides as Electrode Materials for Low Temperature Fuel Cells.* Energies, 2009. **2**(4): p. 873-899.

Harris, D.C., *Charles David Keeling and the Story of Atmospheric CO2 Measurements.* Analytical Chemistry, 2010. **82**(19): p. 7865-7870.

He, D., et al., *Fuel cell anode catalyst performance can be stabilized with a molecularly rigid film of polymers of intrinsic microporosity (PIM).* RSC Advances, 2016. **6**(11): p. 9315-9319.

Hoover, R.R. and Y.V. Tolmachev, *Electrochemical Properties of Pt Coatings on Ni Prepared by Atomic Layer Deposition.* Journal of The Electrochemical Society, 2009. **156**(1): p. A37-A43.

Hsieh, C.-T., et al., *Atomic Layer Deposition of Platinum Nanocatalysts onto Three-Dimensional Carbon Nanotube/Graphene Hybrid.* The Journal of Physical Chemistry C, 2012. **116**(51): p. 26735-26743.

Huong Nguyen, T.G., et al., *Nano-Pt/C electrocatalysts: synthesis and activity for alcohol oxidation.* Advances in Natural Sciences: Nanoscience and Nanotechnology, 2013. **4**(3): p. 035008.

IPCC, *Climate Change 2013: The Physical Science Basis. Contribution of Working Group I to the Fifth Assessment Report of the Intergovernmental Panel on Climate Change*, ed. T.F. Stocker, et al. 2013, Cambridge, United Kingdom and New York, NY, USA: Cambridge University Press. 1535 pp.

Jia, Q., et al., *Structure–property–activity correlations of Pt-bimetallic nanoparticles: A theoretical study.* Electrochimica Acta, 2013. 88: p. 604-613.

Karlberg, G.S., et al., *Cyclic voltammograms for H on Pt(111) and Pt(100) from first principles.* Physical Review Letters, 2007. **99**(12): p. 126101.

Kawasoe, Y., et al., *Preparation and Electrochemical Activities of Pt–Ti Alloy PEFC Electrocatalysts.* Journal of The Electrochemical Society, 2007. **154**(9): p. B969-B975.

Kessels, W.M.M., et al., *Surface reactions during atomic layer deposition of Pt derived from gas phase infrared spectroscopy.* Applied Physics Letters, 2009. **95**(1): p. 013114.

Kim, J., S. Yang, and H. Lee, *Platinum–titanium intermetallic nanoparticle catalysts for oxygen reduction reaction with enhanced activity and durability.* Electrochemistry Communications, 2016. 66: p. 66-70.

King, D.M., et al., *Atomic layer deposition of TiO2 films on particles in a fluidized bed reactor.* Powder Technology, 2008. **183**(3): p. 356-363.

King, D.M., et al., *Atomic layer deposition on particles using a fluidized bed reactor with in situ mass spectrometry.* Surface and Coatings Technology, 2007. **201**(22-23): p. 9163-9171.

King, J.S., et al., *Ultralow Loading Pt Nanocatalysts Prepared by Atomic Layer Deposition on Carbon Aerogels.* Nano Letters, 2008. **8**(8): p. 2405-2409.

Kocha, S.S., *Electrochemical Degradation: Electrocatalyst and Support Durability*, in *Polymer Electrolyte Fuel Cell Degradation,* M.M. Mench, E.C. Kumbur, and T.N. Veziroglu, Editors. 2012, Elsevier: Waltham, MA.

Kuttiyiel, K.A., et al., *Bimetallic IrNi core platinum monolayer shell electrocatalysts for the oxygen reduction reaction.* Energy & Environmental Science, 2012. **5**(1): p. 5297-5304.

Lai, J., R. Luque, and G. Xu, *Recent Advances in the Synthesis and Electrocatalytic Applications of Platinum-Based Bimetallic Alloy Nanostructures.* ChemCatChem, 2015. **7**(20): p. 3206-3228.

Larminie, J. and A. Dicks, *Fuel Cell Systems Explained*, Second Edition. 2003, Hoboken, NJ: John Wiley & Sons Ltd.

Li, H., et al., *A review of water flooding issues in the proton exchange membrane fuel cell.* Journal of Power Sources, 2008. **178**(1): p. 103-117.

Li, J., et al., *Highly dispersed Pt nanoparticle catalyst prepared by atomic layer deposition.* Applied Catalysis B: Environmental, 2010. **97**(1-2): p. 220-226.

Liang, X., et al., *Stabilization of Supported Metal Nanoparticles Using an Ultrathin Porous Shell.* ACS Catalysis, 2011. **1**(10): p. 1162-1165.

Lim, B., et al., *Pd-Pt Bimetallic Nanodendrites with High Activity for Oxygen Reduction.* Science, 2009. 234: p. 1302-1305.

Lin, Y.-H., et al., *Enhancing the Photon-Sensing Properties of ZnO Nanowires by Atomic Layer Deposition of Platinum.* Electrochemical and Solid-State Letters, 2010. **13**(12): p. K93-K95.

Liu, C., et al., *Atomic layer deposition of platinum nanoparticles on carbon nanotubes for application in proton-exchange membrane fuel cells.* Small, 2009. **5**(13): p. 1535-1538.

Lu, H.L., et al., *Atomic Layer Deposition of NiO Films on Si(100) Using Cyclopentadienyl-Type Compounds and Ozone as Precursors.* Journal of The Electrochemical Society, 2008. **155**(10): p. H807-H811.

Lu, J., J.W. Elam, and P.C. Stair, *Atomic layer deposition—Sequential self-limiting surface reactions for advanced catalyst "bottom-up" synthesis.* Surface Science Reports, 2016. 71(2): p. 410-472.

Lu, J., et al., *Coking- and Sintering-Resistant Palladium Catalysts Achieved Through Atomic Layer Deposition.* Science, 2012. **335**(6073): p. 1205-1208.

Lu, J., et al., *Toward atomically-precise synthesis of supported bimetallic nanoparticles using atomic layer deposition.* Nature Communications, 2014. 5: p. 4264.

Lubers, A.M., et al., *Electrochemical hydrogen pumping using a platinum catalyst made in a fluidized bed via atomic layer deposition.* Powder Technology, 2016. 296: p. 72-78.

Lubers, A.M., et al., *Proton Exchange Membrane Fuel Cell Flooding Caused by Residual Functional Groups after Platinum Atomic Layer Deposition.* Electrochimica Acta, 2017. 237: p. 192-198.

Lubers, A.M., et al., *Mechanistic studies for depositing highly dispersed Pt nanoparticles on carbon by use of trimethyl(methylcyclopentadienyl)platinum(IV) reactions with O2 and H2.* Journal of Nanoparticle Research, 2015. **17**(4): p. 179.

Ma, Z., et al., *Surface Modification of Au/TiO2 Catalysts by SiO2 via Atomic Layer Deposition.* Journal of Physical Chemistry C, 2008. 112: p. 9448-9457.

Mackus, A.J.M., et al., *Catalytic Combustion and Dehydrogenation Reactions during Atomic Layer Deposition of Platinum.* Chemistry of Materials, 2012. **24**(10): p. 1752-1761.

Marichy, C., et al., *ALD SnO2 protective decoration enhances the durability of a Pt based electrocatalyst.* Journal of Materials Chemistry A, 2016. **4**(3): p. 969-975.

Markovic, N.M., et al., *Oxygen Reduction Reaction on Pt and Pt Bimetallic Surfaces: A Selective Review.* Fuel Cells, 2001. **1**(2): p. 105-116.

Mauger, S.A., et al., *Fuel Cell Performance Implications of Membrane Electrode Assembly Fabrication with Platinum-Nickel Nanowire Catalysts.* Journal of The Electrochemical Society, 2018. **165**(3): p. F238-F245.

Meléndez-Ceballos, A., et al., *Electrochemical properties of Atomic layer deposition processed CeO2 as a protective layer for the molten carbonate fuel cell cathode.* Electrochimica Acta, 2014. 140: p. 174-181.

Meléndez-Ceballos, A., et al., *Electrochemical behavior of Mx−1Ox (M = Ti, Ce and Co) ultra-thin protective layers for MCFC cathode.* International Journal of Hydrogen Energy, 2014. **39**(23): p. 12233-12241.

Meléndez-Ceballos, A., et al., *TiO2 protective coating processed by Atomic Layer Deposition for the improvement of MCFC cathode.* International Journal of Hydrogen Energy, 2013. **38**(30): p. 13443-13452.

Meng, X., et al., *Atomic layer deposition for nanomaterial synthesis and functionalization in energy technology.* Materials Horizons, 2017. **4**(2): p. 133-154.

Min, M.-k., et al., *Particle Size and Alloying Effects of Pt-based Alloy Catalysts for Fuel Cell Applications.* Electrochimica Acta, 2000. 45: p. 4211-4217.

Moharana, P.L., et al., *Structural and mechanical study of thermally annealed tungsten nitride thin films.* Perspectives in Science, 2016. 8: p. 636-638.

Mukerjee, S., *Particle size and structural effects in platinum electrocatalysis.* Journal of Applied Electrochemistry, 1990. 20: p. 537-548.

Mukerjee, S., et al., *Role of Structural and Electronic Properties of Pt and Pt Alloys on Electrocatalysis of Oxygen Reduction: An In Situ XANES and EXAFS Investigation.* Journal of The Electrochemical Society, 1995. **142**(5): p. 1409-1422.

Mukerjee, S., et al., *Effect of Preparation Conditions of Pt Alloys on Their Electronic, Structural, and Electrocatalytic Activities for Oxygen Reduction-XRD, XAS, and Electrochemical Studies.* Journal of Physical Chemistry, 1995. **99**(13): p. 4577-4589.

Musil, J., et al., *Flexible hydrophobic ZrN nitride films.* Vacuum, 2016. 131: p. 34-38.

Norskov, J.K., et al., *Origin of the Overpotential for Oxygen Reduction at a Fuel-Cell Cathode.* Journal of Physical Chemistry B, 2004. 108: p. 17886-17892.

Park, H.-Y., et al., *Carbon-Supported Ordered Pt-Ti Alloy Nanoparticles as Durable Oxygen Reduction Reaction Electrocatalyst for Polymer Electrolyte Membrane Fuel Cells.* Journal of Electrochemical Science and Technology, 2016. **7**(4): p. 269-276.

Pivovar, B.S., *Extended Surface Electrocatalyst Development*, in *2016 Annual Merit Review and Peer Evaluation Meeting.* 2016, DOE Hydrogen and Fuel Cells Program: https://www.hydrogen.energy.gov/pdfs/review16/fc142_pivovar_2016_o.pdf.

Pivovar, B.S., *Extended Surface Electrocatalyst Development*, in *2017 Annual Merit Review and Peer Evaluation Meeting.* 2017, DOE Hydrogen and Fuel Cells Program: https://www.hydrogen.energy.gov/pdfs/review17/fc142_pivovar_2017_o.pdf.

Puurunen, R.L., *A Short History of Atomic Layer Deposition: Tuomo Suntola's Atomic Layer Epitaxy.* Chemical Vapor Deposition, 2014. **20**(10-11-12): p. 332-344.

Sairanen, E., et al., *Atomic layer deposition in the preparation of Bi-metallic, platinum-based catalysts for fuel cell applications.* Applied Catalysis B: Environmental, 2014. 148-149: p. 11-21.

Sankar, S., et al., *Hydrophobic and Metallophobic Surfaces: Highly Stable Non-wetting Inorganic Surfaces Based on Lanthanum Phosphate Nanorods.* Scientific Reports, 2016. 6: p. 22732.

Sasaki, K., M. Shao, and R. Adzic, *Dissolution and Stabilization of Platinum in Oxygen Cathodes, in Polymer Electrolyte Fuel Cell Durability*, F.N. Buchi, M. Inaba, and T.J. Schmidt, Editors. 2009, Springer New York: New York. p. 7-27.

Setthapun, W., et al., *Genesis and Evolution of Surface Species during Pt Atomic Layer Deposition on Oxide Supports Characterized by in Situ XAFS Analysis and Water-Gas Shift Reaction.* Journal of Physical Chemistry C, 2010. 114: p. 9758-9771.

Sha, Y., et al., *Mechanism for Oxygen Reduction Reaction on Pt3Ni Alloy Fuel Cell Cathode*. The Journal of Physical Chemistry C, 2012. **116**(40): p. 21334-21342.

Shim, J.L., C-R; Lee, H-K; Lee, J-S; Cairns, EJ, *Electrochemical characteristics of Pt-WO3/C and Pt-TiO2/C electrocatalysts in a polymer electrolyte Fuel Cell.* Journal of Power Sources, 2001. 102: p. 172-177.

Shinozaki, K., et al., *Oxygen Reduction Reaction Measurements on Platinum Electrocatalysts Utilizing Rotating Disk Electrode Technique.* Journal of The Electrochemical Society, 2015. **162**(10): p. F1144-F1158.

Skoglund, M.D., et al., *Characterization of Ni@Pt and Co@Pt overlayer catalysts using adsorption, reactivity descriptors, and X-ray absorption spectroscopy.* Applied Catalysis A: General, 2013. 467: p. 355-362.

Srinivasan, S., *Fuel Cell Principles*, in *Fuel Cells: From Fundamentals to Applications.* 2006, Springer: Boston, MA. p. 189-233.

Stamenkovic, V., et al., *Improved Oxygen Reduction Activity on Pt3Ni(111) via Increased Surface Site Availability.* Science, 2007. 26: p. 493-497.

Stamenkovic, V., et al., *Changing the Activity of Electrocatalysts for Oxygen Reduction by Tuning the Surface Electronic Structure.* Angewandte Chemie, 2006. **118**(18): p. 2963-2967.

Stamenkovic, V.R., et al., *Trends in electrocatalysis on extended and nanoscale Pt-bimetallic alloy surfaces.* Nature Materials, 2007. **6**(3): p. 241-247.

Stassi, A., et al., *Electrocatalytic behaviour for oxygen reduction reaction of small nanostructured crystalline bimetallic Pt–M supported catalysts.* Journal of Applied Electrochemistry, 2006. **36**(10): p. 1143-1149.

Takenaka, S. and M. Kishida, *Functionalization of Carbon Nanotube-Supported Precious Metal Catalysts by Coverage with Metal Oxide Layers.* Catalysis Surveys from Asia, 2013. **17**(2): p. 71-84.

Takenaka, S., et al., *High Durability of Carbon Nanotube-Supported Pt Electrocatalysts Covered with Silica Layers for the Cathode in a PEMFC.* Journal of The Electrochemical Society, 2008. **155**(9): p. B929-B936.

Takenaka, S., et al., *Highly active and durable silica-coated Pt cathode catalysts for polymer electrolyte fuel cells: control of micropore structures in silica layers.* Catalysis Science & Technology, 2015. **5**(2): p. 1133-1142.

Takenaka, S., et al., *Highly durable Pd metal catalysts for the oxygen reduction reaction in fuel cells; coverage of Pd metal with silica.* Chemical Communications, 2010. **46**(47): p. 8950-8952.

Takenaka, S., et al., *Highly durable carbon nanotube-supported Pd catalysts covered with silica layers for the oxygen reduction reaction.* Journal of Catalysis, 2011. **279**(2): p. 381-388.

Takenaka, S.M., H.; Nakagawa, K.; Matsune, H.; Tanabe, E.; Kishida, M., *Improvement in the Durability of Pt Electrocatalysts by Coverage with Silica Layers.* Journal of Physical Chemistry C Letters, 2007. 111: p. 15133-15136.

Thomas, C.E., *Fuel cell and battery electric vehicles compared.* International Journal of Hydrogen Energy, 2009. **34**(15): p. 6005-6020.

Tong, X., et al., *Enhanced catalytic activity for methanol electro-oxidation of uniformly dispersed nickel oxide nanoparticles-carbon nanotube hybrid materials.* Small, 2012. **8**(22): p. 3390-3395.

Tran, R., et al., *Surface energies of elemental crystals.* Scientific Data, 2016. 3: p. 160080.

Van Bui, H., F. Grillo, and J.R. van Ommen, *Atomic and molecular layer deposition: off the beaten track.* Chemical Communications, 2016. **53**(1): p. 45-71.

Virkar, A.V. and Y. Zhou, *Mechanism of Catalyst Degradation in Proton Exchange Membrane Fuel Cells.* Journal of The Electrochemical Society, 2007. **154**(6): p. B540-B547.

Wang, Y., et al., *Carbon-Supported W@Pt Nanoparticles with a Pt-Enriched Surface as a Robust Electrocatalyst for Oxygen Reduction Reactions.* ChemistrySelect, 2018. **3**(4): p. 1056-1061.

Wang, Y.J., D.P. Wilkinson, and J. Zhang, *Noncarbon support materials for polymer electrolyte membrane fuel cell electrocatalysts.* Chemical Reviews, 2011. **111**(12): p. 7625-7651.

Wang, Y.-J., et al., *Unlocking the door to highly active ORR catalysts for PEMFC applications: polyhedron-engineered Pt-based nanocrystals.* Energy & Environmental Science, 2018. **11**(2): p. 258-275.

Wroblowa, H.S., Yen-Chi-Pan, and G. Razumney, *Electroreduction of oxygen: A new mechanistic criterion.* Journal of Electroanalytical Chemistry and Interfacial Electrochemistry, 1976. **69**(2): p. 195-201.

Xie, J., et al., *Site-Selective Deposition of Twinned Platinum Nanoparticles on TiSi2 Nanonets by Atomic Layer Deposition and Their Oxygen Reduction Activities.* ACS Nano, 2013. **7**(7): p. 6337-6345.

Yang, C., et al., *Mitigating the Degradation of Carbon-Supported Pt Electrocatalysts by Tungsten Oxide Nanoplates.* Electrochimica Acta, 2016. 188: p. 529-536.

Yang, H., et al., *Structure and Electrocatalytic Activity of Carbon-Supported Pt-Ni Alloy Nanoparticles Toward the Oxygen Reduction Reaction.* Journal of Physical Chemistry B, 2004. 108: p. 11024-11034.

Zenkin, S., et al., *Hydrophobicity of Thin Films of Compounds of Low-Electronegativity Metals.* Journal of the American Ceramic Society, 2014. **97**(9): p. 2713-2717.

Zhang, K., et al., *A highly active, stable and synergistic Pt nanoparticles/Mo2C nanotube catalyst for methanol electro-oxidation.* NPG Asia Materials, 2015. **7**(1): p. e153-e153.

Zhang, Y., et al., *Study of the degradation mechanisms of carbon-supported platinum fuel cells catalyst via different accelerated stress test.* Journal of Power Sources, 2015. 273: p. 62-69.

Zhu, Y., K.A. Dunn, and A.E. Kaloyeros, *Properties of ultrathin platinum deposited by atomic layer deposition for nanoscale copper-metallization schemes.* Journal of Materials Research, 2007. **22**(05): p. 1292-1298.